UNIVERSIDADE D
COIMBRA

Daniela Filipa Domingues Santo

GENE THERAPY MEDIATED BY GLYCOPOLYMERS-BASED NANOCARRIERS IN COMBINATION WITH CHEMOTHERAPEUTIC DRUGS AS A POTENTIAL THERAPEUTIC STRATEGY FOR HEPATOCELLULAR CARCINOMA

Doctoral thesis in Experimental Biology and Biomedicine supervised by Doctor Henrique Faneca, Doctor Jorge Coelho and Doctor Olga Borges and presented to the Institute of Interdisciplinary Research, University of Coimbra

November 2022

Daniela Filipa Domingues Santo

GENE THERAPY MEDIATED BY GLYCOPOLYMERS-BASED NANOCARRIERS IN COMBINATION WITH CHEMOTHERAPEUTIC DRUGS AS A POTENTIAL THERAPEUTIC STRATEGY FOR HEPATOCELLULAR CARCINOMA

Doctoral thesis submitted to the Institute of Interdisciplinary Research of University of Coimbra, to obtain the Degree of Doctor of Philosophy in Experimental Biology and Biomedicine

November 2022

1 2 9 0

UNIVERSIDADE D
COIMBRA

Daniela Filipa Domingues Santo

GENE THERAPY MEDIATED BY GLYCOPOLYMERS-BASED NANOCARRIERS IN COMBINATION WITH CHEMOTHERAPEUTIC DRUGS AS A POTENTIAL THERAPEUTIC STRATEGY FOR HEPATOCELLULAR CARCINOMA

Doctoral thesis submitted to the Institute of Interdisciplinary Research of University of Coimbra, to obtain the Degree of Doctor of Philosophy in Experimental Biology and Biomedicine

Supervisors:
Doctor Henrique Manuel dos Santos Faneca
Doctor Jorge Fernando Jordão Coelho
Doctor Olga Maria Fernandes Borges Ribeiro

Host institutions:
Center for Neuroscience and Cell Biology, University of Coimbra

Funding:
FCT - Portuguese Foundation for Science and Technology
Doctoral degree grant SFRH/BD/132601/2017

Coimbra
2022

Financial support:

AGRADECIMENTOS

Um projeto de doutoramento é uma longa viagem, um roteiro repleto de desafios, frustrações, incertezas, alegrias e muitos percalços...

Trilhar este caminho, só foi possível com a ajuda, o apoio e a força de algumas pessoas às quais pretendo manifestar a minha profunda gratidão.

Assim, ao meu orientador, Doutor Henrique Faneca, agradeço pela orientação científica, pelo incentivo, pela confiança e pela oportunidade de crescer, não só a nível profissional, mas também pessoal.

Ao meu co-orientador, Doutor Jorge Coelho, agradeço pela integração no grupo de investigação Polysyc, e pela possibilidade de desenvolver imensos conhecimentos na área da ciência dos polímeros. Obrigada por todo o seu apoio e confiança.

Ao Doutor Arménio Serra, por todas as sugestões e críticas, que me permitiram pensar com clareza e simplificar os problemas, estou profundamente agradecida.

À Fundação para a Ciência e Tecnologia, pelo financiamento da minha Bolsa de Doutoramento SFRH/BD/132601/2017.

Ao CNC e ao CEMMPRE, um especial agradecimento, pela disponibilização dos serviços e laboratórios necessários para a execução das experiências.

À Doutora Patrícia Mendonça e à Doutora Joana Góis, endereço a minha gratidão, pela solicitude e partilha de conhecimentos, imprescindíveis para dar os primeiros passos na síntese e caracterização de polímeros.

A todos os meus colegas do CNC, em particular aos elementos do laboratório de Vetores e Terapia Génica, agradeço o apoio, a camaradagem e boa disposição. Um especial obrigado à Doutora Dina Pereira pela sua generosidade, conhecimentos partilhados e pela ajuda prestada no laboratório.

A todos os meus colegas do grupo Polysyc, especialmente à Andreia Oliveira, à Vanessa Pereira, à Mónica Fernandes e ao João Costa, agradeço por todas as dúvidas teóricas esclarecidas, por todos os resultados que me ajudaram a analisar e também pela camaradagem. Muito obrigada pela vossa amizade.

À Doutora Rosemeyre Cordeiro, pela ajuda, pela disponibilidade e, principalmente, pelo encorajamento nos momentos mais críticos desta jornada. Rose, agradeço profundamente a oportunidade de ter trabalhado contigo. O teu rigor científico, a tua dedicação e o teu

profissionalismo foram e, sempre serão, um exemplo para mim. Muito obrigada pela tua amizade.

A toda a minha família, agradeço não só pelo apoio, mas, sobretudo, pela amizade, confiança e compreensão ao longo destes anos.

À minha irmã e à minha madrinha, que sempre foram os alicerces da minha vida, o meu muito obrigada.

Ao Ricardo, pelo seu amor, pelo companheirismo, compreensão e apoio incondicional, agradeço pela sua enorme dedicação, generosidade, tolerância e serenidade, com que me brinda todos os dias e, sem as quais não teria sido possível concretizar os grandes desafios destes últimos anos.

RESUMO

O carcinoma hepatocelular (CHC) corresponde a cerca de 75-85% dos tumores primários hepáticos e é a neoplasia com a terceira maior taxa de mortalidade no mundo. Ao longo dos últimos anos foram aprovados diversos inibidores de tirosinas cinases e *checkpoint* imunológicos para o tratamento de doentes com CHC em estádio avançado. No entanto, devido à reduzida taxa de resposta, à elevada toxicidade, à resistência aos fármacos e à, subsequente, recidiva do tumor, o desenvolvimento de novas estratégias antitumorais é absolutamente fundamental.

Nesse contexto, a terapia génica tornou-se uma ferramenta terapêutica promissora para o tratamento do cancro. No entanto, para alcançar os efeitos terapêuticos desejados e minimizar os efeitos secundários, é crucial desenvolver sistemas de transporte e entrega de material genético eficientes e específicos para as células alvo. Os nanossistemas com base em glicopolímeros têm-se destacado devido à sua inerente biocompatibilidade, estabilidade coloidal e alta afinidade de ligação ao recetor das asialoglicoproteínas (ASGPR), um recetor amplamente expresso na superfície das células de CHC. No entanto, o processo de síntese dos glícopolímeros, devido a problemas de solubilização e à necessidade de várias etapas de proteção/desproteção, é bastante trabalhoso e complexo.

Neste projeto, foram desenvolvidos nanossistemas de base glicopolimérica para mediar duas estratégias de terapia génica distintas, as quais foram combinadas com baixas concentrações de agentes quimioterapêuticos, de modo a promover um efeito antitumoral mais acentuado e reduzir potenciais efeitos secundários.

A primeira parte deste trabalho foi focada no desenvolvimento de um nanossistema de entrega de genes altamente eficiente e específico para CHC, de modo a inibir a expressão do oncogene c-MYC e a sensibilizar as células tumorais ao sorafenib (SF). Foi desenvolvida uma biblioteca de glicopolímeros catiónicos, à base do poli-2-aminoetil metacrilato (PAMA) e poli-2-lactobionamidoetil metacrilato (PLAMA), com diferentes composições, estruturas (bloco ou aleatória) e rácios de monómero carbohidrato/catiónico, sintetizados através da técnica de polimerização radicalar por transferência de átomo com ativadores regenerados por transferência de eletrões (ARGET ATRP). Os nanossistemas preparados com o glicopolímero com estrutura aleatória $PAMA_{114}$-*co*-$PLAMA_{20}$ foram os que demonstraram maior eficiência para a entrega de material genético. Estes nanossistemas exibiram uma relação de atividade de

transfecção/citotoxicidade muito melhor do que os nanossistemas preparados com os glicopolímeros em bloco correspondentes. Os nanovetores preparados com o glicopolímero $PAMA_{114}$-*co*-$PLAMA_{20}$ ligam-se especificamente ao recetor das asialogliproteínas e são maioritariamente internalizados através da via endocítica de vesículas revestida por clatrina. Os níveis de c-MYC foram significativamente diminuídos pela expressão do *short hairpin RNA* contra o *c-MYC* (MYC shRNA), resultando na inibição eficiente da proliferação das células tumorais e em elevados níveis de apoptose em modelos 2D e 3D de CHC. Além disso, o silenciamento de *c-MYC* aumentou a sensibilidade das células de CHC para o SF (IC_{50} para MYC shRNA+ SF de 1,9 μM em comparação com 6,9 μM para o controlo shRNA + SF). De um modo geral, os resultados obtidos demonstraram o grande potencial dos nanossistemas $PAMA_{114}$-*co*-$PLAMA_{20}$/MYC shRNA combinados com reduzidas doses de SF para o tratamento do CHC.

A segunda parte do trabalho centrou-se no desenvolvimento de um nanossistema para mediar uma estratégia de terapia de gene suicida. Para avaliar o efeito da amina primária nas propriedades físico-químicas, atividade biológica, biocompatibilidade e especificidade dos nanossistemas, uma mini-biblioteca de glicopolímeros à base de polimetacrilato de amina primária, com grau de polimerização fixo (DP) do LAMA e diferentes valores de DP para o AMA, foi sintetizada por ARGET ATRP. Os glicoplexos gerados demonstraram elevada especificidade para o recetor ASGPR e propriedades físico-químicas adequadas, especialmente em termos de tamanho e carga de superfície, o que permitiu a sua internalização através da endocitose mediada por clatrina. Adicionalmente, a estratégia de terapia de gene suicida *herpes simplex virus-thymidine kinase/ganciclovir* (HSV-TK/GCV), mediada pelos nanossistemas preparados com o glicopolímero $PAMA_{144}$-*co*-$PLAMA_{19}$, resultou numa elevada atividade antitumoral em modelos 2D e 3D de cultura celular de CHC, que foi significativamente incrementada pela combinação com pequenas quantidades de docetaxel.

Em conclusão, os resultados apresentados nesta tese demonstraram o potencial dos glicopolímeros com base em polimetacrilato de amina primária como nanossistemas de transporte e entrega de material genético direcionados ao CHC e destacam a importância das estratégias antitumorais combinadas para o tratamento desta neoplasia.

ABSTRACT

Hepatocellular carcinoma (HCC) accounts for approximately 75–85% of primary liver cancers and is the third leading cause of cancer-related deaths worldwide. In recent years, multiple kinase and immune checkpoint inhibitors have been approved as treatment options for patients with advanced-stage HCC. However, due to the low response rate, drug toxicity, resistance and subsequent tumor relapse, the development of novel strategies against HCC is urgently needed.

In this context, gene therapy has become a promising therapeutic tool for cancer treatment. However, to achieve the desired therapeutic effects and minimize off-target effects, the development of an efficient and targeted gene delivery platform is crucial. In this context, glycopolymers-based nanocarriers have attracted considerable attention due to their biocompatibility, colloidal stability and high binding affinity to the asialoglycoprotein receptor (ASGPR), an overexpressed receptor in HCC cells. However, their synthesis remains laborious and complex, with problems in solubilization and the need for protection/deprotection steps.

In this project, nanocarriers based on glycopolymers were developed to mediate two distinct gene therapy strategies, in combination with low concentrations of chemotherapeutic agents, to promote a higher anti-HCC effect and reduce potential side-effects.

The first part of this work was focused on the development of a highly efficient and HCC-specific gene delivery nanosystem that downregulates *C-MYC* expression and sensitizes tumor cells to low concentrations of sorafenib (SF). To this end, a library of tailor-made cationic glycopolymers, based on poly(2-aminoethyl methacrylate hydrochloride) (PAMA) and poly(2-lactobionamidoethyl methacrylate) (PLAMA), with different compositions, structures (block or random) and carbohydrate/cationic ratios, was synthesized by activators regenerated by electron transfer atom transfer radical polymerization (ARGET-ATRP). Nanocarriers prepared with the random glycopolymer $PAMA_{114}$-*co*-$PLAMA_{20}$ were the most efficient for gene delivery. Moreover, these nanosystems exhibited a much better transfection activity/cytotoxicity ratio than the corresponding nanocarriers based on block glycopolymers. $PAMA_{114}$-*co*-$PLAMA_{20}$-based nanosystems specifically bound to the ASGPR and were internalized by the clathrin-coated pit endocytic pathway. The *c-MYC* levels were significantly downregulated by c-MYC short-hairpin RNA (MYC shRNA), resulting in efficient inhibition of tumor cell proliferation and high levels of apoptosis in 2D and 3D

HCC-tumor models. Moreover, *c-MYC* silencing increased the sensitivity of HCC cells to SF (IC_{50} for MYC shRNA + SF 1.9 μM compared with 6.9 μM for control shRNA + SF). Overall, the data obtained demonstrate the great potential of $PAMA_{114}$-*co*-$PLAMA_{20}$/MYC shRNA nanosystems combined with low doses of SF for the treatment of HCC.

The second part of the work focused in the development of a nanocarrier to mediate a suicide gene therapy strategy. To evaluate the effect of primary amine content on the physicochemical properties, biological activity, biocompatibility and ASGPR specificity of nanocarriers, a mini-library of well-defined glycopolymers based on primary amines and polymethacrylates, with a fixed degree of polymerization (DP) of LAMA and different values of DP of AMA, was synthesized by ARGET ATRP. The glycoplexes generated showed high specificity for ASGPR and possessed suitable physicochemical properties, particularly in terms of size and surface charge, which allowed their internalization via the clathrin-coated pit endocytic pathway. Moreover, the herpes simplex virus-thymidine kinase/ganciclovir (HSV-TK/GCV) suicide gene therapy strategy, mediated by $PAMA_{144}$-*co*-$PLAMA_{19}$-based nanocarriers, resulted in high antitumor activity in 2D and 3D cell culture models of HCC, which was significantly enhanced when combined with small amounts of docetaxel.

Overall, the results presents in this thesis demonstrated the potential of primary-amine polymethacrylate-containing-glycopolymers as HCC-targeted gene delivery nanosystems and highlight the importance of the combined antitumor strategies for the treatment of this disease.

MOTIVATION AND OBJECTIVES

Cancer ranks as a leading cause of death and an important barrier to increasing life expectancy in all countries of the world. Hepatocellular carcinoma (HCC) has a high incidence worldwide and is the third leading cause of cancer mortality. This high mortality rate is due to the fact that HCC is usually detected only at advanced stages of disease and the currently available treatment options are associated with multiple limitations. Although remarkable advances have been made in HCC treatment, the development of new therapeutic strategies is urgently needed. As a promising therapeutic approach, gene therapy is expected to be an effective strategy to control tumor growth in the liver. However, the effective application of this strategy requires the development of nanosystems that allow an efficient and targeted gene delivery into HCC cells. Moreover, the implementation of a multiple-therapeutic approach, combining gene therapy and chemotherapy, could result in a strong and synergistic antitumor activity, with fewer side-effects, thus significantly improving clinical outcomes of HCC patients.

The main goal of this work was to develop a highly efficient and HCC-specific nanosystem for gene delivery and to evaluate the potential of different strategies for the treatment of HCC. These approaches consist of combining gene therapy, mediated by the developed glycopolymer-based nanocarriers, and low concentrations of chemotherapeutic agents to achieve an effective antitumor activity, without causing significant side effects. To accomplish this goal, well-defined lactobionic acid based glycopolymers were synthetized and their potential as HCC-specific gene delivery nanocarriers was evaluated. Subsequently, two distinct antitumor combination strategies were developed: 1) inhibition of *c-MYC* oncogene to sensitize tumor cells to chemotherapy; and 2) combination of HSV-TK/GCV suicide gene therapy with a microtubule-inhibitor agent.

Concerning to sensitization of tumor cells to chemotherapy through gene therapy, c-MYC was downregulated in combination with low concentrations of sorafenib to obtain a powerful antitumor effect. To address this issue, the following objectives were defined:

- Synthesis and characterization of a library of well-defined cationic glycopolymers, based on poly (2-aminoethyl methacrylate hydrochloride) (PAMA) and poly(2-

lactobionamidoethyl methacrylate) (PLAMA), with different compositions, structures (block or random) and carbohydrate/cationic ratios.

- Physicochemical characterization of the polyplexes prepared with the developed glycopolymers.

- Evaluation of the efficiency, biocompatibility and specificity of the glycopolymer-based gene delivery nanosystems in different HCC cell lines.

- Evaluation of the therapeutic potential of *c-MYC* downregulation in HCC cells, through delivery of glycoplexes carrying a DNA plasmid encoding a short hairpin RNA against this protein.

- Assessment of antitumor effect of *c-MYC* inhibition combined with low doses of sorafenib in 2D and 3D HCC cell culture models.

Regarding the combination of HSV-TK/GCV gene therapy strategy with a microtubule-inhibitor, the anti-HCC effect of suicide gene therapy, mediated by a glycopolymer-based nanocarrier, was enhanced when combined with low doses of docetaxel. To accomplish this, the following objectives were defined:

- Synthesis and characterization of a series of tailored made cationic glycopolymers, based on poly (2-aminoethyl methacrylate hydrochloride) (PAMA) and poly(2-lactobionamidoethyl methacrylate) (PLAMA), with fixed degree of polymerization (DP) of LAMA and different DP values of AMA.

- Evaluation of the effect of primary amine content on the physicochemical properties, biological activity, biocompatibility and ASGPR specificity of the nanocarriers.

- Evaluation of the effect of docetaxel on the transfection efficiency of the developed nanocarriers.

- Assessment of the effect of docetaxel on the antitumor activity of HSV-TK/GCV suicide gene therapy strategy mediated by PAMA-*co*-PLAMA-based nanosystems.

THESIS OUTLINE

The main goal of this PhD project was the development of a novel HCC-targeted glycopolymer-based nanosystem to mediate gene therapy with powerful antitumor effect against HCC cells. The PhD dissertation is organized in four chapters:

Chapter 1 provides a literature review on the treatment of hepatocellular carcinoma and gene therapy, with especial emphasis on glycopolymer-based gene delivery nanocarriers

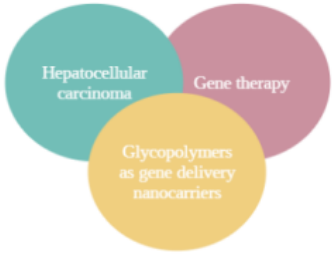

Chapter 2 describes the synthesis of a library of tailored cationic glycopolymers, based on PAMA and PLAMA, with different compositions, structures and carbohydrate/action ratios, by ARGET ATRP. The glycoplexes were subjected to an extensive physicochemical characterization and comprehensive evaluation of biological activity, toxicity and ASGPR specificity. The antitumor effect resulting from the combination of *c-MYC* downregulation, mediated by these HCC-targeted nanosystems, with low concentrations of sorafenib was evaluated.

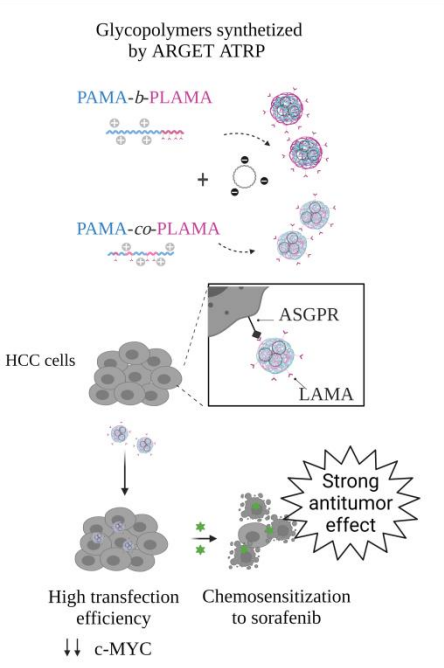

Chapter 3 reports the synthesis of well-defined PAMA-*co*-PLAMA random glycopolymers, with fixed degree of polymerization (DP) of LAMA and different DP values of AMA, to evaluate the effect of the cationic content on physicochemical properties, transfection capacity, cytotoxicity and targeting ability of glycopolymer-based gene delivery nanocarriers. The potential of PAMA-co-PLAMA-based gene delivery nanosystems to mediate HCC-targeted *HSV-TK*/GCV suicide gene therapy strategy in combination with docetaxel was assessed.

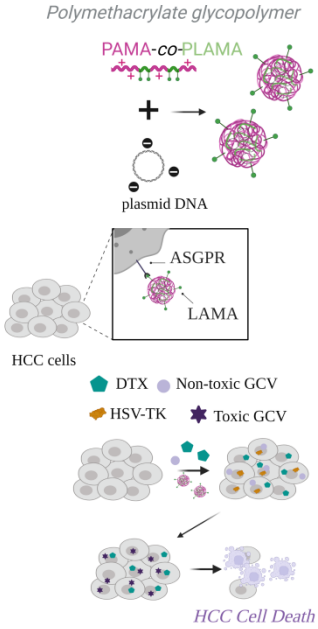

Chapter 4 presents the most relevant conclusions from this PhD research, along with suggestions for future work.

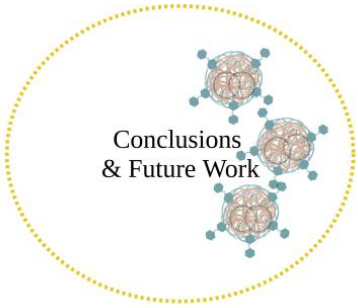

ABREVIATIONS

AAVs - Adeno-associated viruses

AKT - Protein kinase B

AKT- Protein kinase B

ARGET - Activators regenerated by electron transfer atom transfer radical

ASGPR - Asialoglycoprotein receptor

ATRP - Atom transfer radical polymerization

c-MET- Mesenchymal epithelial transition factor

CRISPR- Clustered regularly interspaced short palindromic repeats

DP – Degree of polymerization

DTX – Docetaxel

ERK - Extracellular signal-regulated kinase

ERK- Extracellular signal-regulated kinases

FGFR - fibroblast growth factor receptors

FGFR4 - Fibroblast growth factor receptor 4

GCV - Ganciclovir

HBV - Hepatitis B virus

HBV/HCV – Hepatic B/C virus

HCC – Hepatocellular carcinoma

HCV - Hepatitis C virus

HGF - Hepatocyte growth factor

HSV-TK - Herpes simplex virus-thymidine kinase

IGF - Insulin-like growth factor

MEK - Mitogen-activated protein kinase kinase

MKI - Multikinase inhibitor

mTOR - mammalian target of rapamycin

NAFLD - Non-alcoholic fatty liver disease

NAFLD- Nonalcoholic fatty liver disease

PAMA - Poly(2-aminoethyl methacrylate)

PD-1 - programmed cell death

PDGFRα - platelet-derived growth factor receptor α

PDGFR-β - Platelet-derived growth factor receptor β

PD-L1 – P0rogrammed cell death ligand 1

PDMAEMA - Poly[2-(dimethylamino)ethyl methacrylate]

pDNA- Plasmid DNA

PEI – Polyethylenimine

PGAAs- Poly(glycoamidoamine)s

PI3K - Phosphatidylinositol 3-kinase

PI3K- Phosphatidylinositol-3 kinase

PLAMA - Poly(2-lactobionamidoethyl methacrylate)

PβAE - Poly(β-amino ester)

RAFT - Reversible addition fragmentation chain transfer

SF – Sorafenib

shRNA – Short hairpin RNA

siRNA- Small interfering RNA

TACE - Transarterial chemoembolization

TARE - Transarterial radioembolization

TGFβ - Transforming growth factor beta

TP53- Tumor suppressor p53

VEGFR - Vascular endothelial growth factor receptors

CONTENTS

Agradecimentos ..... **ix**

Resumo ..... **xi**

Abstract ..... **xiii**

Motivation and objectives ..... **xv**

Thesis Outline ..... **xix**

Abreviations ..... **xxi**

List of figures ..... **xxvii**

List of schemes ..... **xxxvii**

List of tables ..... **iv**

Chapter 1 ..... **1**

Gene therapy for hepatocellular carcinoma: with special focus on glycopolymerS-based gene delivery nanocarriers **1**

1.1. Hepatocellular Carcinoma 3

1.1.1. Etiology of HCC 3

1.1.2. Hepatocarcinogenesis 4

1.1.3. Diagnosis and staging 6

1.1.4. Current treatment strategies 7

1.1.5. Emerging novel targeted therapies in HCC 12

1.2. Gene therapy 14

1.2.1. Treatment Modalities Used in Gene Therapy 18

Gene augmentation 19

Gene Silencing 20

Gene editing 21

1.2.2. Combination of gene therapy with other therapeutic agents for treatment of HCC 22

1.2.3. Vectors for gene therapy 23

Viral Vectors 25

Non-Viral Vectors 26

1.3. Glycopolymer-based nanoparticles for gene delivery to cancer cells 28

1.3.1. Carbohydrate-based nanosystems 28

1.3.2. Synthesis of glycopolymers 30
1.3.3. Glycopolymer as nuclei acid delivery nanocarriers 35
Monosaccharides-based nanosystems 35
Disaccharides-based nanosystems 39
1.3.4. Glycopolymers physicochemical properties 41
1.3.5. Interaction with target cells 45
1.3.6. Targeting 46
1.3.7. Intracellular trafficking of glycoplexes 49
1.3.8. Stimuli-responsive glycopolymers 50
1.3.9. Gene therapy mediated by glycopolymer–based nanocarriers 52
1.4. Conclusion 54
1.5. References 55

Chapter 2 77
Targeted downregulation of *MYC* mediated by a highly efficient lactobionic acid-based glycoplex to enhance chemosensitivity in human hepatocellular carcinoma cells 77
..... 77
2.1. Introduction 79
2.2. Materials and methods 81
Antitumor activity 88
2.3. Results and discussion 90
2.3.1. Synthesis and characterization of PAMA-b-PLAMA and PAMA-co-PLAMA glycopolymers 90
2.3.2. Physicochemical characterization of the nanosystems 95
2.3.3. Transfection activity and cytotoxicity of glycopolymer-based polyplexes 98
2.3.4. Asialoglycoprotein receptor-targeted glycoplexes 106
2.3.5. The endocytosis and intracellular fate of glycoplexes 108
2.3.6. *c-MYC* downregulation to enhance sorafenib antitumor effect 111
2.4. Conclusion 115
Acknowledgment 115
2.5. References 116

Chapter 3123Glycopolymers mediate suicide gene therapy in ASGPR-expressing hepatocellular carcinoma cells in tandem with docetaxel.....123

3.1. Introduction 125

3.2. Materials and Methods 128

3.3. Results and Discussion 130

3.3.1. Synthesis and characterization of PAMA-co-PLAMA glycopolymers.....130

3.3.2. Physicochemical Characterization of Nanosystems 132

3.3.3. Transfection activity and cytotoxicity of PAMA-co-PLAMA-based polyplexes.....134

3.3.4. ASGPR mediated targeted gene delivery to HCC cells.....138

3.3.5. The intracellular pathway of PAMA-co-PAMA-based nanocarriers 141

3.3.6. DTX as enhancer of antitumor activity mediated by suicide gene therapy ..144

3.4. Conclusion.....150

Acknowledgment.....150

3.5. References 151

Chapter 4.....157

Concluding remarks and future.....157

perspectives 157

4.1. Concluding remarks.....159

4.2. Future perspectives.....161

Appendices 163

Appendix A.....165

Appendix B.....179

LIST OF FIGURES

Figure 1– Pathogenesis of Hepatocellular Carcinoma.....5

Figure 2– BCLC staging and treatment strategy. *Adaptated from J. Hepatol.* ***2022****, 76 (3), 681–693.* 7

Figure 3– Distribution of completed or ongoing clinical trials according to the targeted diseases.[48] 14

Figure 4– *Ex vivo* and *in vivo* approaches to gene therapy.....15

Figure 5– Treatment modalities used in gene therapy.....19

Figure 6– Vectors for delivery of a therapeutic gene into a target cell. 24

Figure 7– Carbohydrate-based monomers and cationic monomers most commonly used in glycopolymer-based gene delivery nanocarriers. 33

Figure 8– Effect of glycopolymer properties on gene delivery nanosystems performance. ...42

Figure 9– 400 MHz ^{1}H and ^{13}C NMR spectra in D_2O of LAMA monomer. 91

Figure 10– 400 MHz ^{1}H NMR spectrum in D_2O (a) and SEC trace (b) of the $PLAMA_{70}$ homopolymer prepared by ARGET ATRP. 168

Figure 11– Physicochemical properties of the nanosystems: (a) hydrodynamic diameter, (b) zeta potential, (c) TEM imaging, (d) agarose gel electrophoresis assay and (e) DNA complexation efficiency. (a,b) Nanosystems were prepared with 1 μg of plasmid DNA at 50:1 N/P ratio. Statistical analysis of results is available in Table A1 and Table A2 of Appendix A. (c) For TEM analysis, $PAMA_{114}$-*co*-$PLAMA_{20}$-based polyplexes were prepared with 1 μg of plasmid DNA at 50:1 N/P ratio (scale bar = 200 nm). (d) Polyplexes prepared with different glycopolymers (1–$PAMA_{38}$-*co*-$PLAMA_{47}$, 2– $PAMA_{50}$-*b*-$PLAMA_{49}$, 3– $PAMA_{87}$-*co*-$PLAMA_{42}$, 4– $PAMA_{97}$-*b*-$PLAMA_{44}$, 5– $PAMA_{94}$-*co*-$PLAMA_{9}$, 6– $PAMA_{118}$-*b*-$PLAMA_{6}$, 7–$PAMA_{114}$-*co*-$PLAMA_{20}$, 8–$PAMA_{108}$-*b*-$PLAMA_{14}$, 9– $PAMA_{92}$-*co*-$PLAMA_{95}$, 10– $PAMA_{99}$-*b*-$PLAMA_{113}$, 11–$PLAMA_{70}$), at 50/1 N/P ratio, were analyzed by gel electrophoresis. (e) Quantification of Green Safe access to DNA of the different formulations. 96

Figure 12– Biological activity of random- (a) and block- (b) based glycoplexes in HepG2 cells. Nanosystems were prepared by complexing the glycopolymers with 1 μg of plasmid

DNA encoding luciferase (pCMV.Luc) at different N/P ratios. Statistical analysis of results is available in Table A3 of Appendix A.....99

Figure 13– Cytotoxicity of random- (a) and block- (b) based glycoplexes in HepG2 cells. Polyplexes were prepared by complexing the glycopolymers with 1 μg of plasmid DNA encoding luciferase (pCMV.Luc), at different N/P ratios. Statistical analysis of results is available in Table A4 of Appendix A.....101

Figure 14- Transfection activity of random- and diblock-based glycoplexes in Hep3B (a) and Huh-7 (b) cells. Glycoplexes were prepared with 1 μg of pCMV.Luc, at different N/P ratios. 103

Figure 15– Biological activity (a), cell viability (b) and transfection efficiency of different glycoplexes in HepG2 cells (c) and in tumor spheroids (d). Polyplexes were prepared by complexing glycopolymers, $PAMA_{161}$ and PEG_{45}-*b*-$PAMA_{168}$ with 1 μg of pCMV.Luc (a and b) or pCMV.gfp (c), at 50/1 N/P ratio. Asterisks (****p < 0.0001, ***p < 0.001, **p < 0.01, and *p < 0.05) and cardinals (####p < 0.0001, ###p < 0.001, and #p < 0.05) indicate values with statistical significance when compared to those obtained with the standard formulation, PEI-based nanosystem at 25/1 N/P ratio, or with PEG_{45}-*b*-$PAMA_{168}$-based polyplexes, respectively. (d) Polyplexes were prepared by complexing $PAMA_{114}$-*co*-$PLAMA_{20}$-based polyplexes with 0.5 μg of pCMV.gfp, at 50/1 N/P ratios. The cell nucleus was stained by DAPI (blue). Scale bar = 100 μm. 105

Figure 16– Effect of the presence of asialofetuin (a,b) and an antibody against the ASGPR (c) on the biological activity of different nanosystems in HepG2 cells. The biological activity was assessed by luminescence (a,c) and fluorescence microscopy (b) in HepG2 cells transfect with different nanosystems. Biological activity of polyplexes in Hela cells (d). Asialofetuin or antibody against the ASGPR were added to HepG2 cells 1 h before the addition of polyplexes. Polyplexes were prepared by complexing the polymers with 1 μg of pCMV.Luc (a,c,d) or pCMV.gfp (b), at their optimal N/P ratios. Asterisks (****p < 0.0001, ***p < 0.001 and **p < 0.01) correspond to values that differ significantly from those obtained with the same formulations in the absence of asialofetuin or Ab against ASGPR. (b) Fluorescence microscopy (I) and overlapping of fluorescence microscopy and phase contrast images (II) of cells transfected with different formulations at 50:1 N/P ratio (scale bar = 50 μm). (d) Asterisks (*p < 0.05) and cardinals (#p < 0.05) indicate values with statistical significance when compared to those obtained with the standard formulation, PEI-based nanosystem at 25/1 N/P ratio, or with PEG_{45}-*b*-$PAMA_{168}$-based polyplexes, respectively.....107

Figure 17– Effect of endocytosis inhibitors on the transfection ability of $PAMA_{114}$-*co*-$PLAMA_{20}$- (a) and $PAMA_{108}$-*b*-$PLAMA_{14}$- (b) based polyplexes and the influence of asialofetuin in their cell binding and cell internalization (c,d). (a,b) HepG2 cells were treated or not treated (Nt) with endocytosis inhibitors: CPZ (50mM), Fil (1μg/mL) and Amil (0.25mM). Asterisks (***p < 0.001 and **p < 0.01) indicate values with statistical significance when compared to those measured in the control (cells non-treated). (c) Cellular binding /uptake evaluated by flow cytometry, asterisks (**p < 0.01) correspond to values that differ significantly from those obtained with the same formulations in the absence of asialofetuin. (d) Representative confocal microscopic images of cells treated with different nanosystems formulated at 50/1 N/P ratio (scale bar = 10 μm). The acidic cell compartments were labeled with Lysotracker Red DND-9 (red), the cell nucleus was stained by DAPI (blue) and polyplexes were prepared with 1% fluorescein-labeled glycopolymer (green). 109

Figure 18– Antitumor activity promoted by the combination of c-MYC downregulation with sorafenib. HepG2 cells were treated with different therapeutic strategies: c-MYC inhibition mediated by the developed nanosystems (MYC shRNA), chemotherapy (SF), gene therapy combined with chemotherapy (MYC shRNA+ SF), and non-targeting shRNA combined or not with SF (Scr shRNA and scr shRNA + SF). a) c-MYC mRNA levels determined by qRT-PCR. b) Cell viability measured 120 h after transfection with MYC shRNA or Scr shRNA combined or not with 4μM of SF. c) Influence of sorafenib concentration on cell viability following 120 h of MYC silencing. d) Effect of the different treatment approaches on cell proliferation. Cardinals (####p < 0.0001, ###p < 0.001, ##p < 0. 01 and #p< 0. 05) correspond to data from cells treated with the various antitumoral strategies which significantly differ from those obtained with non-treated control. Asterisks (****p <0.0001 and ***p<0.001) correspond to data from cells treated with the combined therapy (MYC shRNA+ SF) which significantly differ from those obtained with cells treated with SF or scr shRNA+SF. e,f) Flow cytometry analysis of apoptosis and necrosis levels using FITC-annexin V/PI double-staining. g) Representative images of overlapping fluorescence microscopy and phase contrast of cells using fluorescein diacetate (green) and propidium iodide (red) staining for imaging live and dead cells, respectively (scale bar = 50 μm).....112

Figure 19- Effect of the c-MYC downregulation combined with SF on tumor spheroids growth. HepG2-spheroids were treated with different antitumor strategies: c-MYC inhibition mediated by glycopolymer-based nanosystems (MYC shRNA), chemotherapy (SF), gene therapy combined with chemotherapy (MYC shRNA+ SF), and non-targeting shRNA

combined or not with SF (Scr shRNA and Scr shRNA + SF). a) The microscopic images (scale bar = 200 μm) for 0 h are phase contrast images, and the microscopic images for 168 h are fluorescence images using fluorescein diacetate (green) and propidium iodide (red) staining for imaging live and dead cells, respectively. b) Asterisks (****p <0.0001, ***p<0.001) correspond to data achieved with spheroids treated with each individual strategy, non-targeted shRNA or non-treated control, which significantly differ from those obtained with spheroids treated with the combined therapy (MYC shRNA + SF).....114

Figure 20– Physicochemical characterization of PAMA-co-PLAMA-based polyplexes. (a) Hydrodynamic diameter and (b) zeta potential of $PAMA_{55}$-*co*-$PLAMA_{21}$-, $PAMA_{73}$-*co*-$PLAMA_{21}$-, $PAMA_{88}$-*co*-$PLAMA_{20}$-, $PLAMA_{70}$-, $PAMA_{161}$- and PEG_{45}-*b*-$PAMA_{168}$-based polyplexes prepared at 50:1 N/P ratio, and $PAMA_{144}$-*co*-$PLAMA_{19}$- based polyplexes formulated at 25:1 N/P ratio. Asterisks (****p < 0.0001, **p < 0.01, and *p < 0.05) indicate values with statistical significance when compared to those obtained with PEG_{45}-*b*-$PAMA_{168}$-based polyplexes. (c) DNA complexation efficiency. (d) Gel electrophoresis of polyplexes prepared with different glycopolymers: L- DNA ladder (1 kb plus), DNA - Plasmid only, 1 - $PAMA_{55}$-*co*-$PLAMA_{21}$, 2 - $PAMA_{73}$-*co*-$PLAMA_{21}$, 3 - $PAMA_{88}$-*co*-$PLAMA_{20}$, 4 - $PAMA_{144}$-*co*-$PLAMA_{19}$, 5 - $PLAMA_{70}$. 133

Figure 21– Transfection activity (a) and cytotoxicity (b) of PAMA-*co*-PLAMA-based nanocarriers in HepG2 cells. Polyplexes were prepared by complexing glycopolymers, $PAMA_{161}$ and PEG_{45}-*b*-$PAMA_{168}$ with DNA plasmid encoding luciferase, at different N/P ratios. Asterisks (****p < 0.0001, ***p < 0.001, **p < 0.01, and *p < 0.05) and cardinals (####p < 0.0001, ###p < 0.001, and #p < 0.05) indicate values with statistical significance when compared to those obtained with the standard formulations, PEI-and PEG_{45}-*b*-$PAMA_{168}$-based polyplexes, respectively.....135

Figure 22– Transfection efficiency assessed by fluorescence microscopy in HepG2 cells. Typical fluorescence images (I) and overlapping (II) of fluorescence microscopy and phase contrast images of cells after transfection with different glycopolymers-based nanocarriers (scale bar = 50 μm).....137

Figure 23– Effect of the presence of asialofetuin and an antibody against the ASGPR on biological activity of PAMA-*co*-PLAMA-based polyplexes in HepG2 cells. Biological activity of polyplexes in Hela cells. (a, b) Asterisks (****p < 0.0001, ***p < 0.001, **p < 0.01, and *p < 0.05) correspond to values that differ significantly from those obtained with e same formulations in the absence of asialofetuin or Ab against ASGPR. (c) Typical

fluorescence images (I) and overlapping of fluorescence microscopy and phase contrast images (II) of cells transfected with different nanocarriers in the presence and absence of asialofetuin (scale bar = 100 μm). d) Asterisks (**p < 0.01 and *p < 0.05) and cardinals (###p < 0.001 and ##p < 0.01 indicate values with statistical significant differences when compared to those obtained with PEI-based nanosystem at 25/1 N/P ratio, or with PEG_{45}-*b*-$PAMA_{168}$-based polyplexes, respectively. 139

Figure 24- Effect of the presence of asialofetuin on cellular uptake of $PAMA_{144}$-*co*-$PLAMA_{19}$- and PEG_{45}-*b*-$PAMA_{168}$-based polyplexes, evaluated by confocal microscopy (a) and flow cytometry (b) and the influence of endocytosis inhibitors on their transfection ability (c). (a) Representative confocal microscopic images of HepG 2 cells treated with $PAMA_{144}$-*co*-$PLAMA_{19}$-based nanocarriers (scale bar = 10 μm): (I) cell nucleus stained by DAPI (blue); (II) acidic cellular compartments stained with Lysotracker Red DND-99 (red); (III) polyplexes prepared with 1% fluorescein-labeled glycopolymer (green); and (IV) overlay of images I−III. (b) Asterisks (*p < 0.05) correspond to values which differed significantly from those obtained with the same formulations in the absence of asialofetuin. (c) HepG2 cells were treated or not treated (Nt) with endocytosis inhibitors: chlorpromazine (50 mM), filipin (1 μg/mL) and amiloride (0.25 mM). Asterisks (***p < 0.001 and *p < 0.05) indicate values with statistical significance compared to those measured in untreated cells (control).....141

Figure 25– Effect of DTX concentration on the biological activity (a) and cytotoxicity (b) of $PAMA_{144}$-*co*-$PLAMA_{19}$-based glycoplexes, prepared at 25/1 N/P ratio, in HepG2 cells. Asterisks (****p < 0.0001, ***p < 0.001, **p < 0.01 and *p < 0.05) indicate values that significantly differ from those measured for $PAMA_{144}$-*co*-$PLAMA_{19}$-based nanocarriers in the absence of DTX. 145

Figure 26- Therapeutic potential of the suicide gene therapy strategy mediated by the glycopolymer-based nanocarrier combined with DTX. Effect on viability (a) and apoptosis levels of HepG2 cells (b, c and d). HepG2 cells were treated with different antitumor strategies: suicide gene therapy ($PAMA_{144}$-*co*-$PLAMA_{19}$/pTK + GCV), chemotherapy (free DTX) and suicide gene therapy combined with chemotherapy ($PAMA_{144}$-*co*-$PLAMA_{19}$/pTK + GCV + DTX). a) The data are expressed as the percentage of cell viability with respect to untreated cells (control). Asterisks (****p <0.0001, ***p<0.001) indicate values that significantly differ from those measured for cells transfected with $PAMA_{144}$-*co*-$PLAMA_{19}$-based nanocarriers, containing 1 μg of pTK plasmid. Cardinals (####p < 0.0001 and ###p < 0.001) correspond to data from cells treated with each individual strategy ($PAMA_{144}$-*co*-

PLAMA$_{19}$/pTK + GCV or DTX) which significantly differ from those obtained with cells treated with the combined therapy (PAMA$_{144}$-*co*-PLAMA$_{19}$/pTK + GCV + DTX). b) Percentage of viable, early apoptotic, late apoptotic/necrotic and necrotic cells obtained from flow cytometry analysis, measured after 72 h of treatment. c) Representative scatter plots of FITC-annexin V vs PI. Q1, necrotic cells; Q2, late apoptotic/necrotic cells; Q3, early apoptotic cells, Q4, viable cells. d) Representative images of overlapping fluorescence microscopy and phase contrast of cells using fluorescein diacetate (green) and propidium iodide (red) staining for imaging live and dead cells, respectively (scale bar = 50 μm).....147

Figure 27– Effect of the suicide gene therapy strategy mediated by the glycopolymer-based nanocarriers combined with DTX on the tumor spheroid growth. HepG2-spheroids were treated with different antitumor strategies: suicide gene therapy (PAMA$_{144}$-*co*-PLAMA$_{19}$/pTK + GCV), DTX and suicide gene therapy combined with DTX (PAMA$_{144}$-*co*-PLAMA$_{19}$/pTK + GCV + DTX). a) Asterisks (****p <0.0001, ***p<0.001) correspond to data achieved with spheroids treated with each individual strategy and non-treated control, which significantly differ from those obtained with spheroids treated with the combined therapy (PAMA$_{144}$-*co*-PLAMA$_{19}$/pTK + GCV + DTX) . b) The microscopic images (scale bar = 200 μm) from 0 h to 120 h are phase contrast images, and the microscopic images for 168 h are fluorescence images using fluorescein diacetate (green) and propidium iodide (red) staining for imaging live and dead cells, respectively. c) PI Mean Fluorescence Intensity (MFI) per spheroid area. 149

Figure A1- 400 MHz ^{1}H NMR spectrum in D_2O (a) and SEC trace (b) of the PAMA$_{114}$-*co*-PLAMA$_{20}$ random copolymer prepared by ARGET ATRP.....168

Figure A2– 400 MHz ^{1}H NMR spectrum in D_2O (a) and SEC trace (b) of the PAMA$_{108}$-*b*-PLAMA$_{14}$ block copolymer prepared by ARGET ATRP. 168

Figure A3– Cytotoxicity of random- and diblock-based glycoplexes in Hep3B (a) and Huh-7 (b) cells. Polyplexes were prepared by complexing the glycopolymers with 1 μg of plasmid DNA encoding luciferase (pCMV.Luc), at different N/P ratios. The results correspond to mean ± SD, achieved from triplicates, and are representative of at least three independent experiments.....174

Figure A4– Representative Z-stack confocal microscopic images of tumor spheroids treated with PEG$_{45}$-*b*-PAMA$_{168}$-based nanosystems formulated at 50/1 N/P ratio. Polyplexes were

prepared by complexing the copolymer with 0.5 μg of pCMV.gfp, at 50/1 N/P ratios. The cell nucleus was stained with DAPI (blue). Scale bar = 100 μm. 174

Figure A5– Effect of the presence of asialofetuin on the biological activity Huh-7 (a) and Hep3B cells transfected with different polyplexes. Asialofetuin was added to cells 1 h before the addition of polyplexes. Polyplexes were prepared by complexing the polymers with 1 μg of pCMV.Luc, at their optimal N/P ratio. The results correspond to mean ± SD, achieved from triplicates, and are representative of at least three independent experiments. Asterisks (****p < 0.0001, ***p < 0.001, **p < 0.01 and *p < 0.05) correspond to values that differ significantly from those obtained with the same formulations in the absence of asialofetuin. 174

Figure A6– Effect of the presence of asialofetuin on the transfection efficiency of HepG2 cells transfected with PEI-based polyplexes and untreated control. Asialofetuin was added to cells 1 h before the addition of polyplexes. Polyplexes were prepared by complexing the polymers with 1 μg of pCMV.GFP, at their optimal N/P ratio. Fluorescence microscopy (I) and overlapping of fluorescence microscopy and phase contrast images (II) of cells transfected with different formulations at 50:1 N/P ratio (scale bar = 50 μm). 175

Figure A7– Effect of endocytosis inhibitors on the transfection activity (a), (b), (c) and toxicity (d), (e), (f) of $PAMA_{114}$-*co*-$PLAMA_{20}$-based polyplexes. HepG2 cells were pretreated with chlorpromazine (50; 75; 100 μM), amiloride (0.25; 0.5; 1 mM) or filipin (0.5; 1; 2 $\mu g.mL^{-1}$) and transfected with $PAMA_{114}$-*co*-$PLAMA_{21}$-based polyplexes prepared with 1 μg of pCMV.Luc at 50/1 N/P ratio. The results correspond to mean ± SD, achieved from triplicates, and are representative of at least three independent experiments. Asterisks (****p <0.0001, ***p < 0.001, **p < 0.01 and *p < 0.05) indicate values that differ significantly from those measured in the control (cells not-treated with endocytosis inhibitors).....176

Figure A8– Effect of endocytosis inhibitors on the transfection activity (a), (b), (c) and toxicity (d), (e), (f) of $PAMA_{108}$-*b*-$PLAMA_{14}$-based polyplexes. HepG2 cells were pretreated with chlorpromazine (50; 75; 100 μM), amiloride (0.25; 0.5; 1 mM) or filipin (0.5; 1; 2 $\mu g.mL^{-1}$) and transfected with $PAMA_{108}$-*b*-$PLAMA_{14}$-based polyplexes prepared with 1 μg of pCMV.Luc at 50/1 N/P ratio. The results correspond to mean ± SD, achieved from triplicates, and are representative of at least three independent experiments. Asterisks (****p <0.0001, ***p < 0.001, **p < 0.01 and *p < 0.05) indicate values that differ significantly from those measured in the control (cells not-treated with endocytosis inhibitors).....176

Figure A9– Effect of asialofetuin on cellular uptake of polyplexes in HepG2 cells evaluated by confocal microscopy. Asialofetuin was added to the cells 1 h before the addition of the polyplexes. Polyplexes were prepared by complexing the polymers, containing 1% of fluorescein-labeled glycopolymer, with 1 μg of pCMV.Luc, at their optimal N/P ratio. Scale bar = 10 μm. (I) cell nucleus stained by DAPI (blue); (II) acidic cell compartments labeled with Lysotracker Red DND-99 (red); (III) polyplexes were prepared with 1% fluorescein-labeled glycopolymer (green); (IV) overlay of images I−III. 177

Figure A10– Effect of the non-targeting shRNA combined or not with SF (Scr shRNA and Scr shRNA + SF) on tumor spheroids growth. The microscopic images (scale bar = 200 μm) for 0 h are phase contrast images, and the microscopic images for 168 h are fluorescence images using fluorescein diacetate (green) and propidium iodide (red) staining for imaging live and dead cells, respectively. 178

Figure B1– ^{1}H (a) and ^{13}C (b) NMR spectra (D_2O, 400 MHz) for the LAMA monomer..... 187

Figure B2– ^{1}H NMR spectrum (D_2O, 400 MHz) (a) and SEC trace (b) of the $PAMA_{144}$-*co*-$PLAMA_{19}$ random copolymer prepared by ARGET ATRP..... 188

Figure B3– SEC traces of the PAMA-*co*-PLAMA random copolymers prepared by ARGET ATRP. 188

Figure B4– ^{1}H NMR spectrum (D_2O, 400 MHz) (a) and SEC trace (b) of the $PLAMA_{38}$-Br homopolymer prepared by ARGET ATRP. 189

Figure B5– Potentiometric titration curves of PAMA-co-PLAMA glycopolymers. Glycopolymers were dissolved in acidic water (pH=3) and the polymeric solutions were acidified to pH 2 with 1% (V/V) HCl and titrated with 0.1M NaOH. 190

Figure B6– Effect of the presence of asialofetuin on the transfection efficiency of PEI- and PEG_{45}-*b*-$PAMA_{168}$ based polyplexes in HepG2 cells.. 190

Figure B7– Effect of the presence of asialofetuin and an antibody against the ASGPR on biological activity of PAMA-*co*-PLAMA-based polyplexes in Hep3B cells. 191

Figure B8– Cellular internalization of PAMA-*co*-PLAMA-based polyplexes evaluated by flow cytometry..... 192

Figure B9– Effect of endocytosis inhibitors on the transfection activity (a), (b), (c) and toxicity (d), (e), (f) of $PAMA_{114}$-*co*-$PLAMA_{21}$-based polyplexes. 193

Figure B10– Effect of endocytosis inhibitors on the transfection activity (a), (b), (c) and toxicity (d), (e), (f) of PEG_{45}-*b*-$PAMA_{168}$-based polyplexes.....194

Figure B11–Therapeutic potential of the suicide gene therapy strategy mediated by the glycopolymer-based nanocarrier combined with docetaxel in HepG2 cells.. 195

LIST OF SCHEMES

Scheme 1- The general mechanism of ATRP. 34

Scheme 2- Random and block methacrylate-based glycopolymers were synthetized by ARGET ATRP. ASGPR-specific internalization and clathrin-mediated endocytosis lead to high transfection efficiency in HCC cells. Downregulation of c-MYC expression by MYC shRNA resulted in a high sensitization of HepG2 cells to SF. 81

Scheme 3 - ARGET ATRP of AMA and LAMA for the synthesis of random (a) and block (b) glycopolymers. 94

Scheme 4- Schematic illustration of the proposed anti-HCC therapeutic strategy based on the combinatorial effects of DTX with suicide gene therapy-mediated by PAMA-*co*-PLAMA-based glycoplexes. 127

Scheme 5- Synthesis of for the random PAMA-*co*-PLAMA glycopolymers by ARGET ATRP. 131

Scheme A1– Synthesis of 2-lactobionamidoethyl methacrylate (LAMA).a) Lactobionic acid was dissolved in anhydrous methanol at 50 ºC, in the presence of trifluoroacetic acid ($C_2HF_3O_2$), to obtain lactobionolactone. b) Lactobionolactone was dissolved in methanol, followed by the addition of 2-aminoethyl methacrylate hydrochloride, triethylamine (Net3) and hydroquinone at room temperature. 167

LIST OF TABLES

Table 1– FDA-approved targeted drugs for HCC. 9

Table 2- Clinical trials of molecular targeted therapy for advanced HCC. 12

Table 3– Current EMA and FDA approved gene therapy products. 16

Table 4- Summary of viral vectors characteristics. 25

Table 5- Advantages and challenges ahead of the carbohydrate-based nanosystems. 29

Table 6 - Composition and molecular weight parameters of glycopolymers synthetized by ARGET ATRP.....92

Table 7- Composition and molecular weight parameters of glycopolymers prepared by ARGET ATRP.....131

Table A1– Statistical analysis of data presented in Figure 9a. 168

Table A2– Statistical analysis of data presented in Figure 9b. 169

Table A3– Statistical analysis of data presented inFigure 10a and 10b.. 170

Table A4– Statistical analysis of data presented in Figure 11. 171

CHAPTER 1

GENE THERAPY FOR HEPATOCELLULAR CARCINOMA: WITH SPECIAL FOCUS ON GLYCOPOLYMERS-BASED GENE DELIVERY NANOCARRIERS

This chapter was partially based on a review paper – *in preparation.*

1.1.Hepatocellular Carcinoma

Cancer is a leading cause of death in all countries of the world and an important barrier to increasing life expectancy. The World Health Organization (WHO) estimates that there were 19.3 million new cancer cases and nearly 10.0 million cancer deaths in 2020.[1] Liver cancer is the seventh most commonly diagnosed cancer worldwide and the third most common cause of cancer death, after lung and colorectal cancers.[1] The main reasons for the high mortality rate in patients with liver cancer are the lack of good molecular markers for diagnosis and the tumor resistance to existing anticancer drugs. For example, there were approximately 906,000 new cases of liver cancer in 2020 that will result in an estimated 830,000 deaths.[1] Primary liver cancer include hepatocellular carcinoma (HCC) (75%-85% of the cases) and intrahepatic cholangiocarcinoma (10%-15%), as well as other rare forms.[1] The worldwide incidence and mortality of HCC is heterogeneous because of differences in the degree of exposure to environmental and infectious risk factors, availability of healthcare resources, and ability to detect and effectively treat HCC at an earlier stage. Almost 85% of HCC cases occur in low and middle-resource countries, particularly in Eastern Asia and sub-Saharan Africa, where medical and social care resources are often limited.[2] The occurrence of HCC is usually observed in males to a greater extent than in females. This differential distribution by sex is thought to be related to a higher exposure of men to risk factors, as well as a possible effect of sex hormones on HCC risk. Testosterone is a positive regulator of hepatocyte cell-cycle regulators, which may promote hepatocarcinogenesis, whereas estradiol suppresses cell-cycle regulators preventing the development of HCC.[3] The age of onset of HCC varies in different parts of the world, with the average age at HCC diagnosis being above 60 years in Japan, North America and European countries, and in the age range of 30–60 years in parts of Asia and most African countries. The incidence and mortality of HCC continue to grow, particularly due to the obesity pandemic, and HCC mortality is expected to increase 41% worldwide by 2040.[1]

1.1.1. Etiology of HCC

HCC is a complex disease associated with multiple pathogenic mechanisms and caused by a variety of risk factors. The large majority of HCC cases occur as a result of chronic liver disease.[2] The main risk factors for HCC are viral (chronic hepatitis B and C), metabolic (diabetes and nonalcoholic fatty liver disease (NAFLD)), toxic (alcohol and aflatoxins) and immune system-related disorders.[2] The major risk factors vary by

region. In Africa and East Asia, chronic HBV infection is the main cause of HCC, whereas in the Western world chronic HCV infection is the most common cause of liver disease. However, the etiology of HCC appears to be changing as the prevalence of viral hepatitis declines and obesity, diabetes and NAFLD increase in most developed countries.

1.1.2. Hepatocarcinogenesis

Similar to many other tumors, the development of HCC is a highly complex multistep process associated with genetic and epigenetic aberrations, and alterations in multiple molecular signaling pathways.[4] In general, after hepatic injury caused by one of the several risk factors, inflammation and the subsequent and continuous cycles of hepatocyte necrosis-regeneration lead to chronic liver disease that culminates in cirrhosis. Cirrhosis is characterized by the formation of abnormal liver nodules surrounded by collagen deposition, and scarring of the liver. Within the fibrotic liver, alterations in molecular pathways, epigenetic changes, and somatic mutations may occur leading to HCC (Figure 1).[4] However, the cellular and molecular basis of hepatocarcinogenesis may differ among etiological factors.[4] For example, virus-induced hepatocarcinogenesis may result from DNA microdeletions, as a consequence of viral integration into the host genome, oxidative stress, and targeted activation of oncogenic pathways by various viral proteins.[5]

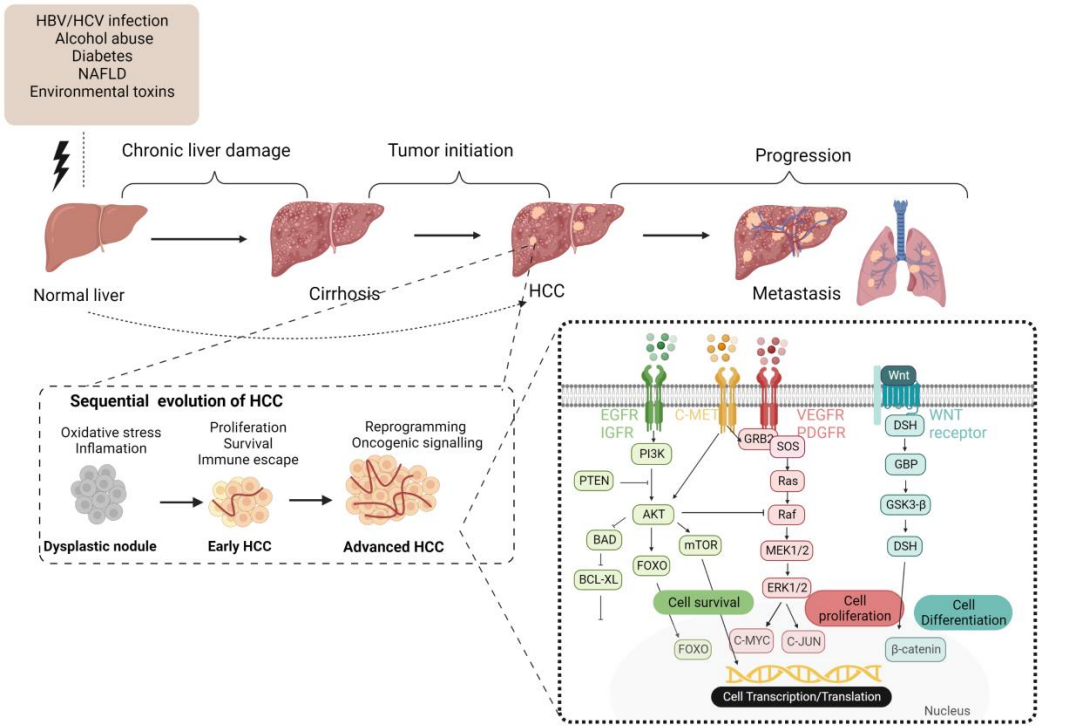

Figure 1– Pathogenesis of Hepatocellular Carcinoma.

The molecular analysis of human HCC has revealed many genetic alterations that result in the activation of key oncogenes, such as β-catenin, *c-MYC*, ErbB receptor family members, mesenchymal epithelial transition factor (*c-MET*) and its ligand hepatocyte growth factor (*HGF*), and in the inactivation or loss of tumor suppressor genes, such as tumor suppressor protein p53 (TP53). In addition to genetic aberrations, different epigenetic alterations, such as modification of histone tails (acetylation, methylation, phosphorylation, etc.) and hypermethylation of various cancer-related genes have also been identified in human HCC.[6] Alterations in multiple signaling pathways that regulate tumor cell proliferation, differentiation, angiogenesis, invasion and metastasis are also involved in the initiation and progression of HCC. These include the RAF/mitogen-activated protein kinase kinase (MEK)/extracellular signal-regulated kinases (ERK) pathway, phosphatidylinositol-3 kinase (PI3K)/protein kinase B (AKT)/mammalian target of rapamycin (mTOR) cascade, wingless/integrated (Wnt)/β-catenin pathway, insulin-like growth factor (IGF) pathway, HGF/c-MET pathway and vascular endothelial growth factor (VEGF) pathway [7](Figure 1). In addition, the tumor immune microenvironment plays a critical role in the development and progression of HCC.[8]

Cancer cells bypass the immune system's surveillance mechanisms by creating an immunosuppressive environment and/or avoiding the recognition by immune cells.

1.1.3. Diagnosis and staging

The diagnosis of HCC can be established based on noninvasive imaging without biopsy confirmation. The American Association for the Study of Liver Diseases (AASLD) and the European Association for the Study of the Liver (EASL) guidelines state that the diagnosis of HCC can be made radiologically if a new ≥1 cm mass is found, demonstrating arterial phase hyperenhancement and venous washout in a cirrhotic liver, using either cross-sectional, multiphase, contrast-enhanced computed tomography (CT) or magnetic resonance imaging (MRI).[9]

In the majority of solid tumors, staging is determined by pathological examination of surgically resected tissue, resulting in the tumor-node-metastasis (TNM) classification. However, the TNM staging system does not take into account the patient's degree of liver dysfunction and performance status, which are critical facts that need to be considered in making clinical decisions for patients with HCC. The Barcelona Clinic Liver Cancer (BCLC) classification is currently the most widely used standard staging system for HCC.[10] The BCLC staging system classifies HCC into five stages (0, A, B, C and D) and provides the estimated median survival and recommended treatments for patients at each stage (Figure 2).

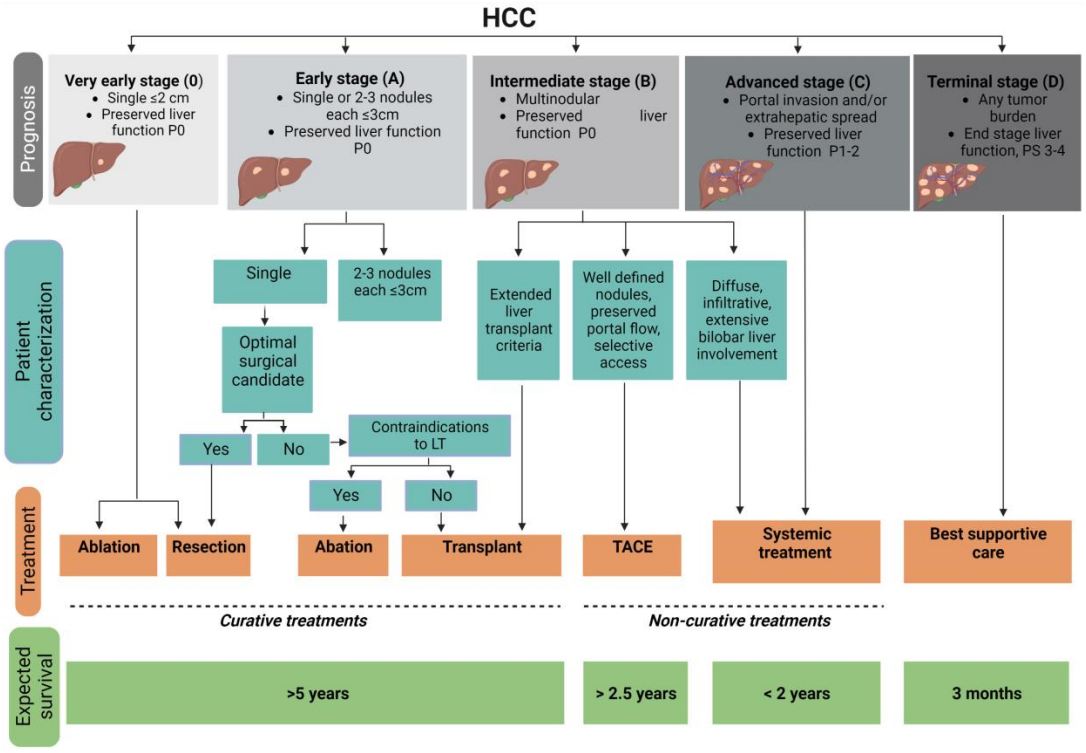

Figure 2– BCLC staging and treatment strategy. *Adaptated from J. Hepatol.* ***2022****, 76 (3), 681–693.*

Despite several other staging systems have been proposed, this is the only one with robust prospective validation and it is routinely used as a main stratifying factor in clinical trials.

1.1.4. Current treatment strategies

In the last 10 years, there have been significant advances in the treatment of HCC.[11] The available therapeutic options can be divided into curative and noncurative strategies (Figure 2).[9] Effective curative therapies include surgical resection, orthotopic liver transplantation, and ablative techniques, such as thermal ablation. These therapeutic approaches offer the chance of long-term response and improved survival. On the other hand, aiming at improving survival by slowing tumor progression, noncurative therapies include transarterial chemoembolization (TACE), transarterial radioembolization (TARE) and systemic chemotherapy.

Surgical resection is a recommended treatment option for patients with resectable disease in the absence of clinically significant portal hypertension (CSPH). However, nearly 70% of patients develop recurrent HCC after resection.[12] In patients with

alcoholic cirrhosis with CSPH and hepatic decompensation with early-stage HCC that meets Milan criteria (1 tumor up to 5 cm, or two to three tumors with the largest being <3 cm) liver transplantation is the treatment of choice. This treatment option is very effective for early-stage HCC, because it removes not only the tumor but also the diseased liver, which has impaired function and is prone to developing recurrent HCC. However, transplantation is limited by the extreme shortage of available liver allografts and the need for lifelong immunosuppression. Local tumor ablation is another potentially curative treatment used in patients with early-stage HCC. Destruction or ablation of tumor cells can be achieved by modifying local tumor temperature (radiofrequency, microwave, laser, cryotherapy) or by the injection of chemical substances (ethanol, acetic acid, and boiling saline).[13] This procedure can be performed percutaneously or during laparoscopy, and is currently considered the best option for HCC patients who are not candidates for surgical resection. Locoregional therapies, such as TACE and TARE, are treatment options for patients with intermediate-stage HCC who are not eligible for curative treatments[14]. TACE combines intra-arterial infusion of cytotoxic chemotherapeutic agents with delivery of embolization particles into the tumor-feeding artery to achieve strong cytotoxic and ischemic effects.[15] Drug-eluting beads (DEBs) have been developed to minimize ischemic damage to non-tumorous tissues and increased tumor concentration of chemotherapeutic agents. TARE has emerged as an alternative therapy to TACE. This intratumoral brachytherapy consists of the delivery of radioactive glass or resin microspheres loaded with a β-emitting yttrium-90 isotope into the arteries that supply the HCC tumour.[16]

Despite advances in early detection and diagnosis, more than 80% of patients are diagnosed with advanced disease, because HCC is asymptomatic in the early stages. These patients usually have a very poor prognosis, and treatment options are mainly palliative, aiming to reduce or to alleviate a locally advanced disease.[17] In addition, therapeutic options for advanced HCC are limited, due to the resistance of tumor cells to conventional chemotherapy and the underline liver dysfunction that hinders the delivery of drugs. Systemic therapy with doxorubicin (DNA-binding alkylating agent), cisplatin (antimetabolite drug), or docetaxel (microtubule inhibitor) results in low objective response rates and severe side effects.[18,19]

During the past decades, research has shed light on the molecular and genetic profiles of HCC, leading to a greater number of *druggable* targets, such as intracellular signaling proteins, angiogenesis factors, peptide growth factors and their receptors, cell cycle regulators, and transcription factors.[20] Sorafenib is a small-molecule multikinase inhibitor (MKI) that targets tumor angiogenesis and proliferation pathways by blocking the vascular endothelial growth factor receptor (VEGFR) 1-3, platelet-derived growth factor receptor β (PDGFR-β), and myc.[21] It was the first agent to achieve a statistically significant improvement in overall survival in patients with advanced HCC.[22] In a randomized phase III clinical trial, sorafenib was shown to prolong median overall survival by 2–3 months in patients with advanced-stage HCC (median overall survival of 10.7 months in the sorafenib group versus 7.9 months in the placebo group in the SHARP trial).[22] Based on these results, in 2007 sorafenib was approved by the Food and Drug Administration (FDA) for advanced HCC as first-line standard treatment.

Although sorafenib provides a remarkable survival benefit in patients with advanced HCC, its administration causes several adverse effects, including fatigue, diarrhea, skin irritation, hand-foot syndrome, hypertension, bleeding, weight loss, infection, and peripheral nerve sensory disorders. These adverse side effects result from the lack of cell specificity and water insolubility of sorafenib, making it necessary to administer high doses to ensure an effective treatment. However, in most cases, this leads to dosage reduction or treatment discontinuation. In a study to predict survival of HCC patients who permanently discontinued sorafenib, due to tumor progression, liver decompensation, or adverse effects, the median survival post-sorafenib was only 4.1 months.[19]

In recent years, due to improved knowledge of the hepatocarcinogenesis process and numerous clinical trials in HCC, major breakthroughs have been made in the development of new molecularly targeted drugs.[23] Since 2017, the FDA has approved several drugs for the treatment of HCC, including MKI (regorafenib, lenvatinib, cabozantinib, ramucirumab), immune checkpoint inhibitors (ICI) (nivolumab and pembrolizumab), and two combination regimens (nivolumab plus ipilimumab and bevacizumab plus atezolizumab) (Table 1).

Table 1– FDA-approved targeted drugs for HCC.

Drug	Therapeutic line	Target	Indication	Approved year
Sorafenib	1	Multitargeted TK	Unresectable HCC	2007
Nivolumab	2	PD-1	HCC treated previously with sorafenib	2017
Regorafenib	2	Multitargeted TK	HCC treated previously with Sorafenib	2017
Lenvantinib	1	Multitargeted TK	Unresectable HCC	2018
Pembrolizumab	2	PD-1	HCC treated previously with sorafenib	2018
Cabozantinib	2	Multitargeted TK	HCC treated previously with sorafenib	2019
Ramucirumab	2	VEGFR	HCC treated previously with sorafenib and AFP ≥ 400 ng/mL	2019
Nivolumab + Ipilimumab	2	PD-1/CTLA-4	HCC treated previously with sorafenib	2019
Atezolizumab + Bevacizumab	1	PD-L1/ VEGF	Unresectable HCC	2020
Tremelimumb + Durvalumab	1	CTLA-4/ PD-L1	Unresectable HCC	2022

Lenvatinib, a multikinase inhibitor targeting vascular endothelial growth factor receptor (VEGFR1–3), fibroblast growth factor receptors (FGFR1–4), platelet-derived growth factor receptor α (PDGFRα) and proto-oncogene tyrosine-protein kinase receptors RET and KIT, was approved in 2018 as a first-line systemic therapy for HCC. In the phase III REFLECT trial, lenvatinib proved to be noninferior to sorafenib and the median overall survival with lenvatinib was 13.6 versus 12.3 months with sorafenib.[24] Moreover, progression-free survival, time to disease progression and objective response rate were also improved with lenvatinib compared with sorafenib. Regorafenib is an oral inhibitor that inhibits many angiogenic and tumorigenic kinases, including VEGFR1–3, tyrosine kinase with immunoglobulin and epidermal growth factor homology domain 2 (TIE2), PDGFRβ, FGFR1, BRAF, RET, and KIT. In the phase III RESORCE trial, conducted in patients who had progressed on prior sorafenib treatment,

regorafenib had a longer overall survival than placebo (mOS, 10.6 vs. 7.8 months).[25] The phase III CELESTIAL trial showed that treatment with cabozantinib, an inhibitor of tyrosine kinases including MET, AXL and VEGF receptors, resulted in a significant improvement in median overall survival compared with placebo in patients with advanced HCC previously treated with sorafenib (mOS 10.2 vs. 8.0 months).[26] Cabozantinib was approved in 2019 for patients with HCC previously treated with sorafenib. In 2019, ramucirumab, a human anti-VEGFR-2 monoclonal antibody, demonstrated to improve overall survival in patients with advanced HCC and serum AFP levels ≥400 ng/ml.[27]

Improved knowledge of the role of the immune microenvironment in the development and progression of HCC has changed the treatment landscape for HCC.[28] ICI have emerged as a promising treatment option for advanced- stage HCC. In 2017 the FDA approved the use of nivolumab, a human monoclonal antibody against programmed cell death protein 1 (PD-1), as a second line treatment for advanced HCC in patients previously treated with sorafenib.[29] The PD-1/programmed cell death ligand 1 (PD-L1) engagement blocks T cell receptor signal transduction, inhibits T cell proliferation and secretion of cytotoxic mediators, leading to tumour immune escape. Blocking the PD-1 pathway could promote an antitumor immune response. Pembrolizumab, a monoclonal antibody that blocks PD-1, demonstrated durable antitumor activity and promising overall survival (17 months), in the multicenter phase II KEYNOTE-224 trial, and received accelerated approval from the FDA in 2018. To achieve more satisfactory therapeutic response rates than ICI monotherapy, combination therapies based on ICIs have been extensively explored for the treatment of HCC.[30] Nivolumab in combination with ipilimumab (cytotoxic T-lymphocyte associated protein 4 (CTLA-4) inhibitor) demonstrated clinically meaningful response rates and long-term survival benefit in HCC (mOS was 22.2 months), being approved for advanced HCC patients that progressed on sorafenib treatment.[31]Since antiangiogenic multikinase inhibitors or specific VEGF/VEGFR inhibitors may enhance antitumor immune activity through multiple mechanisms, namely by promoting the M1 polarization of tumor-associated macrophages (TAM), increasing CD4+ and CD8+ T cell infiltration and function, and suppressing regulatory T cells, the combination of antiangiogenics agents and ICIs may represent an evolution of current treatment approaches.[30] The combination of

atezolizumab, an IgG1 monoclonal antibody that specifically binds to PD-L1 and disrupts its interaction with PD-1, and bevacizumab, a humanized anti-VEGF monoclonal antibody that suppresses angiogenesis, was the first combination that proved to be more effective than sorafenib in the first-line treatment of advanced HCC. The median OS of this combination regime was 19.2 months, 5.8 months longer than sorafenib.[31] The combination of durvalumab and tremelimumab, monoclonal antibodies against PD-L1 and CTLA-4 immune checkpoints, respectively, was studied in the large phase 3 HIMALAYA trial. This combination regimen displayed superior efficacy and a more favorable benefit-risk profile than sorafenib, and was approved by the FDA in October 2022 for the treatment of HCC.[32]

1.1.5. Emerging novel targeted therapies in HCC

Over the past three years, rapid advances in molecular targeted therapies have dramatically changed the treatment landscape for advanced HCC.[33] The recent FDA approval of the atezolizumab + bevacizumab and tremelimumab + durvalumab regimens, as standard treatments, is considered a milestone and an encouraging breakthrough in the treatment of advanced HCC. In addition to these approved targeted therapies, several clinical trials are currently testing different molecular therapies for advanced HCC (Table 2).[34]

Table 2– Clinical trials of molecular targeted therapy for advanced HCC.

Target	Trial name	Drug	Setting	Phase
c-MET	NCT01755767	Tivantinib	2nd	III
	NCT01988493	Tepotinib	1st	Ib/II
	NCT01737827	Capmatinib	1st	II
FGFR4	NCT02508467	Fisogatinib (BLU554)	1st/2nd	I
	NCT02834780	H3B-652	2nd	I
TFG-β	NCT02178358	Galunisertib	2nd	II
c-MYC	NCT05497453	OTX-2002	2nd	Ib/II

Mesenchymal epithelial transition factor (c-MET) is a tyrosine kinase receptor for hepatocyte growth factor (HGF). Abnormal activation of the MET/HGF pathway is involved in HCC progression by promoting cell proliferation, survival and invasion, and

even by inducing drug resistance.[35] c-MET inhibitors are being investigated in several studies for their potential use in HCC patients as first-or second-line therapy. [36,37,38]

The transforming growth factor β (TGFβ) pathway has dual antitumor and protumor functions: in the early stage, the TFG-β ligand may be beneficial for promoting cell cycle arrest and apoptosis, whereas in the advanced stage, it promotes cell invasion, angiogenesis, epithelial-to-mesenchymal transition (EMT), immunosuppression and drug resistance.[35] These findings provide an important rationale for blocking the TGFβ pathway to circumvent HCC aggressiveness and resistance to therapies.[39]

Blocking the fibroblast growth factor receptor 4 (FGFR4) pathway is another promising approach in HCC.[40] Activation of this signaling pathway leads to cell proliferation, EMT, angiogenesis and invasion. While no significant difference was detected in FGFR4 expression between HCC and surrounding liver cells, FGF19 (one of the three endogenous ligands) was significantly overexpressed in HCC. Moreover, FGF19 expression was associated with early tumor recurrence and resistance to sorafenib, making this pathway a promising therapeutic target. [41,42]

MYC is a transcription factor recognized as a "master regulator" of cell metabolism and proliferation. Due to its important role as primary oncoprotein regulating many aspects of hepatocarcinogenesis, namely cell proliferation, growth, differentiation and immune response, it provides a unique opportunity for the development of novel anti-HCC therapies.[43,44] OTX-2002 is an mRNA therapeutic delivered via lipid nanoparticles designed to pre-transcriptionally downregulate the expression of MYC, through epigenetic modulation, potentially overcoming MYC autoregulation.[45] An open-label phase 1/2 study (NCT05497453) is evaluating the safety, tolerability, pharmacokinetics, pharmacodynamics, and preliminary antitumor activity of OTX-2002 in HCC patients, both as a single agent and in combination with standard therapy.

The results of recent clinical trials indicate that single-drug therapy may not be sufficient for the treatment of HCC. Therefore these molecular targeted drugs have been evaluated in combination with other multiple tyrosine kinase inhibitors or ICIs.[34] In addition, it is critical to find biomarkers that can predict the treatment response to guide the systemic therapy strategy.

1.2. Gene therapy

The completion of the human genome sequence opened the door and paved the way for the development of gene-based therapeutics to treat human diseases.[46] This unprecedented scientific achievement has enhanced the understanding of the causes of disease at the molecular level, improved the diagnosis and classification of disorders based on genetic profiles, and has been enabling the development of new therapeutics. In this context, gene therapy is a promising avenue to eradicate a wide range of diseases involving genetic factors such as cancer, cardiovascular diseases, degenerative neurological disorders, and many others. According to the European Medicines Agency (EMA), a gene therapy product generally consists of a vector or delivery formulation/system containing a genetic construct ("therapeutic sequence") engineered to regulate, repair, replace, add, or delete a specific genetic sequence associated with the disease and/or its treatment.[46] In 1990, the first clinical trial of gene therapy was started using retroviral-mediated transfer of the adenosine deaminase (ADA) gene into the T cells of two children with severe combined immunodeficiency (SCID).[47] Since then, despite the several setbacks suffered in gene therapy clinical trials, research has still been focused on the development of safe and efficient gene delivery systems for transferring foreign nucleic acids into human cells, and success stories continue to accumulate. To date, more than 3180 new gene therapy clinical trials have been completed, are ongoing or have been approved worldwide. The overwhelming majority of gene therapy clinical trials have addressed cancer (67.4%) and monogenic diseases (11.6%) (**Figure 3**).[48]

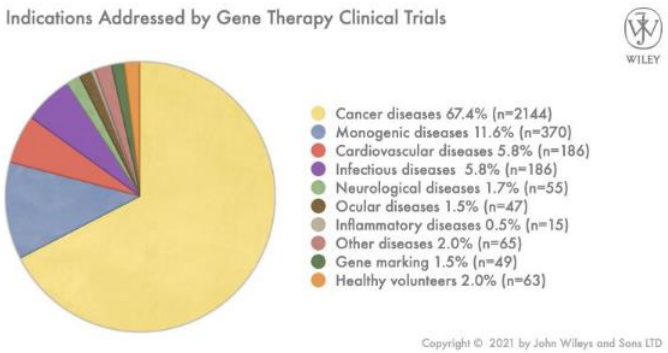

Figure 3– Distribution of completed or ongoing clinical trials according to the targeted diseases.[48]

Two fundamental strategies have been used in gene therapy: *ex vivo* or *in vivo* gene delivery (Figure 4).[49]

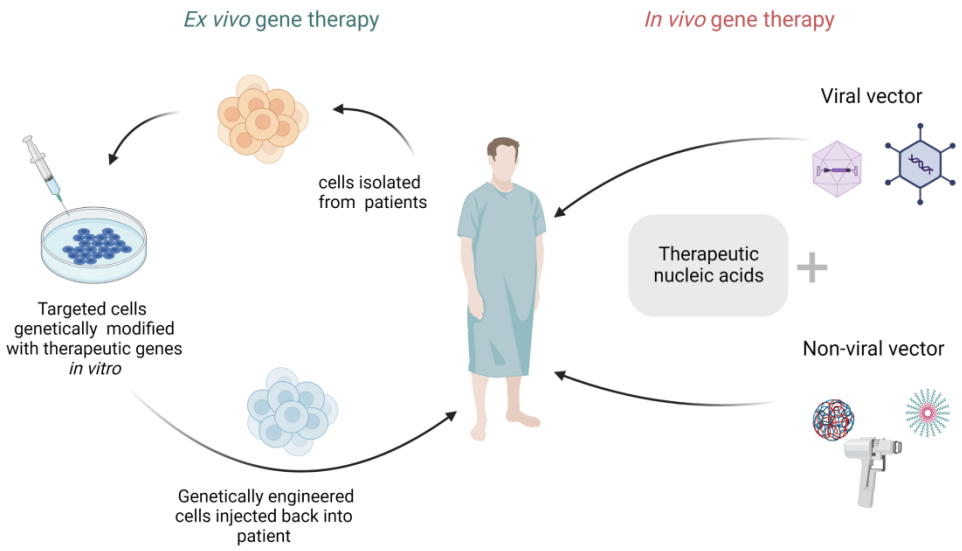

Figure 4– *Ex vivo* and *in vivo* approaches to gene therapy.

Ex vivo gene therapy involves taking cells from the patient or a donor, cultured them in a laboratory, transducing them with a therapeutic gene, and reinfusing them into the patient. Chimeric Antigen Receptor T cells (CAR-T cells) are the most commonly used cells in *ex vivo* protocols. The patient's T-cells are genetically modified to produce a new receptor, called Chimeric Antigen Receptor (CAR), hence the name CAR-T cells. This receptor varies for each cancer type, is specific to molecules overexpressed and/or exclusively expressed in cancer cells, and gives CAR-T cells the ability to specifically bind to cancer cells without harming healthy cells.[50] Glypican-3, alpha fetoprotein, cluster of differentiation 147 (CD147), mucin-1, epithelial cell adhesion molecule (EpCAM) and New York esophageal squamous cell carcinoma 1 (NY-ESO 1) are the most common CAR to target HCC cells.[51] *In vivo* gene therapy is a strategy in which genetic material is delivered through a vector in order to alter the genetic repertoire of target cells for therapeutic purposes. Depending on the cell type to be modified, gene therapy can be divided into two categories: somatic and germline gene therapy. In germline gene therapy, the therapeutic genes are integrated into the genome of germ cells, such as eggs and sperm. This makes the therapy heritable, and can be passed on to

future generations, which raise several ethical issues and hinders its application in many countries. In somatic gene therapy, the therapeutic genes are introduced into the somatic cells and this genetic modification cannot be passed on to descendants.

Thanks to advances in genetic engineering and biotechnology, the field of gene therapy has exploded in recent years with the approval of diverse drug products by the FDA and EMA (Table 3)[52]. The first oncolytic virus approved by the FDA and EMA as an anticancer therapy was talimogene laherparepvec (Imlygic®), which was approved in 2015 for the treatment of melanoma.[53] It is a modified herpes simplex virus type 1 (HSV-1) that has been engineered to selectively replicate in tumor cell, reducing viral pathogenicity and promoting immunogenicity through deletion of the viral genes ICP34.5 and insertion of the gene coding for human cytokine granulocyte macrophage colony-stimulating factor (GM-CSF).[54] Local release of GM-CSF promotes the recruitment of dendritic cells and macrophages into the tumor, which facilitates antigen presentation and enhances the tumor specific immune response.

Table 3– Current EMA and FDA approved gene therapy products.

Drug	Year of approval	Approving agency	Indications	Vector	Approaches
Breyanzi	2021	FDA	Refractory large B-cell lymphoma	Retroviral	*Ex vivo*
Carvykti	2022	FDA	Refractory multiple myeloma	Lentiviral	*Ex vivo*
Abcema	2021	FDA	Refractory multiple myeloma	Lentiviral	*Ex vivo*
Tecartus	2021	FDA	Refractory mantle cell lymphoma / refractory acute lymphoblastic leukaemia	Retroviral	*Ex vivo*
Zynteglo	2019/ 2022	EMA/FDA	B- thalassemia	Lentiviral	*Ex vivo*
Vaxzevria	2021	FDA/EMA	COVID-19	Adenovirus	*In vivo*
Ad26.COV 2.S	2021	FDA/EMA	COVID-19	Adenovirus	*In vivo*
mRNA-1273	2020	FDA	COVID-19	Lipid-complex mRNA	*In vivo*
Comirnaty	2020	FDA	COVID-19	Lipid-complex mRNA	*In vivo*
Zolgensma	2019	FDA	Spinal muscular atrophy	AAV	*In vivo*
Waylivra	2019	EMA	Familial chylomicronemia syndrome	Oligonucleotide	*In vivo*
Onpattro	2018	FDA	Amyloidosis	Lipid-complex siRNA	*In vivo*
Tegsedi	2018	EMA	Amyloidosis	oligonucleotide	*In vivo*
Luxturna	2018	FDA	Retinal dystrophy	AAV	*In vitro*
Yescarta	2018/ 2017	EMA/FDA	Large B-cell lymphoma	Retroviral – CD19	*Ex vivo*
Kymriah	2017	EMA/FDA	B-Cell precursor acute lymphoblastic leukemia and large B-Cell lymphoma	LentiviralCD19	*Ex vivo*
Spinraza	2016	FDA/EMA	Spinal muscular atrophy	Oligonucleotide	*In vivo*
Exondys U.S.	2016	FDA	Duchenne muscular dystrophy	Oligonucleotide	*In vivo*
Zalmoxis	2016	EMA	Restore s immune system HSCT Transplant	Retroviral-ΔLNGFR/ HSV1-TK	*Ex vivo*
Strimvelis	2016	EMA	ADA-SCID	Retroviral-ADA	*Ex vivo*

Imlygic	2015	FDA/EMA	Melanoma	HSV1-GM-CSF	*In vivo*
Kynamro	2013	FDA	Homozygous familial hypercholesterolemia	Oligonucleotide	*In vivo*
Glybera UniQure	2012	EMA	Familial lipoprotein lipase deficiency and pancreatitis attacks	rAAV1-LPL	*In vivo*
Vitravene	1998/ 1999	FDA/EMA	Cytomegalovirus retinitis	Oligonucleotide	*In vivo*

1.2.1. Treatment Modalities Used in Gene Therapy

In the context of cancer, there are three basic gene therapy strategies: gene augmentation, which consists in the introduction of a specific gene into target cells in which the endogenous gene is absent/underexpressed, or the introduction of a specific exogenous gene that expresses a therapeutic protein; gene silencing, which involves the downregulation of an overexpressed or pathogenic gene; and gene editing, which is the permanent manipulation of a gene in a patient's genome (Figure 5).

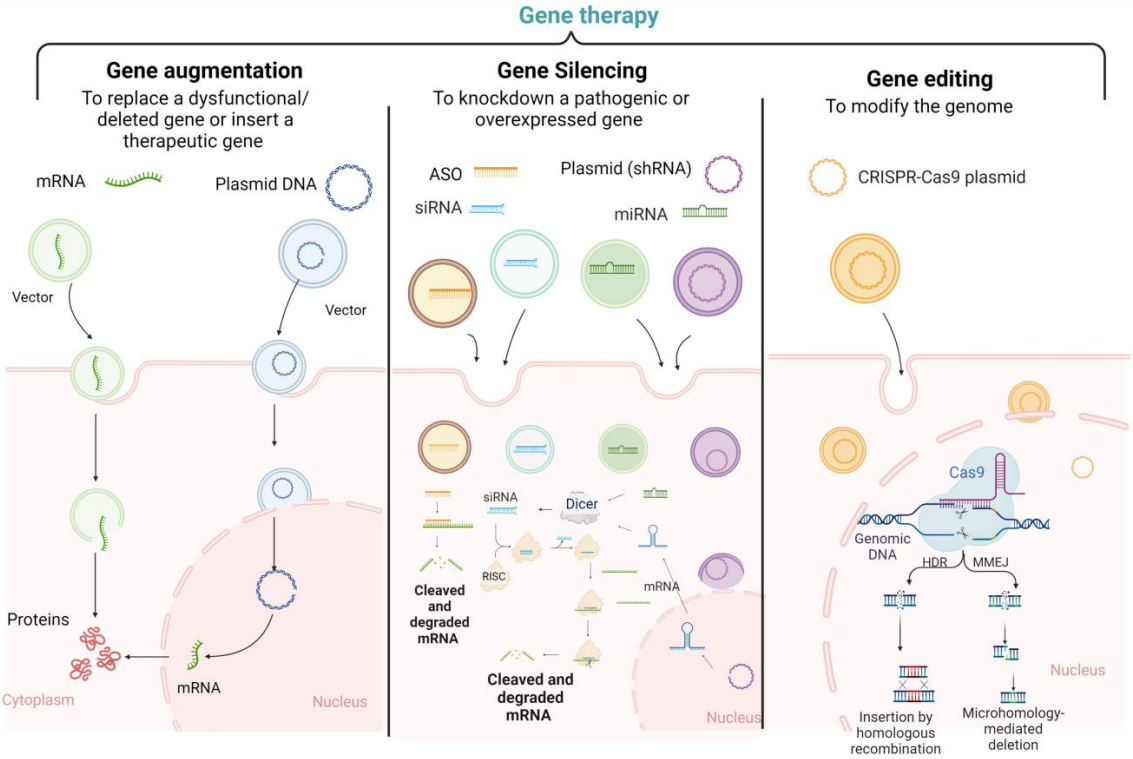

Figure 5– Treatment modalities used in gene therapy.

Gene augmentation

Gene augmentation involves the introduction of a new therapeutic gene or the insertion of a functional gene into a non-specific region of the host genome, to replace a dysfunctional or deleted gene, in order to achieve a desired therapeutic effect. Generally, this can be accomplished by the introduction of the required gene or the messenger RNA (mRNA) that encodes the desired protein (Figure 5). These nucleic acids are introduced into the target cells to express the functional or therapeutic protein through viral or non-viral vectors, a process termed transduction or transfection, respectively. The intracellular delivery of pDNA is challenging because of its large molecular size and the need to translocate it to the cell nucleus, where it is transcribed into the corresponding mRNA. Alternatively, intracellular delivery of mRNA is much easier than that of pDNA due to its smaller molecular size and to its ability to act directly in the cytoplasm, eliminating the need for the challenging nuclear delivery.[55] In addition, mRNA does not integrate into the host genome, reducing the risk of mutagenicity. Nevertheless, delivery of pDNA usually results in much higher and more sustained protein expression than that obtained with mRNA. In the context of cancer, multiple approaches can be endorsed, such as the delivery of tumor suppressor genes[56],

immune-stimulatory genes[57], apoptotic-related genes[58] or suicide genes[59]. For example, a phase I/II clinical trial currently underway to evaluated the safety, immunogenicity, and preliminary efficacy of GNOS-PV02 (personalized DNA vaccine that encodes up to 40 patient-specific neoantigens), in combination with INO-9012 (plasmid-encoded IL-12) and Pembrolizumab (ICI) in patients with advanced HCC (NCT04251117). Preliminary results, obtained with the first 12 patients, indicate that no serious adverse drug events were reported with the treatment and the objective response rate was 25% (3/12 partial response, 5/12 stable disease, 4/12 progressive disease).[60] In addition, analysis of peripheral blood and tumor tissue identified novel and significantly expanded T cell clones after vaccination, which may trigger tumor regression.

HSV-TK/GCV strategy, the most commonly used suicide gene therapy approach in clinical trials, is based on the insertion into tumor cells of a gene encoding the herpes simplex virus thymidine kinase (HSV-TK), which converts ganciclovir (GCV) into ganciclovir monophosphate, which in turn is converted by cellular kinases to ganciclovir triphosphate.[61,62] Since the latter compound is an analog of deoxyguanosine triphosphate, inhibition of DNA polymerase and/or incorporation into DNA occurs, causing chain termination and tumor cell death.[63] In addition, suicide gene therapy leads to better therapeutic outcomes because the bystander effect involves the neighboring cancer cells, thus eliminating the need to deliver the therapeutic gene to all tumor cells.[64] This effect is mainly explained by passive diffusion of the activated drug and by transfer through gap junctions and/or apoptotic bodies generated by dying cells that can be taken up by non-transfected cells.

Gene Silencing

This approach consists of silencing the expression of pathogenic or overexpressed genes responsible for supporting pathological conditions of multiple diseases, such as cancer. Increased expression of several oncogenes promotes tumor cell survival by suppressing apoptosis and regulation of cell cycle. Therefore, inhibition of oncogenes or their upstream genes represents an attractive approach for the development of novel antitumor strategies. In general, antisense oligonucleotides (ASO) or RNA interference (RNAi) techniques are the most common used for gene silencing.[65] Antisense oligonucleotides are small-sized single-stranded nucleic acids that have a complementary sequence to a target mRNA. After binding to the specific mRNA, they

inhibit mRNA translation into the corresponding protein by steric hindrance of ribosomes and induction of RNase H endonuclease activity to cleave the target mRNA. ASO can also be engineered to bind to the double-stranded DNA in the nucleus, forming a triple helix that cannot be transcribed into mRNA. RNA interference (RNAi) is a post-transcriptional mechanism of gene silencing in which small RNA molecules (such as small interfering RNA (siRNA); small hairpin RNA (shRNA); or microRNA (miRNA)) are introduced into the target cells where they interact with specific proteins in the cytosol to form the RNA-induced silencing complex (RISC) that specifically binds to the target mRNA and induces its cleavage to prevent its translation into the corresponding protein, thus resulting in gene silencing (Figure 5).

Gene editing

Gene-editing technology has the potential to cure a variety of diseases involving genetic factors, such as monogenic diseases and cancer, by directly targeting the genome and the genetic mutations.[66] This technology is based on genetically engineered DNA-cleaving enzymes, namely zinc finger nucleases (ZFNs), transcription activator-like effector nucleases (TALENs), clustered regularly interspaced short palindromic repeats (CRISPR) and the associated endonuclease Cas9 (CRISPR/Cas9), which can be reprogrammed to cleave a precise target sequence and create a double-strand break (DSB) at a specific location (Figure 5).[67] Once the target gene has been cleaved by one of these nucleases, repair of the DSB can occur by two different mechanisms: nonhomologous end joining (NHEJ) and homology-dependent repair (HDR). In the NHEJ, the target region is eliminated by joining the DSB, and it can be used to silence or correct a gene associated with the disease. On other hand, in the HDR method, a homologous sequence can be introduced into the DSB allowing exogenous DNA to be inserted either to correct an existing gene or to add a new one. For example, Yu Qi et al developed a lactose-derived biopolymer to mediate the delivery of pCas9-survivin, which targets and knocks down survivin oncogene, resulting in efficient gene editing and high anticancer activity in orthotopic HCC mouse models.[68] In contrast to gene augmentation and suppression, therapeutics based on gene editing promote a permanent effect on the genome, and have, therefore, raised important ethical issues. Nevertheless, there have been remarkable progresses in gene editing in recent years, most notably

with CRISPR/Cas9, and several clinical trials using gene-editing technologies have been completed or are underway.[69]

1.2.2. Combination of gene therapy with other therapeutic agents for treatment of HCC

Hepatocellular carcinoma cells developed complex signaling network to escape death induced by chemotherapeutics agents.[70] Therefore, the antitumor efficacy of a single-target therapeutic strategy is severely compromised. Combination therapy, a treatment modality that combines two or more therapeutic agents, is a promising approach to improve the therapeutic index by simultaneously blocking multiple signaling pathways in tumor cells.[70] Particularly, combining chemotherapy with gene and/or immunogene therapy is an effective strategy to sensitize cancer cells to drug response and achieve an additive/synergistic antitumor effect with a lower chemotherapeutic dose and consequently with fewer side effects.[71,72] This approach potentially reduces drug resistance[73,74] while providing therapeutic benefits in anticancer therapy, such as reducing tumor growth and metastatic potential, arresting mitotically active cells, reducing cancer stem cell population[75] and enhancing antitumor immune response[76,77]. For example, Zhang Linlin et al. developed N, N, N-trimethyl chitosan nanoparticles grafted with p-mercaptobenzoic acid for the co-delivery of paclitaxel (PTX), survivin shRNA-expressing plasmid and recombinant human interleukin-2.[78] This redox-responsive nanocarrier allows the controlled co-delivery release of paclitaxel in the cell cytoplasm, due to the reductive cleavage of the disulfide crosslinks in their hydrophobic core, which further improved the antitumor efficacies and decreased the systemic side effects of PTX. This triple co-delivery system exhibited synergistic in vivo antitumor efficacies and improved antitumor immune responses. C. Song et al developed a therapeutic strategy to enhance the anti-HCC effect of sorafenib, by delivering this drug together with a immunoglobulin mucin-3 (Tim-3) siRNA through chitosan-based nanoparticles.[73] Downregulation of TIM-3, an immune checkpoint molecule, not only inhibited the tumor growth in an orthotopic H22 mouse hepatoma tumor model, but also induced an immune response improving the recruitment of cytotoxic T cells to kill tumor cells. In addition, sorafenib induced extensive tumor apoptosis by inhibiting tumor angiogenesis. In another approach, the antitumor effect was enhanced by combining an anti-microtubule drug with gene therapy.[79] Paclitaxel, one of the most

commonly used chemotherapeutic agents against cancer, binds to tubulin and promotes microtubules stabilization avoiding their depolymerization, leading to G2/M cell cycle arrest and cell death. In addition, because microtubules play a crucial role in intracellular dynamics, including the transport of nanoparticles to lysosomes after their internalization by endocytosis, this drug can be used to enhance the transfection ability of nanocarriers, by helping to overcome the endolysosomal entrapment.[80] Paclitaxel-mediated enhanced gene transfection was achieved by co-administration of paclitaxel and p53 gene with a cationic-based nanoparticle. Paclitaxel-enhanced p53 gene expression resulted in an antitumor synergistic effect, with a large cell population at sub G1 and G2/M phases, which induced significant cell apoptosis.[81] Despite the additive/synergistic effects of gene therapy combination with other therapeutic agents, the development of targeted-co-delivery nanocarriers remains challenging, mainly because of the different physicochemical properties of therapeutic agents.

1.2.3. Vectors for gene therapy

Clinical outcomes of gene therapy are often limited by various technical barriers to gene delivery. The most critical challenge for successful gene therapy is the safe and effective delivery of the therapeutic nucleic acid into target cells. A delivery system is essential to protect the genetic material from enzymatic degradation and to facilitate its internalization into target cells, as hydrophilic and anionic nucleic acids do not have any property that confers them specificity to target cells and cannot effectively penetrate the cell membrane.[82] Therefore, several approaches have been developed to deliver the genetic material into target cells (Figure 6).

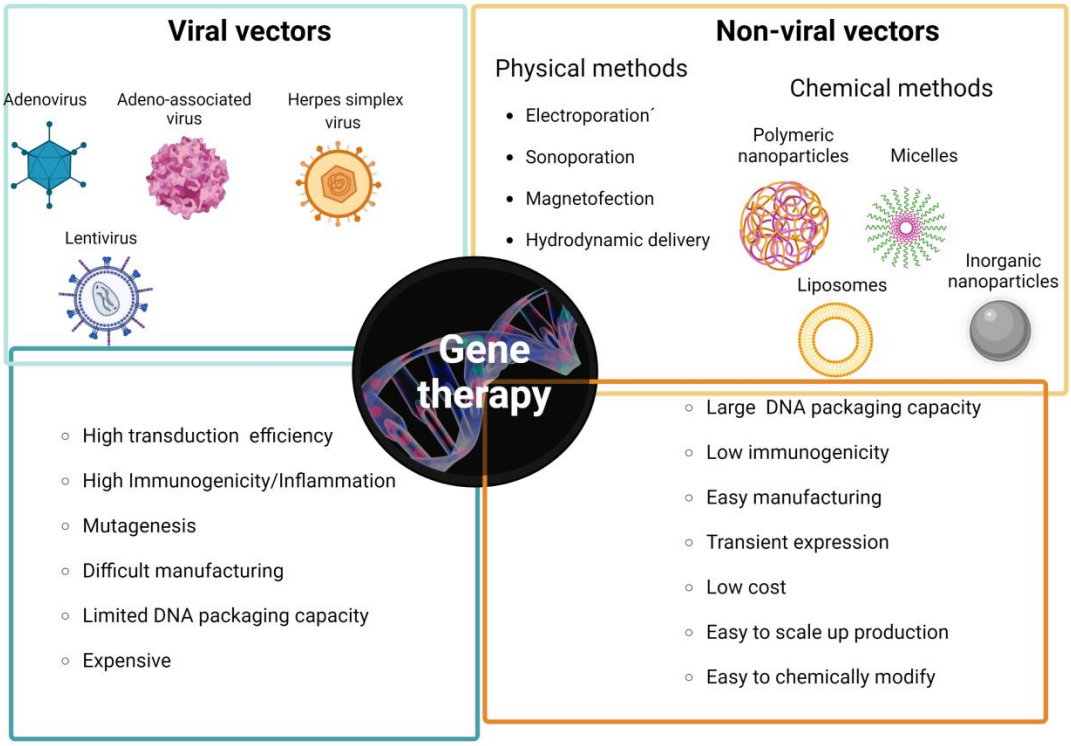

Figure 6– Vectors for delivery of a therapeutic gene into a target cell.

By far, the most popular vehicles for delivering nucleic acids into cells are viral vectors. Several viruses, in which all or parts of the viral coding regions were replaced with a therapeutic gene, have been used and engineered to develop delivery vectors. These vectors can achieve high transfection efficiency, and represent the majority of DNA delivery systems currently in clinical trials. However, viral vectors have several drawbacks, including immunogenicity, carcinogenesis, severe inflammatory responses, low target specificity, limited DNA packaging capacity and high production costs. To address some of these concerns, particularly with regards to biosafety, non-viral vectors have been extensively studied. Non-viral vectors are less toxic and far less immunogenic than their viral counterparts. Other potential advantages of non-viral vectors include the ability to carry a larger genetic payload, ease of large-scale production, capability to be repeatedly administered and the ability to be stored without refrigeration. In addition, the recent approval of two lipid-based mRNA vaccines against SARS-CoV-2 coronavirus has further sparked the interest in non-viral gene delivery systems.[83]

Viral Vectors

The most common viral vectors used in gene therapy include adenoviruses, adeno-associated viruses (AAVs), retroviruses, lentiviruses (a subtype of retrovirus) and herpes simplex virus (HSV).[84] Generally, viral vectors have a regulatory cassette, which controls stable or transient somatic expression of the transgene as an episome or a chromosomal integrant, and a protein capsid and/or envelope that condense the genetic payload and the transgene of interest, which produce a therapeutic effect. Several factors play a role in the choice of a particular vector, such as its packaging capacity, its host range, its gene expression profile or its tendency to elicit immune responses (Table 4).

Table 4– Summary of viral vectors characteristics.

	Adenovirus	**AAV**	**HSV**	**Retrovirus**	**Lentivirus**
Genome	dsDNA	ssDNA	dsDNA	ssRNA	RNA
Tropism	Dividing and non-dividing cells	Dividing and non-dividing cells	Dividing and non-dividing cells	Dividing cells	Dividing and non-dividing cells
Host genome integration	No, episomal	Both episomal and chromosomal insertion (<0.1%)	No,Episomal	Chromosomal insertion	Chromosomal insertion
Transgene expression	Transient	Potentially long -lasting	Long lasting	Long lasting	Long lasting
Packaging capacity (kb)	8	<5	>30	8	8
Limitation	High immune response	Small packaging capacity	Transient gene expression in neurons	Potential oncogenicity	Potential oncogenicity
Major advantage	Efficient transduction of most cells	Non-inflammatory and non-pathogenic	Large packaging capacity .	Long term gene expression in most cells	Long term gene expression in most cells

Actually, adenovirus has been the most commonly used vector in gene therapy clinical trials (17.5%). The main characteristics of this type of vector are: the ability to carry a large DNA load; the capacity to infect both dividing and nondividing cells; and a high but transient level of gene expression. Retroviruses can reverse transcribe their genetic

material (single-stranded RNA) into double-stranded DNA and integrate it into the genome of host cells. The main advantages of retroviral vectors, which were the first vectors used in gene therapy clinical trials, are their ability to carry a large DNA load (8 Kb) and their capacity to integrate the transgene into the host genome, resulting in long-term gene expression. However, retroviral vectors require cell division to integrate their DNA into the host genome and, therefore, they can only transduce dividing cells. In addition, retroviral vectors present the risk of randomly inserting their DNA into the host chromosomes, potentially leading to an insertional mutagenesis. Lentivirus, a subtype of retrovirus, is another important viral vector for gene therapy, commonly used in *ex vivo* applications. These vectors are capable of transducing both dividing and nondividing cells, allow long-term gene expression, and have a lower risk of genotoxicity and insertional mutagenesis when compared to retroviral vectors. The herpes simplex virus is an enveloped virus with a double-stranded DNA genome of over 150 kb. Key characteristics of HSV vectors include their ability to evade the immune system, their capacity to deliver large amounts of DNA and multiple genes, and their intrinsic or artificially generated cell-specific lytic property. While viral vectors are very efficient as gene delivery carriers, they also have some weaknesses, particularly with respect to safety issues. They can induce host immune and inflammatory responses, have the potential to form replication-competent virions, induce tumorigenic mutations, and generate active viral particles through recombination. They also pose problems related to large-scale manufacture, limitation of the size of inserted foreign transgenes and high production costs. Considerable efforts have been made to reduce pathogenicity and immunogenicity, promote site-specific integration and allow regulation of transgene expression, and this has been shown to ameliorate the safety problems.

Non-Viral Vectors

Non-viral vectors have several important advantages over viral systems, including lower immunogenicity or inflammatory response; no packaging limitation; construction flexibility; facile fabrication; low production costs; and reproducibility.[85] Non-viral vectors can be divided into two main groups: physical and chemical approaches.

Physical methods rely on the application of physical forces to temporarily destabilize the cell membrane and increase its permeability, allowing the internalization of exogenous molecules, such as DNA.[86] This destabilization can be achieved through the

use of high intensity electrical pulses (electroporation), ultrasound (sonoporation), magnetic fields (magnetofection) or a hydrodynamic force (hydrodynamic delivery). Since the application of physical-based methods is significantly limited by the observed cell damage and low levels of transgene expression, gene delivery can be achieved using chemical-based vectors, which bind and shuttle nuclei acids to target cells. Chemical vectors can generally be categorized as inorganic-, lipid-, peptide- and polymer-based systems.[87] Cationic lipids are the most widely explored alternative to viral vectors for gene delivery.[88] Cationic lipids are amphiphilic molecules consisting of a polar headgroup linked to a hydrophobic tail by a spacer (linker). The cationic headgroups bind to the negatively charged phosphate groups of the nucleic acids via electrostatic interactions and, during the self-assembly process, the genetic material wraps with the amphiphilic molecules in a multilamellar fashion. The lipid/DNA complexes formed are designated as lipoplexes. Some examples of headgroups of cationic lipids are: primary, secondary, tertiary, or quaternary amines, guanidine, imidazole, pyridinium and phosphorus groups. The hydrophobic region is generally composed of aliphatic chains (saturated or unsaturated), cholesterol, or other steroid rings. The linkers between the hydrophobic tail and the polar headgroup are usually amino, carbamate, or ester linkages, which often influence the transfection efficiency, stability and biocompatibility of the lipid.[89] The transfection efficiency of lipoplexes depends on several parameters, namely the structure of the lipids (headgroup type, number of cationic charges, linker type, type of hydrophobic tail, or overall geometric shape), ratio of cationic to neutral lipids, and the lipid/DNA charge ratio.[90]

Polymer-based nanoparticles, prepared from natural or synthetic polymers, have attracted increasing interest for gene delivery, because of their synthetic tunability and versatility, low production costs, large loading capacity, extended shelf life, and immunocompatibility.[91] In general, the positive charges of cationic polymers interact with the negative charges of nucleic acids, through electrostatic interactions, to form nanoscale polyplexes. These interactions should protect the genetic material from enzymatic degradation, while allowing efficient unpacking and subsequent release of nucleic acids inside the target cells. Some of the most commonly used cationic polymers for gene delivery are chitosan[92], poly(L-lysine), polyethylenimine (PEI), poly(β-amino ester) (PβAE)[93], and nitrogen-containing poly(methacrylate)s[94]. PEI has

been widely explored for *in vitro* and *in vivo* gene delivery and is considered the gold standard for polymer-based non-viral gene nanocarriers. The relative ease with which the physicochemical properties of polymer-based nanocarriers can be fine-tuned, by varying the chemical composition, molecular weight or architecture of the polymers, makes it possible to overcome a number of extracellular and intracellular barriers associated with the gene delivery process.[95] In addition, the integration of degradable components, targeting moieties and stimuli-responsive functional groups helps to overcome these barriers.[96,97]

Despite the attractive properties of these nanosystems, polymer-based nanocarriers are less efficient than viral vectors and can be cytotoxic. Various approaches such as the use anionic shielding polymers[98], conjugation of peptides[98] or fluorination of polymers[99] have been used to improve transfection efficiency while reducing cytotoxicity. Moreover, PEGylation of nanocarriers shields the surface charge of nanoparticles, reducing the opsonization and uptake by mononuclear phagocyte system and consequently increasing the half-life of nanoparticles, which improves extravasation at the tumor site through the enhanced permeability and retention effect (EPR). However, this strategy leads to the development of immunological responses and difficult the interactions between nanocarriers and cell membranes, reducing the cellular internalization and the endosomal escape of nanocarriers.[100] Alternatively, functionalization with carbohydrates can camouflage nanocarriers, prolong their circulation time in the bloodstream and allow their specific cellular uptake, increasing their gene delivery efficiency and specificity.

1.3. Glycopolymer-based nanoparticles for gene delivery to cancer cells

1.3.1. Carbohydrate-based nanosystems

In recent years, carbohydrate-based polymers have attracted increasing interest in the field of drug and gene delivery.[101] Recent innovations in synthetic approaches have enabled the synthesis of well-defined carbohydrate-based polymers, modification of their structure and determination of structure−activity relationships.[102] These tailored polymers can be readily prepared in various formulations, such as nanoparticles, micelles, and hydrogels, to deliver multiple therapeutic agents. Moreover, they are

derived from low-cost renewable natural resources, are composed of various repeating units (i.e., monosaccharides, oligosaccharides, and polysaccharides), and have functional groups suitable for a wide range of chemical functionalizations. Compared to other synthetic polymers, carbohydrate-based polymers have inherent tunability, chirality and unique degradability *in vivo*. The differences in the stereochemistry of the hydroxyl groups result in a specific three-dimensional configuration and spatial arrangement, which brings different biological and pharmacokinetic properties. Carbohydrate-based nanosystems display numerous desirable properties, such as reducing toxicity and immunogenicity, improving serum stability, lowering freezing point, and promoting targeted delivery of cargos. An overview of the advantages and major challenges in the application of carbohydrate-based polymers as gene delivery nanosystems is shown in Table 5.

Table 5- Advantages and challenges ahead of the carbohydrate-based nanosystems.

Advantages	Challenges
• Surface chemistry can be modulated to reduce impact in the nanoparticles toxicity, immunogenicity, and biodistribution • Increase hydrophilicity of nanocarriers • High steric stabilization against opsonisation and phagocytosis • Improved pharmacokinetics/ pharmacodynamics profile • Reduce self-aggregation tendency of the nanoparticles • Effective internalization in target cells • Site-specific delivery with reduced side-effects	• Nanoparticles stability during storage, in contact with blood and tissues • Scale up and time of production • Low transfection efficiency • Steric hindrance and charge shielding on cationic polymers • Limited *in vivo* clinical research

Depending on the role of the carbohydrate in the polymer structure, carbohydrate-based polymers can be classified into the following categories: polysaccharide derivatives, in which the carbohydrate is the main polymer composition; sugar-linked polymers, in which a sugar is used as a branching site or backbone; and glycopolymers, in which carbohydrate residues are conjugated as pendent groups.[103] Polysaccharides, because of their molecular diversity, are considered promising candidates for non-viral gene delivery that can be modified to fine-tune their physicochemical properties.[104] The naturally-occurring polysaccharides can be easily modified by chemical conjugation due to their diverse functional groups such as hydroxyl, carboxyl, and amino groups. These chemical modification methods, such as carboxymethylation, acetylation or phosphorylation, improve the biological activity of polysaccharides by changing their properties, namely their degradation profile, molecular weight and solubility.[105] For example, chitosan, one of the most studied polysaccharides as gene delivery nanocarrier, has been modified to obtain several derivatives with improved transfection efficiency.[106] Sugar linked-polymers, a less exploited type of sugar-based polymer, use a carbohydrate as a branching site or backbone. For example, Synatschke et al. used a core-first approach with functionalized sugars with multiple initiation sites for sequential polymerization of 2-(dimethylamino)ethyl methacrylate (DMAEMA) by atom transfer radical polymerization (ATRP), to obtain star-shaped polycations for gene delivery.[107] On the other hand, glycopolymers are synthetic polymers containing carbohydrate groups, generally monosaccharides and/or oligosaccharides, on their side chains. Cationic glycopolymers have attracted tremendous attention due to their unique ability to mimic naturally occurring polysaccharides, promoting the specific recognition by carbohydrate-binding proteins (lectins) and increasing the biocompatibility of gene delivery nanosystems.[108] Another approach that has also been widely explored to prepare carbohydrate-based nanoparticles is the post-functionalization of nanocarriers (organic, inorganic or hybrid) with carbohydrate derivatives.[109] In this work, however, we focus mainly on gene delivery nanosystems based on glycopolymers.

1.3.2. Synthesis of glycopolymers

In recent years, the development of novel synthesis techniques has led to major advances in the generation of glycopolymer-based gene delivery nanocarriers.[102] Linear glycopolymers, with a monosaccharide and/or oligosaccharide pendant group in a

repeating unit, are the most explored class of carbohydrate-based polymers due to the simplicity of their synthesis. In general, there are two approaches to synthesize glycopolymers: by post-functionalization of pre-synthetized polymers or by reversible deactivation radical polymerizations (RDRP) techniques (

Figure 7).

Post-functionalization of polymeric backbones with sugar unities is the most common technique for preparing synthetic glycopolymers.[110] This method provides more flexibility in terms of attaching different carbohydrate units to the pre-synthetized polymer backbone and is an efficient way to prepare functional polymers that cannot be polymerized directly from monomers due to low tolerance to functional group during polymerization. For example, glycosylation can be chemically achieved through reductive amination, click chemistry or coupling reactions for conjugation via esters or amides. In particular, click chemistry, namely copper-catalysed azide–alkyne cycloadditions (CuAAC)[111] and radical thiol-ene reaction[112], are the most commonly used organic reactions either for the synthesis of sugar-based monomers or for the subsequent modification to prepare glycopolymers.[113] Moreover, these techniques allow the precise control over the degree of chemical modification, which is critical for quantitative analysis of glycosylation of nanocarriers.[114] For example, Zhou Ye et al. developed a highly efficient nanosystem, to mediate a therapeutic strategy for HCC, based on rhodamine B (RhB) -end-labeled cationic poly[2-(dimethylamino)ethyl methacrylate] (PDMAEMA) and hydrophobic poly(3-azido-2-hydroxypropyl methacrylate) (PGMA-N3) segments post-functionalized with galactose for co-delivery of Bcl-2 siRNA and doxorubicin.[115] The RhB-PDMAEMA-*co*-PGMA copolymers were synthetized via atom transfer radical polymerization (ATRP) of DMAEMA and GMA-N3 using an RhB-based atom ATRP initiator. Then, the target glycopolymers were prepared by CuAAC click reaction of the corresponding RhB-PDMAEMA-c-PGMA-N3 with propargyl α-d-galactopyranoside.

In addition to post-polymerization modification technique, glycopolymers have also been synthesized by RDRP techniques, such as ATRP and reversible addition fragmentation chain transfer (RAFT) polymerization (

Figure 7). These methods have provided researchers with additional tools to prepare well-defined carbohydrate-based polymers with a variety of compositions,

stereochemistry, architectures and end-group functionalities. In general, glycopolymers are synthetized by polymerization of protected monomers, pre-synthesized by glycosylation of vinyl compounds, followed by the deprotection reaction of the resulting glycopolymers.[116] However, incomplete deprotection of carbohydrate residues can increase the polymer hydrophobicity, which can change the physicochemical properties of glycopolymer-based nanocarriers and reduce their biological activity.[117] Therefore, to avoid troublesome protection/deprotection procedures efforts have been made to synthesize glycopolymers without protecting-groups. RAFT is the most commonly used polymerization technique to prepare well-defined telechelic glycopolymers for gene delivery applications. RAFT is a useful and versatile approach, due to its tolerance to a wide range of functional groups, relatively mild reaction conditions and the absence of metal catalysts. RAFT polymers are synthesized via a chain transfer process that requires the use of chain transfer agents (CTAs), typically dithioesther, trithiocarbonate or xanthates compounds. RAFT also requires a radical initiator, such as azobisisobutyronitrile (AIBN), to start the polymerization. Narain and Reineke's groups have synthetized well-defined glycopolymers, with different architectures, compositions and low polydispersity, using RAFT, to develop gene delivery nanosystems. The most commonly used are methacrylamide-based copolymers, containing cationic monomers, such as 3-aminopropyl methacrylamide[118] or 2-amino ethyl methacrylamide[119,120], and carbohydrate-derived monomers, namely 3-gluconamidopropyl methacrylamide[121] and 2-lactobionamidoethyl methacrylamide.[122,123] Recently, M.R. Bockman et al. reported the synthesis of a N-acetyl-D-galactosamine (GalNAc)-derived monomer via a new improved two-step, high-yielding route and a newly CTA bearing a GalNAc end-group functionality, to prepare various diblock copolymers with N-(2-aminoethyl) methacrylamide (AEMA) via RAFT polymerization.[124]

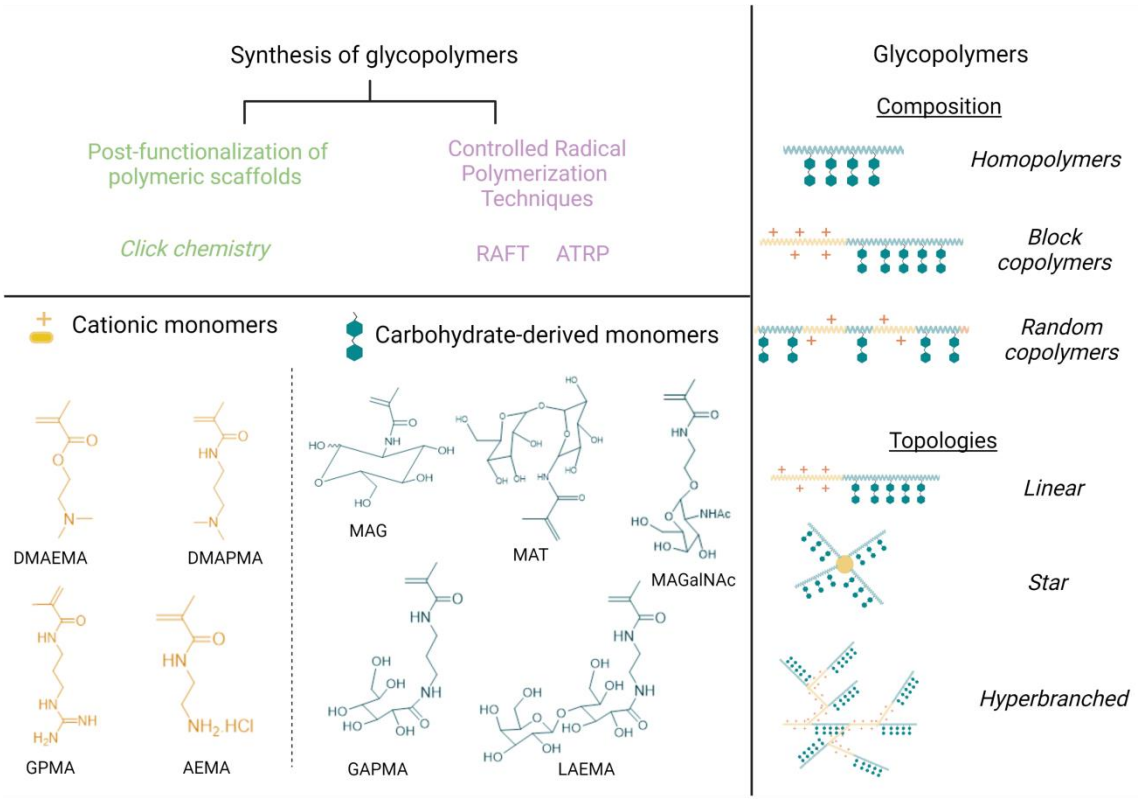

Figure 7– Carbohydrate-based monomers and cationic monomers most commonly used in glycopolymer-based gene delivery nanocarriers.

ATRP has proven to be a versatile and robust technique for the synthesis of well-defined polymers.[125] Through this technique, it is possible to prepare glycopolymers with controlled molecular weight, low molar mass dispersity (*Đ*), complex architecture, and high chain-end functionality. ATRP is mediated by a transition metal, usually copper, and an alkyl halide initiator for the polymerization of vinyl monomers containing polar group. The excellent tolerance of ATRP to functional groups allows direct polymerization of unprotected saccharide monomers. ATRP technique is based on a reversible electrontransfer reaction from a dormant specie (Pn^{-X}), usually a halogen derivative, to a transition metal salt (Mt^{m+}/L) (Scheme 1).[126] This process leads to the formation of propagating radicals (Pn*) and the metal complex in the higher oxidation state ($X\text{-}Mt^{m+1}/L$). The formed radical species can be added to one or more vinyl monomer units. Due to the reversibility of the reaction, the radicals can also react with the oxidized metal complexes, $X\text{-}Mt^{m+1}/L$, restoring the dormant species and the transition metal complex (Mt^{m}/L) in the lower oxidation state. The rapid chemical equilibrium between a very low concentration of propagating radicals and a much larger

concentration of dormant species suppresses bimolecular termination and chain transfer reactions, and promotes an effective process control allowing the preparation of polymers with a narrow molecular weight distribution. Armes and Narain reported the first example of well-defined carbohydrate-based polymers, with low polydispersity, prepared by the ring-opening reaction of 2-aminoethyl methacrylate with *D*-gluconolactone, followed by the atom transfer radical polymerization under mild conditions without recourse to protecting group chemistry.[127]

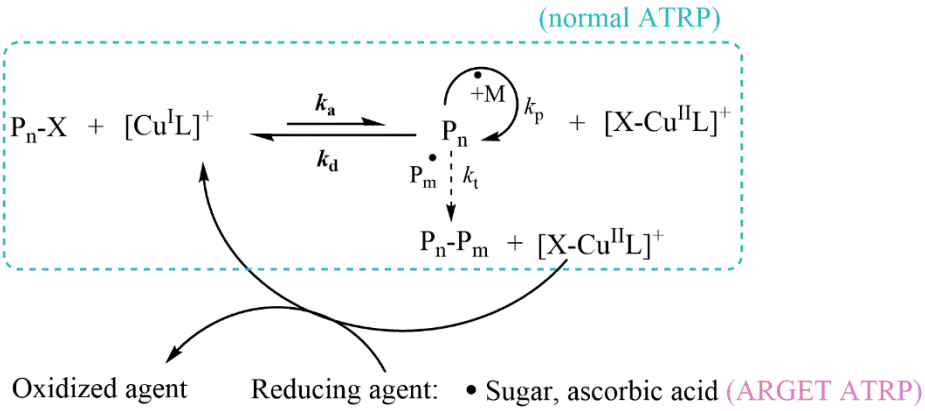

Scheme 1- The general mechanism of ATRP.

Despite the great performance of ATRP in the development of nanocarriers to gene delivery, due to its robustness, and to composition and architecture versatility of final polymers, as well as to great cost benefit when compared to RAFT, the need of a transition metal catalyst, generally copper, is a problem especially in the preparation of biomaterials[125]. The cytotoxic effect caused by the presence of the metal on the ATRP based polymers has led to improvements in ATRP technique that have produced new variants, in which the copper concentration has been lowered to the ppm range, such as supplemental activator and reducing agent (SARA) ATRP, initiators for continuous activator regeneration (ICAR) ATRP , electrochemically mediated ATRP (eATRP) and activators regenerated by electron transfer (ARGET ATRP).[128] This could be a remarkable step toward the tailored construction of well-defined copolymers for targeted gene delivery. However, to the best of our knowledge, our work is the first report of ARGET ATRP synthetized glycopolymers used for this purpose.

ARGET ATRP employs reducing agents to continuously regenerate the activator complex (Scheme 1**)**.[129] In this method ppm amounts of the oxidatively stable Cu^{II}

species are used to start the reaction, and the rate of reduction by reducing agents determines the rate of polymerization. Several biocompatible reducing agents such as ascorbic acid and glucose have been investigated. In addition, to improve tolerance to oxygen, reducing agents can be added slowly to regulate the rate of polymerization. ARGET ATRP also reduces some catalyst-induced side reactions and polymers with high chain end functionality can be prepared, allowing the synthesis of block copolymers. The synthesis of poly(2-aminoethyl methacrylate) (PAMA) and PEG-*b*-PAMA via ARGET ATRP under mild conditions was reported by our research group.[130,131] This method yielded homopolymers and block copolymers with a good control over molecular weights ($Đ < 1.2$) and with high chain-end functionality, which also showed high potential as gene delivery systems.

1.3.3. Glycopolymer as nuclei acid delivery nanocarriers

Monosaccharides-based nanosystems

Polyamine-based nanosystems, such as PEI-based polyplexes, have been shown a high ability to deliver DNA, but their transfection efficiency is associated with cytotoxicity. In contrast, carbohydrate-based nanoparticles stand out as biocompatible nanocarriers, but their clinical translation is hampered by low transfection efficiency. Therefore, cationic glycopolymers have been shown to be ideal carriers containing cationic regions to ensure DNA binding, as well as carbohydrates groups for increased biocompatibility and colloidal stability. In addition, the incorporation of carbohydrates into cationic polymers may help promote interactions with lectins involved in several extracellular and intracellular steps of the gene delivery process, thereby improving the transfection efficiency of nanocarriers.[132,108] To determine whether the biocompatibility of a PEI-like polymer can be improved upon incorporation of monosaccharides into the polymer backbone, a library of glycopolymers, designed as poly(glycoamidoamine)s (PGAAs), was prepared by Reineke group. PGAAs were synthetized by step-growth polymerization of linear monosaccharides, L-tartarate, D-glucarate, meso-galactarate and D-mannarate, with linear oligoethyleneamines containing between one and four secondary amines.[133] The number and stereochemistry of hydroxyl groups influence the cell surface binding and internalization, the mechanism of intracellular trafficking and, consequently, the biological activity. In general, the galactarate polymer with four

ethyleneamine units (G4) promoted the greatest cellular internalization of pDNA and the highest luciferase gene expression among PGAAs.[134] The performance of these nanocarriers can be explained by their stronger binding affinity with DNA, their enhanced ability to protect nucleic acids from degradation by DNases, and their stability under serum rich conditions. Another factor contributing to the efficacy of PGAAs is their ability to degrade under physiological conditions, which likely promotes gene expression, through enhanced nucleic acid unpacking and release, and contributes to their nontoxic nature.[135] The PGAA G4 has been commercialized as a glycofect transfection reagent. In addition, this class of glycopolymers was particularly relevant because the PGAA platform allowed careful tuning of their chemical structure for the analysis of structure-activity relationships.[136,133,134] To evaluate the contribution of hydroxyl groups to PGAA degradation, hydroxylated monosaccharides were replaced with analogous structures containing an alkyl chain in place of carbohydrates (oxylate, succinate, and adipate).[135] These nonhydroxylated polymers did not degrade readily under aqueous conditions at physiological temperature and were less efficient in promoting transgene expression than the degradable PGAA.[135,137] Therefore, amines and hydroxyl groups along the backbone of these polyamides play a synergistic role in promoting amide degradation. Chen-Chang Lee and colleagues also evaluated the biological effect of increasing the number of methylene units between amines and introducing branching structures.[138] In general, glycopolymers with higher amine density in the repeat unit cannot improve transfection efficiency without increasing cytotoxicity. Branched structures were found to be less toxic but have lower delivery efficiency than linear analogues of the same molecular weight, possible due to lower protonation of the amine groups. With the goal of improving the polymer system, several modifications of the PGAA structures have been explored, such as the use of ring-closed monosaccharides or guanidium-based charge centers.[139] In addition, to enhance the nanoparticles/cell interactions, different transfection methodology has been used.[140] Anderson and co-workers have further modified PGAAs by ring-opening reactions with epoxides[141] with various lengths of lipophilic alkyl side chains. The obtained modified polymer-brush materials were formulated into nanoparticles by combining them with cholesterol, $mPEG_{2000}$-DMG (1,2-dimyristoyl-sn-glycero-3-phosphoethanolamine-N-[methoxy-$(polyethyleneglycol)_{2000}$]), and siRNA using a

microfluidic techniques. These vehicles exhibited significant improved delivery efficiency for siRNA *in vivo*, demonstrating that the alkyl tails can improve the transfection performance of PGAA[141]. The lipophilic modification of the polymers facilitates the interaction between polyplexes and the cell membrane and subsequently improves transgene expression. However, these membrane-disrupting properties also increase the cytotoxicity of the polymers[142]. Although PGAA-based nanocarriers allow efficient delivery of nucleic acids, both *in vitro* and *in vivo*, these nanocarriers aggregate to about 300 nm in the presence of salt and serum.[134]

Colloidal stability under physiological conditions is a crucial parameter for gene delivery nanocarriers. The carbohydrate decoration of polyplexes confers a hydrophilic corona to nanosystems, making them less susceptible to opsonisation and providing the robust serum stability required for their systemic delivery. In an effort to prevent colloidal aggregation in the presence of serum, Smith and co-workers developed biocompatible glucose-based core-shell nanocarriers to deliver genetic material to HeLa (human cervix adenocarcinoma) and U-87 (human glioblastoma) cells.[143] Three glycopolymers, consisting of a 2-deoxy-2-methacrylamido glucopyranose block (MAG) of fixed length (n=46) and a primary amine-containing AEMA of varying length (n=21, 39, 49), were synthesized via aqueous RAFT polymerization. In general, the nanocarriers prepared with these diblock glycopolymers were found to be colloidally stable in the presence of serum, throughout the transfection period, maintaining constant the hydrodynamic diameter (~100nm). However, under serum-rich conditions these nanocarriers exhibited much lower transgene expression than the positive controls (lipofetacmine and glycofect). Another strategy to improve the colloidal stability and cryostability of nanocarriers for gene delivery is the incorporation of trehalose, an α-glucose dimer linked by 1,1-glycosidic bond.[144,145] Trehalose-based polymers have been synthetized by RAFT polymerization[144] or via a copper (I) catalyzed click reaction[111]. These structures contain a trehalose moiety to increase biocompatibility and stability against aggregation, an amide-triazole group to promote nucleic acid binding, and an oligoamine unit to facilitate DNA encapsulation and interaction with the cell surface. Srinivasachari et al. developed trehalose-based oligoethyleneamines delivery vehicles with 1−4 ethyleneamines between the trehalose groups along the backbone and demonstrated that transfection efficiency increased with increasing amine number.[146]

Kizjakina and co-workers showed that increasing amine density (5 or 6 amines per repeat unit) did not improve transfection efficiency, but end group functionalization of trehalose with carboxyl or oligoethyleneamines resulted in higher transgene expression in primary neonatal human skin fibroblasts and rat mesenchymal stem cells, in the presence of serum.[147] Another strategy to enhance the transfection efficiency was the addition of heparin, a negatively charged glycoprotein, to trehalose-based polyplexes to form ternary complexes[148]. Heparin-treated polyplexes showed improved cell surface binding, and efficient uptake and intracellular trafficking of polyplexes to the nucleus, resulting in higher transgene expression in HepG2 (HCC) and U-87 cells and primary fibroblasts. To deliver a large plasmid encoding for a Cas9 derivative (dCas-VP64), targeted to the promoter of collagen type VII, trehalose-heparin polyplexes were coformulated with dexamethasone, a corticosteroid that expands the nuclear pore complex.[149] This formulation was found to increase functional collagen expression in primary human dermal fibroblasts (HDFs) and to induce pluripotent stem cells (iPSCs) by 5- and 20-fold, respectively, compared with trehalose-based nanocarriers without the additive. In another approach, to prepare a series of diblock glycopolymers a methacrylamido trehalose monomer, 6-methacrylamido-6-deoxy trehalose (MAT) was polymerized and then chain-extended with AEMA.[144] These diblock glycopolymers ensured colloidal stability of polyplexes in the presence of serum and allowed efficient siRNA-induced luciferase knockdown in U-87 gliobastoma cells without significant cytotoxicity. Moreover, trehalose-based diblock copolymers allowed the lyophilization of siRNA polyplexes and their resuspension in a solution, without loss of biological function and without altering their size and morphology. Furthermore, the biodistribution and efficacy of gene delivery nanocarriers were studied *in vivo*, using two different injection techniques.[145] Whereas slow infusion via the tail vein led to nonspecific internalization in the liver, kidney, spleen, and lungs, rapid hydrodynamic injection of the nanocarriers promoted very specific localization of the polyplexes in the mouse liver and showed excellent transgene expression. In addition to the carbohydrates or cationic monomers used and their ratios in the copolymers, their distribution in the glycopolymer sequence plays a crucial role in the physicochemical and biological properties of gene delivery nanocarriers. In this context, a library of well-defined glycopolymers composed of 3-gluconamidopropyl methacrylamide (GAPMA) and the

primary amine 3-aminopropyl methacrylamide (APMA) or AEMA was synthetized using RAFT polymerization technique.[118] These polymers differ from each other in their composition (block or random polymers), molecular weights, and monomer ratio (carbohydrate to cationic segment). The physicochemical and biological properties of these glycopolymer-based nanocarriers depend on the polymer composition and content of carbohydrate residues. Under serum-rich conditions, nanosystems based on random glycopolymers showed lower toxicity and higher transgene expression than those prepared with the corresponding block copolymers. To evaluate the role of serum proteins in gene expression as a function of glycopolymer composition, the cellular uptake of random- and block-based polyplexes was assessed after incubation with or without FITC-BSA. In the presence of BSA, compared to random copolymer-based polyplexes, block glycopolymer-based nanocarriers were poorly internalized by cells, which may explain their lower transfection activity.[118] The lower uptake of block copolymer-based polyplexes could be due to their lower zeta potential, which is further reduced in the presence of negatively charged serum proteins. Moreover, increasing carbohydrate content in the copolymers resulted in a decrease in transfection efficiency.[118]

Mannose is a promising molecule for targeted gene delivery to dendritic cells and tumor-associated macrophages, which play a key role in tumor invasion, proliferation and metastasis. In recent years, great efforts have been made to improve the transfection performance of nanocarriers in macrophages, which are recognized as a hard-to-transfect immune cell type.[150] Different glycopolymers based on linear PEI[151] or branched PEI conjugated with mannose have been developed for gene delivery to immune cells.[152] Recently, a cationic diblock copolymer of PEG and poly {N-[N-(2-aminoethyl)-2-aminoethyl]aspartamide} (pAsp(DET)) was synthetized, by anionic ring opening polymerization, and conjugated with 2′-azidoethyl-O-α-D-mannopyranoside, via click reaction, to form polyplexes with pDNA.[153] These polyplexes exhibited low toxicity and much higher transfection activity in IC-21 macrophages than mannose-free polyplexes.

Disaccharides-based nanosystems

Lactobionic acid, known for its biocompatibility and biodegradability, has rapidly emerged as a strategic functionalization molecule in the development of liver-specific gene delivery nanocarriers.[154] This multifunctional galactosylated moiety display the ability to form an amide bond between its carboxyl group and the amine groups of monomers or functional polymers, and is widely used to formulate polymer-based nanoparticles.[154] The most commonly studied glycopolymer, as nanocarrier for gene delivery, contains the 2-lactobionamidoethyl methacrylamido (LAEMA) and AEMA, a disaccharide- and primary amine-based methacrylamide monomers, respectively. Narain group synthetized a library of stable galactose-containing glycopolymers, with block and random compositions, and different molecular weights, by RAFT, using LAEMA and AEMA as monomers.[155] The physicochemical properties of these glycopolymers had a significant impact on their toxicity and gene delivery efficiency in HepG2 cells. The nanocarriers based on diblock glycopolymers showed high colloidal stability and maintained their size (<150 nm) consistently over 24 hours in the presence of serum. These nanosystems contain most of the condensed DNA in the core and have higher carbohydrate content in the shell, avoiding interactions and, consequently, aggregation with serum proteins. In contrast, in glycopolymer-based random polyplexes complexation with DNA is random and carbohydrates and cationic segments are equally likely to be found on the surface of the polyplexes. This work showed that the incorporation of carbohydrate units into the glycopolymer greatly decreased the cytotoxicity of nanocarriers, but compromised their transfection efficiency. On the other hand, increasing the length of the cationic block promoted higher binding affinity, stable polyplex formation, and high transgene expression, but increased cytotoxicity is a critical challenge. Therefore, to increase the biocompatibility of the delivery system, an oxaborole polymer poly(N-isopropylacrylamide-*co*-5-methacrylamido-1,2-benzoxaborole), P(NIPAm-*co*-AAm-*co*-MAAmBO) was conjugated to a P(LAEMA-*co*-AEMA) glycopolymer.[156] The strong binding between oxaborole and the cis-hydroxyl groups of galactose enables rapid crosslinking of the polymer chains, which improved nucleic acid protection and increased physiological stability. Moreover, conjugation with oxaborole polymers reduced the intrinsic toxicity of glycopolymer, probably by reducing the interaction with the cell membranes, due to masking the amine residues on the surface of polyplexes. Benzoxaborole-glycopolymer polyplexes,

constituted of AEMA and 2-methacryloyloxyethyl phosphorylcholine (MPC) and 2-hydroxyethyl methacrylate (HEMA), were also prepared to improve the biocompatibility of the nanosystems.[157] The biocompatibility and low protein absorption given by MPC and HEMA, combined with the reversible responsiveness of the oxaborole motifs, resulted in a biodegradable nontoxic nanocarrier, with high transfection efficiency. To evaluate the potential of poly-[3(Dimethylamino)propyl] methacrylamido (PDMAPMA) as non-viral vector, Singhsa and co-workers prepared a series of random and block glycopolymers by aqueous RAFT.[122] These tertiary amine containing polymers were further extended with AEMA, or with N-(3-aminopropyl) morpholine methacrylamide (MPMA), a tertiary amine in heterocyclic ring and with LAEMA. In general, these glycopolymers were characterized by high polydispersity values ($M_n/M_w > 1.4$), especially the copolymers composed by all the monomers. All glycopolymers showed good complexation ability with siRNA at low weight ratios, but in the presence of serum their hydrodynamic diameters were about 300−600 nm and the zeta potential values were 2−6 mV. In general, all nanocarriers exhibited much better biocompatibility in HeLa cells, compared with lipofectamine. Regarding the transfection efficiency, polyplexes prepared with $PDMAPMA_{65}$-*b*-$PLAEMA_{15}$ glycopolymers promoted higher epidermal growth factor receptor (EGFR) downregulation. However, for the other glycopolymers knockdown of EGFR protein with control siRNA was also observed, resulting in off-target silencing. In a different approach to developed disaccharides-based glycopolymers, branched PEI was modified with lactose, via reductive amination, to generate gene delivery nanocarriers.[158] As expected, electrophoresis data showed that larger amounts of bPEI-Lac than of bPEI were required for complete DNA condensation. Despite the substantial increase of nanocarrier size due to lactose conjugation, these nanosystems exhibited lower cytotoxicity and higher levels of gene expression in HeLa cells than those obtained with bPEI.

1.3.4. Glycopolymers physicochemical properties

As indicated by structure-activity relationship studies, the performance of glycopolymers as gene delivery nanocarriers depends on the type of the charge center[159], the type of carbohydrate[138], the degree of polymerization of both cationic and

carbohydrate-based monomers[118], the distribution of monomers on the glycopolymer sequence[159], and the N/P ratio of the polyplexes[108] (Figure 8).

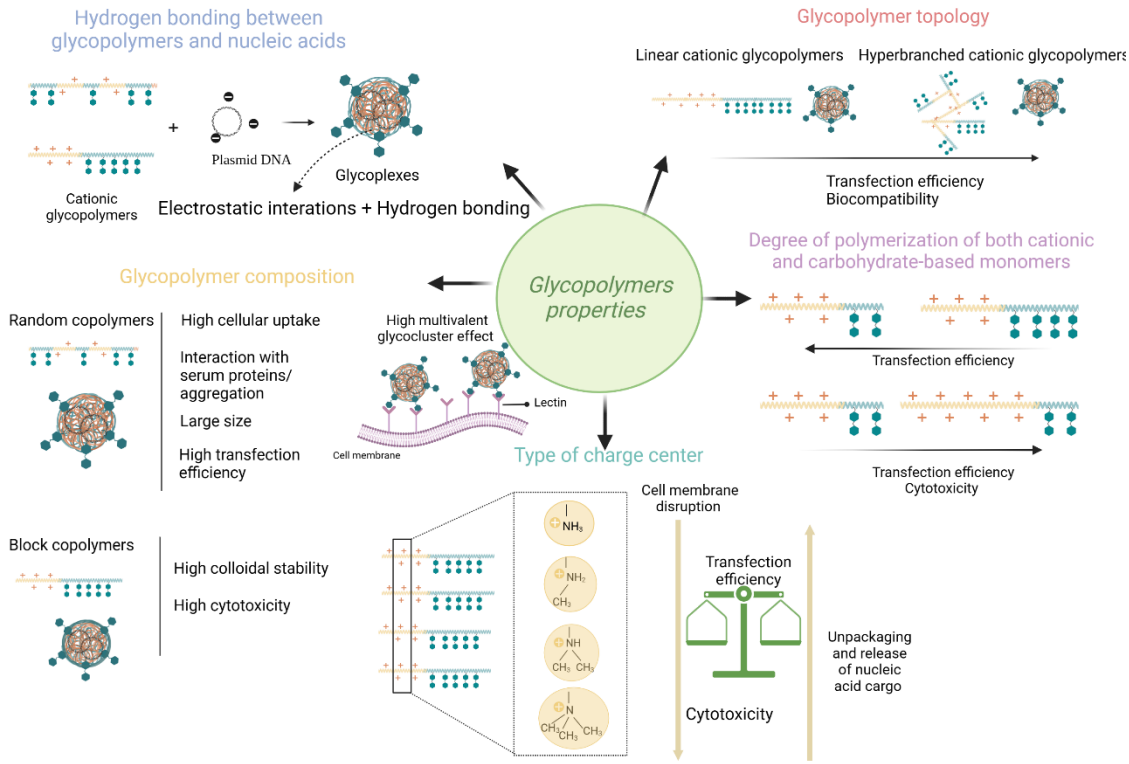

Figure 8– Effect of glycopolymer properties on gene delivery nanosystems performance.

In addition to the electrostatic interaction between the genetic material and the cationic polymers, hydrogen bonds between secondary amines and/or triazole nitrogens and the guanine/thymine nucleobases facilitate DNA condensation of polyplexes.[160,161] This combination of electrostatics and hydrogen bonds reduces the need for excess cationic charge and, ultimately lowers the cytotoxicity of the nanocarrier. Moreover, the hydroxyl groups of PGAA, through hydrogen bonding, activate the carbonyl groups of the amide bond for hydrolysis. This facilitates polymer degradation, resulting in the release of pDNA from the polyplexes and increased gene expression[135].

Cationic glycopolymers used for the formation of polyplexes have a different composition of charge centers, ranging from primary, secondary or tertiary amines. The different nature of the amines and the arrangement of these charges along the polymer backbone (random or block) alters the pKa values and the hydrophobicity profiles of the glycopolymers. These properties can affect the strength of nucleic acid binding, nanocarriers charge, the interaction with cell membranes and, consequently, the

cytotoxicity of the carrier. To evaluate the effect of the nature of the charge center on the biological properties of polyplexes, a series of diblock glycopolymers were synthetized by polymerizing MAG with methacrylate-based monomers with different levels of methyl substitution on the cationic amine moieties.[162] Cellular internalization studies revealed that all of the developed nanosystems were efficiently internalized by cells. However, with increasing amount of methyl groups on the amine (secondary < tertiary < quaternary) the transfection efficiency of the nanocarriers in HepG2 cells decreased. These results were explained by the higher binding affinity of tertiary- and quaternary-glycopolymers with pDNA, which do not allow its efficient release for gene expression. MAG was also copolymerized with a methacrylamide monomer containing primary-amine AEMA and tertiary amine moiety DMAEMA via RAFT, varying the ratio of primary to tertiary amine.[159] The effect of the tertiary amine content of glycopolymers on cell membrane integrity was evaluated by propidium iodide (PI) staining after transfection. The results showed that as the amount of tertiary amine increased, cell permeability to PI increased, which may be explained by the greater membrane disruption/destabilization effect of hydrophobic methyl groups of tertiary amines (especially when not protonated). An optimal balance between high transfection efficiency and low toxicity was achieved with polyplexes prepared with a glycopolymer composed of a higher primary amine block and a short tertiary amine block.[163]

In general, increasing the length of the cationic block increases the transfection efficiency of glycopolymer-based nanocarriers. On the other hand, increasing the carbohydrate content reduces their transfection ability. Therefore, the ratio of carbohydrate to cationic block is another critical factor for successful transfection. The glycopolymers with similar cationic content but high carbohydrate residues showed decreased gene expression.[118] The increase in sugar content resulted in a decrease in transfection efficiency due to reduced DNA binding and protection and decreased cellular uptake of genetic material. Cationic polymers with different degrees of sugar decoration (0, 9, and 33%) were synthesized by ring-opening reaction of PGMA with ethanolamine and a lactobionic acid-derived aminosaccharide (Lac-NH2) and were used to form polyplexes with EGFR siRNA.[164] The glycopolymer-based nanocarriers with the highest sugar content were found to be less effective in EGFR knockdown, which can be explained by their lower surface charge. An optimal balance between

biocompatibility and gene transfection efficiency was obtained for PGMA-based glycopolymers with a sugar decoration degree of 9%.

The number of hydroxyl groups and stereochemistry of carbohydrate components (*D*-glucarate, meso-galactarate, *D*-mannarate or *L*-tartarate) in PGAA-based nanocarriers resulted in different gene expression profiles, which was related to differences in polymer-pDNA binding affinity, DNase protective ability, polyplexes stability, and cellular internalization profiles.[165, 134] The galactaramide and tartaramide analogs exhibited higher delivery efficiency than glucaramide and mannaramide structures.[139] Narain and colleagues showed that galactose derived hyperbranched polymers (PAEMA-*co*-PLAEMA) promoted high transgene expression than the glucose-derived analog (PAEMA-*co*-GAPMA).[139] The longer carbohydrate chain of galactose derived polymers masks the charge of the cationic moiety leading to a higher LD_{50} than glucose-derived polymers. In general, hyperbranched cationic polymers resulted in high transgene expression and low toxicity, compared to their linear analogs. As mentioned above, hyperbranched glycopolymers with high galactose content showed improved transfection activity in the presence and absence of serum. Hyperbranched glycopolymers (15-38 kDa) were hemocompatible *in vitro*, and their cytotoxicity was found to depend on the type of cell line used and the polymer concentration.[166] Hyperbranched PGAA demonstrated to be less toxic than linear versions with a similar chemical structure, due to a lower density of secondary amines from the branching units. [139] However, the transfection activity of these glyco-nanocarriers was found to be less dependent on the shape of the polymers, and stereochemistry of the carbohydrates moieties dominated their biological effects.

The distribution of carbohydrate and cationic moieties along the glycopolymer sequence also play a critical role in the gene delivery performance of nanocarriers. A library of tailor made glycopolymers, with low dispersity, known molecular weight and composition, was prepared and their transfection efficiency was evaluated in HeLa and HepG2.[118,120] Different distributions of monomers on glycopolymers resulted in the formation of polyplexes with different biophysical properties. Glycoplexes prepared with random copolymers were larger than polyplexes based on block copolymers.[155] In the presence of serum, nanocarriers prepared with random glycopolymers resulted in high transgene expression and low toxicity, compared with their block analogs. This

improvement in transfection efficiency in the presence of serum was explained by the interaction between serum proteins/polyplex complexes and proteoglycans on the cell surface, which increased their cellular internalization. However, nanocarriers based on random glycopolymers showed aggregation, probably due to the exposure of amine content on the surface of these nanovectors. To reduce the aggregation of random-based polyplexes and maintain high transgene expression, random-block copolymers were synthetized.[167] Similarly, Jingjing Sun et al observed that amino-acid-based random glycopolymers exhibited higher transfection efficiency than the corresponding block glycopolymers-based nanocarriers.[116] Random and diblock copolymers composed by 2-(α-d-mannopyranosyloxy)ethyl methacrylate (ManEMA), a manose monomer derivative, and DMAEMA were synthetized by aqueous RAFT polymerization.[168] Despite their similar ability to condense DNA, random glycopolymers promoted higher transfection efficiency in HeLa cells than the corresponding diblock copolymers. In addition, the turbidimetric assay showed that random copolymers are much more efficient multivalent ligands for clustering of Concanavalin A, a lectin that specifically binds glucose and mannose, than block copolymers.

Another factor with a strong influence on transfection efficiency, stability, hemocompatibility, and biodistribution is the N/P ratio (amine to phosphate) of glycoplexes.[169] Phillips, H. R. and co-workers demonstrated that polyplexes prepared with the diblock copolymer PMAG-*b*-MAEMt at an N/P ratio of 5 did not affect coagulation, while the same nanocarriers prepared at an N/P ratio of 15 induced coagulation.

1.3.5. Interaction with target cells

The interaction of nanocarriers with target cells and their subsequent intracellular transport strongly influence their transfection efficiency. An efficient gene delivery nanosystem must result in a strong accumulation in tumor microenvironment, without affecting surrounding normal cells. Passive targeting of nanocarriers through the enhanced permeability and retention effect (EPR effect) has been widely explored in cancer therapy.[170] This effect is based on pathological angiogenesis, in which abnormal and weakly modulated vascularization results in walls with large pores that allow the extravasation of nanocarriers into the tumor. Moreover, poor lymphatic clearance of

tumors, as a consequence of rapid tumor mass development, enhances intratumor accumulation and retention of nanosystems. However, the EPR effect is only a pathway for the extravasation of nanoparticles from the bloodstream into the tumor microenvironment, and its efficacy is highly variable due to the complex and heterogeneous tumor-milieu. After accumulation in the tumor region, nanocarriers functionalized with ligands, specifically recognized by membrane receptors on the surface of cancer cells, are internalized via receptor-induced endocytosis. These approaches, termed active targeting, increase the specificity of the gene delivery systems to cancer cells, consequently improving their transfection efficiency in the target tissue and reducing the side effects usually associated with nonspecific gene delivery nanocarriers.

1.3.6. Targeting

Glycotargeting is a magic bullet approach for the delivery of genetic material by receptor-mediated endocytosis due to the interactions between cell-surface lectins and carbohydrate-based nanocarriers.[110] The C-type lectin receptors (CLRs) express single or multiple carbohydrate recognition domains and bind to different carbohydrates such as lactose, mannose, fructose, galactose, and N-acetyl-D-glucosamine. In general, tumor cells have a very high affinity toward sugar moieties such as lactose, fructose, galactose, and mannose via lectin-like receptors. The asialoglycoprotein receptor (ASGPR) has attracted enormous attention for active targeting of HCC with glycopolymer-based nanocarriers.[115,171] The ASGPR consists of two units: the major ASGPR-1 unit with a molecular weight of 48 kDa and a minor 40 kDa big subunit, ASGPR-2.[172] The role of ASGPR is to eliminate asialoglycoproteins by specifically recognizing their galactose or galactosamine residues, a process that is Ca^{2+}-dependent. This receptor is expressed predominantly on hepatocytes and only to a minor extent in nonhepatic cells.[172] The non-parenchymal cells, namely liver endothelial and Kupffer cells possess a mannose receptor. This receptor is also abundant in dendritic cells and macrophages, playing a critical role in immune response.

Glycopolymers have been widely used to prepare multivalent ligands to target lectin receptors. These high valency ligands exhibit enhanced binding activity compared with their corresponding monovalent targeting moieties, a phenomenon designed “cluster

glycoside effect".[173] For example, compared to monovalent structures, the triantennary structures have more than a thousand-fold higher affinity for the ASGPR, as measured by the half-maximum inhibitory concentration (IC_{50}).[174] However, the synthesis of these triantennary structures requires multiple reaction steps that are time and labor intensive, making imperative the development of alternative ligands. Reineke and co-workers conjugated azide-modified β-*D*-galactose units to a PGAA backbone by a copper (I)-catalyzed/azide alkyne "click" reaction and evaluated the effect of galactose substitution and carbohydrate linker length on ASGPR-mediated cell uptake in the HCC HepG2 cell line.[175] The distance between carbohydrate functionality and polymer backbone showed no correlation with targeting ability, as demonstrated by other authors.[176] Although, polymers with a high degree of carbohydrate substitution were internalized mainly by ASGPR-mediated endocytosis, non-specific endocytosis by charge mediated cell surface interactions was also observed. However, high conjugation densities were difficult to achieve due to the limitation of modification after polymerization. To overcome this limitation, a methacrylamido GalNac monomer was synthetized and copolymerized with AEMA to obtain well-defined PMAGalNAc-*b*-AEMA block copolymers.[132] These block glycopolymers formed polyplexes with pDNA that were more colloidally stable than nanocarriers formed with polycations copolymerized from a PEG block. Moreover, these glycopolymers resulted in higher transgene expression in ASGPR-rich cells (HepG2) compared to ASGPR-free cells (HeLa). The PMAGalNAc-based nanocarriers showed an exceptional strong binding affinity to ASGPR, which was two orders of magnitude higher than ASF and five orders of magnitude higher than monomeric GalNAc. Biodistribution experiments in mice revealed that PMAGalNAc-based nanovectors accumulated in the liver via interactions with ASGPRs, whereas PEI and the glucose-derived nontargeted control showed higher uptake in the lungs. The MAGalNAc was also copolymerized with the monomer 3-guanidinopropyl methacrylamide (GPMA) to obtain block glycopolymers with high membrane permeability. [177] Nanocarriers obtained with GPMA homopolymers were shown to be internalized via both energy-dependent and independent pathways, whereas polyplexes formed with block glycopolymers were internalized by endocytosis. The higher cellular internalization of guanidinium homopolymer-based polyplexes at 4°C and their higher cytotoxicity, as compared with glycoplexes, suggest that they were taken up by direct

membrane penetration. Notably, the incorporation of a hydrophilic carbohydrate block significantly reduced the toxicity and promoted higher transfection efficiency in HepG2 cells. [177] As mentioned before, the Narain group developed a series of block and random galactose-based copolymers that exhibited high gene transfection efficiency and low cytotoxicity in HepG2 and Huh7.5 cells.[155] The transfection efficiency of these nanocarriers was negligible in ASGPR deficient cells (HeLa and SK-HEP-1), whereas PEI and PAEMA-based polyplexes still exhibited high reporter gene expression in those cells. Thus, the internalization of homopolymer based polyplexes was driven by the electrostatic interaction between polyplexes and cell membrane, whereas the uptake of glycoplexes is due to the strong interactions of the galactose residues of the nanocarrier with the overexpressed ASGPR. Moreover, uptake of glycopolymer-based nanocarriers decreases significantly in the presence of free asialofetuin, confirming that these nanocarriers were recognized and internalized by ASGPR. To further strengthen the ability to target hepatocytes, dual-targeting nanocarriers have been developed.[178,179] For example, Zheng et al. synthetized a dual-targeting chitosan-based nanosystem, containing galactose of lactobionic acid and glycyrrhetinic acid, which are effective ligands of the overexpressed hepatocyte receptors, the ASGPR and glycyrrhetinic acid receptor, respectively.[180]

Macrophage-targeted gene therapy is a promising alternative approach to polarize M2-like macrophages into M1-like macrophages, which have antitumor effects. Qijing Chen et al prepared a series of nanoparticles based on a cationic lipid-like compound G0-C14 and PLGA-PEG modified with different carbohydrates, including mannose, galactose, dextran, and a mixture of mannose and galactose.[181] Incorporation of carbohydrate moieties, particularly mannose and dextran, improved active targeting to macrophages and transfection efficiency of nanocarriers.[182] Nadine Leber et al synthetized amphiphilic block copolymers bearing an α-mannosyl moiety to prepare nanohydrogel particles for specific targeting of M2-polarized macrophages, through the overexpressed mannose receptor CD206.[183] Effective ManNP-guided siRNA delivery was confirmed by sequence-specific gene knockdown of CSF-1R exclusively in M2-type macrophages, whereas the expression level in M1-polarized macrophages was not affected.

1.3.7. Intracellular trafficking of glycoplexes

After ligand-receptor interaction, the nanocarriers must be internalized by the cell to deliver the genetic material. Cellular internalization of polyplexes has been shown to occur via an energy-independent pathway, such as direct cell penetration, or via energy-dependent endocytic pathways.[91] The best characterized endocytosis routes include clathrin-mediated endocytosis, caveolin -dependent endocytosis, clathrin- and caveolin-independent pathways, macropinocytosis, and phagocytosis. Clathrin-mediated endocytosis is the main method for internalization of ASGPR-targeted nanocarriers, because recognition and binding of a ligand to the receptor triggers the membrane budding with the formation of clathrin-coated vesicles. Subsequently, these clathrin-coated endocytic vesicles lose their coating and fused with early endosomes that become late endosomes, as their pH decreases (pH 5.0-6.0). If nanocarriers fail to escape from the endocytic pathway they are likely transported via the late endosomes to lysosomes, whose acidic lumen (pH ≈ 4.5) and high digestive enzymes content facilitate the payload degradation. Therefore, effective endosomal escape of DNA into the cytoplasm is necessary for efficient gene delivery and subsequent transgene expression. Endolysosomal escape of polymer-based nanocarriers has been mainly explained by the proton sponge hypothesis or by direct membrane permeabilization. The proton sponge theory states that the amino groups of polymers, which have a broad buffering capacity in the pH range of endosomes (pH 4−7), act as potent “proton sponges” during the ATPase-driven acidification of endosomes. Buffering against this acidification results in a passive influx of chloride ions that cause osmotic swelling of the endosome leading to its rupture and subsequent release of the entrapped nanocarriers into the cytosol. Alternatively, free polymer chains present together with the polyplexes, intercalate into the endosomal membrane, leading to its destabilization and the formation of nano-holes that allow the escape of the polyplexes. PGAA polymers were used as a model system to study the cellular pathways that are associated with successful transfection.[184] Cellular internalization of PGAA-based polyplexes occurs primarily through actin- and dynamin-dependent pathways, such as caveolae- and clathrin-mediated endocytosis. The author observed that caveolae/raft-mediated endocytosis was the predominant uptake route leading to efficient nuclear delivery and transgene expression. Using confocal microscopy, Ingle et al demonstrated that filopodia, actin projections extending

from the cell surface, actively detect glycoplexes in the extracellular milieu, steer toward them, and internalize these particles into vesicles, that are then transported along actin to the main cell body to deliver the nucleic acids near to the nucleus.[185] Intracellular trafficking has been shown to involve a combination of proton-sponge-mediated endosomal release or active transport to the Golgi and the endoplasmic reticulum, which is adjacent to the outer nuclear membranes and provides transport to the nucleus and subsequent transgene expression.[186] In addition, PGAA-based nanocarriers that exhibited the highest nuclear envelope permeability also displayed the highest transfection efficiency.[187] This enhanced nuclear import of glycosylated nanocarriers may be explained by the interaction between the glycopolymers present on the particles surface and the nuclear shuttling lectins.[188]

To overcome the obstacles of cellular internalization and endosomal entrapment, Yi-Yang Peng and co-workers have prepared different galactose-based nanocarriers conjugated with arginine-rich cell-penetrating peptides.[189] Block P[LAEMA(2-lactobionamidoethyl methacrylamide)$_{37}$]-*b*-P[FPMA(4-formyl phenyl methacrylate)$_2$-*co*-DMA(N,N-dimethylacrylamide)$_2$] and two random [P(LAEMA$_{23}$-*co*-FPMA$_3$) and P(LAEMA$_{25}$-*co*-FPMA$_2$-*co*-DMA$_2$)] glycopolymers were synthetized by RAFT followed by the conjugation with an arginine-rich peptide via a Schiff base reaction. The peptide incorporation clearly enhanced the cellular internalization of polyplexes, leading to efficient siRNA delivery and, consequently, EGFR silencing in a cervical cancer cell line. The efficient escape from the endosomes was promoted by an acid degradable imine bond, which is cleaved in the acidic environment of the endosomes.

1.3.8. Stimuli-responsive glycopolymers

To enhance the successful systemic delivery of nucleic acids, polymeric materials can be designed to respond to an internal or external stimulus, such as pH, redox state, enzyme levels, light or temperature, resulting in controlled release of the loaded genetic material.[190] Delivery and release of nucleic acids into the cytoplasm (siRNA and mRNA) or nucleus (plasmid DNA) is a crucial step and a major challenge in the gene delivery process.

Thermoresponsive polymers modify their physical properties in a response to temperature changes, which makes them excellent candidate nanocarriers for drug and

gene delivery, because the temperature of the tumor microenvironment is different from that of healthy tissues. For example, thermoresponsive glycopolymers were prepared by RAFT and crosslinked with acid labile crosslinks, to obtain dual sensitivity (pH and thermosensitive) nanocarriers for efficient delivery of nuclei acid.[191] These glyconanogels showed high DNA complexation efficiency at physiological temperature, low toxicity and degradation in acidic environments. Moreover, these nanosystems allowed simultaneous encapsulation of proteins and DNA plasmid, and exhibited high transgene expression in HepG2 cells.[192]

Differences in pH in various intracellular environments, such as the cytoplasm, endosomes, lysosomes, endoplasmic reticulum, Golgi bodies, mitochondria, and nuclei, have been explored to improve gene delivery. Glycopolymers with acid-labile bonds or protonatable functionalities can be used to facilitate the endosomal release of nanocarriers by increasing the rate of hydrolysis or by changing the polymer protonation.[193] To allow endosomal pH-responsive protonation and the subsequent release of the entrapped nucleic acids into the cytosol, the pKa of cationic polymers should be low (4-7). Degradable galactose-based cationic hyperbranched polymers bearing an acid sensitive crosslinker, 2,2-dimethacroyloxypropane (DEP), were synthetized via RAFT and their ability to mediate EGFR knockdown in cervical carcinoma was evaluated.[123] The crosslinker incorporated into these glycopolymers contains a hydrolysable ketal group, which allows degradation of the polymer into smaller fragments in an acidic environment, thereby reducing cytotoxicity. Moreover, the faster release of the siRNA from the endolysosomal pathway improved transfection efficiency. Additionally, to reduce cytotoxicity by lowering the cationic charge distribution in these nanocarriers, cationic hyperbranched polymers, based on di(ethylene glycol) methyl ether methacrylate (DEGMA), were also prepared from the RAFT copolymerization of AEMA, DEGMA and DEP.[194] Due to the temperature responsiveness of DEGMA, incubation of polyplex components at a temperature below the lower critical solution temperature (LCST), can easily allow complexation of siRNA with the cationic polymer. Then, with the subsequent increase in temperature, above the LCST, more stable and compact polyplex nanoparticles can be obtained. These acid degradable cationic nanocarriers based on hyperbranched polymer resulted in 95% of EGFR silencing in HeLa cells. Oxaborole-based polymers, due to their stimuli-

responsive properties, are another class of gene delivery vectors, in which the methacrylamide benzoxaborole (MAAmBO) residues with the hydroxyl groups of the glycopolymer sugars allow reversible crosslinking of the polymer chains in response to temperature, pH, and the presence of free glucose. This reversible interaction has shown to provide effective release of the siRNA cargo inside the cancer cells displaying 60% of gene silencing.[156]

Furthermore, disulfide linkages are often incorporated into the glycopolymer chain to form highly cross-linked polyplexes that prevent dissociation under extracellular conditions and promote gene release at the target sites. In intracellular reductive environments, where the glutathione concentration is 50–1000 fold higher than in the extracellular environment, these polyplexes dissociate and facilitate the release of the genetic cargo. For example, Peng and coworkers developed an efficient, biocompatible, and redox-responsive nanocarrier for EGFR siRNA delivery in cervical carcinoma.[119] For this purpose, hyperbranched polymers were synthesized by RAFT using LAEMA, AEMA and a redox-responsive crosslinker N,N-bis(methacryloyl) cystamine (BMAC). The high intracellular concentration of glutathione triggered the reduction of the disulfide bond of the crosslinker, cleaving the glycopolymers, which promoted the rapid release of the payloads in the cytosol. These redox-responsive galactose-based nanocarriers exhibited excellent colloidal stability, high transfection efficiency and minimal toxicity in HeLa cells.

1.3.9. Gene therapy mediated by glycopolymer–based nanocarriers

Cationic glycopolymers have improved the properties and delivery capabilities of polymeric-based nanosystems for gene delivery in unprecedented ways, including colloidal stability, reduced cytotoxicity, lyoprotection and tissue-specific targeting. Despite their promising properties, there are few examples of glycopolymers as gene delivery nanocarriers for *in vivo* gene therapy approaches. Expression of microRNA-99a (miR-99a) is substantially downregulated in HCC and significantly correlated with poor prognosis of HCC patients.[195] To restore miR-99a expression, Cai et al. developed dual-targeted nanoparticles, based on the (polyethylene glycol)-poly(D,L-lactide-co-glycolide)-poly(L-lysine)-lactobionic acid (mPEG-PLGA-PLL-LA) glycopolymer, which were additionally post-functionalized with the antibody against vascular

endothelial growth factor.[179] The targeted nanoparticles showed excellent specificity for HepG2 cells and their transfection efficiency was proved by the suppression of mTOR expression, a target gene of miR-99a. Downregulation of this target gene resulted in suppression of proliferation and inhibition of the migration and invasion of HepG2 cells. Moreover, *in vivo* results showed that transfection via dual-targeted functionalized nanoparticles resulted in the inhibition of tumor xenograft growth in HCC-bearing mice without systemic toxicity. The miR-122, another critical tumor suppressor microRNA, could inhibit hepatocarcinogenesis, epithelial–mesenchymal transition, and angiogenesis by targeting a myriad of genes, namely Bcl-2, ADAM17, Wnt1 and AKT3.[196] To achieve a synergistic antitumor effect, Q. Ning and coworkers developed a galactosylated-chitosan-5-fluorouracil-based nanosystem to codeliver the anticancer drug fluorouracil (5-FU) and miR-122.[197] This glycopolymer-prodrug-based nanocarrier showed high blood and salt stability and an excellent biocompatibility in both normal liver cells (L02 cells) and endothelial cells. The combination of gene therapy and chemotherapy induced HepG2 cells apoptosis, cell cycle arrest, inhibited cell proliferation, migration and invasion and downregulated the expression of Bcl-2 and ADAM17, as well as suppressed tumor growth *in vivo*. Overexpression of p21-activated protein kinase 1 (PAK1) positively correlates with tumor progression, metastasis and poor prognosis in HCC patients. To downregulated the expression of PAK1, Zheng and coworkers modified chitosan with lactobionic acid and glycyrrhetinic acid and produced nanoparticles, that complexed a PAK1siRNA, using the ionic gelation method.[180] PAK1 silencing significantly decreased cell proliferation, invasion, and migration, and led to an obvious increase of apoptosis levels in Hep3B and HepG2 cells. In addition, the intravenous administration of nanoparticles/PAK1siRNA via tail vein in a HCC xenograft mouse model resulted in the accumulation of nanocarriers in the tumor tissue via the EPR effect, followed by dual-ligand-receptor-mediated endocytosis. The effective gene delivery mediated by the nanocarriers provided downregulation of PAK1, leading to apoptosis of HCC cells via the PAK1/MEK/ERK signalling pathway. A novel copolymer consisting of branched PEI cross-linked by myo-inositol and conjugated with a galactose-grafted PEG chain (LA-PegPI) was synthetized by Liu et al to develop HCC-targeted nanoparticles to deliver a plasmid DNA containing the IL-15 gene (pIL-15), a cytokine that is involved in the activation of

antitumor effector cells.[171] These polyplexes exhibited low cytotoxicity and high transfection efficiency in ASGPR-expressing cells (HepG2). Moreover, pIL-15 loaded nanoparticles effectively inhibited tumor growth and prolonged the survival time of tumor-bearing mice through innate and adaptive antitumor immune responses, namely by the activation of antitumor CD8+ T cells and NK cells and by the upregulation of the cytokines IFN-γ, TNF, and IL12. In a different strategy, Ganbold T. and coworkers conjugated mannose with 6-amino-6-deoxy-curdlan to develop nanoparticles that targeted primary macrophages with siRNA against tumor necrosis factor α (TNFα).[198] Competitive blocking experiments, with mannan (a natural ligand for the mannose receptor (CD206) on the surface of macrophage) showed that these glycopolymer-based nanocarriers were internalized by macrophages through receptor-mediated endocytosis. These nanosystems efficiently delivered siRNA against TNFα to lipopolysaccharide-stimulated primary mouse peritoneal macrophages *in vitro* and *in vivo* and induced significant silencing of TNFα at both the mRNA and protein levels.

1.4. Conclusion

Hepatocellular carcinoma is a global health problem due to its increasing prevalence and high mortality worldwide. Despite the great progress made in recent years in the fields of targeted molecular therapy, immunotherapy and combinatorial approaches, the goal is far from being achieved. The accumulation of knowledge regarding genetic and epigenetic factors is crucial to elucidate the biological features of hepatocarcinogenesis and to develop new therapeutic approaches to overcome this disease. Gene therapy is emerging as a promising therapeutic strategy that circumvents the limitations of pharmacological treatments, namely the chemoresistance and the potential side effects. However, the development of a scalable gene delivery nanosystem, with high transfection efficiency, low toxicity and tumor cell-specificity, is the critical step for the clinical translation of this therapeutic strategy. Glycopolymer-based nanosystems have attracted considerable attention due to their high biocompatibility, selective-delivery and colloidal stability. Particularly, the introduction of new polymerization methods has yielded well-defined glycopolymers with different compositions and architectures, which are being used to prepare novel nanosystems for gene delivery with better targeting capability to HCC cells and high transfection efficiency.

1.5.References

(1) Sung, H.; Ferlay, J.; Siegel, R. L.; Laversanne, M.; Soerjomataram, I.; Jemal, A.; Bray, F. Global Cancer Statistics 2020: GLOBOCAN Estimates of Incidence and Mortality Worldwide for 36 Cancers in 185 Countries. *CA. Cancer J. Clin.* **2021**, *71* (3), 209–249.

(2) Singal, A. G.; Lampertico, P.; Nahon, P. Epidemiology and Surveillance for Hepatocellular Carcinoma: New Trends. *J. Hepatol.* **2020**, *72* (2), 250–261.

(3) Pok, S.; Barn, V. A.; Wong, H. J.; Blackburn, A. C.; Board, P.; Farrell, G. C.; Teoh, N. C. Testosterone Regulation of Cyclin E Kinase: A Key Factor in Determining Gender Differences in Hepatocarcinogenesis. *J. Gastroenterol. Hepatol.* **2016**, *31* (6), 1210–1219.

(4) Farazi, P. A.; DePinho, R. A. Hepatocellular Carcinoma Pathogenesis: From Genes to Environment. *Nat. Rev. Cancer* **2006**, *6* (9), 674–687.

(5) Tokino, T.; Tamura, H.; Hori, N.; Matsubara, K. Chromosome Deletions Associated with Hepatitis B Virus Integration. *Virology* **1991**, *185* (2), 879–882.

(6) Braghini, M. R.; Lo Re, O.; Romito, I.; Fernandez-Barrena, M. G.; Barbaro, B.; Pomella, S.; Rota, R.; Vinciguerra, M.; Avila, M. A.; Alisi, A. Epigenetic Remodelling in Human Hepatocellular Carcinoma. *J. Exp. Clin. Cancer Res.* **2022**, *41* (1), 107.

(7) Whittaker, S.; Marais, R.; Zhu, a X. The Role of Signaling Pathways in the Development and Treatment of Hepatocellular Carcinoma. *Oncogene* **2010**, *29* (36), 4989–5005.

(8) Donne, R.; Lujambio, A. The Liver Cancer Immune Microenvironment: Therapeutic Implications for Hepatocellular Carcinoma. *Hepatology* **2022**, *n/a* (n/a).

(9) Marrero, J. A.; Kulik, L. M.; Sirlin, C. B.; Zhu, A. X.; Finn, R. S.; Abecassis, M. M.; Roberts, L. R.; Heimbach, J. K. Diagnosis, Staging, and Management of Hepatocellular Carcinoma: 2018 Practice Guidance by the American Association for the Study of Liver Diseases. *Hepatology* **2018**, *68* (2), 723–750.

(10) Reig, M.; Forner, A.; Rimola, J.; Ferrer-Fàbrega, J.; Burrel, M.; Garcia-Criado,

Á.; Kelley, R. K.; Galle, P. R.; Mazzaferro, V.; Salem, R.; et al. BCLC Strategy for Prognosis Prediction and Treatment Recommendation: The 2022 Update. *J. Hepatol.* **2022**, *76* (3), 681–693.

(11) Su, T.-H.; Hsu, S.-J.; Kao, J.-H. Paradigm Shift in the Treatment Options of Hepatocellular Carcinoma. *Liver Int.* **2022**, *42* (9), 2067–2079.

(12) Tabrizian, P.; Jibara, G.; Shrager, B.; Schwartz, M.; Roayaie, S. Recurrence of Hepatocellular Cancer After Resection: Patterns, Treatments, and Prognosis. *Ann. Surg.* **2015**, *261* (5).

(13) Bailey, C. W.; Sydnor, M. K. Current State of Tumor Ablation Therapies. *Dig. Dis. Sci.* **2019**, *64* (4), 951–958.

(14) Llovet, J. M.; De Baere, T.; Kulik, L.; Haber, P. K.; Greten, T. F.; Meyer, T.; Lencioni, R. Locoregional Therapies in the Era of Molecular and Immune Treatments for Hepatocellular Carcinoma. *Nat. Rev. Gastroenterol. Hepatol.* **2021**, *18* (5), 293–313.

(15) Raoul, J.-L.; Forner, A.; Bolondi, L.; Cheung, T. T.; Kloeckner, R.; de Baere, T. Updated Use of TACE for Hepatocellular Carcinoma Treatment: How and When to Use It Based on Clinical Evidence. *Cancer Treat. Rev.* **2019**, *72*, 28–36.

(16) Kallini, J. R.; Gabr, A.; Salem, R.; Lewandowski, R. J. Transarterial Radioembolization with Yttrium-90 for the Treatment of Hepatocellular Carcinoma. *Adv. Ther.* **2016**, *33* (5), 699–714.

(17) Yang, J. D.; Hainaut, P.; Gores, G. J.; Amadou, A.; Plymoth, A.; Roberts, L. R. A Global View of Hepatocellular Carcinoma: Trends, Risk, Prevention and Management. *Nat. Rev. Gastroenterol. Hepatol.* **2019**, *16* (10), 589–604.

(18) Hebbar, M.; Ernst, O.; Cattan, S.; Dominguez, S.; Oprea, C.; Mathurin, P.; Triboulet, J. P.; Paris, J. C.; Pruvot, F. R. Phase II Trial of Docetaxel Therapy in Patients with Advanced Hepatocellular Carcinoma. *Oncology* **2006**, *70* (2), 154–158.

(19) Cidon, E. U. Systemic Treatment of Hepatocellular Carcinoma: Past, Present and Future. *World J. Hepatol.* **2017**, *9* (18), 797–807.

(20) Huang, A.; Yang, X.-R.; Chung, W.-Y.; Dennison, A. R.; Zhou, J. Targeted Therapy for Hepatocellular Carcinoma. *Signal Transduct. Target. Ther.* **2020**, *5* (1), 146.

(21) Cervello, M.; Bachvarov, D.; Lampiasi, N.; Cusimano, A.; Azzolina, A.; McCubrey, J. a.; Montalto, G. Molecular Mechanisms of Sorafenib Action in Liver Cancer Cells. *Cell Cycle* **2012**, *11* (15), 2843–2855.

(22) Llovet, J. M.; Ricci, S.; Mazzaferro, V.; Hilgard, P.; Gane, E.; Blanc, J.-F.; de Oliveira, A. C.; Santoro, A.; Raoul, J.-L.; Forner, A.; et al. Sorafenib in Advanced Hepatocellular Carcinoma. *N. Engl. J. Med.* **2008**, *359* (4), 378–390.

(23) Zhang, H.; Zhang, W.; Jiang, L.; Chen, Y. Recent Advances in Systemic Therapy for Hepatocellular Carcinoma. *Biomark. Res.* **2022**, *10* (1), 3.

(24) Kudo, M.; Finn, R. S.; Qin, S.; Han, K.-H.; Ikeda, K.; Piscaglia, F.; Baron, A.; Park, J.-W.; Han, G.; Jassem, J.; et al. Lenvatinib versus Sorafenib in First-Line Treatment of Patients with Unresectable Hepatocellular Carcinoma: A Randomised Phase 3 Non-Inferiority Trial. *Lancet* **2018**, *391* (10126), 1163–1173.

(25) Bruix, J.; Qin, S.; Merle, P.; Granito, A.; Huang, Y.-H.; Bodoky, G.; Pracht, M.; Yokosuka, O.; Rosmorduc, O.; Breder, V.; et al. Regorafenib for Patients with Hepatocellular Carcinoma Who Progressed on Sorafenib Treatment (RESORCE): A Randomised, Double-Blind, Placebo-Controlled, Phase 3 Trial. *Lancet* **2017**, *389* (10064), 56–66.

(26) Abou-Alfa, G. K.; Meyer, T.; Cheng, A.-L.; El-Khoueiry, A. B.; Rimassa, L.; Ryoo, B.-Y.; Cicin, I.; Merle, P.; Chen, Y.; Park, J.-W.; et al. Cabozantinib in Patients with Advanced and Progressing Hepatocellular Carcinoma. *N. Engl. J. Med.* **2018**, *379* (1), 54–63.

(27) Zhu, A. X.; Kang, Y.-K.; Yen, C.-J.; Finn, R. S.; Galle, P. R.; Llovet, J. M.; Assenat, E.; Brandi, G.; Pracht, M.; Lim, H. Y.; et al. Ramucirumab after Sorafenib in Patients with Advanced Hepatocellular Carcinoma and Increased α-Fetoprotein Concentrations (REACH-2): A Randomised, Double-Blind, Placebo-Controlled, Phase 3 Trial. *Lancet Oncol.* **2019**, *20* (2), 282–296.

(28) Llovet, J. M.; Castet, F.; Heikenwalder, M.; Maini, M. K.; Mazzaferro, V.; Pinato, D. J.; Pikarsky, E.; Zhu, A. X.; Finn, R. S. Immunotherapies for Hepatocellular Carcinoma. *Nat. Rev. Clin. Oncol.* **2022**, *19* (3), 151–172.

(29) El-Khoueiry, A. B.; Sangro, B.; Yau, T.; Crocenzi, T. S.; Kudo, M.; Hsu, C.; Kim, T.-Y.; Choo, S.-P.; Trojan, J.; Welling 3rd, T. H.; et al. Nivolumab in

Patients with Advanced Hepatocellular Carcinoma (CheckMate 040): An Open-Label, Non-Comparative, Phase 1/2 Dose Escalation and Expansion Trial. *Lancet* **2017**, *389* (10088), 2492–2502.

(30) Cheng, A.-L.; Hsu, C.; Chan, S. L.; Choo, S.-P.; Kudo, M. Challenges of Combination Therapy with Immune Checkpoint Inhibitors for Hepatocellular Carcinoma. *J. Hepatol.* **2020**, *72* (2), 307–319.

(31) El-Khoueiry, A. B.; Yau, T.; Kang, Y.-K.; Kim, T.-Y.; Santoro, A.; Sangro, B.; Melero, I.; Kudo, M.; Hou, M.-M.; Matilla, A.; et al. Nivolumab (NIVO) plus Ipilimumab (IPI) Combination Therapy in Patients (Pts) with Advanced Hepatocellular Carcinoma (AHCC): Long-Term Results from CheckMate 040. *J. Clin. Oncol.* **2021**, *39* (3_suppl), 269.

(32) Abou-Alfa, G. K.; Chan, S. L.; Kudo, M.; Lau, G.; Kelley, R. K.; Furuse, J.; Sukeepaisarnjaroen, W.; Kang, Y.-K.; Dao, T. V; De Toni, E. N.; et al. Phase 3 Randomized, Open-Label, Multicenter Study of Tremelimumab (T) and Durvalumab (D) as First-Line Therapy in Patients (Pts) with Unresectable Hepatocellular Carcinoma (UHCC): HIMALAYA. *J. Clin. Oncol.* **2022**, *40* (4_suppl), 379.

(33) Faivre, S.; Rimassa, L.; Finn, R. S. Molecular Therapies for HCC: Looking Outside the Box. *J. Hepatol.* **2020**, *72* (2), 342–352.

(34) Chakraborty, E.; Sarkar, D. Emerging Therapies for Hepatocellular Carcinoma (HCC). *Cancers (Basel).* **2022**, *14* (11), 1–23.

(35) Meng, W.; Chen, T. Association between the HGF/C-MET Signaling Pathway and Tumorigenesis, Progression and Prognosis of Hepatocellular Carcinoma (Review). *Oncol Rep* **2021**, *46* (3), 191.

(36) Rimassa, L.; Assenat, E.; Peck-Radosavljevic, M.; Pracht, M.; Zagonel, V.; Mathurin, P.; Rota Caremoli, E.; Porta, C.; Daniele, B.; Bolondi, L.; et al. Tivantinib for Second-Line Treatment of MET-High, Advanced Hepatocellular Carcinoma (METIV-HCC): A Final Analysis of a Phase 3, Randomised, Placebo-Controlled Study. *Lancet Oncol.* **2018**, *19* (5), 682–693.

(37) Xiong, W.; Hietala, S. F.; Nyberg, J.; Papasouliotis, O.; Johne, A.; Berghoff, K.; Goteti, K.; Dong, J.; Girard, P.; Venkatakrishnan, K.; et al. Exposure–response Analyses for the MET Inhibitor Tepotinib Including Patients in the Pivotal

VISION Trial: Support for Dosage Recommendations. *Cancer Chemother. Pharmacol.* **2022**, *90* (1), 53–69.

(38) Qin, S.; Chan, S. L.; Sukeepaisarnjaroen, W.; Han, G.; Choo, S. P.; Sriuranpong, V.; Pan, H.; Yau, T.; Guo, Y.; Chen, M.; et al. A Phase II Study of the Efficacy and Safety of the MET Inhibitor Capmatinib (INC280) in Patients with Advanced Hepatocellular Carcinoma. *Ther. Adv. Med. Oncol.* **2019**, *11*, 1758835919889001–1758835919889001.

(39) Kelley, R. K.; Gane, E.; Assenat, E.; Siebler, J.; Galle, P. R.; Merle, P.; Hourmand, I. O.; Cleverly, A.; Zhao, Y.; Gueorguieva, I.; et al. A Phase 2 Study of Galunisertib (TGF-B1 Receptor Type I Inhibitor) and Sorafenib in Patients With Advanced Hepatocellular Carcinoma. *Clin. Transl. Gastroenterol.* **2019**, *10* (7), e00056–e00056.

(40) Wang, H.; Yang, J.; Zhang, K.; Liu, J.; Li, Y.; Su, W.; Song, N. Advances of Fibroblast Growth Factor/Receptor Signaling Pathway in Hepatocellular Carcinoma and Its Pharmacotherapeutic Targets . *Frontiers in Pharmacology* . 2021.

(41) Kim, R. D.; Sarker, D.; Meyer, T.; Yau, T.; Macarulla, T.; Park, J.-W.; Choo, S. P.; Hollebecque, A.; Sung, M. W.; Lim, H.-Y.; et al. First-in-Human Phase I Study of Fisogatinib (BLU-554) Validates Aberrant FGF19 Signaling as a Driver Event in Hepatocellular Carcinoma. *Cancer Discov.* **2019**, *9* (12), 1696–1707.

(42) Mercade, T. M.; Moreno, V.; John, B.; Morris, J. C.; Sawyer, M. B.; Yong, W. P.; Gutierrez, M.; Karasic, T. B.; Sangro, B.; Sheng-Shun, Y.; et al. A Phase I Study of H3B-6527 in Hepatocellular Carcinoma (HCC) or Intrahepatic Cholangiocarcinoma (ICC) Patients (Pts). *J. Clin. Oncol.* **2019**, *37* (15_suppl), 4095.

(43) Lin, C. P.; Liu, C. R.; Lee, C. N.; Chan, T. S.; Liu, H. E. Targeting C-Myc as a Novel Approach for Hepatocellular Carcinoma. *World J. Hepatol.* **2010**, *2* (1), 16–20.

(44) Casey, S. C.; Tong, L.; Li, Y.; Do, R.; Walz, S.; Fitzgerald, K. N.; Gouw, A. M.; Baylot, V.; Gutgemann, I.; Eilers, M.; et al. MYC Regulates the Antitumor Immune Response through CD47 and PD-L1. *Science (80-.).* **2016**, *352* (6282), 227–231.

(45) Senapedis, W.; Figueroa, E.; Gallagher, K.; Farelli, J.; Lyng, R.; O'Donnell, C.; Newman, J.; McCauley, T. Epigenetic Modulation of the MYC Oncogene as a Potential Novel Therapy for HCC. *Cancer Res.* **2022**, *82* (12_Supplement), 2629.

(46) Venter, J. C.; Adams, M. D.; Myers, E. W.; Li, P. W.; Mural, R. J.; Sutton, G. G.; Smith, H. O.; Yandell, M.; Evans, C. A.; Holt, R. A.; et al. The Sequence of the Human Genome. *Science (80-.).* **2001**, *291* (5507), 1304–1351.

(47) Blaese, R. M.; Culver, K. W.; Miller, A. D.; Carter, C. S.; Fleisher, T.; Clerici, M.; Shearer, G.; Chang, L.; Chiang, Y.; Tolstoshev, P.; et al. T Lymphocyte-Directed Gene Therapy for ADA− SCID: Initial Trial Results After 4 Years. *Science (80-.).* **1995**, *270* (5235), 475–480.

(48) Gene Therapy Clinical Trials Worldwide. The Journal of Gene Medicine. *https://a873679.fmphost.com/fmi/webd/GTCT*.

(49) Cring, M. R.; Sheffield, V. C. Gene Therapy and Gene Correction: Targets, Progress, and Challenges for Treating Human Diseases. *Gene Ther.* **2022**, *29* (1), 3–12.

(50) D'Aloia, M. M.; Zizzari, I. G.; Sacchetti, B.; Pierelli, L.; Alimandi, M. CAR-T Cells: The Long and Winding Road to Solid Tumors. *Cell Death Dis.* **2018**, *9* (3), 282.

(51) Guo, J.; Tang, Q. Recent Updates on Chimeric Antigen Receptor T Cell Therapy for Hepatocellular Carcinoma. *Cancer Gene Ther.* **2021**, *28* (10), 1075–1087.

(52) Kulkarni, J. A.; Witzigmann, D.; Thomson, S. B.; Chen, S.; Leavitt, B. R.; Cullis, P. R.; van der Meel, R. The Current Landscape of Nucleic Acid Therapeutics. *Nat. Nanotechnol.* **2021**, *16* (6), 630–643.

(53) Rehman, H.; Silk, A. W.; Kane, M. P.; Kaufman, H. L. Into the Clinic: Talimogene Laherparepvec (T-VEC), a First-in-Class Intratumoral Oncolytic Viral Therapy. *J. Immunother. Cancer* **2016**, *4* (1), 53.

(54) Liu, B. L.; Robinson, M.; Han, Z.-Q.; Branston, R. H.; English, C.; Reay, P.; McGrath, Y.; Thomas, S. K.; Thornton, M.; Bullock, P.; et al. ICP34.5 Deleted Herpes Simplex Virus with Enhanced Oncolytic, Immune Stimulating, and Anti-Tumour Properties. *Gene Ther.* **2003**, *10* (4), 292–303.

(55) Kowalski, P. S.; Rudra, A.; Miao, L.; Anderson, D. G. Delivering the Messenger: Advances in Technologies for Therapeutic MRNA Delivery. *Mol. Ther.* **2019**, *27*

(4), 710–728.

(56) Xue, W.-J.; Feng, Y.; Wang, F.; Guo, Y.-B.; Li, P.; Wang, L.; Liu, Y.-F.; Wang, Z.-W.; Yang, Y.-M.; Mao, Q.-S. Asialoglycoprotein Receptor-Magnetic Dual Targeting Nanoparticles for Delivery of RASSF1A to Hepatocellular Carcinoma. *Sci. Rep.* **2016**, *6* (1), 22149.

(57) Wang, Y.; Tiruthani, K.; Li, S.; Hu, M.; Zhong, G.; Tang, Y.; Roy, S.; Zhang, L.; Tan, J.; Liao, C.; et al. MRNA Delivery of a Bispecific Single-Domain Antibody to Polarize Tumor-Associated Macrophages and Synergize Immunotherapy against Liver Malignancies. *Adv. Mater.* **2021**, *33* (23), 2007603.

(58) Liu, C.-H.; Chern, G.-J.; Hsu, F.-F.; Huang, K.-W.; Sung, Y.-C.; Huang, H.-C.; Qiu, J. T.; Wang, S.-K.; Lin, C.-C.; Wu, C.-H.; et al. A Multifunctional Nanocarrier for Efficient TRAIL-Based Gene Therapy against Hepatocellular Carcinoma with Desmoplasia in Mice. *Hepatology* **2018**, *67* (3), 899–913.

(59) Kumar, S. U.; Wang, H.; Telichko, A. V; Natarajan, A.; Bettinger, T.; Cherkaoui, S.; Massoud, T. F.; Dahl, J. J.; Paulmurugan, R. Ultrasound Triggered Co-Delivery of Therapeutic MicroRNAs and a Triple Suicide Gene Therapy Vector by Using Biocompatible Polymer Nanoparticles for Improved Cancer Therapy in Mouse Models. *Adv. Ther.* **2021**, *4* (5), 2000197.

(60) Yarchoan, M.; Gane, E.; Marron, T.; Rochestie, S.; Cooch, N.; Peters, J.; Csiki, I.; Perales-Puchalt, A.; Sardesai, N. 453 Personalized DNA Neoantigen Vaccine (GNOS-PV02) in Combination with Plasmid IL-12 and Pembrolizumab for the Treatment of Patients with Advanced Hepatocellular Carcinoma. *J. Immunother. Cancer* **2021**, *9* (Suppl 2), A481 LP-A481.

(61) Sheikh, S.; Ernst, D.; Keating, A. Prodrugs and Prodrug-Activated Systems in Gene Therapy. *Mol. Ther.* **2021**, *29* (5), 1716–1728.

(62) Sangro, B.; Mazzolini, G.; Ruiz, M.; Ruiz, J.; Quiroga, J.; Herrero, I.; Qian, C.; Benito, A.; Larrache, J.; Olagüe, C.; et al. A Phase I Clinical Trial of Thymidine Kinase-Based Gene Therapy in Advanced Hepatocellular Carcinoma. *Cancer Gene Ther.* **2010**, *17* (12), 837–843.

(63) Vaughan, H. J.; Zamboni, C. G.; Hassan, L. F.; Radant, N. P.; Jacob, D.; Mease, R. C.; Minn, I.; Tzeng, S. Y.; Gabrielson, K. L.; Bhardwaj, P.; et al. Polymeric Nanoparticles for Dual-Targeted Theranostic Gene Delivery to Hepatocellular

Carcinoma. *Sci. Adv.* **2022**, *8* (29), eabo6406.

(64) Horikawa, M.; Koizumi, S.; Oishi, T.; Yamamoto, T.; Ikeno, M.; Ito, M.; Yamasaki, T.; Amano, S.; Sameshima, T.; Mitani, Y.; et al. Potent Bystander Effect and Tumor Tropism in Suicide Gene Therapy Using Stem Cells from Human Exfoliated Deciduous Teeth. *Cancer Gene Ther.* **2022**.

(65) Kole, R.; Krainer, A. R.; Altman, S. RNA Therapeutics: Beyond RNA Interference and Antisense Oligonucleotides. *Nat. Rev. Drug Discov.* **2012**, *11* (2), 125–140.

(66) Doudna, J. A. The Promise and Challenge of Therapeutic Genome Editing. *Nature* **2020**, *578* (7794), 229–236.

(67) Taha, E. A.; Lee, J.; Hotta, A. Delivery of CRISPR-Cas Tools for in Vivo Genome Editing Therapy: Trends and Challenges. *J. Control. Release* **2022**, *342*, 345–361.

(68) Qi, Y.; Liu, Y.; Yu, B.; Hu, Y.; Zhang, N.; Zheng, Y.; Yang, M.; Xu, F.-J. A Lactose-Derived CRISPR/Cas9 Delivery System for Efficient Genome Editing In Vivo to Treat Orthotopic Hepatocellular Carcinoma. *Adv. Sci.* **2020**, *7* (17), 2001424.

(69) Kong, H.; Ju, E.; Yi, K.; Xu, W.; Lao, Y.-H.; Cheng, D.; Zhang, Q.; Tao, Y.; Li, M.; Ding, J. Advanced Nanotheranostics of CRISPR/Cas for Viral Hepatitis and Hepatocellular Carcinoma. *Adv. Sci.* **2021**, *8* (24), 2102051.

(70) Mokhtari, R. B.; Homayouni, T. S.; Baluch, N.; Morgatskaya, E.; Kumar, S.; Das, B.; Yeger, H. Combination Therapy in Combating Cancer. *Oncotarget; Vol 8, No 23* **2017**.

(71) Qin, S.-Y.; Cheng, Y.-J.; Lei, Q.; Zhang, A.-Q.; Zhang, X.-Z. Combinational Strategy for High-Performance Cancer Chemotherapy. *Biomaterials* **2018**, *171*, 178–197.

(72) Lohitesh, K.; Chowdhury, R.; Mukherjee, S. Resistance a Major Hindrance to Chemotherapy in Hepatocellular Carcinoma: An Insight. *Cancer Cell Int.* **2018**, *18* (1), 44.

(73) Song, C.; Zhang, J.; Wen, R.; Li, Q.; Zhou, J.; Xiaoli liu; Wu, Z.; Lv, Y.; Wu, R. Improved Anti-Hepatocellular Carcinoma Effect by Enhanced Co-Delivery of Tim-3 SiRNA and Sorafenib via Multiple PH Triggered Drug-Eluting

Nanoparticles. *Mater. Today Bio* **2022**, *16*, 100350.

(74) Krstic, J.; Reinisch, I.; Schindlmaier, K.; Galhuber, M.; Riahi, Z.; Berger, N.; Kupper, N.; Moyschewitz, E.; Auer, M.; Michenthaler, H.; et al. Fasting Improves Therapeutic Response in Hepatocellular Carcinoma through P53-Dependent Metabolic Synergism. *Sci. Adv.* **2022**, *8* (3), eabh2635.

(75) Wu, C. X.; Wang, X. Q.; Chok, S. H.; Man, K.; Tsang, S. H. Y.; Chan, A. C. Y.; Ma, K. W.; Xia, W.; Cheung, T. T. Blocking CDK1/PDK1/β-Catenin Signaling by CDK1 Inhibitor RO3306 Increased the Efficacy of Sorafenib Treatment by Targeting Cancer Stem Cells in a Preclinical Model of Hepatocellular Carcinoma. *Theranostics* **2018**, *8* (14), 3737–3750.

(76) Xiao, Y.; Chen, J.; Zhou, H.; Zeng, X.; Ruan, Z.; Pu, Z.; Jiang, X.; Matsui, A.; Zhu, L.; Amoozgar, Z.; et al. Combining P53 MRNA Nanotherapy with Immune Checkpoint Blockade Reprograms the Immune Microenvironment for Effective Cancer Therapy. *Nat. Commun.* **2022**, *13* (1), 758.

(77) Rawal, S.; Patel, M. M. Threatening Cancer with Nanoparticle Aided Combination Oncotherapy. *J. Control. Release* **2019**, *301*, 76–109.

(78) Zhang, L.; Li, Q.; Chen, J.; Tang, C.; Yin, C. Enhanced Antitumor Efficacy of Glutathione-Responsive Chitosan Based Nanoparticles through Co-Delivery of Chemotherapeutics, Genes, and Immune Agents. *Carbohydr. Polym.* **2021**, *270*, 118384.

(79) Wang, Y.; Gao, S.; Ye, W.-H.; Yoon, H. S.; Yang, Y.-Y. Co-Delivery of Drugs and DNA from Cationic Core–shell Nanoparticles Self-Assembled from a Biodegradable Copolymer. *Nat. Mater.* **2006**, *5* (10), 791–796.

(80) Wang, Y.; Gao, S.; Ye, W.-H.; Yoon, H. S.; Yang, Y.-Y. Co-Delivery of Drugs and DNA from Cationic Core-Shell Nanoparticles Self-Assembled from a Biodegradable Copolymer. *Nat. Mater.* **2006**, *5* (October), 791–796.

(81) Zhao, F.; Yin, H.; Li, J. Supramolecular Self-Assembly Forming a Multifunctional Synergistic System for Targeted Co-Delivery of Gene and Drug. *Biomaterials* **2014**, *35* (3), 1050–1062.

(82) Singh, V.; Khan, N.; Jayandharan, G. R. Vector Engineering, Strategies and Targets in Cancer Gene Therapy. *Cancer Gene Ther.* **2022**, *29* (5), 402–417.

(83) Milane, L.; Amiji, M. Clinical Approval of Nanotechnology-Based SARS-CoV-2

MRNA Vaccines: Impact on Translational Nanomedicine. *Drug Deliv. Transl. Res.* **2021**, *11* (4), 1309–1315.

(84) Bulcha, J. T.; Wang, Y.; Ma, H.; Tai, P. W. L.; Gao, G. Viral Vector Platforms within the Gene Therapy Landscape. *Signal Transduct. Target. Ther.* **2021**, *6* (1).

(85) Sharma, D.; Arora, S.; Singh, J.; Layek, B. A Review of the Tortuous Path of Nonviral Gene Delivery and Recent Progress. *Int. J. Biol. Macromol.* **2021**, *183* (June), 2055–2073.

(86) Alsaggar, M.; Liu, D. Chapter One - Physical Methods for Gene Transfer. In *Nonviral Vectors for Gene Therapy*; Huang, L., Liu, D., Wagner, E. B. T.-A. in G., Eds.; Academic Press, 2015; Vol. 89, pp 1–24.

(87) Lostalé-Seijo, I.; Montenegro, J. Synthetic Materials at the Forefront of Gene Delivery. *Nat. Rev. Chem.* **2018**, *2* (10), 258–277.

(88) Buck, J.; Grossen, P.; Cullis, P. R.; Huwyler, J.; Witzigmann, D. Lipid-Based DNA Therapeutics: Hallmarks of Non-Viral Gene Delivery. *ACS Nano* **2019**, *13* (4), 3754–3782.

(89) Zhi, D.; Bai, Y.; Yang, J.; Cui, S.; Zhao, Y.; Chen, H.; Zhang, S. A Review on Cationic Lipids with Different Linkers for Gene Delivery. *Adv. Colloid Interface Sci.* **2018**, *253*, 117–140.

(90) Ponti, F.; Campolungo, M.; Melchiori, C.; Bono, N.; Candiani, G. Cationic Lipids for Gene Delivery: Many Players, One Goal. *Chem. Phys. Lipids* **2021**, *235*, 105032.

(91) Kumar, R.; Santa Chalarca, C. F.; Bockman, M. R.; Bruggen, C. Van; Grimme, C. J.; Dalal, R. J.; Hanson, M. G.; Hexum, J. K.; Reineke, T. M. Polymeric Delivery of Therapeutic Nucleic Acids. *Chem. Rev.* **2021**, *121* (18), 11527–11652.

(92) Sargazi, S.; Siddiqui, B.; Qindeel, M.; Rahdar, A.; Bilal, M.; Behzadmehr, R.; Mirinejad, S.; Pandey, S. Chitosan Nanocarriers for MicroRNA Delivery and Detection: A Preliminary Review with Emphasis on Cancer. *Carbohydr. Polym.* **2022**, *290*, 119489.

(93) Cordeiro, R. A.; Serra, A.; Coelho, J. F. J.; Faneca, H. Poly(β-Amino Ester)-Based Gene Delivery Systems: From Discovery to Therapeutic Applications. *J. Control. Release* **2019**, *310*, 155–187.

(94) Santo, D.; Cordeiro, R. A.; Sousa, A.; Serra, A.; Coelho, J. F. J.; Faneca, H. Combination of Poly[(2-Dimethylamino)Ethyl Methacrylate] and Poly(β-Amino Ester) Results in a Strong and Synergistic Transfection Activity. *Biomacromolecules* **2017**, *18* (10), 3331–3342.

(95) Piotrowski-Daspit, A. S.; Kauffman, A. C.; Bracaglia, L. G.; Saltzman, W. M. Polymeric Vehicles for Nucleic Acid Delivery. *Adv. Drug Deliv. Rev.* **2020**, *156*, 119–132.

(96) Krhač Levačić, A.; Berger, S.; Müller, J.; Wegner, A.; Lächelt, U.; Dohmen, C.; Rudolph, C.; Wagner, E. Dynamic MRNA Polyplexes Benefit from Bioreducible Cleavage Sites for in Vitro and in Vivo Transfer. *J. Control. Release* **2021**, *339*, 27–40.

(97) Ye, L.; Liu, H.; Fei, X.; Ma, D.; He, X.; Tang, Q.; Zhao, X.; Zou, H.; Chen, X.; Kong, X.; et al. Enhanced Endosomal Escape of Dendrigraft Poly-L-Lysine Polymers for the Efficient Gene Therapy of Breast Cancer. *Nano Res.* **2022**, *15* (2), 1135–1144.

(98) Richter, F.; Leer, K.; Martin, L.; Mapfumo, P.; Solomun, J. I.; Kuchenbrod, M. T.; Hoeppener, S.; Brendel, J. C.; Traeger, A. The Impact of Anionic Polymers on Gene Delivery: How Composition and Assembly Help Evading the Toxicity-Efficiency Dilemma. *J. Nanobiotechnology* **2021**, *19* (1), 292.

(99) Lou, B.; De Koker, S.; Lau, C. Y. J.; Hennink, W. E.; Mastrobattista, E. MRNA Polyplexes with Post-Conjugated GALA Peptides Efficiently Target, Transfect, and Activate Antigen Presenting Cells. *Bioconjug. Chem.* **2019**, *30* (2), 461–475.

(100) Zalba, S.; ten Hagen, T. L. M.; Burgui, C.; Garrido, M. J. Stealth Nanoparticles in Oncology: Facing the PEG Dilemma. *J. Control. Release* **2022**, *351*, 22–36.

(101) Wang, J.; Wang, D.; Zhang, Y.; Dong, J. Synthesis and Biopharmaceutical Applications of Sugar-Based Polymers: New Advances and Future Prospects. *ACS Biomater. Sci. Eng.* **2021**, *7* (3), 963–982.

(102) Pramudya, I.; Chung, H. Recent Progress of Glycopolymer Synthesis for Biomedical Applications. *Biomater. Sci.* **2019**, *7* (12), 4848–4872.

(103) Zhang, Y.; Chan, J. W.; Moretti, A.; Uhrich, K. E. Designing Polymers with Sugar-Based Advantages for Bioactive Delivery Applications. *J. Control. Release* **2015**, *219*, 355–368.

(104) Hong, S. J.; Ahn, M. H.; Sangshetti, J.; Choung, P. H.; Arote, R. B. Sugar-Based Gene Delivery Systems: Current Knowledge and New Perspectives. *Carbohydr. Polym.* **2018**, *181* (September 2017), 1180–1193.

(105) Xie, L.; Shen, M.; Hong, Y.; Ye, H.; Huang, L.; Xie, J. Chemical Modifications of Polysaccharides and Their Anti-Tumor Activities. *Carbohydr. Polym.* **2020**, *229* (September 2019), 115436.

(106) Chuan, D.; Jin, T.; Fan, R.; Zhou, L.; Guo, G. Chitosan for Gene Delivery: Methods for Improvement and Applications. *Adv. Colloid Interface Sci.* **2019**, *268*, 25–38.

(107) Synatschke, C. V.; Schallon, A.; Jérôme, V.; Freitag, R.; Müller, A. H. E. Influence of Polymer Architecture and Molecular Weight of Poly(2-(Dimethylamino)Ethyl Methacrylate) Polycations on Transfection Efficiency and Cell Viability in Gene Delivery. *Biomacromolecules* **2011**, *12* (12), 4247–4255.

(108) Van Bruggen, C.; Hexum, J. K.; Tan, Z.; Dalal, R. J.; Reineke, T. M. Nonviral Gene Delivery with Cationic Glycopolymers. *Acc. Chem. Res.* **2019**, *52* (5), 1347–1358.

(109) Das, R.; Mukhopadhyay, B. A Brief Insight to the Role of Glyconanotechnology in Modern Day Diagnostics and Therapeutics. *Carbohydr. Res.* **2021**, *507*, 108394.

(110) Gadekar, A.; Bhowmick, S.; Pandit, A. A Glycotherapeutic Approach to Functionalize Biomaterials-Based Systems. *Adv. Funct. Mater.* **2020**, *30* (44).

(111) Srinivasachari, S.; Liu, Y.; Prevette, L. E.; Reineke, T. M. Effects of Trehalose Click Polymer Length on PDNA Complex Stability and Delivery Efficacy. *Biomaterials* **2007**, *28* (18), 2885–2898.

(112) Lau, U. Y.; Pelegri-O'Day, E. M.; Maynard, H. D. Synthesis and Biological Evaluation of a Degradable Trehalose Glycopolymer Prepared by RAFT Polymerization. *Macromol. Rapid Commun.* **2018**, *39* (5), 1700652.

(113) Slavin, S.; Burns, J.; Haddleton, D. M.; Becer, C. R. Synthesis of Glycopolymers via Click Reactions. *Eur. Polym. J.* **2011**, *47* (4), 435–446.

(114) Williams, E. G. L.; Hutt, O. E.; Hinton, T. M.; Larnaudie, S. C.; Le, T.; MacDonald, J. M.; Gunatillake, P.; Thang, S. H.; Duggan, P. J. Glycosylated Reversible Addition–Fragmentation Chain Transfer Polymers with Varying

Polyethylene Glycol Linkers Produce Different Short Interfering RNA Uptake, Gene Silencing, and Toxicity Profiles. *Biomacromolecules* **2017**, *18* (12), 4099–4112.

(115) Ye, Z.; Wu, W. R.; Qin, Y. F.; Hu, J.; Liu, C.; Seeberger, P. H.; Yin, J. An Integrated Therapeutic Delivery System for Enhanced Treatment of Hepatocellular Carcinoma. *Adv. Funct. Mater.* **2018**, *28* (18).

(116) Sun, J.; Sheng, R.; Luo, T.; Wang, Z.; Li, H.; Cao, A. Synthesis of Diblock/Statistical Cationic Glycopolymers with Pendant Galactose and Lysine Moieties: Gene Delivery Application and Intracellular Behaviors. *J. Mater. Chem. B* **2016**, *4* (27), 4696–4706.

(117) Zhao, Y.; Zhang, Y.; Wang, C.; Chen, G.; Jiang, M. Role of Protecting Groups in Synthesis and Self-Assembly of Glycopolymers. *Biomacromolecules* **2017**, *18* (2), 568–575.

(118) Ahmed, M.; Narain, R. The Effect of Polymer Architecture, Composition, and Molecular Weight on the Properties of Glycopolymer-Based Non-Viral Gene Delivery Systems. *Biomaterials* **2011**, *32* (22), 5279–5290.

(119) Peng, Y. Y.; Diaz-Dussan, D.; Kumar, P.; Narain, R. Tumor Microenvironment-Regulated Redox Responsive Cationic Galactose-Based Hyperbranched Polymers for SiRNA Delivery. *Bioconjug. Chem.* **2019**, *30* (2), 405–412.

(120) Quan, S.; Kumar, P.; Narain, R. Cationic Galactose-Conjugated Copolymers for Epidermal Growth Factor (EGFR) Knockdown in Cervical Adenocarcinoma. *ACS Biomater. Sci. Eng.* **2016**, *2* (5), 853–859.

(121) Ahmed, M.; Deng, Z.; Liu, S.; Lafrenie, R.; Kumar, A.; Narain, R. Cationic Glyconanoparticles: Their Complexation with DNA, Cellular Uptake, and Transfection Efficiencies. *Bioconjug. Chem.* **2009**, *20* (11), 2169–2176.

(122) Singhsa, P.; Diaz-Dussan, D.; Manuspiya, H.; Narain, R. Well-Defined Cationic N-[3-(Dimethylamino)Propyl]Methacrylamide Hydrochloride-Based (Co)Polymers for SiRNA Delivery. *Biomacromolecules* **2018**, *19* (1), 209–221.

(123) Peng, Y. Y.; Diaz-Dussan, D.; Kumar, P.; Narain, R. Acid Degradable Cationic Galactose-Based Hyperbranched Polymers as Nanotherapeutic Vehicles for Epidermal Growth Factor Receptor (EGFR) Knockdown in Cervical Carcinoma. *Biomacromolecules* **2018**, *19* (10), 4052–4058.

(124) Bockman, M. R.; Dalal, R. J.; Kumar, R.; Reineke, T. M. Facile Synthesis of GalNAc Monomers and Block Polycations for Hepatocyte Gene Delivery. *Polym. Chem.* **2021**, *12* (28), 4063–4071.

(125) Gonçalves, S. de Á.; Vieira, R. P. Current Status of ATRP-Based Materials for Gene Therapy. *React. Funct. Polym.* **2020**, *147*, 104453.

(126) Baker, S. L.; Kaupbayeva, B.; Lathwal, S.; Das, S. R.; Russell, A. J.; Matyjaszewski, K. Atom Transfer Radical Polymerization for Biorelated Hybrid Materials. *Biomacromolecules* **2019**, *20* (12), 4272–4298.

(127) Narain, R.; Armes, S. P. Synthesis of Low Polydispersity, Controlled-Structure Sugar Methacrylate Polymers under Mild Conditions without Protecting Group Chemistry. *Chem. Commun.* **2002**, *2* (23), 2776–2777.

(128) Pan, X.; Fantin, M.; Yuan, F.; Matyjaszewski, K. Externally Controlled Atom Transfer Radical Polymerization. *Chem. Soc. Rev.* **2018**, *47* (14), 5457–5490.

(129) Jakubowski, W.; Matyjaszewski, K. Activators Regenerated by Electron Transfer for Atom-Transfer Radical Polymerization of (Meth)Acrylates and Related Block Copolymers. *Angew. Chemie Int. Ed.* **2006**, *45* (27), 4482–4486.

(130) Mendonça, P. V.; Averick, S. E.; Konkolewicz, D.; Serra, A. C.; Popov, A. V.; Guliashvili, T.; Matyjaszewski, K.; Coelho, J. F. J. Straightforward ARGET ATRP for the Synthesis of Primary Amine Polymethacrylate with Improved Chain-End Functionality under Mild Reaction Conditions. *Macromolecules* **2014**, *47* (14), 4615–4621.

(131) Santo, D.; Mendonça, P. V; Lima, M. S.; Cordeiro, R. A.; Cabanas, L.; Serra, A.; Coelho, J. F. J.; Faneca, H. Poly(Ethylene Glycol)-Block-Poly(2-Aminoethyl Methacrylate Hydrochloride)-Based Polyplexes as Serum-Tolerant Nanosystems for Enhanced Gene Delivery. *Mol. Pharm.* **2019**, *16* (5), 2129–2141.

(132) Dhande, Y. K.; Wagh, B. S.; Hall, B. C.; Sprouse, D.; Hackett, P. B.; Reineke, T. M. N-Acetylgalactosamine Block-Co-Polycations Form Stable Polyplexes with Plasmids and Promote Liver-Targeted Delivery. *Biomacromolecules* **2016**, *17* (3), 830–840.

(133) Liu, Y.; Wenning, L.; Lynch, M.; Reineke, T. M. New Poly(D-Glucaramidoamine)s Induce DNA Nanoparticle Formation and Efficient Gene Delivery into Mammalian Cells. *J. Am. Chem. Soc.* **2004**, *126* (24), 7422–7423.

(134) Liu, Y.; Reineke, T. M. Poly(Glycoamidoamine)s for Gene Delivery: Stability of Polyplexes and Efficacy with Cardiomyoblast Cells. *Bioconjug. Chem.* **2006**, *17* (1), 101–108.

(135) Liu, Y.; Reineke, T. M. Degradation of Poly(Glycoamidoamine) DNA Delivery Vehicles: Polyamide Hydrolysis at Physiological Conditions Promotes DNA Release. *Biomacromolecules* **2010**, *11* (2), 316–325.

(136) Liu, Y.; Reineke, T. M. Hydroxyl Stereochemistry and Amine Number within Poly(Glycoamidoamine)s Affect Intracellular DNA Delivery. *J. Am. Chem. Soc.* **2005**, *127* (9), 3004–3015.

(137) Prevette, L. E.; Lynch, M. L.; Reineke, T. M. Amide Spacing Influences PDNA Binding of Poly(Amidoamine)S. *Biomacromolecules* **2010**, *11* (2), 326–332.

(138) Lee, C. C.; Liu, Y.; Reineke, T. M. General Structure-Activity Relationship for Poly(Glycoamidoamine)s: The Effect of Amine Density on Cytotoxicity and DNA Delivery Efficiency. *Bioconjug. Chem.* **2008**, *19* (2), 428–440.

(139) Taori, V. P.; Lu, H.; Reineke, T. M. Structure-Activity Examination of Poly(Glycoamidoguanidine)s: Glycopolycations Containing Guanidine Units for Nucleic Acid Delivery. *Biomacromolecules* **2011**, *12* (6), 2055–2063.

(140) Agrawal, P.; Ingle, N. P.; Boyle, W. S.; Ward, E.; Tolar, J.; Dorfman, K. D.; Reineke, T. M. Fast, Efficient, and Gentle Transfection of Human Adherent Cells in Suspension. *ACS Appl. Mater. Interfaces* **2016**, *8* (14), 8870–8874.

(141) Dong, Y.; Dorkin, J. R.; Wang, W.; Chang, P. H.; Webber, M. J.; Tang, B. C.; Yang, J.; Abutbul-Ionita, I.; Danino, D.; Derosa, F.; et al. Poly(Glycoamidoamine) Brushes Formulated Nanomaterials for Systemic SiRNA and MRNA Delivery in Vivo. *Nano Lett.* **2016**, *16* (2), 842–848.

(142) Wu, Y.; Smith, A. E.; Reineke, T. M. Lipophilic Polycation Vehicles Display High Plasmid DNA Delivery to Multiple Cell Types. *Bioconjug. Chem.* **2017**, *28* (8), 2035–2040.

(143) Smith, A. E.; Sizovs, A.; Grandinetti, G.; Xue, L.; Reineke, T. M. Diblock Glycopolymers Promote Colloidal Stability of Polyplexes and Effective PDNA and SiRNA Delivery under Physiological Salt and Serum Conditions. *Biomacromolecules* **2011**, *12* (8), 3015–3022.

(144) Sizovs, A.; Xue, L.; Tolstyka, Z. P.; Ingle, N. P.; Wu, Y.; Cortez, M.; Reineke, T.

M. Poly(Trehalose): Sugar-Coated Nanocomplexes Promote Stabilization and Effective Polyplex-Mediated SiRNA Delivery. *J. Am. Chem. Soc.* **2013**, *135* (41), 15417–15424.

(145) Tolstyka, Z. P.; Phillips, H.; Cortez, M.; Wu, Y.; Ingle, N.; Bell, J. B.; Hackett, P. B.; Reineke, T. M. Trehalose-Based Block Copolycations Promote Polyplex Stabilization for Lyophilization and in Vivo PDNA Delivery. *ACS Biomater. Sci. Eng.* **2016**, *2* (1), 43–55.

(146) Srinivasachari, S.; Liu, Y.; Zhang, G.; Prevette, L.; Reineke, T. M. Trehalose Click Polymers Inhibit Nanoparticle Aggregation and Promote PDNA Delivery in Serum. *J. Am. Chem. Soc.* **2006**, *128* (25), 8176–8184.

(147) Kizjakina, K.; Bryson, J. M.; Grandinetti, G.; Reineke, T. M. Cationic Glycopolymers for the Delivery of PDNA to Human Dermal Fibroblasts and Rat Mesenchymal Stem Cells. *Biomaterials* **2012**, *33* (6), 1851–1862.

(148) Boyle, W. S.; Senger, K.; Tolar, J.; Reineke, T. M. Heparin Enhances Transfection in Concert with a Trehalose-Based Polycation with Challenging Cell Types. *Biomacromolecules* **2017**, *18* (1), 56–67.

(149) Boyle, W. S.; Twaroski, K.; Woska, E. C.; Tolar, J.; Reineke, T. M. Molecular Additives Significantly Enhance Glycopolymer-Mediated Transfection of Large Plasmids and Functional CRISPR-Cas9 Transcription Activation Ex Vivo in Primary Human Fibroblasts and Induced Pluripotent Stem Cells. *Bioconjug. Chem.* **2019**, *30* (2), 418–431.

(150) Dalle Vedove, E.; Costabile, G.; Merkel, O. M. Mannose and Mannose-6-Phosphate Receptor–Targeted Drug Delivery Systems and Their Application in Cancer Therapy. *Adv. Healthc. Mater.* **2018**, *7* (14), 1701398.

(151) Sun, X.; Chen, S.; Han, J.; Zhang, Z. Mannosylated Biodegradable Polyethyleneimine for Targeted DNA Delivery to Dendritic Cells. *Int. J. Nanomedicine* **2012**, *7*, 2929–2942.

(152) Zhang, Y.; Wang, Y.; Zhang, C.; Wang, J.; Pan, D.; Liu, J.; Feng, F. Targeted Gene Delivery to Macrophages by Biodegradable Star-Shaped Polymers. *ACS Appl. Mater. Interfaces* **2016**, *8* (6), 3719–3724.

(153) Lopukhov, A. V; Yang, Z.; Haney, M. J.; Bronich, T. K.; Sokolsky-Papkov, M.; Batrakova, E. V; Klyachko, N. L.; Kabanov, A. V. Mannosylated Cationic

Copolymers for Gene Delivery to Macrophages. *Macromol. Biosci.* **2021**, *21* (4), 2000371.

(154) Alonso, S. Exploiting the Bioengineering Versatility of Lactobionic Acid in Targeted Nanosystems and Biomaterials. *J. Control. Release* **2018**, *287* (August), 216–234.

(155) Thapa, B.; Kumar, P.; Zeng, H.; Narain, R. Asialoglycoprotein Receptor-Mediated Gene Delivery to Hepatocytes Using Galactosylated Polymers. *Biomacromolecules* **2015**, *16* (9), 3008–3020.

(156) Diaz-Dussan, D.; Nakagawa, Y.; Peng, Y. Y.; Sanchez, L. V.; Ebara, M.; Kumar, P.; Narain, R. Effective and Specific Gene Silencing of Epidermal Growth Factor Receptors Mediated by Conjugated Oxaborole and Galactose-Based Polymers. *ACS Macro Lett.* **2017**, *6* (7), 768–774.

(157) Diaz-Dussan, D.; Peng, Y.-Y.; Kumar, P.; Narain, R. Oncogenic Epidermal Growth Factor Receptor Silencing in Cervical Carcinoma Mediated by Dynamic Sugar-Benzoxaborole Polyplexes. *ACS Macro Lett.* **2020**, *9* (10), 1464–1470.

(158) Albuquerque, L. J. C.; Alavarse, A. C.; Carlan da Silva, M. C.; Zilse, M. S.; Barth, M. T.; Bellettini, I. C.; Giacomelli, F. C. Sweet Vector for Gene Delivery: The Sugar Decoration of Polyplexes Reduces Cytotoxicity with a Balanced Effect on Gene Expression. *Macromol. Biosci.* **2018**, *18* (2), 1–9.

(159) Sprouse, D.; Reineke, T. M. Investigating the Effects of Block versus Statistical Glycopolycations Containing Primary and Tertiary Amines for Plasmid DNA Delivery. *Biomacromolecules* **2014**, *15* (7), 2616–2628.

(160) Prevette, L. E.; Kodger, T. E.; Reineke, T. M.; Lynch, M. L. Deciphering the Role of Hydrogen Bonding in Enhancing PDNA-Polycation Interactions. *Langmuir* **2007**, *23* (19), 9773–9784.

(161) Jung, S.; Lodge, T. P.; Reineke, T. M. Complexation between DNA and Hydrophilic-Cationic Diblock Copolymers. *J. Phys. Chem. B* **2017**, *121* (10), 2230–2243.

(162) Haibo Li, Mallory A. Cortez, Haley R. Phillips, Yaoying Wu, and T. M. R. Poly(2 Deoxy 2 Methacrylamido Glucopyranose) b Poly(Methacrylate Amine)s: Optimization of Diblock Glycopol Ycations for Nucleic Acid Delivery. *ACS Macro Lett.* **2013**, *2* (3).

(163) Wu, Y.; Wang, M.; Sprouse, D.; Smith, A. E.; Reineke, T. M. Glucose-Containing Diblock Polycations Exhibit Molecular Weight, Charge, and Cell-Type Dependence for Pdna Delivery. *Biomacromolecules* **2014**, *15* (5), 1716–1726.

(164) Chen, Y.; Diaz-Dussan, D.; Peng, Y.-Y.; Narain, R. Hydroxyl-Rich PGMA-Based Cationic Glycopolymers for Intracellular SiRNA Delivery: Biocompatibility and Effect of Sugar Decoration Degree. *Biomacromolecules* **2019**, *20* (5), 2068–2074.

(165) Liu, Y.; Reineke, T. M. Poly(Glycoamidoamine)s for Gene Delivery. Structural Effects on Cellular Internalization, Buffering Capacity, and Gene Expression. *Bioconjug. Chem.* **2007**, *18* (1), 19–30.

(166) Ahmed, M.; Lai, B. F. L.; Kizhakkedathu, J. N.; Narain, R. Hyperbranched Glycopolymers for Blood Biocompatibility. *Bioconjug. Chem.* **2012**, *23* (5), 1050–1058.

(167) Ahmed, M.; Jawanda, M.; Ishihara, K.; Narain, R. Impact of the Nature, Size and Chain Topologies of Carbohydrate-Phosphorylcholine Polymeric Gene Delivery Systems. *Biomaterials* **2012**, *33* (31), 7858–7870.

(168) Obata, M.; Kobori, T.; Hirohara, S.; Tanihara, M. Aqueous RAFT Synthesis of Block and Statistical Copolymers of 2-(α-d-Mannopyranosyloxy)Ethyl Methacrylate with 2-(N,N-Dimethylamino)Ethyl Methacrylate and Their Application for Nonviral Gene Delivery. *Polym. Chem.* **2015**, *6* (10), 1793–1804.

(169) Phillips, H. R.; Tolstyka, Z. P.; Hall, B. C.; Hexum, J. K.; Hackett, P. B.; Reineke, T. M. Glycopolycation-DNA Polyplex Formulation N/P Ratio Affects Stability, Hemocompatibility, and in Vivo Biodistribution. *Biomacromolecules* **2019**, *20* (4), 1530–1544.

(170) Spiess, M. The Asialoglycoprotein Receptor: A Model for Endocytic Transport Receptors. *Biochemistry* **1990**, *29* (43), 10009–10018.

(171) Liu, L.; Zong, Z. M.; Liu, Q.; Jiang, S. S.; Zhang, Q.; Cen, L. Q.; Gao, J.; Gao, X. G.; Huang, J. D.; Liu, Y.; et al. A Novel Galactose-PEG-Conjugated Biodegradable Copolymer Is an Efficient Gene Delivery Vector for Immunotherapy of Hepatocellular Carcinoma. *Biomaterials* **2018**, *184* (September), 20–30.

(172) Huang, X.; Leroux, J. C.; Castagner, B. Well-Defined Multivalent Ligands for Hepatocytes Targeting via Asialoglycoprotein Receptor. *Bioconjug. Chem.* **2017**, *28* (2), 283–295.

(173) Lee, R. T.; Lee, Y. C. Affinity Enhancement by Multivalent Lectin-Carbohydrate Interaction. *Glycoconj. J.* **2000**, *17* (7–9), 543–551.

(174) Lee, Y. C.; Townsend, R. R.; Hardy, M. R.; Lönngren, J.; Arnarp, J.; Haraldsson, M.; Lönn, H. Binding of Synthetic Oligosaccharides to the Hepatic Gal/GalNAc Lectin. Dependence on Fine Structural Features. *J. Biol. Chem.* **1983**, *258* (1), 199–202.

(175) Lee, C. C.; Grandinetti, G.; McLendon, P. M.; Reineke, T. M. A Polycation Scaffold Presenting Tunable "Click" Sites: Conjugation to Carbohydrate Ligands and Examination of Hepatocyte-Targeted PDNA Delivery. *Macromol. Biosci.* **2010**, *10* (6), 585–598.

(176) Williams, E. G. L.; Hutt, O. E.; Hinton, T. M.; Larnaudie, S. C.; Le, T.; Macdonald, J. M.; Gunatillake, P.; Thang, S. H.; Duggan, P. J. Glycosylated Reversible Addition-Fragmentation Chain Transfer Polymers with Varying Polyethylene Glycol Linkers Produce Different Short Interfering RNA Uptake, Gene Silencing, and Toxicity Profiles. *Biomacromolecules* **2017**, *18* (12), 4099–4112.

(177) Tan, Z.; Dhande, Y. K.; Reineke, T. M. Cell Penetrating Polymers Containing Guanidinium Trigger Apoptosis in Human Hepatocellular Carcinoma Cells Unless Conjugated to a Targeting N-Acetyl-Galactosamine Block. *Bioconjug. Chem.* **2017**, *28* (12), 2985–2997.

(178) Liu, S.; Gao, Y.; A, S.; Zhou, D.; Greiser, U.; Guo, T.; Guo, R.; Wang, W. Biodegradable Highly Branched Poly(β-Amino Ester)s for Targeted Cancer Cell Gene Transfection. *ACS Biomater. Sci. Eng.* **2017**, *3* (7), 1283–1286.

(179) Cai, C.; Xie, Y.; Wu, L.; Chen, X.; Liu, H.; Zhou, Y.; Zou, H.; Liu, D.; Zhao, Y.; Kong, X.; et al. PLGA-Based Dual Targeted Nanoparticles Enhance MiRNA Transfection Efficiency in Hepatic Carcinoma. *Sci. Rep.* **2017**, *7* (March), 1–12.

(180) Zheng, Q. C.; Jiang, S.; Wu, Y. Z.; Shang, D.; Zhang, Y.; Hu, S. B.; Cheng, X.; Zhang, C.; Sun, P.; Gao, Y.; et al. Dual-Targeting Nanoparticle-Mediated Gene Therapy Strategy for Hepatocellular Carcinoma by Delivering Small Interfering

RNA. *Front. Bioeng. Biotechnol.* **2020**, *8* (June), 1–17.

(181) Chen, Q.; Gao, M.; Li, Z.; Xiao, Y.; Bai, X.; Boakye-Yiadom, K. O.; Xu, X.; Zhang, X.-Q. Biodegradable Nanoparticles Decorated with Different Carbohydrates for Efficient Macrophage-Targeted Gene Therapy. *J. Control. Release* **2020**, *323*, 179–190.

(182) Pan, Z.; Kang, X.; Zeng, Y.; Zhang, W.; Peng, H.; Wang, J.; Huang, W.; Wang, H.; Shen, Y.; Huang, Y. A Mannosylated PEI–CPP Hybrid for TRAIL Gene Targeting Delivery for Colorectal Cancer Therapy. *Polym. Chem.* **2017**, *8* (35), 5275–5285.

(183) Leber, N.; Kaps, L.; Yang, A.; Aslam, M.; Giardino, M.; Klefenz, A.; Choteschovsky, N.; Rosigkeit, S.; Mostafa, A.; Nuhn, L.; et al. α-Mannosyl-Functionalized Cationic Nanohydrogel Particles for Targeted Gene Knockdown in Immunosuppressive Macrophages. *Macromol. Biosci.* **2019**, *19* (7), 1–12.

(184) McLendon, P. M.; Fichter, K. M.; Reineke, T. M. Poly(Glycoamidoamine) Vehicles Promote PDNA Uptake through Multiple Routes and Efficient Gene Expression via Caveolae-Mediated Endocytosis. *Mol. Pharm.* **2010**, *7* (3), 738–750.

(185) Ingle, N. P.; Hexum, J. K.; Reineke, T. M. Polyplexes Are Endocytosed by and Trafficked within Filopodia. *Biomacromolecules* **2020**.

(186) Fichter, K. M.; Ingle, N. P.; McLendon, P. M.; Reineke, T. M. Polymeric Nucleic Acid Vehicles Exploit Active Interorganelle Trafficking Mechanisms. *ACS Nano* **2013**, *7* (1), 347–364.

(187) Grandinetti, G.; Reineke, T. M. Exploring the Mechanism of Plasmid DNA Nuclear Internalization with Polymer-Based Vehicles. *Mol. Pharm.* **2012**, *9* (8), 2256–2267.

(188) Tammam, S. N.; Azzazy, H. M. E.; Lamprecht, A. How Successful Is Nuclear Targeting by Nanocarriers? *J. Control. Release* **2016**, *229*, 140–153.

(189) Peng, Y.-Y.; Hu, H.; Diaz-Dussan, D.; Zhao, J.; Hao, X.; Narain, R. Glycopolymer–Cell-Penetrating Peptide (CPP) Conjugates for Efficient Epidermal Growth Factor Receptor (EGFR) Silencing. *ACS Macro Lett.* **2022**, *11* (4), 580–587.

(190) Sun, M.; Wang, K.; Oupický, D. Advances in Stimulus-Responsive Polymeric

Materials for Systemic Delivery of Nucleic Acids. *Adv. Healthc. Mater.* **2018**, *7* (4), 1–17.

(191) Sunasee, R.; Wattanaarsakit, P.; Ahmed, M.; Lollmahomed, F. B.; Narain, R. Biodegradable and Nontoxic Nanogels as Nonviral Gene Delivery Systems. *Bioconjug. Chem.* **2012**, *23* (9), 1925–1933.

(192) Ahmed, M.; Narain, R. Intracellular Delivery of DNA and Enzyme in Active Form Using Degradable Carbohydrate-Based Nanogels. *Mol. Pharm.* **2012**, *9* (11), 3160–3170.

(193) Peeler, D. J.; Sellers, D. L.; Pun, S. H. PH-Sensitive Polymers as Dynamic Mediators of Barriers to Nucleic Acid Delivery. *Bioconjug. Chem.* **2019**, *30* (2), 350–365.

(194) Peng, Y.-Y.; Diaz-Dussan, D.; Vani, J.; Hao, X.; Kumar, P.; Narain, R. Achieving Safe and Highly Efficient Epidermal Growth Factor Receptor Silencing in Cervical Carcinoma by Cationic Degradable Hyperbranched Polymers. *ACS Appl. Bio Mater.* **2018**, *1* (4), 961–966.

(195) Ning, S.; Liu, H.; Gao, B.; Wei, W.; Yang, A.; Li, J.; Zhang, L. MiR-155, MiR-96 and MiR-99a as Potential Diagnostic and Prognostic Tools for the Clinical Management of Hepatocellular Carcinoma. *Oncol Lett* **2019**, *18* (3), 3381–3387.

(196) Tsai, W.-C.; Hsu, P. W.-C.; Lai, T.-C.; Chau, G.-Y.; Lin, C.-W.; Chen, C.-M.; Lin, C.-D.; Liao, Y.-L.; Wang, J.-L.; Chau, Y.-P.; et al. MicroRNA-122, a Tumor Suppressor MicroRNA That Regulates Intrahepatic Metastasis of Hepatocellular Carcinoma. *Hepatology* **2009**, *49* (5), 1571–1582.

(197) Ning, Q.; Liu, Y.-F.; Ye, P.-J.; Gao, P.; Li, Z.-P.; Tang, S.-Y.; He, D.-X.; Tang, S.-S.; Wei, H.; Yu, C.-Y. Delivery of Liver-Specific MiRNA-122 Using a Targeted Macromolecular Prodrug toward Synergistic Therapy for Hepatocellular Carcinoma. *ACS Appl. Mater. Interfaces* **2019**, *11* (11), 10578–10588.

(198) Ganbold, T.; Baigude, H. Design of Mannose-Functionalized Curdlan Nanoparticles for Macrophage-Targeted SiRNA Delivery. *ACS Appl. Mater. Interfaces* **2018**, *10* (17), 14463–14474.

CHAPTER 2

TARGETED DOWNREGULATION OF MYC MEDIATED BY A HIGHLY EFFICIENT LACTOBIONIC ACID-BASED GLYCOPLEX TO ENHANCE CHEMOSENSITIVITY IN HUMAN HEPATOCELLULAR CARCINOMA CELLS

The contents of this chapter were adapted from:
Santo, D..; Mendonça, P. V; Serra, A. C.; Coelho, J. F. J.; Faneca, H. Targeted downregulation of MYC mediated by a highly efficient lactobionic acid-based glycoplex to enhance chemosensitivity in human hepatocellular carcinoma cells, International Journal of Pharmaceutics (*under review*).

2.1. Introduction

Hepatocellular carcinoma (HCC) represents about 75–85% of primary liver cancers and is the third leading cause of cancer-related deaths worldwide.[1] Although remarkable progress has been made in recent years, the therapeutic efficacy of current treatments is still not satisfactory, with a very low 5-year survival rate (16.6%).[2] Sorafenib (SF), approved as the first-line therapy for unresectable HCC, blocks multiple receptor tyrosine kinase signaling pathways, inhibiting downstream kinases activity to prevent tumour growth by anti-angiogenic, antiproliferative and/or pro-apoptotic effects.[3] However, this chemotherapeutic drug exhibits low therapeutic efficacy and it therapeutic outcome is severely limited by drug resistance and severe side effects.[4] Therefore, novel antitumor strategies that have both higher therapeutic efficiency and lower side effects are urgently needed for HCC.

c-MYC is a transcription factor that regulates the expression of a myriad of gene products involved in cell proliferation, apoptosis, differentiation and other critical biological processes associated with carcinogenesis.[5] *c-MYC* amplification is frequently observed in HCC patients at younger age and with poor prognosis.[6] Several studies have shown that inhibition of *c-MYC* induces the regression and differentiation of liver tumors.[7] In addition, Che-Pin Lin and co-workers demonstrated that c-MYC inhibition by 10058-F4, a small-molecule c-MYC inhibitor, enhances the chemosensitivity of tumor cells to low-doses of chemotherapeutic agents.[8] However, the low concentration of these small-molecule inhibitors in tumors, due to rapid metabolism, limits their clinical application. Therefore, gene therapy capable of specifically silencing c-*MYC* may be considered a potentially useful chemosensitization strategy to improve the response of HCC cells to chemotherapy.

Despite the significant advances in the field of gene therapy, the development of efficient and targeted gene delivery platforms is crucial to achieve the desired therapeutic effects and minimize off-target effects.[9,10,11] In this context, cationic glycopolymers, cationic copolymers with pendant carbohydrate groups, have attracted considerable attention due to their unique ability to mimic naturally occurring polysaccharides, to increase the biocompatibility of gene delivery nanosystems and to promote carbohydrate-specific recognition by cell surface receptors.[12,13,14] In particular, nanocarriers functionalized with lactobionic acid exhibit high binding affinity with the asialoglycoprotein receptor (ASGPR), a target receptor overexpressed in tumour cells, making these nanovehicles a promising tool for HCC-specific gene delivery.[15,16,17] The

glycocluster effect promoted by the multivalence of glycopolymers can circumvent the weak binding affinity of these glycoproteins to the receptor, enhancing the cellular internalization.[18,19] Reineke's and Narain's groups have extensively worked on the synthesis of cationic glycopolymers and on the evaluation of their efficiency in gene delivery as a function of various polymer properties, such as molecular weight[20], cationic content[21], carbohydrate content[22] and architecture[23]. Some of the most commonly used glycopolymers are methacrylamide-based copolymers, prepared by copolymerization between primary amine monomers, such as 3-aminopropyl methacrylamide[24] or 2-amino ethyl methacrylamide[25,23] and carbohydrate-derived monomers, namely 3-gluconamidopropyl methacrylamide[26] and 2-lactobionamidoethyl methacrylamide.[27,28,29] The positive charges of these glycopolymers interact with the negative charges of nucleic acids through electrostatic interactions, while the carbohydrate residues can facilitate DNA condensation through hydrogen bonding, to form stable glycoplexes.[30] In general, nanocarriers prepared with random cationic glycopolymers showed high transgene expression with low cytotoxicity compared to their block counterparts.[31,32] Nevertheless, most reports have shown that nanosystems based on glycopolymers have lower transfection ability than the corresponding polyplexes based on cationic homopolymers.[33,24]

In this work, a highly efficient ASGPR-targeted glycopolymer-based gene delivery nanosystem was developed to downregulate the expression of c-MYC and further sensitizes tumor cells to sorafenib. First, a library of well-defined cationic glycopolymers, based on poly (2-aminoethyl methacrylate hydrochloride) (PAMA) and poly(2-lactobionamidoethyl methacrylate) (PLAMA), with different compositions, structure (block or random) and carbohydrate/cationic ratios, was synthesized by activators regenerated by electron transfer atom transfer radical polymerization (ARGET ATRP) (Scheme 2). The best formulations of glycoplexes were subjected to extensive physicochemical characterization and comprehensive evaluation of biological activity, toxicity and ASGPR specificity. The antitumor effect of c-MYC downregulation, promoted by a short hairpin RNA against this protein, in combination with low concentration of SF was evaluated in 2D and 3D tumor models of HCC.

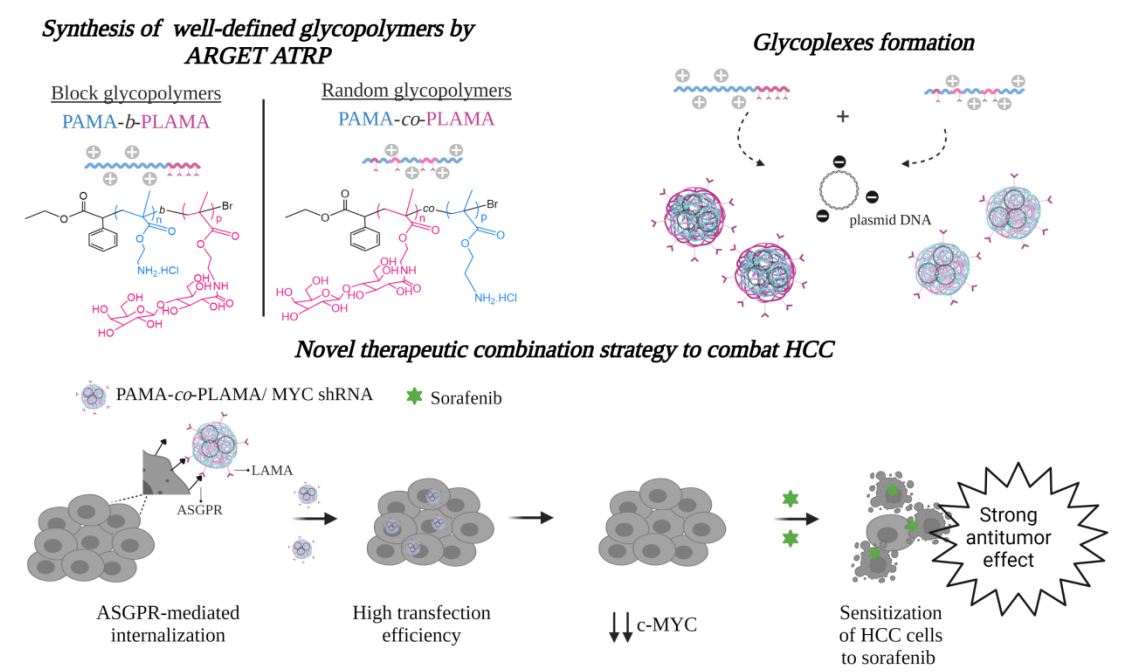

Scheme 2– Random and block methacrylate-based glycopolymers were synthetized by ARGET ATRP. ASGPR-specific internalization and clathrin-mediated endocytosis lead to high transfection efficiency in HCC cells. Downregulation of c-MYC expression by MYC shRNA resulted in a high sensitization of HepG2 cells to SF.

2.2.Materials and methods

Materials

2-Aminoethyl methacrylate hydrochloride (AMA; ≥95%, Polysciences), ascorbic acid (AscA; Sigma-Aldrich), ASGPR Monoclonal Antibody (Thermo Fisher), asialofetuin (Sigma-Aldrich), amiloride hydrochloride (Sigma-Aldrich), bovine serum albumin (BSA; Sigma-Aldrich), chlorpromazine (Sigma-Aldrich), copper(II) bromide (CuBr2; 99.999%, Sigma-Aldrich), deuterium oxide (D_2O; +99.9% D, Euroiso-top), DC protein assay kit (Bio-Rad), 4,6-diamidino-2-phenylindole (DAPI, Thermo Fisher Scientific), dimethylformamide (DMF, Fisher Scientific), Dulbecco's modified Eagle's medium-high glucose (DMEM-HG; Sigma-Aldrich), D-luciferin sodium salt (99%, Synchem), ethyl α-bromophenyl acetate (EBPA; Alfa Aesar), filipin (Sigma-Aldrich), fluorescein o-methacrylate monomer (FMO, Sigma-Aldrich), fluoroshield (Sigma-Aldrich), Green Safe (Nzytech), lactobionic acid (Thermo Scientific), Lysotrack Red DND-99 (Thermo Fisher Scientific), PEI (branched, Mw 25000, Sigma-Aldrich), plasmids DNA encoding

luciferase (pCMV.Luc), green fluorescent protein (GFP, pCMV.gfp) (Vical), resazurin sodium salt (Sigma-Aldrich) and 2-propanol (Fisher Scientific) were used as received. Methanol (Fisher Chemical) was dried over CaH_2 and distilled before use. Triethylamine (≥99.5%, Sigma-Aldrich) was distilled before use. Tris(pyridine-2-ylmethyl)amine (TPMA) was synthesized as reported in the literature.[34]

Synthesis and characterization of glycopolymers

Techniques

A syringe pump (KDS Scientific, Legato 101) was used for the continuous feeding of the reducing agent (AscA) at the rate of 1 μL/min during ARGET ATRP.

The molecular weight parameters of the polymers were determined by a size exclusion chromatography (SEC) system equipped with an online degasser, a refractive index (RI) detector and the set of columns: Shodex OHpak SB-G guard column, OHpak SB-804HQ and OHpak SB-802.5HQ. The polymers were eluted at a flow rate of 0.5 mL/min with 0.1 M Na_2SO_4 (aq)/1 wt% acetic acid/0.02% NaN_3 at 40 °C. Before the injection, the samples were filtered through a polytetrafluoroethylene (PTFE) membrane with 0.2 μm pore. The system was calibrated with five narrow polyethylene glycol (PEG) standards and the polymers number-average molecular weight (M_n^{SEC}) and dispersity ($Đ = M_w/M_n$) were determined by conventional calibration using the Clarity software version 2.8.2.648.400

MHz ^{1}H NMR spectra were recorded on a Bruker Avance III 400 MHz spectrometer, with a 5-mm TIX triple resonance detection probe, in D_2O. Conversion of monomers was determined by integration of monomers and internal standard (dimethylformamide) NMR signals using the MestRenova software version: 10.0.1-14719.

Synthesis of 2-lactobionamidoethyl methacrylate (LAMA)

LAMA was synthesized according to a previously described procedure.[35] First, lactobionic acid was converted into the corresponding lactobionolactone. For this purpose, lactobionic acid (4.0 g, 11.2 mmol) was dissolved in anhydrous methanol (25 mL) at 50 ºC, in the presence of trifluoroacetic acid as a catalyst (0.1 g, 1.1 mmol), followed by vacuum distillation to recover lactobionolactone. After that, lactobionolactone (1.5 g, 4.5 mmol) was dissolved in methanol at 50 ºC, followed by the addition of 2-aminoethyl methacrylate hydrochloride (1.5 g, 9.0 mmol), triethylamine (1.27 mL) and hydroquinone (0.05 g) at room temperature. The mixture

was stirred for 6 h, concentrated by rotary evaporation and precipitated in 2-propanol. The white solid formed was filtered, washed with 2-propanol and dried under vacuum. The final yield of LAMA after purification was 81%.

Typical procedure for the synthesis of PAMA-co-PLAMA by ARGET ATRP

AMA (2.18 g, 13.8 mmol), LAMA (1 g, 2.13 mmol), $CuBr_2$ (11.8 mg, 53.5 μmol), TPMA (61.8 mg, 213 μmol) and EBPA (25.9 mg, 106 μmol) were dissolved in water/dimethylformamide (DMF) mixture (50/50, V/V) (3.5 mL). The mixture was added to a 10 mL round-bottom Schlenk flask, equipped with a magnetic stir bar, and purged with nitrogen for 30 min. The flask was placed in an oil bath at 60 °C and a deoxygenated ascorbic acid (AscA) aqueous solution (43 mM) was continuously injected into the reaction medium using a syringe pump at the rate of 1 μL/min. The reaction was stopped after 3 h, and a sample was collected for ^{1}H nuclear magnetic resonance (NMR) spectroscopy to determine the monomer (AMA/LAMA) conversion and for aqueous size exclusion chromatography (SEC) to determine the molecular weight and dispersity of the copolymer. The final reaction mixture was dialyzed (dialysis membrane MWCO = 3500) against deionized water, and the glycopolymer was recovered by freeze-drying.

Typical procedure for synthesis of PAMA-b-PLAMA by "one-pot" ARGET ATRP

Briefly, AMA (0.3 g, 1.72 mmol), $CuBr_2$ (1.7 mg, 7.8 μmol), TPMA (9.0 mg, 31 μmol) and EBPA (3.8 mg, 15.6 μmol) were dissolved in 1.2 mL of water/DMF mixture (50/50, V/V). The mixture was added to a 10 mL Schlenk flask, equipped with a magnetic stir bar, and purged with nitrogen for 30 min. The flask was placed in an oil bath at 35 °C and a deoxygenated AscA aqueous solution (10 mM) was continuously injected into the reaction medium, using a syringe pump, at the rate of 1 μL/min. When the monomer conversion reached more than 90%, a degassed mixture of LAMA (0.15g, 312 μmol) in 2 mL of water/DMF (50/50, V/V) was added to the Schlenk flask, under a nitrogen atmosphere, and the temperature was increased to 60 ºC. The reaction was allowed to proceed until maximum LAMA conversion was achieved. Monomer conversion was determined by ^{1}H NMR spectroscopy and the molecular weight and dispersity were determined by aqueous SEC. The final reaction mixture was dialyzed (dialysis membrane MWCO = 3500) against deionized water, and the glycopolymer was recovered by freeze-drying.

Synthesis of fluorescein-labeled glycopolymer

AMA (0.54g, 3.7 mmol), LAMA (0.25 g, 532 μmol), FMO (53.3 mg, 133 μmol), $CuBr_2$ (2.97 mg, 13.3 μmol), TPMA (15.5 mg, 53 μmol), and EBPA (6.5 mg, 26 μmol) were dissolved in water/DMF mixture (50/50, V/V) (3.5mL). The mixture was added to a 10 mL round-bottom Schlenk flask, equipped with a magnetic stir bar, and purged with nitrogen for 30 min. The flask was placed in an oil bath at 60 °C and a deoxygenated AscA aqueous solution (43 mM) was continuously injected into the reaction medium, using a syringe pump, at the rate of 1 μL/min. The reaction was stopped after 3 h and a sample was collected for ^{1}H NMR spectroscopy to determine the monomer (AMA and LAMA) conversion. The final reaction mixture was dialyzed (dialysis membrane MWCO = 3500) against deionized water and the glycopolymer was recovered by freeze-drying.

Formulation of polyplexes

Polymers were dissolved in Milli-Q water and mixed with 1μg of pCMV.Luc, pCMV.gfp or pshRNA at the desired polymer/DNA N/P (+/−) charge ratio. The mixture was incubated at room temperature for 15 min. The complexes were used immediately after their preparation.

Physicochemical characterization of the polyplexes

Polyplexes were characterized using different techniques, including dynamic light scattering (DLS), electrophoresis, and transmission electron microscopy (TEM).

The particle size distribution and average hydrodynamic diameter were determined by DLS on a Zetasizer Nano-ZS (Malvern Instruments Ltd. UK), with Zetasizer 7.13 software. The zeta potential measurements were performed using a Zetasizer Nano-ZS (Malvern Instruments Ltd., UK) coupled to laser Doppler electrophoresis and determined using a Smoluchovski model. To further analyze the particle size and morphology, TEM was performed as previously described[36].

The accessibility to DNA of polyplexes was analyzed using the Green Safe intercalation assay. The polyplexes were prepared as described above, and after 15 min, 50 μL of each sample was transferred into a black 96-well plate. Then, 50 μL of Green Safe solution (0.00002 % (V/V)) was added to polyplexes. Following 10 min incubation, fluorescence was measured in a SpectraMax Gemini EM fluorometer

(Molecular Devices, Sunnyvale, CA, USA) at the excitation wavelength of 490 nm and emission wavelength of 530 nm. The fluorescence scale was calibrated such that the initial fluorescence of Green Safe (50 μL of Green Safe solution was added to 50 μL of Milli-Q water) was set as residual fluorescence. The value of fluorescence obtained with 1 μg of naked DNA (control) was set as 100%. The amount of DNA available to interact with the probe was calculated by subtracting the values of residual fluorescence from those obtained for the samples and expressed as the percentage of the control. To evaluate the complexation of DNA with copolymers, electrophoresis was performed in agarose gel, as previously described[36] .

Cell culture

Human hepatocellular carcinoma cells (HepG2, Hep3B and HuH-7 cell lines) and human epithelial cervical carcinoma cells (HeLa cell line) were maintained at 37 °C, under 5% CO_2, in DMEM-HG cell culture medium, supplemented with 10% (V/V) heat inactivated fetal bovine serum (FBS, Sigma-Aldrich, MO, USA), penicillin (100 U/mL) and streptomycin (100 μg/mL). All cells were grown in monolayers and were detached by treatment with a 0.25% trypsin solution (Sigma-Aldrich, MO, USA).

Transfection activity

The biological activity of the different polyplexes was determined by luminescence, using a plasmid containing the reporter gene luciferase (pCMV.Luc), in HepG2, Hep3B, HuH-7 and HeLa cells[37]. Briefly, the HepG2 (8×10^4 cells/well), Hep3B (3.5×10^4 cells/well), HuH-7 (3.5×10^4 cells/well) and HeLa (5×10^4 cells/well) cells were seeded onto 48-well culture plates 24 h prior to incubation with polyplexes. After 4 h of incubation with polyplexes, the transfection medium was replaced with fresh DMEM-HG and the cells were further incubated for 48 h. At this time, the cells were washed with PBS solution lysed. The quantification of luciferase expression in cell lysates was evaluated by measuring the light production by luciferase in a Synergy HT luminometer (Biotek, USA). The protein content of the lysates was measured by the DC protein assay reagent (Biorad, CA, USA) using BSA as a standard. The data were expressed as relative light units of luciferase per milligram of the total cell protein. For the competitive studies, the cell culture medium, containing 1 mg/mL of asialofetuin or 40 μg/ml of antibody against the ASGPR, was added to cells 30 min before the addition of nanosystems and maintained during the 4 h of transfection. In the endocytic pathway

studies, the culture medium containing various endocytosis inhibitors (50 μM Chlorpromazine, 0.25 mM amiloride or 2 μg/mL Filipin) was added to cells 1 h before the polyplex addition and maintained during the 4 h of transfection.

Transfection efficiency

To evaluate the transfection efficiency of the formulations, GFP expression was analyzed in the transfected cells by fluorescence microscopy.[38] Briefly, 1.5×10^5 HepG2 cells/well were seeded on 24-well plates (the wells were previously covered with a coverslip) and, after 24 h, polyplexes containing 2 μg of pCMV.gfp were added to the cells. After 4 h of incubation (5% CO_2 at 37 °C), the transfection medium was replaced with DMEM-HG containing 10% (V/V) FBS and antibiotics and the cells were further incubated for 48 h. Then, the cells were washed with PBS, fixed with 4% paraformaldehyde for 15 min at room temperature, and mounted in Fluoroshield medium. The images (original magnification ×20) were obtained on an Axio Imager Z2 microscope (Zeiss, Munich, Germany) using an AxioCam HRc camera (Zeiss, Germany). For the flow cytometry analysis of GFP expression after 48h of transfection the cells were washed and resuspended in PBS and immediately analyzed in a FACSCalibur flow cytometer (Becton Dickinson, NJ, USA). Live cells were gated by forward/side scattering from a total of 20 000 events and the data were analyzed using FlowJo software.

Cell viability assay

Cell viability under different experimental conditions was assessed by an Alamar Blue assay. After 48 h of transfection, the cells were incubated with DMEM containing 10% (V/V) Alamar Blue dye, prepared from a 0.1 mg mL^{-1} stock solution of Alamar Blue. After 1 h incubation period at 37 °C, the absorbance of the medium was measured at 570 and 600 nm in SPECTRAmax PLUS 384 spectrophotometer (Molecular Devices, USA). Cell viability was calculated, as percentage of the nontreated control cells, according to the formula: $[(A_{570} - A_{600})$ of treated cells × 100]/$[(A_{570} - A_{600})$ of control cells].

Cell uptake

Polyplexes were prepared with 1% of fluorescein-labeled FMO_2-*co*-$PAMA_{103}$-*co*-$PLAMA_{19}$ at their optimal N/P ratio. HepG2 cells were seeded on 24-well plates at a

density of 1.6×10^5 cells/well and, after 24 h, polyplexes containing the glycopolymer labeled with fluorescein were added to cells previously covered with 0.5 mL of DMEM-HG with serum. After 4 h of incubation (5% CO_2 at 37 °C), cells were washed twice with PBS, detached with trypsin and then washed and resuspended in PBS. In the competitive studies, the culture medium containing 2 mg/mL of asialofetuin was added to cells 30 min before the addition of the nanosystems and maintained during the 4 h of transfection. Live cells were gated by forward/side scattering from a total of 20 000 events and data was analyzed using FlowJo software.

Intracellular distribution of polyplexes

Confocal laser scanning microscopy was used to visualize the intracellular distribution of polyplexes prepared with 1% of fluorescein-labeled glycopolymer at their optimal N/P ratio. The HepG2 cells were seeded in 24-well culture plates (previously covered with a coverslip) at an initial density of 1.5×10^5 cells/well and, after 24 h, polyplexes were added. In the competitive studies, the culture medium containing 2 mg/mL of asialofetuin was added to cells 30 min before the addition of the nanosystems and maintained during the 4 h of transfection. After this period of incubation (5% CO_2 at 37 °C), the transfection medium was removed and the cells were washed with PBS and incubated for 30 min with 200 nM Lysotrack Red DND-99, which labels the acidic compartments of living cells. Cells were then washed three times with PBS and fixed with 4% paraformaldehyde solution for 15 min at room temperature. Nuclei labeling was accomplished through 5 min of incubation at room temperature with the fluorescent DNA binding dye DAPI (1 μg/mL). The cells were then mounted in Fluoroshield medium, and images were taken in a Zeiss LSM 710 Axio Observer microscope (Zeiss, Gottingen, Germany) with a Plan-Apochromat 63×/1.40 oil differential interference contrast (DIC) M27 objective at the excitation wavelengths of 405 nm for DAPI (blue), 488 nm for fluorescein (green) and 561 nm for Lysotracker (red).

3D Multicellular tumor spheroids preparation and transfection efficiency evaluation

HepG2 cells, suspended in complete cell culture medium, were seeded at a density of 3×10^3 cells/well in 96-well round-bottomed ultra-low attachment microplates (Corning® Costar®), spun down at 500 rpm for 3 min and incubated at 37 °C in a humidified atmosphere of 5% CO_2. After the initial 3 days of formation, spheroids were incubated with $PAMA_{114}$-*co*-$PLAMA_{21}$- and PEG_{45}-*b*-$PAMA_{168}$-based polyplexes,

prepared at 50/1 N/P ratio with 0.5 μg of pCMV.gfp, for 72 hours at 37 °C in a humidified atmosphere of 5% CO_2. To assess the transfection efficiency of the formulations, GFP expression was evaluated in these spheroids by confocal laser scanning microscopy. Firstly, the spheroids were gently washed with PBS and fixed with 4% paraformaldehyde solution for 1 h at room temperature. After that, nuclei labeling was accomplished through 30 min of incubation, at room temperature, with the fluorescent DNA binding dye DAPI (1 μg/mL). The spheroids were then carefully transferred with a tip for a coverslip and mounted in Fluoroshield medium. The Z-Stack images were taken in a Zeiss LSM 710 Axio Observer microscope (Zeiss, Gottingen, Germany) with a Plan-Apochromat 20x/0.8 and Plan-Apochromat 40×/1.40 oil differential interference contrast (DIC) M27 objectives, at the excitation wavelengths of 405 nm for DAPI (blue) and 488 nm for fluorescein (green).

Antitumor activity

The *in vitro* antitumor activity promoted by *c-MYC* inhibition, SF or their combination was evaluated in HepG2 cells. shRNA-mediated knockdown of human *c-MYC* was performed with the pLKO.1 lentiviral plasmids containing a c-MYC shRNA (pMYC shRNA) or a scrambled control (p*Scr* shRNA) sequence (Sigma). $PAMA_{114}$-*co*-$PLAMA_{20}$-based polyplexes, loading 1 μg of pScr shRNA or pMYC shRNA, were added to HepG2 cells. Following 4 h of incubation the medium was replaced with fresh DMEM-HG. Twenty-four hours after, the medium was replaced with DMEM-HG with 0, 2, 4, 6 or 8 μM of sorafenib and cells were further incubated for 5 days under the normal culture conditions (5% CO_2 at 37 °C).

For quantification of c-MYC mRNA expression levels, real-time polymerase chain reaction (RT-PCR) assay was performed. Briefly, after 48 h of transfection, RNA was isolated using NucleoSpin® RNA Plus (Macherey-Nagel) according to manufacturer instructions. Then, cDNA was synthesized using SuperScript™ IV VILO™ Master Mix (ThermoFisher). The forward and reverse primer sequences of the c-MYC gene were GGCTCCTGGCAAAAGGTCA and CTGCGTAGTTGTGCTGATGT, respectively (Quiagen). RT-PCR was performed in a reaction mixture containing specific primers, FastStart Universal SYBR Green Master in a StepOnePlus™ Real-Time PCR System, from Thermo Fisher. Each reaction was performed in duplicate, by adding 6 μl of master mix to 4 μl of template cDNA. Threshold values for threshold cycle determination (Ct) were generated automatically by the StepOne™ software v2.2.2.

Relative mRNA levels were determined following the Pfaffl method in comparison with control cells.

The cell viability was assessed at 48, 72, 96 and 120 hours by the Alamar Blue assay. After each measurement, the medium, with or without SF, was replaced. The effect of the developed therapeutic strategy on HepG2 cells proliferation was measured by hemocytometer cell counting method after 48, 72 or 96 hours of treatment.

The cell death mechanisms involved in the studied therapeutic strategies were evaluated, in 24-well culture plates, by flow cytometry using FITC-Annexin and PI probes. After 96 h of incubation with $PAMA_{114}$-*co*-$PLAMA_{20}$/pMYC shRNA; $PAMA_{114}$-*co*-$PLAMA_{20}$/pScr shRNA; $PAMA_{114}$-*co*-$PLAMA_{20}$/pMYC shRNA + SF; $PAMA_{114}$-*co*-$PLAMA_{20}$/pScr shRNA + SF; or SF alone (4μM), cell media and detached cells were harvested, washed with PBS and resuspended in 100 μL of binding buffer (10 mM HEPES (pH 7.4), 2.5 mM $CaCl_2$, 140 mM NaCl) to which 2 μL of FITC annexin V and 1 μL of PI (0.05 mg/mL) were added. Samples were incubated for 5 min in the dark at RT and then analyzed (10,000 events) in a FACSCalibur flow cytometer (Becton Dickinson, USA). The data were analyzed using FlowJo software.

For fluorescence images, live/dead staining of HepG2 cells was carried out using fluorescein diacetate (5 mg/mL in acetone) and propidium iodide (2mg/mL in PBS). After incubating for 15 minutes, the cells were washed with PBS and DMEM without phenol red was added. The images (original magnification ×10) were immediately acquired in an Axio Observer Z1 widefield microscope using a digital CMOS camera (ORCA Flash 4.0) (Zeiss®, Germany).

To evaluate the antitumor effect of the developed therapeutic strategy in a 3D cell culture model, $3x10^3$ $HepG^2$ cells per well were seeded in 96-well culture round-bottom ultralow attachment microplates. After the initial 3 days of formation, spheroids were incubated with $PAMA_{144}$-*co*-$PLAMA_{19}$-based polyplexes, prepared at 50/1 N/P ratio with 0.5 μg of pMYC shRNA or pScr shRNA per well. Following 48 h of incubation, the medium was replaced by medium with or without SF (4 μM) every 48 h. Microscopy images were taken at 0 h and 168 h. The images (original magnification: x20 (plan apochromat objectives)) were acquired in an Axio Observer Z1 widefield microscope using a digital CMOS camera (ORCA Flash 4.0) (Zeiss®,Germany) and processed with Zen Blue software (Zeiss®, Germany). Analysis of spheroid areas was performed using a well-established image analysis algorithm of the Zen Blue software. For fluorescence images, live/dead staining of spheroids was carried out using

fluorescein diacetate (5 mg/mL in acetone) and propidium iodide (5 mg/mL in PBS). After incubating for 45 minutes, the spheroids were washed with PBS and visualized immediately.

Statistical analysis

All the results correspond to mean ± standard deviation SD, achieved from triplicates, are representative of at least three independent experiments and analyzed using GraphPad Prism (version 6.01 GraphPad Software Inc., San Diego, CA, USA). The statistical significance of differences between data was evaluated by one-way analysis of variance (ANOVA) using Dunnett test or by two-way ANOVA using Dunnett, Sidak or Turkey tests. p-Values < 0.05 were considered as statistically significant.

2.3. Results and discussion

2.3.1. Synthesis and characterization of PAMA-b-PLAMA and PAMA-co-PLAMA glycopolymers

To prepare well-defined methacrylate-based glycopolymers and further develop a highly efficient and HCC-specific gene delivery nanosystem, a series of PAMA-*co*-PLAMA random and PAMA-*b*-PLAMA block glycopolymers were synthetized by ARGET ATRP. Lactobionic acid stands out as a multifunctional galactosylated molecule with unique biocompatibility, biodegradability, functionality and asialoglycoprotein receptor specificity.[15,39] In this work, LAMA, am inexpensive lactobionic-acid derivative monomer, was synthetized by reacting AMA with lactobionolactone without using protecting group chemistry (Scheme A1, Appendix A).[35]

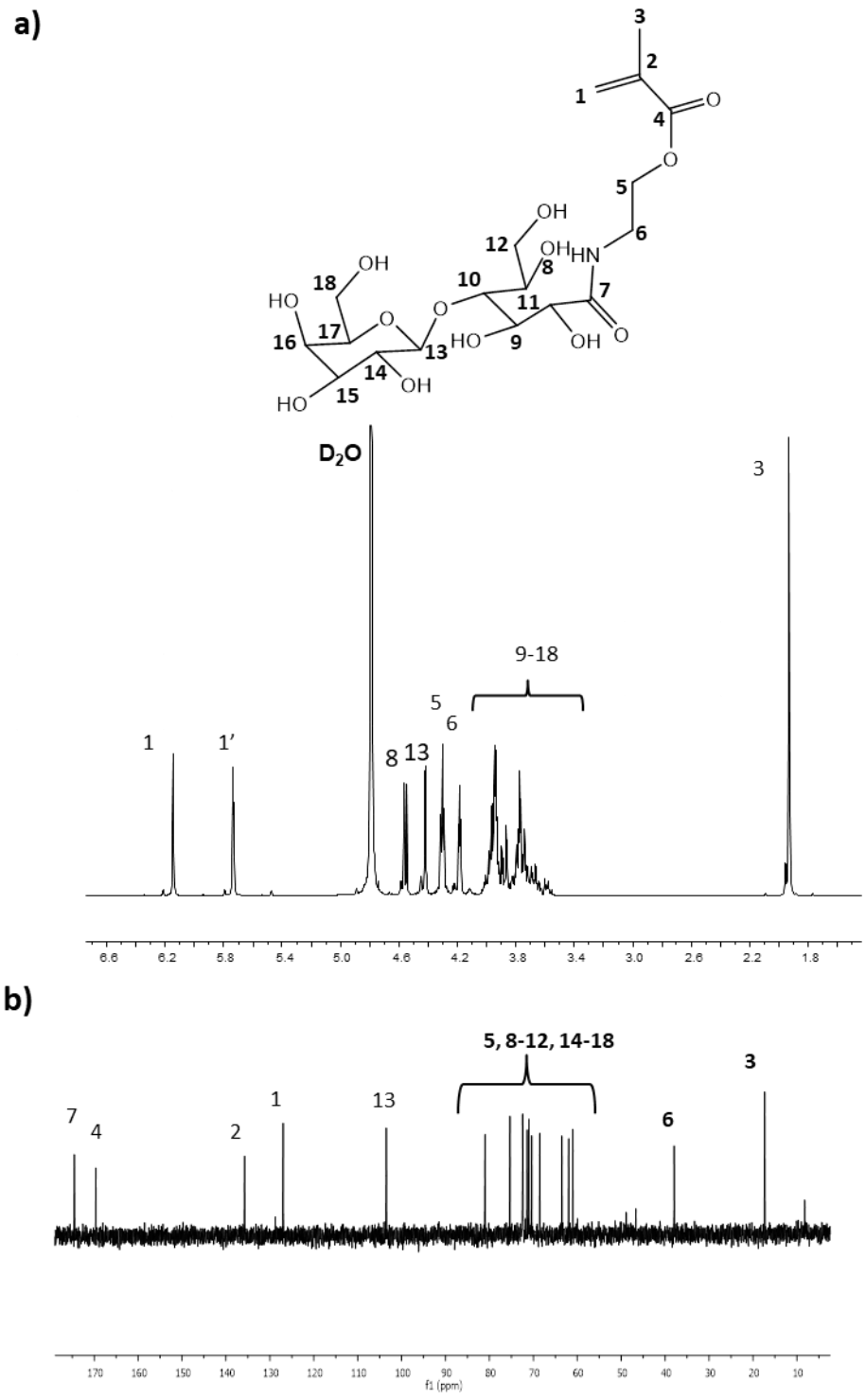

Figure 9– 400 MHz ^{1}H and ^{13}C NMR spectra in D_2O of LAMA monomer.

The chemical structure of LAMA monomer was confirmed by ^{1}H and ^{13}C NMR spectroscopy **Figure 9** and it is in accordance with literature.[35] Then, AMA, a recognized hard-to-polymerize primary amine methacrylate-containing monomer, which ensures the polyplex formation via electrostatic interactions with genetic the

material, was further polymerized with LAMA through ARGET ATRP. Previously, LAMA and AMA were polymerized by ATRP in 3:2 methanol/water or in isopropanol (IPA)/water mixtures, using CuBr/ bipyridine complex as a catalyst, to obtain different AMA- and LAMA-block copolymers.[35,40] However, due to the lack of chain-end functionality of PAMA-Br, the preparation of well-defined block copolymers was not possible.[40] To overcome this critical problem, the synthesis of well-defined copolymers was carried out using ARGET ATRP in a 1:1 DMF/water mixture, using a slow feeding of ascorbic acid for the regeneration of the activator.[41] Compared to the normal ATRP, the synthesis of glycopolymers using this method may be more advantageous because it allows control over the molecular weight of the polymers using a much lower concentration of the metal catalyst.[42] In addition, this synthesis approach enabled the copolymerization of both monomers without the problematic multistep protection/deprotection reactions typical for the synthesis of glycopolymers.

To evaluate the effects of glycopolymer composition and carbohydrate/cationic ratio on transfection capacity, cytotoxicity and targeting ability of the obtained polyplexes, different carbohydrate homopolymers, cationic homopolymers, random and diblock copolymers with different degrees of polymerization (DP) values of AMA and LAMA were synthetized (Table 6).

Table 6 - Composition and molecular weight parameters of glycopolymers synthetized by ARGET ATRP.

Polymer composition	M_n^{th} **x** $10^{3\,a}$	M_n^{SEC} **x** $10^{3\,b}$	$Đ$
$PLAMA_{70}$	33.1	37.7	1.03
$PAMA_{161}$ [c]	25.7	26.9	1.10
PEG_{45}-*b*-$PAMA_{168}$ [c]	29.9	28.8	1.10
$PAMA_{38}$-*co*-$PLAMA_{47}$	29.9	28.8	1.10
$PAMA_{87}$-*co*-$PLAMA_{42}$	34.3	26.0	1.18
$PAMA_{94}$-*co*-$PLAMA_{9}$	20.1	21.0	1.15
$PAMA_{114}$-*co*-$PLAMA_{20}$	28.5	35.1	1.05
$PAMA_{92}$-*co*-$PLAMA_{95}$	60.3	49.4	1.15
$PAMA_{50}$-*b*-$PLAMA_{49}$	32.1	32.1	1.21
$PAMA_{97}$-*b*-$PLAMA_{44}$	37.1	34.5	1.11

$PAMA_{\mathbf{108}}$-*b*-$PLAMA_{\mathbf{14}}$	24.5	26.0	1.20
$PAMA_{\mathbf{118}}$-*b*-$PLAMA_{\mathbf{6}}$	21.7	23.7	1.21
$PAMA_{\mathbf{90}}$-*b*-$PLAMA_{\mathbf{113}}$	73.1	52.5	1.05

M_n, number-average molecular weight; $Đ$, dispersity (M_w/M_n). [a] Determined from monomer conversion. For random glycopolymers M_n^{th} = [(AMA conversion/100) × DP_{AMA} × M_{WAMA}] + [(LAMA conversion/100) × DP_{LAMA} × $M_{W\ LAMA}$] + $M_{W,\ EBPA}$ For diblock glycopolymers: M_n^{th} = [(LAMA conversion/100) × DP_{LAMA} × $M_{W\ LAMA}$] + $M_{W,\ PAMA\text{-}Br}$; [b] Determined by SEC using conventional calibration with PEG standards. [c] The synthesis and characterization of $PAMA_{161}$ and PEG_{45}-*b*-$PAMA_{168}$ can be found in a previous report.[37]

The PAMA-*b*-PLAMA diblock copolymers were prepared by "one-pot" ARGET ATRP, i.e. AMA was first allowed to react until a near quantitative conversion was achieved (> 91%), and then LAMA was added to the reaction mixture to form the second block (Scheme 3). For comparative purposes, analogous PAMA-*co*-PLAMA random copolymers (similar DP value of both blocks) were also synthetized by ARGET ATRP to evaluate the effect of polymer structure on the performance of the nanosystems.

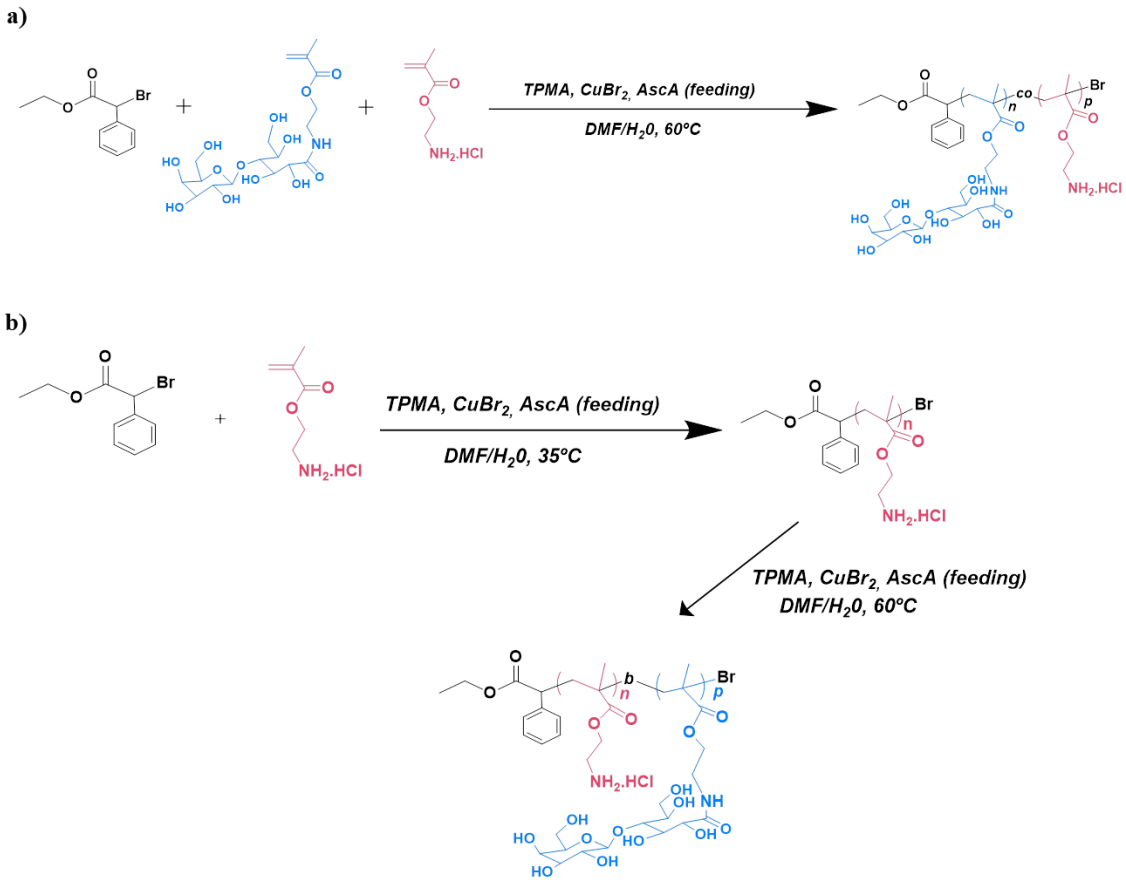

Scheme 3– ARGET ATRP of AMA and LAMA for the synthesis of random (a) and block (b) glycopolymers.

The PAMA homopolymer and PEG-*b*-PAMA block copolymer were also synthesized by the same method, to serve as control samples, as we previously confirmed their potential as gene delivery systems.[37] The polymers were purified by dialysis against water and then lyophilized yielding solids with high water solubility, which allowed their application as gene delivery systems. The structure of the polymers was confirmed by ^{1}H NMR spectroscopy (Figure 10, Figure A1 and Figure A2, Appendix A) and the molecular weights were determined by SEC (Figure 10, Figure A1 and Figure A1, Appendix A).The obtained results showed that the developed ARGET ATRP method yielded homopolymers, random glycopolymers and block glycopolymers with good control over molecular weight, as illustrated by representative monomodal SEC chromatograms (Figure 10, Figure A1 and Figure A2, Appendix A), and the low dispersity values ($Đ \leq 1.2$,Table 6).

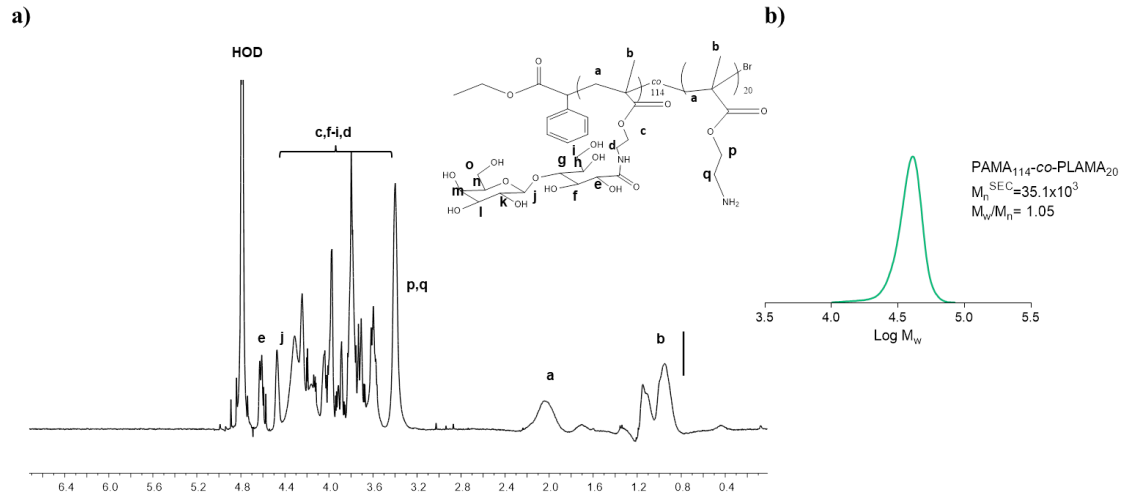

Figure 10–400 MHz ^{1}H NMR spectrum in D_2O (a) and SEC trace (b) of the $PAMA_{114}$-*co*-$PLAMA_{20}$ random copolymer prepared by ARGET ATRP.

To the best of our knowledge, galactose methacrylate-based copolymers synthetized by ARGET ATRP have never been investigated for the preparation of gene delivery carriers.

2.3.2. Physicochemical characterization of the nanosystems

The physicochemical properties of the polymeric-based nanosystems have a major impact on their ability to mediate gene delivery into target cells. To correlate the biological activity with the physicochemical properties of the developed glycopolymer-based nanosystems, we evaluated their ability to condense and protect DNA, their size, and their surface charge (Figure 11).

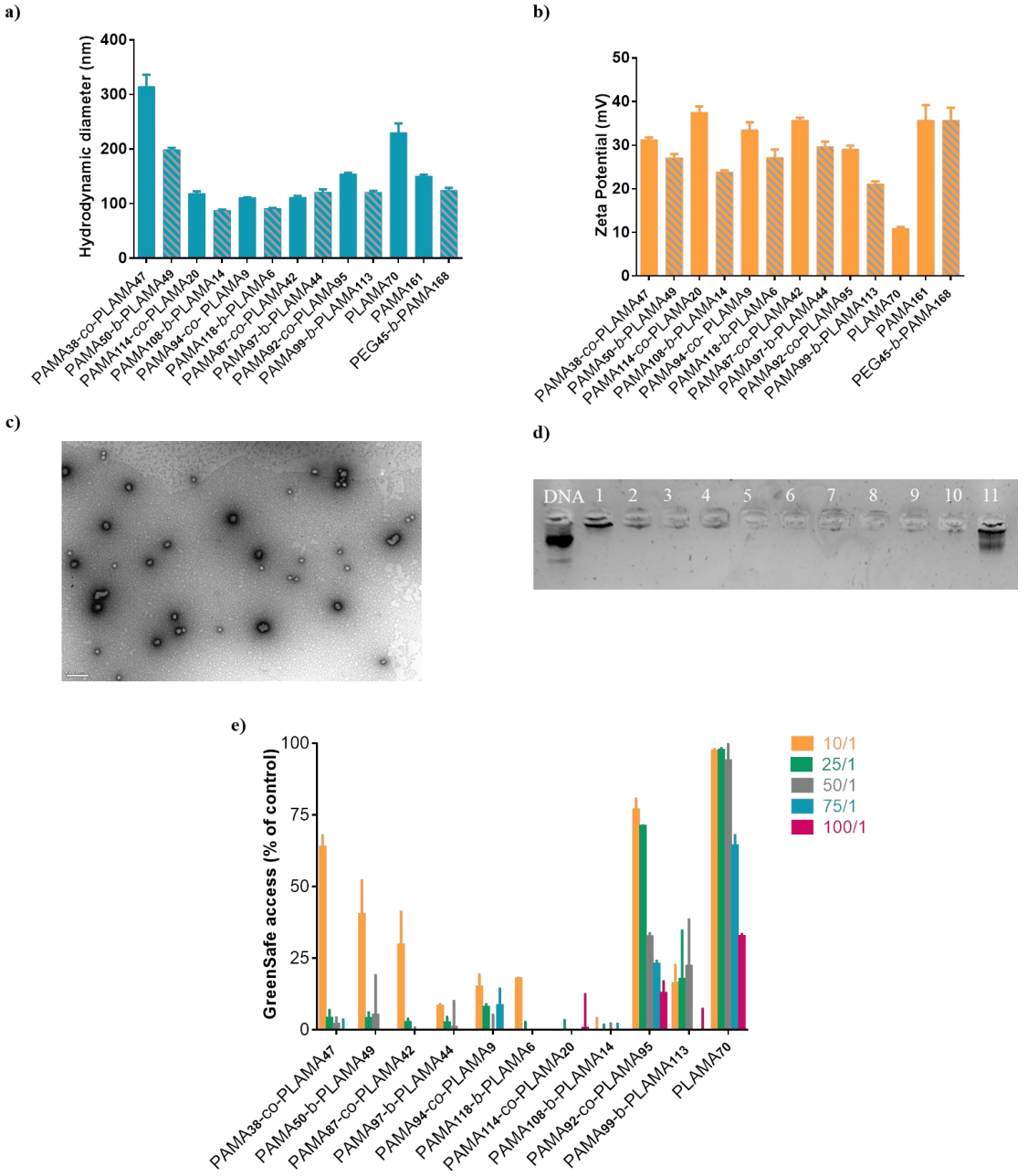

Figure 11– Physicochemical properties of the nanosystems: (a) hydrodynamic diameter, (b) zeta potential, (c) TEM imaging, (d) agarose gel electrophoresis assay and (e) DNA complexation efficiency. (a,b) Nanosystems were prepared with 1 µg of plasmid DNA at 50:1 N/P ratio. Statistical analysis of results is available in Table A1 and Table A2 of Appendix A. (c) For TEM analysis, $PAMA_{114}$-*co*-$PLAMA_{20}$-based polyplexes were prepared with 1 µg of plasmid DNA at 50:1 N/P ratio (scale bar = 200 nm). (d) Polyplexes prepared with different glycopolymers (1–$PAMA_{38}$-*co*-$PLAMA_{47}$, 2– $PAMA_{50}$-*b*-$PLAMA_{49}$, 3– $PAMA_{87}$-*co*-$PLAMA_{42}$, 4– $PAMA_{97}$-*b*-$PLAMA_{44}$, 5– $PAMA_{94}$-*co*-$PLAMA_{9}$, 6– $PAMA_{118}$-*b*-$PLAMA_{6}$, 7– $PAMA_{114}$-*co*-$PLAMA_{20}$, 8–$PAMA_{108}$-*b*-$PLAMA_{14}$, 9– $PAMA_{92}$-*co*-$PLAMA_{95}$, 10– $PAMA_{99}$-*b*-$PLAMA_{113}$, 11–$PLAMA_{70}$), at 50/1 N/P ratio, were analyzed by gel electrophoresis. (e) Quantification of Green Safe access to DNA of the different formulations.

From the DLS measurements, presented in Figure 11, it is evident that the size of the developed nanosystems depends on both the DP value of AMA and the composition of the glycopolymers. The results show that glycopolymers with a low DP of AMA, such as $PAMA_{38}$-*co*-$PLAMA_{47}$, form larger polyplexes than copolymers with a higher cationic content. The increase of AMA content in the glycopolymers improved their DNA condensation ability and decreased the size of the nanocarriers, even for copolymers with higher carbohydrate content. Morphological characterization by TEM imaging (Figure 11c) revealed that $PAMA_{114}$-*co*-$PLAMA_{20}$-based polyplexes had a spherical shape and a small particle size, confirming the DLS data. Moreover, the results presented in Figure 1a showed that the size of the developed nanosystems depends on the structure of the glycopolymer. In general, polyplexes prepared with block copolymers were smaller than the corresponding random glycopolymers, suggesting that the complexation of DNA by both types of macromolecules is different. In the case of the PAMA-*b*-PLAMA glycopolymers, the plasmid DNA was complexed by the PAMA segment of the glycopolymer in the core of the nanocarrier, leaving a shell of the PLAMA block.

Regarding the zeta potential of the developed nanosystems, the results presented in Figure 11b shows that their surface charge depends on their carbohydrate/cationic ratio and the composition of the glycopolymer. The nanocarriers prepared at N/P ratio of 50/1, exhibited a positive surface charge, ranging from +10 to +40 mV. As expected, the nanocarriers prepared with PLAMA homopolymer exhibited lower zeta potential than the nanosystems prepared with a cationic containing glycopolymer. The latter nanocarriers exhibited high positive zeta potential values, similar to those obtained for PEG_{45}-*b*-$PAMA_{168}$-based polyplexes, regardless the glycopolymer composition. These galactose-containing polyplexes were prepared at an N/P ratio of 50/1, corresponding to an excess of positive charge that could justify the cationic surface of these PAMA-*co*-PLAMA- and PAMA-*b*-PLAMA- based nanocarriers. Some authors have studied the influence of glycopolymer carbohydrate/cationic ratio on the physicochemical properties of polyplexes, showing that the incorporation of carbohydrate moieties in nanocarriers leads to a decrease in their surface charge compared to the corresponding cationic polymer-based nanosystems.[33] However, in these studies, the nanocarriers were formulated using glycopolymers with a typical carbohydrate/cationic ratio of 0.9 - 1.0 and were prepared at N/P ratios lower than 10/1.[24] Moreover, our results showed that random glycopolymers produced polyplexes with higher positive zeta potential values

than their corresponding block copolymers. This fact could be justified by their different structural rearrangement during polyplex formation. While diblock glycopolymers assemble in a core-shell configuration, the random glycopolymers exhibit a random distribution of cationic and carbohydrate moieties, with equal probability of displaying these segments on the surface of the polyplexes.[33]

The Green Safe intercalation assay was performed to evaluate whether the developed nanocarriers are able to condense the plasmid DNA. The results presented in Figure 11e show a decrease in the green safe fluorescence with the increase in the N/P ratio of the polyplexes for all the developed nanosystems, except for the PLAMA-based nanocarriers. This shows that increasing the content of cationic segments in the glycopolymers leads to a higher degree of condensation and protection of DNA. The glycoplexes prepared with PLAMA homopolymers, in which the condensation of DNA occurs only via hydrogen bonds, presented the highest levels of intercalating agent access. This very low condensation ability, observed for all tested N/P ratios of PLAMA-based glycoplexes, could result in a poor performance in terms of gene delivery, possibly releasing DNA earlier than expected or allowing its degradation before it reaches the nucleus. In addition, it was found that the $PAMA_{92}$-*co*-$PLAMA_{95}$-based polyplexes exhibited a high degree of green safe access, which could be explained by the high content of LAMA and the random distribution of cationic charges. The data obtained in the green safe accessibility assays were confirmed by the agarose gel electrophoresis assay (Figure 11d).

2.3.3. Transfection activity and cytotoxicity of glycopolymer-based polyplexes

To evaluate the potential of PLAMA-based glycopolymers as gene delivery nanocarriers, a preliminary study was performed in HepG2 cells using luciferase as a reporter gene.

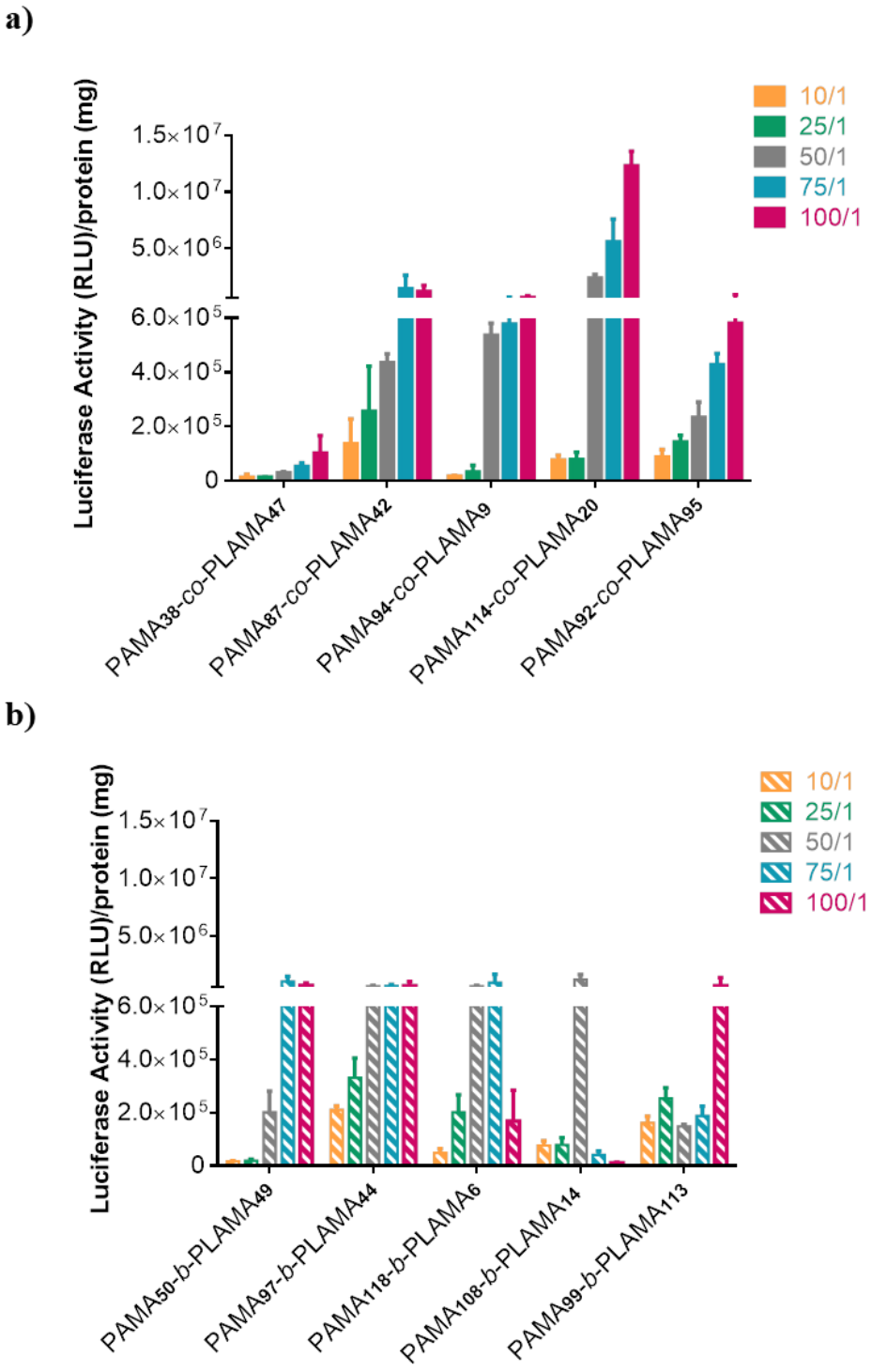

Figure 12– Biological activity of random- (a) and block- (b) based glycoplexes in HepG2 cells. Nanosystems were prepared by complexing the glycopolymers with 1 μg of plasmid DNA encoding luciferase (pCMV.Luc) at different N/P ratios. Statistical analysis of results is available in Table A3 of Appendix A.

As shown in Figure 12, the ability of the different nanosystems to effectively deliver genetic material into HepG2 cells depends on their composition and N/P ratio. For

polyplexes prepared with random glycopolymers, transgene expression was enhanced with increasing N/P ratio (Figure 12a). Moreover, the results showed that polyplexes based on $PAMA_{87}$-*co*-$PLAMA_{42}$- and $PAMA_{114}$-*co*-$PLAMA_{20}$ exhibited higher transgene expression than nanocarriers based on $PAMA_{38}$-*co*-$PLAMA_{47}$. This suggests that in nanosystems prepared with glycopolymers of similar molecular weight, the transfection activity is enhanced by increasing the content of the cationic component (PAMA). This fact can be possibly justified by the higher DNA condensation ability as well as by the final structure of the nanosystems, which could allow an improved interaction with the cells, leading to a higher gene delivery efficiency. Moreover, these polyplexes prepared from glycopolymers with a higher content of AMA could most likely be involved in a greater interaction with the endosomal membrane, promoting their efficient escape from the endolysosomal pathway into the cytoplasm, thus leading to an increase in their transfection capacity.[43]

For diblock glycopolymers, transgene expression was also improved by the increase of the N/P ratio (Figure 12b). The results also showed that glycoplexes prepared with block copolymers generally exhibited lower level of transgene expression than those prepared with the corresponding random copolymers. In contrast to what was observed with random-based glycoplexes, the transfection activity obtained at high N/P ratios was not improved by the increase in the AMA content. For example, nanocarriers prepared with $PAMA_{50}$-*b*-$PLAMA_{49}$, the glycopolymer with shortest chain length of PAMA, had similar transfection levels as $PAMA_{97}$-*b*-$PLAMA_{44}$-based polyplexes. The higher condensation of genetic material by diblock glycopolymers may lead to limited DNA unpacking inside the cells, which could partially justify the lower transfection ability when compared to that obtained with polyplexes prepared with random glycopolymers (Figure 11e).

The cell viability studies, performed in HepG2 cells, showed that the cytotoxicity of the developed nanosystems was dependent on their N/P ratio, on the composition and carbohydrate/cationic ratio of the glycopolymers (Figure 13).

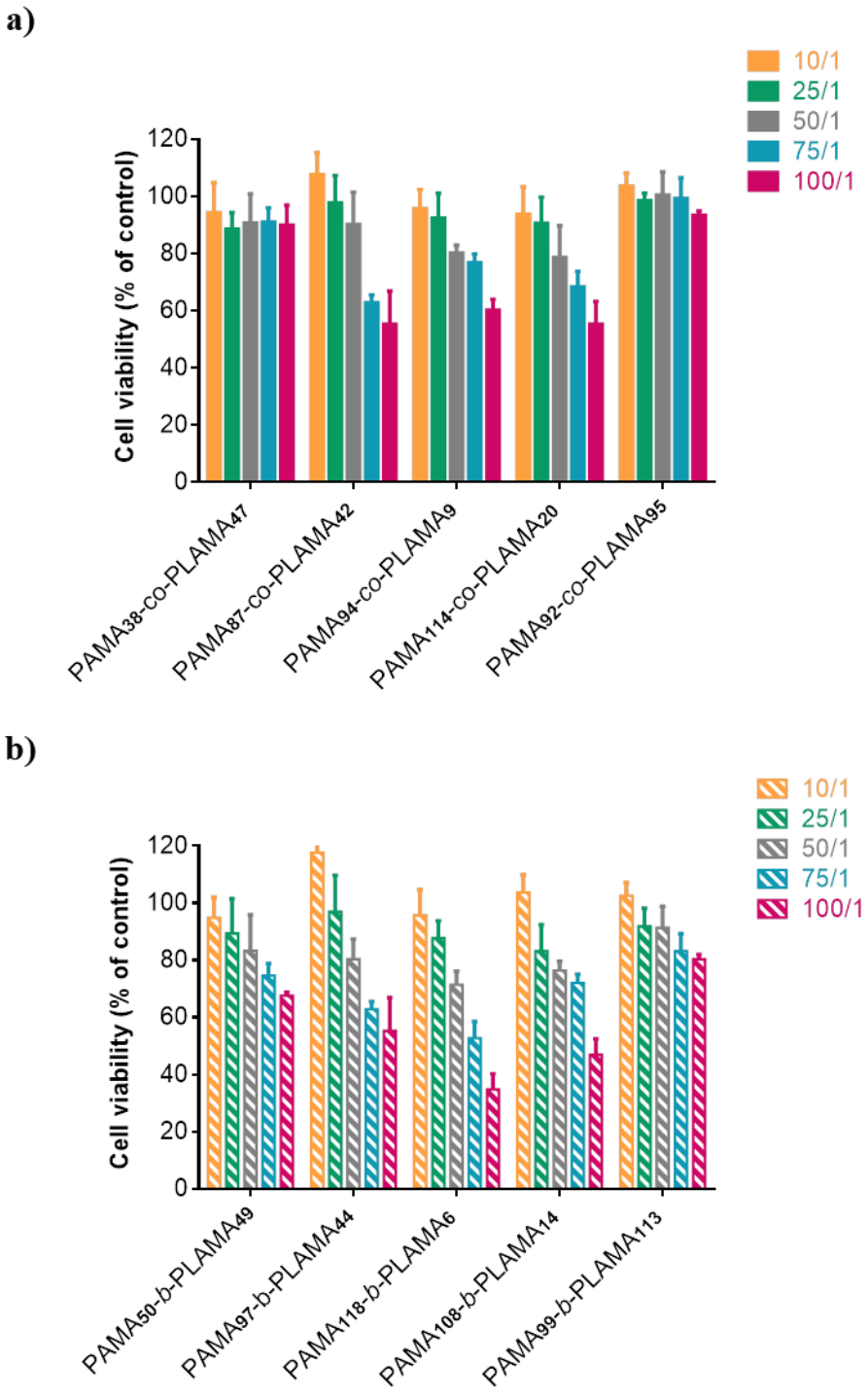

Figure 13– Cytotoxicity of random- (a) and block- (b) based glycoplexes in HepG2 cells. Polyplexes were prepared by complexing the glycopolymers with 1 µg of plasmid DNA encoding luciferase (pCMV.Luc), at different N/P ratios. Statistical analysis of results is available in Table A4 of Appendix A.

For both random and block glycopolymers-based nanosystems, cell viability decreased with the increase of N/P ratio and with the increase of DP from AMA. The significant

cytotoxicity observed with polyplexes prepared at the highest N/P ratios and DP of AMA can be explained by the multiple and strong interactions that can occur between glycoplexes and the cytoplasmic membrane or intracellular organelles, causing membrane destabilization, which in turn affects the metabolic activity of the cells.[44] On the other hand, the data also showed that the increase in the proportion of carbohydrates relatively to the cationic content improves the biocompatibility of the developed nanosystems. It is expected that the increase of the LAMA content decreases the density of the positive charge of the cationic polymer, thus reducing the cytotoxicity of the polyplexes. The structure (block *versus* random) of the glycopolymers also played a crucial role in the cytotoxicity of the developed nanocarriers, as reported by other authors.[33,31] The polyplexes prepared with block copolymers exhibited higher cytotoxicity than the nanosystems prepared with random copolymers, suggesting that the block configurations are less able to mask the cationic content of the glycopolymers than the corresponding random copolymers.

To evaluate the robustness of the developed nanocarriers as gene delivery systems to HCC, transfection assays were performed in two other hepatocellular carcinoma cell lines, Hep3B and Huh-7 cells (Figure 14).

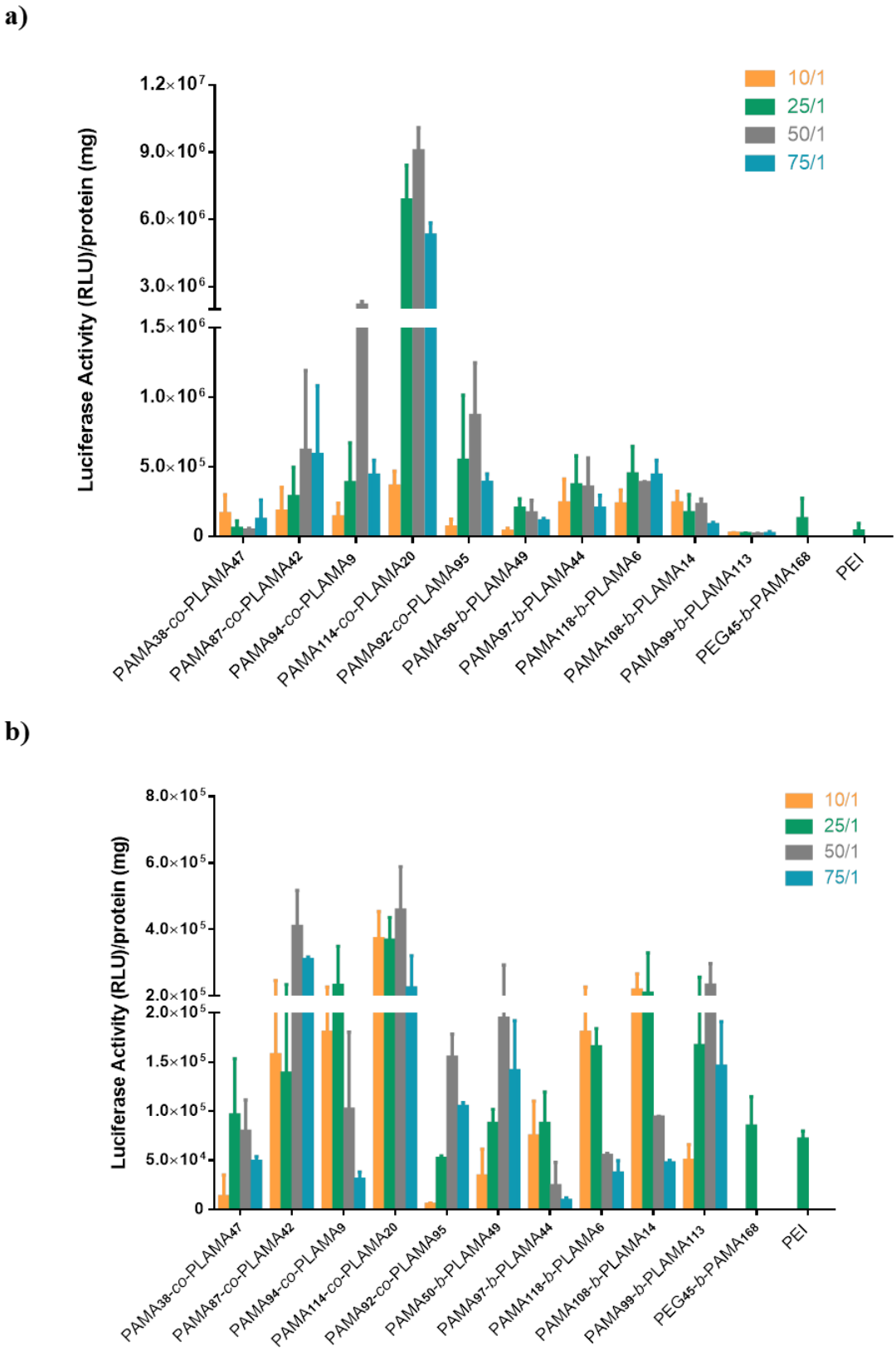

Figure 14- Transfection activity of random- and diblock-based glycoplexes in Hep3B (a) and Huh-7 (b) cells. Glycoplexes were prepared with 1 μg of pCMV.Luc, at different N/P ratios.

Remarkably, in both Hep3B and Huh-7 cells, $PAMA_{114}$-*co*-$PLAMA_{20}$-based nanosystems, prepared at 25/1 and 50/1 N/P ratios, showed the highest level of luciferase expression. Regarding cytotoxicity, as observed in HepG2 cells, the data obtained showed that increasing the N/P ratio of the nanosystems and increasing the cationic content of the glycopolymer resulted in lower cell viability (Figure A3, Appendix A).

In general, incorporation of carbohydrate moieties into polymer-based nanocarriers reduces their transfection efficiency. For example, Nairin´s group investigated the potential of methacrylamide-based glycopolymers as nanosystems for gene delivery and showed that incorporation of carbohydrate units reduced both toxicity and transfection activity.[33] The authors demonstrated that the glycopolymers-based nanosystems resulted in lower transgene expression than poly (2-amino ethyl methacrylamide) $PAEMA_{90}$-based polyplexes. However, as shown in the data presented in Figure 15a, the biological activity of $PAMA_{114}$-*co*-$PLAMA_{20}$- and $PAMA_{108}$-*b*-$PLAMA_{14}$-based nanosystems, was much higher than that of polyplexes based on $PAMA_{161}$- and PEG_{45}-*b*-$PAMA_{168}$, suggesting that the gene delivery capacity of nanocarriers prepared with methacrylate-based glycopolymers can be significantly enhanced by these hydrophilic moities (at least for certain carbohydrate/cationic ratios). These results may be partially justified by the higher susceptibility of methacrylate-based copolymers to hydrolysis compared to their acrylamide counterparts, which may facilitate the release of DNA for transcription in the nucleus. [45] In addition, methacrylamide-based copolymers generally have higher p*K*a values, which have a lower buffering capacity and, consequently, a lesser ability to promote the endolysosomal escape of nanocarriers and thus transgene expression.[46] Regarding to carbohydrate/cationic moieties distribution, in general random-based glycopolymers exhibited higher potential as gene delivery nanocarrier than their corresponding block-based glycopolymers.[47] However, for most of the developed nanocarriers, with the exception of $PAMA_{114}$-*co*-$PLAMA_{20}$- and $PAMA_{108}$-*b*-$PLAMA_{14}$-based nanosystems, it was not found a significant difference in terms of biological activity between the block- and random-based glycoplexes (Figure 15a). In addition, the results showed that further increasing the carbohydrate content, as in the case of $PAMA_{92}$-*co*-$PLAMA_{95}$-based nanocarriers, resulted in lower transgene expression. As shown by other authors, the decrease in transfection activity with increasing carbohydrate content could be explained by the stereo effect promoted by galactose units, which could reduce cellular internalization and endosomal escape.[22] In

this context, polyplexes based on $PAMA_{114}$-*co*-$PLAMA_{20}$ showed the highest transfection activity at a carbohydrate/cationic molar ratio of 0.2.

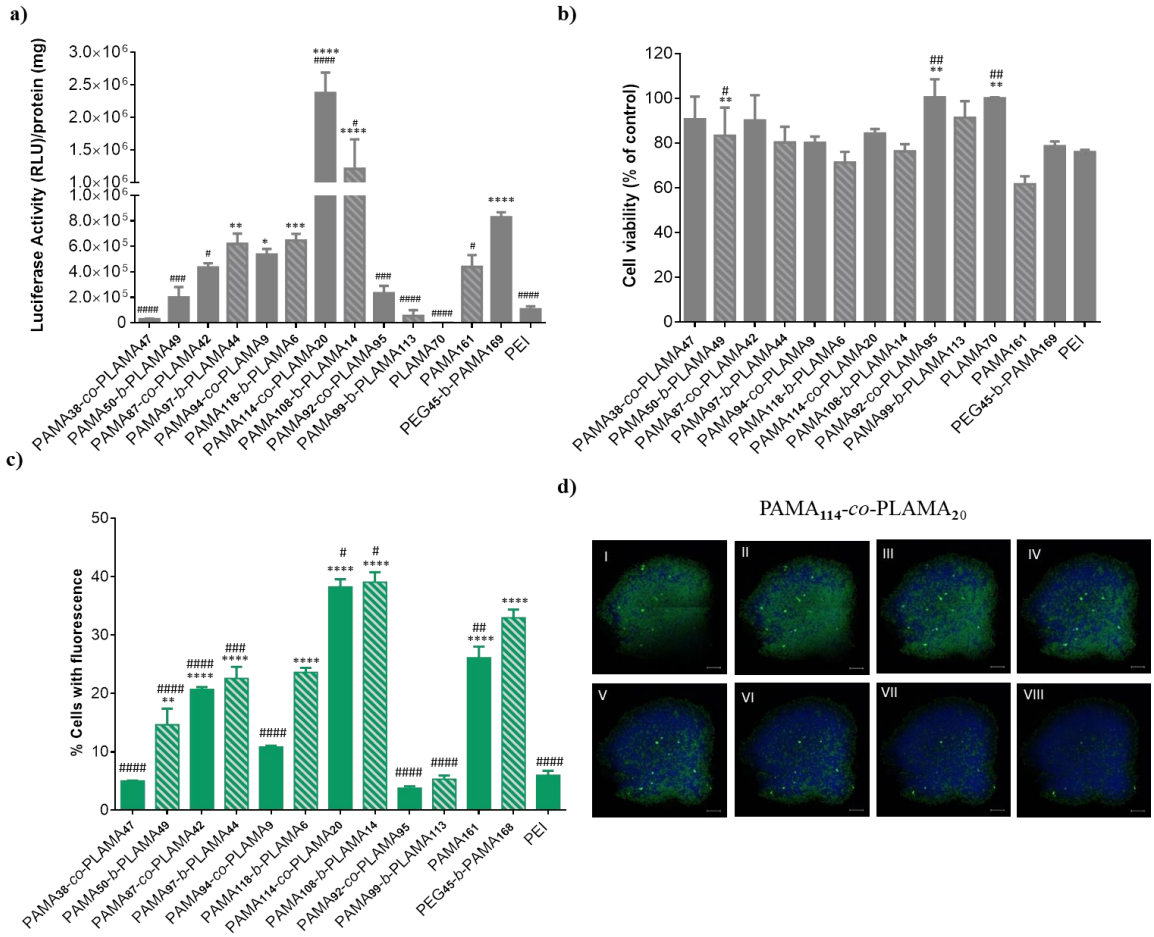

Figure 15– Biological activity (a), cell viability (b) and transfection efficiency of different glycoplexes in HepG2 cells (c) and in tumor spheroids (d). Polyplexes were prepared by complexing glycopolymers, $PAMA_{161}$ and PEG_{45}-*b*-$PAMA_{168}$ with 1 μg of pCMV.Luc (a and b) or pCMV.gfp (c), at 50/1 N/P ratio. Asterisks (****p < 0.0001, ***p < 0.001, **p < 0.01, and *p < 0.05) and cardinals (####p < 0.0001, ###p < 0.001, and #p < 0.05) indicate values with statistical significance when compared to those obtained with the standard formulation, PEI-based nanosystem at 25/1 N/P ratio, or with PEG_{45}-*b*-$PAMA_{168}$-based polyplexes, respectively. (d) Polyplexes were prepared by complexing $PAMA_{114}$-*co*-$PLAMA_{20}$-based polyplexes with 0.5 μg of pCMV.gfp, at 50/1 N/P ratios. The cell nucleus was stained by DAPI (blue). Scale bar = 100 μm.

The results presented in Figure 15b show that PEI-, $PAMA_{161}$- and PEG_{45}-*b*-$PAMA_{168}$-based polyplexes exhibit higher cytotoxicity than most PLAMA containing nanocarriers, confirming the high ability of carbohydrate moieties to mask the cationic charge of nanosystems, and thus improve their biocompatibility. To evaluate the effects of glycopolymer composition and carbohydrate/cationic ratio on the percentage of

transfected cells, flow cytometry analysis was performed after transfection of cells with the developed glycoplexes prepared with pCMV.gfp (Figure 15c). The obtained results showed that transfection of HepG2 cells with $PAMA_{114}$-*co*-$PLAMA_{20}$- and $PAMA_{108}$-*b*-$PLAMA_{14}$-based polyplexes resulted in a large number of GFP-expressing cells. Moreover, these nanocarriers promoted a much higher percentage of transfected cells than the PEI-based polyplexes, which are recognized as the gold standard for polymerbased gene delivery nanosystems.[48]

Taking together the results of biological activity and cytotoxicity in different HCC cell lines, it was demonstrated that the $PAMA_{114}$-*co*-$PLAMA_{20}$-based polyplexes are the best formulation, promoting the highest transfection activity with lower cytotoxicity.

Since 3D tumor spheroids provide more realistic spatial and pharmacologically relevant information and bridge the experimental gap between *in vivo* and *in vitro* results, we investigated the potential of $PAMA_{114}$-*co*-$PLAMA_{20}$-based polyplexes as gene nanocarrier in tumor spheroids obtained with HepG2 cells.[49] The results shown in Figure 15d demonstrate that $PAMA_{114}$-*co*-$PLAMA_{20}$-based polyplexes could transfect not only the surface cells of tumor spheroids, but also cells in the nucleus of the spheroids. In contrast, nanocarriers based on PEG_{45}-*b*-$PAMA_{168}$ showed reduced transfection capacity, being observed only a slight GFP expression in the spheroids surface (Figure A4, Appendix A). The accentuated difference between these two formulations was even more pronounced in 3D HepG2 cell cultures than in 2D ones cell cultures, which may be due to an increase in ASGPR levels in tumor spheroids.[50] Therefore, this novel nanocarrier revealed a high ability to penetrate and deliver genetic material into 3D tumor masses.

2.3.4. Asialoglycoprotein receptor-targeted glycoplexes

The ASGPR binds specifically to galactose or *N*-acetylgalactosamine terminal residues of desialylated glycoproteins and the binding affinity increases with the valence of the sugar residues via a phenomenon known as the cluster effect.[51] To determine whether the developed nanosystems are specifically recognized by the ASGPR of HCC cells, the effect of a high concentration of free asialofetuin (a specific ligand of the ASGPR used as a competitive agent) and an antibody against the ASGPR, on the biological activity of the glycoplexes was investigated.

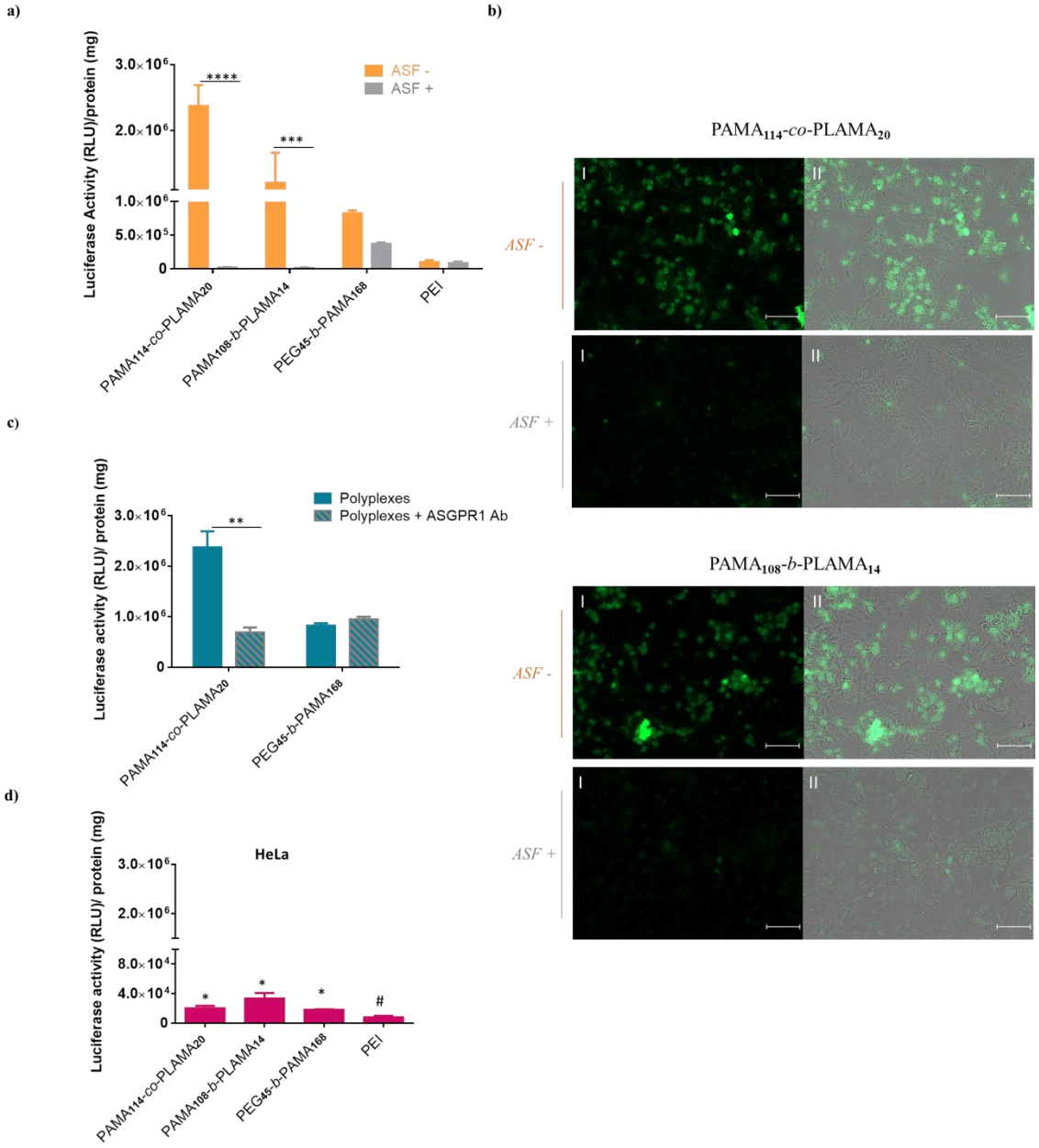

Figure 16– Effect of the presence of asialofetuin (a,b) and an antibody against the ASGPR (c) on the biological activity of different nanosystems in HepG2 cells. The biological activity was assessed by luminescence (a,c) and fluorescence microscopy (b) in HepG2 cells transfect with different nanosystems. Biological activity of polyplexes in Hela cells (d). Asialofetuin or antibody against the ASGPR were added to HepG2 cells 1 h before the addition of polyplexes. Polyplexes were prepared by complexing the polymers with 1 μg of pCMV.Luc (a,c,d) or pCMV.gfp (b), at their optimal N/P ratios. Asterisks (****$p < 0.0001$, ***$p < 0.001$ and **$p < 0.01$) correspond to values that differ significantly from those obtained with the same formulations in the absence of asialofetuin or Ab against ASGPR. (b) Fluorescence microscopy (I) and overlapping of fluorescence microscopy and phase contrast images (II) of cells transfected with different formulations at 50:1 N/P ratio (scale bar = 50 μm). (d) Asterisks (*$p < 0.05$) and cardinals (#$p < 0.05$) indicate values with statistical significance when compared to those obtained with the standard formulation, PEI-based nanosystem at 25/1 N/P ratio, or with PEG_{45}-*b*-$PAMA_{168}$-based polyplexes, respectively.

The results presented in Figure 16a showed that the presence of asialofetuin drastically reduces the transgene expression of $PAMA_{114}$-*co*-$PLAMA_{20}$- and $PAMA_{108}$-*b*-$PLAMA_{14}$-based polyplexes, whereas it did not significantly alter the biological activity of PEG_{45}-*b*-$PAMA_{168}$- and PEI-based nanocarriers. This assay was also performed in Huh-7 and Hep3B cells, ASGPR-rich cell lines, where a similar decrease in the biological activity of the developed glycoplexes was observed in the presence of asialofetuin (Figure A5, Appendix *A*). Fluorescence microscopy data also indicated that asialofetuin binds to the ASGPR, blocking the internalization of the developed glycoplexes and thus resulting in a notably lower number of GFP-expressing cells than in the absence of asialofetuin (Figure 16b). On the other hand, the transfection efficiency of the nanosystems prepared with PEI was not significantly affected by incubation with asialofetuin, supporting the observation that the developed glycoplexes are specifically recognized by the ASGPR on the surface of HepG2 cells (Figure 5, Appendix A). In addition, transfection activity was also assessed in the presence of an antibody against the ASGPR. A strong reduction in the biological activity of the $PAMA_{114}$-*co*-$PLAMA_{20}$-based polyplexes, but not with the PEG_{45}-*b*-$PAMA_{168}$-based ones, was observed (Figure 16c). Moreover, the biological activity of these formulations was also examined in ASGPR-deficient cells (Hela cells) (Figure 16d).[52,33] The obtained results showed that the higher transfection activity of galactose-containing nanocarriers, achieved in HepG2, Hep3b and Huh-7 cells, compared to PEI-based nanosystems, was not observed in Hela cells. Therefore, all these results clearly indicate that the developed glycoplexes have the ability to specifically bind to the ASGPR, via the galactose residues, which significantly enhances their cell internalization and consequently their transfection activity.

2.3.5. The endocytosis and intracellular fate of glycoplexes

The ASGPR specifically binds to the galactose terminal residues of desialylated glycoproteins and then internalizes them via clathrin-coated pit endocytosis. To elucidate the endocytic mechanism involved in the cell internalization of $PAMA_{114}$-*co*-$PLAMA_{20}$- and $PAMA_{108}$-*b*-$PLAMA_{14}$-based polyplexes, their biological activity was studied in the presence of various endocytosis inhibitors: chlorpromazine, which inhibits clathrin-mediated endocytosis; filipin, which prevents caveolae-mediated endocytosis; and amiloride, which inhibits macropinocytosis. Several concentrations of each inhibitor were tested to determine the lowest drug concentration at which the

inhibitor is active, without causing high cytotoxicity (Figure A7 and Figure A8, Appendix A).

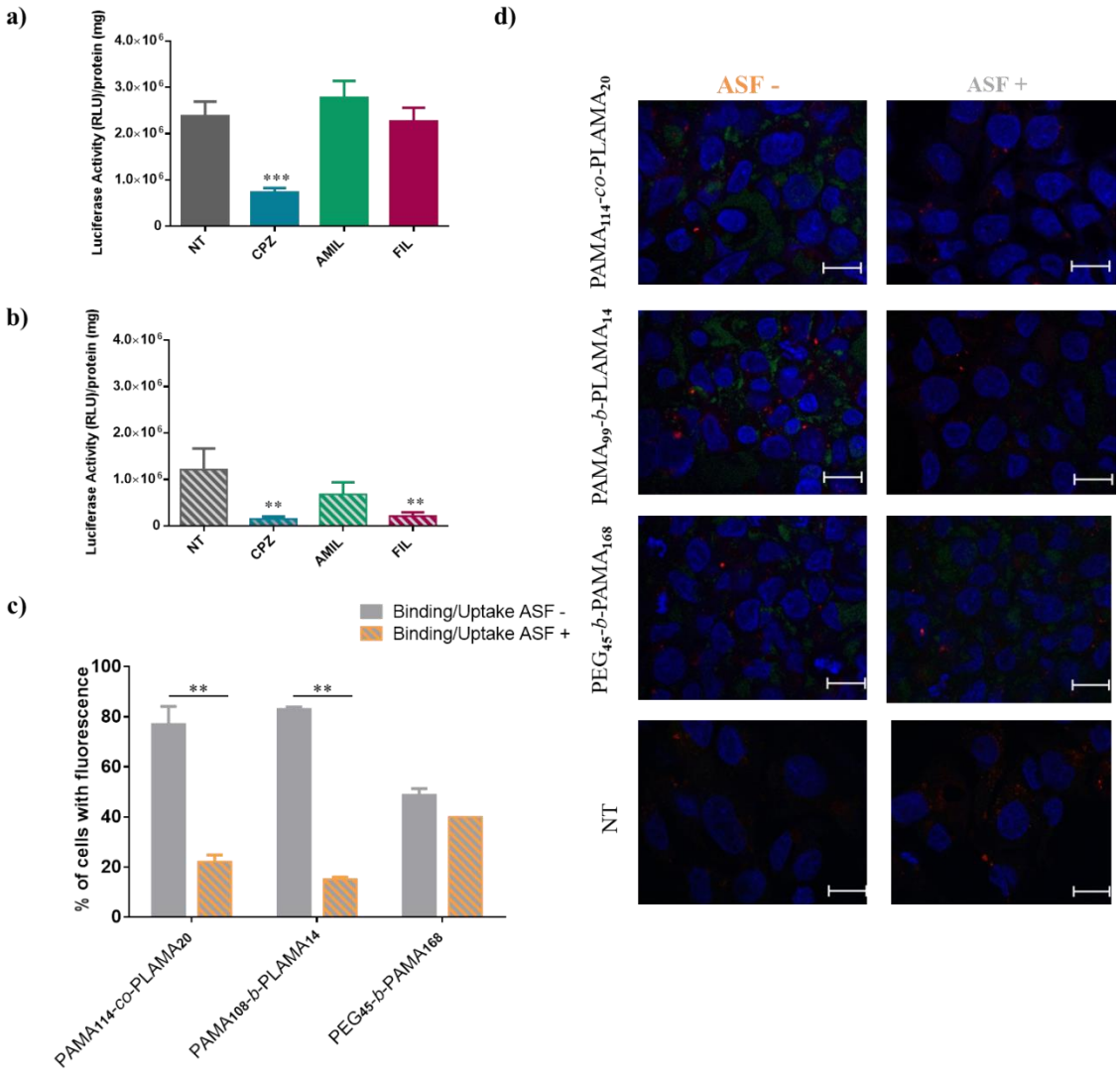

Figure 17– Effect of endocytosis inhibitors on the transfection ability of $PAMA_{114}$-*co*-$PLAMA_{20}$- (a) and $PAMA_{108}$-*b*-$PLAMA_{14}$- (b) based polyplexes and the influence of asialofetuin in their cell binding and cell internalization (c,d). (a,b) HepG2 cells were treated or not treated (Nt) with endocytosis inhibitors: CPZ (50mM), Fil (1μg/mL) and Amil (0.25mM). Asterisks (***$p < 0.001$ and **$p < 0.01$) indicate values with statistical significance when compared to those measured in the control (cells non-treated). (c) Cellular binding /uptake evaluated by flow cytometry, asterisks (**$p < 0.01$) correspond to values that differ significantly from those obtained with the same formulations in the absence of asialofetuin. (d) Representative confocal microscopic images of cells treated with different nanosystems formulated at 50/1 N/P ratio (scale bar = 10 μm). The acidic cell compartments were labeled with Lysotracker Red DND-9 (red), the cell nucleus was stained by DAPI (blue) and polyplexes were prepared with 1% fluorescein-labeled glycopolymer (green).

As shown in Figure 17a and Figure A7a, preincubation of HepG2 cells with chlorpromazine resulted in a significant decrease in luciferase expression, suggesting that the clathrin-coated pit endocytic pathway is associated with the internalization of the developed PAMA$_{114}$-*co*-PLAMA$_{20}$-based nanosystems. This observation confirms the involvement of ASGPR in their cellular internalization due to the specific binding of the galactose molecules to this receptor. Regarding the PAMA$_{108}$-*b*-PLAMA$_{14}$-based polyplexes, the obtained results (Figure 17b and Figure A8a) showed that the transgene expression was negatively affected by the preincubation with chlorpromazine and filipin, suggesting the involvement of both clathrin- and caveolae-mediated endocytic pathways. This inhibition was not due to the cytotoxicity of the endocytic inhibitors, since no significant changes in cell viability were observed at the selected concentrations (Figure A7 and Figure A8, Appendix A). Therefore, the higher transfection activity of the polyplexes prepared with the PAMA$_{114}$-*co*-PLAMA$_{20}$ random glycopolymer, compared with the polyplexes prepared with the block glycopolymer PAMA$_{108}$-*b*-PLAMA$_{14}$ may also be due to their different internalization mechanisms.

The cellular uptake of the developed nanosystems containing 1% of fluorescein-labeled PAMA-*co*-PLAMA glycopolymer was assessed by flow cytometry and confocal microscopy, in the presence or absence of asialofetuin (Figure 17). The results presented in Figure 17d show that a substantial amount of PAMA$_{114}$-*co*-PLAMA$_{20}$- and PAMA$_{108}$-*b*-PLAMA$_{14}$-based nanocarriers, prepared at 50/1 N/P ratio, was observed inside almost all cells. Moreover, cellular uptake of polyplexes prepared with galactose-containing copolymers was significantly inhibited after pretreatment with asialofetuin, whereas PEG$_{45}$-*b*-PAMA$_{168}$-based polyplexes showed a similar extent of cellular internalization, regardless of preincubation with asialofetuin (Figure A9, Appendix A). Moreover, the developed formulations did not colocalize with lysosomal compartments (red fluorescence), suggesting that they efficiently escape from the endolysosomal pathway to the cytoplasm, preventing the nucleic acid degradation inside the lysosomes (Figure 17d and Figure A9). These nanosystems has a high content of PAMA, which contains primary amines that can potentially interact with and disrupt endosomal membranes, promoting the release of the polyplexes into the cell cytoplasm.[53] This fact also contributes to the great potential of PAMA-based polyplexes as nanosystems for gene delivery. Moreover, ASGPR-mediated cell binding and internalization of the engineered nanocarriers was confirmed by flow cytometry (Figure 17c). As expected,

the uptake of $PAMA_{114}$-*co*-$PLAMA_{20}$- and $PAMA_{108}$-*b*-$PLAMA_{14}$-based nanocarriers decreased drastically in the presence of asialofetuin. On the other hand, asialofetuin pretreatment did not significantly affect the cellular internalization of PEG_{45}-*b*-$PAMA_{168}$-based polyplexes (Figure 17c and Figure A10, Appendix A).

Overall, these results demonstrate that $PAMA_{114}$-*co*-$PLAMA_{20}$-based polyplexes bind specifically to the ASGPR, being internalized via clathrin mediated endocytosis, and efficiently escape from endolysosomal pathway, resulting in high transfection activity.

2.3.6. c-MYC downregulation to enhance sorafenib antitumor effect

c-MYC has been found to be highly expressed in HCC, and its overexpression has been associated with proliferation, differentiation and apoptosis inhibition of HCC cells.[54] To downregulate c-*MYC* expression in HCC cells, in order to sensitize them to SF, HepG2 cells were transfected with $PAMA_{114}$-*co*-$PLAMA_{21}$-based glycoplexes carrying a DNA plasmid that encodes a short hairpin RNA against this protein. RT-PCR assays were performed to investigate the inhibition extent of *c-MYC* mRNA levels in HepG2 cells and, as illustrated in Figure 18a, a strong (72% decrease with MYC shRNA) and specific (no significant effect with Scr shRNA) reduction in *c-MYC* mRNA levels was observed.

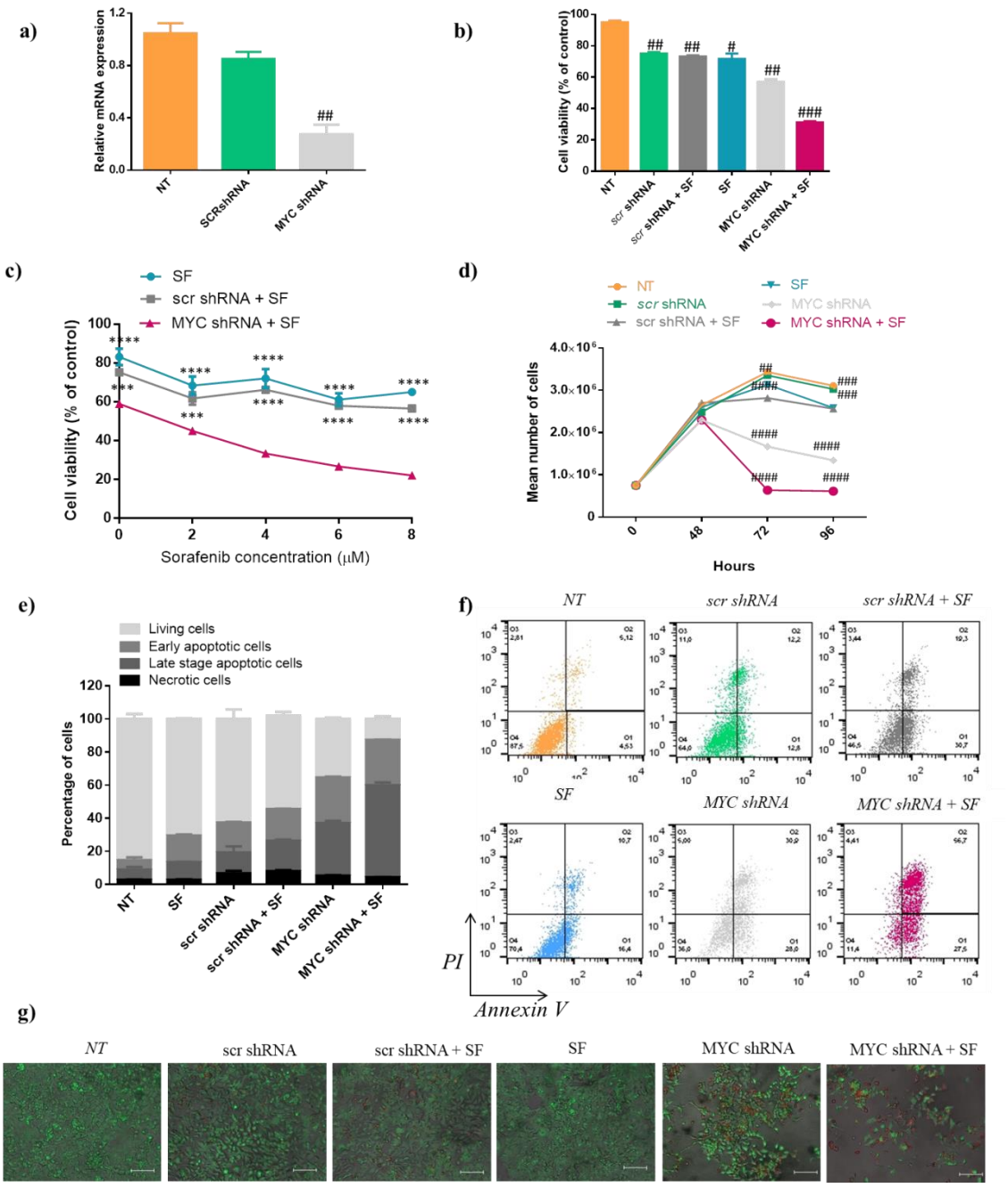

Figure 18– Antitumor activity promoted by the combination of *c-MYC* downregulation with sorafenib. HepG2 cells were treated with different therapeutic strategies: *c-MYC* inhibition mediated by the developed nanosystems (MYC shRNA), chemotherapy (SF), gene therapy combined with chemotherapy (MYC shRNA+ SF), and non-targeting shRNA combined or not with SF (Scr shRNA and scr shRNA + SF). a) *c-MYC* mRNA levels determined by qRT-PCR. b) Cell viability measured 120 h after transfection with MYC shRNA or Scr shRNA combined or not with 4μM of SF. c) Influence of sorafenib concentration on cell viability following 120 h of MYC silencing. d) Effect of the different treatment approaches on cell proliferation. Cardinals (####p < 0.0001, ###p < 0.001, ##p < 0. 01 and #p< 0. 05) correspond to data from cells treated with the various antitumoral strategies which significantly differ from those obtained with non-treated control. Asterisks (****p <0.0001 and ***p<0.001) correspond to data from cells treated with the combined therapy (MYC shRNA+ SF) which significantly differ from those obtained with cells treated with SF or scr shRNA+SF. e,f) Flow cytometry analysis of apoptosis and necrosis levels using FITC-annexin V/PI double-staining. g) Representative images of overlapping fluorescence microscopy and phase contrast of cells using

fluorescein diacetate (green) and propidium iodide (red) staining for imaging live and dead cells, respectively (scale bar = 50 μm).

The sensitization of tumor cells to chemotherapeutic agents by gene therapy modulation has been explored to improve the antitumor effect.[55,56] The cytotoxicity of different concentrations of SF in combination with MYC shRNA or Scr shRNA was measured to clarify whether *c-MYC* downregulation could enhance the sensitivity of HepG2 cells to SF (Figure 18b). The results showed that the combined treatment exhibited much higher cytotoxicity than the strategy that included only SF (IC_{50} of 9.6 μM). For example, at a SF concentration of 4 μM, the viability of HepG2 cells treated with Scr shRNA was 70%. In contrast, cell viability decreased significantly to 33% when cells were transfected with MYC shRNA (Figure 18c). The IC_{50} values of SF combined with Scr shRNA or MYC shRNA were 6.97 μM and 1.99 μM, respectively. The sensitization factor (SF_{50}), defined as the IC_{50} of SF for Scr shRNA-treated control cells divided by the IC_{50} of SF in combination with gene silencing treatment (MYC shRNA) was 3.5. The main advantage of this combinatorial strategy is the reduction in the chemotherapeutic drug concentration required to induce cell-death, thereby increasing the therapeutic effect and reducing the possibility of adverse effects. However, most of the combinatorial strategies developed use non-targeted nanocarriers to deliver genetic material.[57] Herein, the developed nanocarriers have the ability to specifically deliver the DNA plasmid into HCC cells, decreasing the expression of *c-MYC,* which sensitize the tumors cells to SF and reduce the concentration of this cytotoxic drug. In general, suppression of c-MYC expression leads to a migration, invasion and tumor cell proliferation inhibition[58]. Therefore, the effect of the developed combinatorial therapeutic strategy on tumor cells proliferation was evaluated (Figure 18d). The results showed that *c-MYC* downregulation significantly decreased the tumor cell proliferation, while treatment with the non-targeting shRNA did not affect the cell division ability, presenting a proliferation profile similar to non-treated controls cells. Moreover, this anti-proliferative effect was significantly enhanced by the combination with SF, which has slight only a slight effect when used as single-therapy.

To clarify the mechanisms involved in the antitumor activity of the individual and combined strategies, the extent of apoptosis and necrosis/late apoptosis was evaluated by cell staining with annexin V and PI. As illustrated in Figure 18e and 18f, after 120 h of treatment, the levels of apoptotic cells obtained with the proposed combined

therapeutic strategy (MYC shRNA + SF) were much higher than those registered with the single-therapies (MYC shRNA or SF). Moreover, for the combined strategy more necrotic/late apoptotic (red) than viable cells (green) were observed, in contrast to the single therapeutic strategies (Figure 18g). Most importantly, SF, as single therapy, did not induce significantly cell death at the tested concentration (4μM), as shown by the absence of necrotic/late apoptotic cells and by the normal cell morphology. These data further demonstrate that SF-induced apoptosis was synergistically enhanced by *c-MYC* downregulation.

To further verify the robustness of the developed therapeutic approach, the antitumor effect of the combined strategy (MYC shRNA+ SF) and the individual approaches, gene therapy (MYC shRNA) or chemotherapy (SF), was evaluated in HepG2 tumor spheroids.

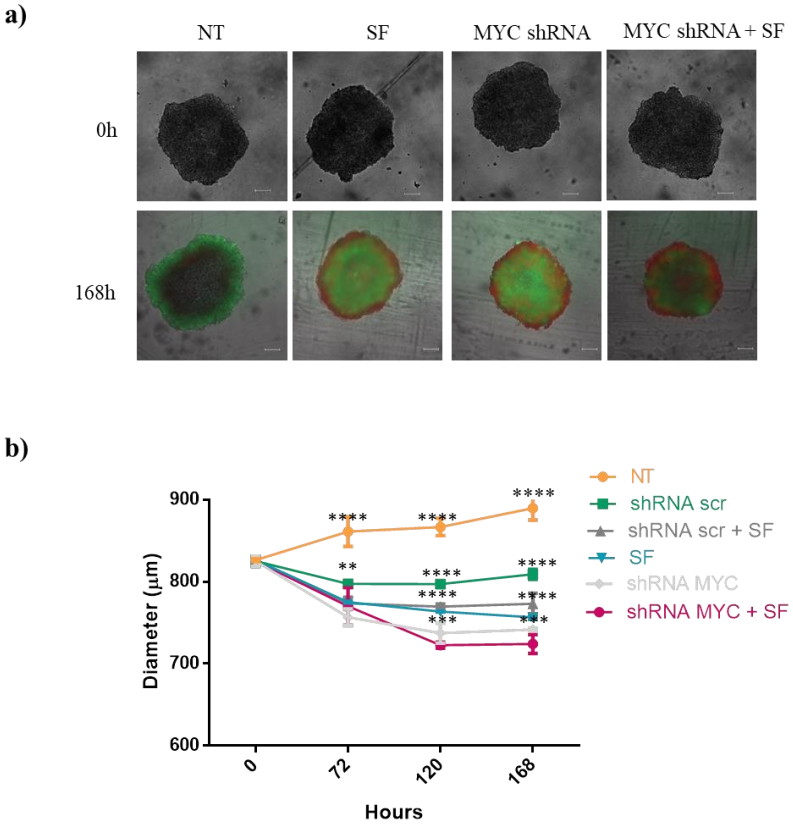

Figure 19- Effect of the c-MYC downregulation combined with SF on tumor spheroids growth. HepG2-spheroids were treated with different antitumor strategies: c-MYC inhibition mediated by glycopolymer-based nanosystems (MYC shRNA), chemotherapy (SF), gene therapy combined with chemotherapy (MYC shRNA+ SF), and non-targeting shRNA combined or not with SF (Scr shRNA and Scr shRNA + SF). a) The microscopic images (scale bar = 200 μm) for 0 h are phase contrast images, and the microscopic images for 168 h are fluorescence images using fluorescein diacetate (green) and propidium iodide (red) staining for imaging live and dead cells, respectively. b) Asterisks (****p <0.0001, ***p<0.001) correspond to data achieved with spheroids treated with each individual strategy, non-targeted shRNA or non-treated

control, which significantly differ from those obtained with spheroids treated with the combined therapy (MYC shRNA + SF).

The results showed that after 168 hours of treatment with our combined antitumor strategy the area of tumor spheroids decreased by ~19%, whereas the area of non-treated tumor spheroids increased by 8% **(**Figure 19 and Figure A10, Appendix A). Moreover, at the end of the treatment with the combination of MYC shRNA and SF the ratio of necrotic (red)/viable cells (green) was much higher than that obtained with the single treatments, chemotherapy (SF) or gene therapy (MYC shRNA), demonstrating the therapeutic potential of this combined strategy.

2.4. Conclusion

In this study, we developed a novel lactobionic acid-based nanocarrier and evaluated the antitumor effect resulting from the combination of c-MYC downregulation, mediated by these HCC-targeted nanosystems, with low concentration of sorafenib. A library of well-defined random and block glycopolymers was synthesized by ARGET ATRP. These polymethacrylate-based glycopolymers demonstrated the ability to form gene delivery nanocarriers with suitable physicochemical properties, high transfection efficiency, biocompatibility and ASGPR-specificity. Among the different synthesized glycopolymers, it was found that the $PAMA_{114}$-*co*-$PLAMA_{20}$-based nanocarrier exhibited higher transfection activity than the corresponding block-glycopolymers- and cationic homopolymer-based nanosystems. Moreover, the expression of *c-MYC* was significantly inhibited by $PAMA_{114}$-*co*-$PLAMA_{20}$/MYC shRNA nanosystems, which markedly increased the sensitivity of tumor cells to SF treatment, resulting in a substantial decrease of tumor cells proliferation and a significant enhancement of apoptosis/necrosis levels. Overall, the obtained results demonstrated the potential of $PAMA_{114}$-*co*-$PLAMA_{20}$-based nanocarriers as a HCC-targeted gene delivery nanosystem and showed that sensitization of tumor cells to SF through *c-MYC* silencing is a promising strategy for the treatment of HCC.

Acknowledgment

This work was financed by the European Regional Development Fund (ERDF) through the COMPETE 2020 program (Operational Program for Competitiveness and Internationalization) and Portuguese national funds via FCT – Fundação para a Ciência e a Tecnologia, under projects: IF/01007/2015, POCI-01-0145-FEDER-30916,

UIDB/04539/2020 and UIDP/04539/2020. Daniela Santo acknowledges FCT for the Grant: SFRH/BD/132601/2017.

The ^{1}H NMR data was collected at the UC-NMR facility which is supported in part by FEDER – European Regional Development Fund through the COMPETE Programme (Operational Programme for Competitiveness) and by National Funds through FCT (Portuguese Foundation for Science and Technology) through grants REEQ/481/QUI/2006, RECI/QEQ-QFI/0168/2012, CENTRO-07-CT92-FEDER-002012, and Rede Nacional de Ressonância Magnética Nuclear (RNRMN).

2.5.References

(1) Sung, H.; Ferlay, J.; Siegel, R. L.; Laversanne, M.; Soerjomataram, I.; Jemal, A.; Bray, F. Global Cancer Statistics 2020: GLOBOCAN Estimates of Incidence and Mortality Worldwide for 36 Cancers in 185 Countries. *CA. Cancer J. Clin.* **2021**, *71* (3), 209–249.

(2) Huang, A.; Yang, X. R.; Chung, W. Y.; Dennison, A. R.; Zhou, J. Targeted Therapy for Hepatocellular Carcinoma. *Signal Transduct. Target. Ther.* **2020**, *5* (1).

(3) Llovet, J. M.; Ricci, S.; Mazzaferro, V.; Hilgard, P.; Gane, E.; Blanc, J.-F.; de Oliveira, A. C.; Santoro, A.; Raoul, J.-L.; Forner, A.; et al. Sorafenib in Advanced Hepatocellular Carcinoma. *N. Engl. J. Med.* **2008**, *359* (4), 378–390.

(4) Tang, W.; Chen, Z.; Zhang, W.; Cheng, Y.; Zhang, B.; Wu, F.; Wang, Q.; Wang, S.; Rong, D.; Reiter, F. P.; et al. The Mechanisms of Sorafenib Resistance in Hepatocellular Carcinoma: Theoretical Basis and Therapeutic Aspects. *Signal Transduct. Target. Ther.* **2020**, *5* (1), 87.

(5) Chen, H.; Liu, H.; Qing, G. Targeting Oncogenic Myc as a Strategy for Cancer Treatment. *Signal Transduct. Target. Ther.* **2018**, *3* (1), 5.

(6) Kaposi-Novak, P.; Libbrecht, L.; Woo, H. G.; Lee, Y.-H.; Sears, N. C.; Conner, E. A.; Factor, V. M.; Roskams, T.; Thorgeirsson, S. S. Central Role of C-Myc during Malignant Conversion in Human Hepatocarcinogenesis. *Cancer Res.* **2009**, *69* (7), 2775–2782.

(7) Lin, C. P.; Liu, C. R.; Lee, C. N.; Chan, T. S.; Liu, H. E. Targeting C-Myc as a Novel Approach for Hepatocellular Carcinoma. *World J. Hepatol.* **2010**, *2* (1), 16–20.

(8) Lin, C. P.; Liu, J. D.; Chow, J. M.; Liu, C. R.; Eugene Liu, H. Small-Molecule c-Myc Inhibitor, 10058-F4, Inhibits Proliferation, Downregulates Human Telomerase Reverse Transcriptase and Enhances Chemosensitivity in Human Hepatocellular Carcinoma Cells. *Anticancer. Drugs* **2007**, *18* (2), 161–170.

(9) Ning, Q.; Liu, Y.-F.; Ye, P.-J.; Gao, P.; Li, Z.-P.; Tang, S.-Y.; He, D.-X.; Tang, S.-S.; Wei, H.; Yu, C.-Y. Delivery of Liver-Specific MiRNA-122 Using a Targeted Macromolecular Prodrug toward Synergistic Therapy for Hepatocellular Carcinoma. *ACS Appl. Mater. Interfaces* **2019**, *11* (11), 10578–10588.

(10) Park, S.-C.; Heo, H.; Jang, M.-K. Polyethylenimine Grafted-Chitosan Based Gambogic Acid Copolymers for Targeting Cancer Cells Overexpressing Transferrin Receptors. *Carbohydr. Polym.* **2022**, *277*, 118755.

(11) Sharma, D.; Arora, S.; Singh, J.; Layek, B. A Review of the Tortuous Path of Nonviral Gene Delivery and Recent Progress. *Int. J. Biol. Macromol.* **2021**, *183*, 2055–2073.

(12) Van Bruggen, C.; Hexum, J. K.; Tan, Z.; Dalal, R. J.; Reineke, T. M. Nonviral Gene Delivery with Cationic Glycopolymers. *Acc. Chem. Res.* **2019**, *52* (5), 1347–1358.

(13) Zhang, Y.; Chan, J. W.; Moretti, A.; Uhrich, K. E. Designing Polymers with Sugar-Based Advantages for Bioactive Delivery Applications. *J. Control. Release* **2015**, *219*, 355–368.

(14) Zhao, L.; Li, Y.; Pei, D.; Huang, Q.; Zhang, H.; Yang, Z.; Li, F.; Shi, T. Glycopolymers/PEI Complexes as Serum-Tolerant Vectors for Enhanced Gene Delivery to Hepatocytes. *Carbohydr. Polym.* **2019**, *205*, 167–175.

(15) Lu, J.; Wang, J.; Ling, D. Surface Engineering of Nanoparticles for Targeted Delivery to Hepatocellular Carcinoma. *Small* **2018**, *14* (5), 1702037.

(16) Warrier, D. U.; Dhanabalan, A. K.; Krishnasamy, G.; Kolge, H.; Ghormade, V.; Gupta, C. R.; Ambre, P. K.; Shinde, U. A. Novel Derivatives of Arabinogalactan, Pullulan & Lactobionic Acid for Targeting Asialoglycoprotein Receptor: Biomolecular Interaction, Synthesis & Evaluation. *Int. J. Biol. Macromol.* **2022**, *207*, 683–699.

(17) Perrone, F.; Craparo, E. F.; Cemazar, M.; Kamensek, U.; Drago, S. E.; Dapas, B.; Scaggiante, B.; Zanconati, F.; Bonazza, D.; Grassi, M.; et al. Targeted Delivery of SiRNAs against Hepatocellular Carcinoma-Related Genes by a Galactosylated

Polyaspartamide Copolymer. *J. Control. Release* **2021**, *330*, 1132–1151.

(18) Miura, Y.; Hoshino, Y.; Seto, H. Glycopolymer Nanobiotechnology. *Chem. Rev.* **2016**, *116* (4), 1673–1692.

(19) González-Cuesta, M.; Ortiz Mellet, C.; García Fernández, J. M. Carbohydrate Supramolecular Chemistry: Beyond the Multivalent Effect. *Chem. Commun.* **2020**, *56* (39), 5207–5222.

(20) Ahmed, M.; Narain, R. The Effect of Molecular Weight, Compositions and Lectin Type on the Properties of Hyperbranched Glycopolymers as Non-Viral Gene Delivery Systems. *Biomaterials* **2012**, *33* (15), 3990–4001.

(21) Dhande, Y. K.; Wagh, B. S.; Hall, B. C.; Sprouse, D.; Hackett, P. B.; Reineke, T. M. N-Acetylgalactosamine Block-Co-Polycations Form Stable Polyplexes with Plasmids and Promote Liver-Targeted Delivery. *Biomacromolecules* **2016**, *17* (3), 830–840.

(22) Chen, Y.; Diaz-Dussan, D.; Peng, Y.-Y.; Narain, R. Hydroxyl-Rich PGMA-Based Cationic Glycopolymers for Intracellular SiRNA Delivery: Biocompatibility and Effect of Sugar Decoration Degree. *Biomacromolecules* **2019**, *20* (5), 2068–2074.

(23) Peng, Y. Y.; Diaz-Dussan, D.; Kumar, P.; Narain, R. Tumor Microenvironment-Regulated Redox Responsive Cationic Galactose-Based Hyperbranched Polymers for SiRNA Delivery. *Bioconjug. Chem.* **2019**, *30* (2), 405–412.

(24) Ahmed, M.; Narain, R. The Effect of Polymer Architecture, Composition, and Molecular Weight on the Properties of Glycopolymer-Based Non-Viral Gene Delivery Systems. *Biomaterials* **2011**, *32* (22), 5279–5290.

(25) Quan, S.; Kumar, P.; Narain, R. Cationic Galactose-Conjugated Copolymers for Epidermal Growth Factor (EGFR) Knockdown in Cervical Adenocarcinoma. *ACS Biomater. Sci. Eng.* **2016**, *2* (5), 853–859.

(26) Ahmed, M.; Deng, Z.; Liu, S.; Lafrenie, R.; Kumar, A.; Narain, R. Cationic Glyconanoparticles: Their Complexation with DNA, Cellular Uptake, and Transfection Efficiencies. *Bioconjug. Chem.* **2009**, *20* (11), 2169–2176.

(27) Diaz-Dussan, D.; Nakagawa, Y.; Peng, Y. Y.; Sanchez, L. V.; Ebara, M.; Kumar, P.; Narain, R. Effective and Specific Gene Silencing of Epidermal Growth Factor Receptors Mediated by Conjugated Oxaborole and Galactose-Based Polymers. *ACS Macro Lett.* **2017**, *6* (7), 768–774.

(28) Singhsa, P.; Diaz-Dussan, D.; Manuspiya, H.; Narain, R. Well-Defined Cationic

N-[3-(Dimethylamino)Propyl]Methacrylamide Hydrochloride-Based (Co)Polymers for SiRNA Delivery. *Biomacromolecules* **2018**, *19* (1), 209–221.

(29) Peng, Y. Y.; Diaz-Dussan, D.; Kumar, P.; Narain, R. Acid Degradable Cationic Galactose-Based Hyperbranched Polymers as Nanotherapeutic Vehicles for Epidermal Growth Factor Receptor (EGFR) Knockdown in Cervical Carcinoma. *Biomacromolecules* **2018**, *19* (10), 4052–4058.

(30) Prevette, L. E.; Kodger, T. E.; Reineke, T. M.; Lynch, M. L. Deciphering the Role of Hydrogen Bonding in Enhancing PDNA-Polycation Interactions. *Langmuir* **2007**, *23* (19), 9773–9784.

(31) Sun, J.; Sheng, R.; Luo, T.; Wang, Z.; Li, H.; Cao, A. Synthesis of Diblock/Statistical Cationic Glycopolymers with Pendant Galactose and Lysine Moieties: Gene Delivery Application and Intracellular Behaviors. *J. Mater. Chem. B* **2016**, *4* (27), 4696–4706.

(32) Sprouse, D.; Reineke, T. M. Investigating the Effects of Block versus Statistical Glycopolycations Containing Primary and Tertiary Amines for Plasmid DNA Delivery. *Biomacromolecules* **2014**, *15* (7), 2616–2628.

(33) Thapa, B.; Kumar, P.; Zeng, H.; Narain, R. Asialoglycoprotein Receptor-Mediated Gene Delivery to Hepatocytes Using Galactosylated Polymers. *Biomacromolecules* **2015**, *16* (9), 3008–3020.

(34) Britovsek, G. J. P.; England, J.; White, A. J. P. Non-Heme Iron(II) Complexes Containing Tripodal Tetradentate Nitrogen Ligands and Their Application in Alkane Oxidation Catalysis. *Inorg. Chem.* **2005**, *44* (22), 8125–8134.

(35) Narain, R.; Armes, S. P. Synthesis and Aqueous Solution Properties of Novel Sugar Methacrylate-Based Homopolymers and Block Copolymers. *Biomacromolecules* **2003**, *4* (6), 1746–1758.

(36) Santo, D.; Cordeiro, R. A.; Sousa, A.; Serra, A.; Coelho, J. F. J.; Faneca, H. Combination of Poly[(2-Dimethylamino)Ethyl Methacrylate] and Poly(β-Amino Ester) Results in a Strong and Synergistic Transfection Activity. *Biomacromolecules* **2017**, *18* (10), 3331–3342.

(37) Santo, D.; Mendonça, P. V; Lima, M. S.; Cordeiro, R. A.; Cabanas, L.; Serra, A.; Coelho, J. F. J.; Faneca, H. Poly(Ethylene Glycol)-Block-Poly(2-Aminoethyl Methacrylate Hydrochloride)-Based Polyplexes as Serum-Tolerant Nanosystems for Enhanced Gene Delivery. *Mol. Pharm.* **2019**, *16* (5), 2129–2141.

(38) Cordeiro, R. A.; Santo, D.; Farinha, D.; Serra, A.; Faneca, H.; Coelho, J. F. J.

High Transfection Efficiency Promoted by Tailor-Made Cationic Tri-Block Copolymer-Based Nanoparticles. *Acta Biomater.* **2017**, *47*, 113–123.

(39) Alonso, S. Exploiting the Bioengineering Versatility of Lactobionic Acid in Targeted Nanosystems and Biomaterials. *J. Control. Release* **2018**, *287* (August), 216–234.

(40) Read, E. S.; Thompson, K. L.; Armes, S. P. Synthesis of Well-Defined Primary Amine-Based Homopolymers and Block Copolymers and Their Michael Addition Reactions with Acrylates and Acrylamides. *Polym. Chem.* **2010**, *1* (2), 221–230.

(41) Mendonça, P. V.; Averick, S. E.; Konkolewicz, D.; Serra, A. C.; Popov, A. V.; Guliashvili, T.; Matyjaszewski, K.; Coelho, J. F. J. Straightforward ARGET ATRP for the Synthesis of Primary Amine Polymethacrylate with Improved Chain-End Functionality under Mild Reaction Conditions. *Macromolecules* **2014**, *47* (14), 4615–4621.

(42) Baker, S. L.; Kaupbayeva, B.; Lathwal, S.; Das, S. R.; Russell, A. J.; Matyjaszewski, K. Atom Transfer Radical Polymerization for Biorelated Hybrid Materials. *Biomacromolecules* **2019**, *20* (12), 4272–4298.

(43) Bus, T.; Traeger, A.; Schubert, U. S. The Great Escape: How Cationic Polyplexes Overcome the Endosomal Barrier. *J. Mater. Chem. B* **2018**, *6* (43), 6904–6918.

(44) Tan, Z.; Dhande, Y. K.; Reineke, T. M. Cell Penetrating Polymers Containing Guanidinium Trigger Apoptosis in Human Hepatocellular Carcinoma Cells Unless Conjugated to a Targeting N-Acetyl-Galactosamine Block. *Bioconjug. Chem.* **2017**, *28* (12), 2985–2997.

(45) Li, H.; Cortez, M. A.; Phillips, H. R.; Wu, Y.; Reineke, T. M. Poly(2-Deoxy-2-Methacrylamido Glucopyranose)-b -Poly(Methacrylate Amine)s: Optimization of Diblock Glycopolycations for Nucleic Acid Delivery. *ACS Macro Lett.* **2013**, *2* (3), 230–235.

(46) Van De Wetering, P.; Moret, E. E.; Schuurmans-Nieuwenbroek, N. M. E.; Van Steenbergen, M. J.; Hennink, W. E. Structure-Activity Relationships of Water-Soluble Cationic Methacrylate/Methacrylamide Polymers for Nonviral Gene Delivery. *Bioconjug. Chem.* **1999**, *10* (4), 589–597.

(47) Sun, J.; Sheng, R.; Luo, T.; Wang, Z.; Li, H.; Cao, A. Synthesis of Diblock/Statistical Cationic Glycopolymers with Pendant Galactose and Lysine

Moieties: Gene Delivery Application and Intracellular Behaviors. *J. Mater. Chem. B* **2016**, *4* (27), 4696–4706.

(48) Chen, Y.; Liu, C.; Yang, Z.; Sun, Y.; Chen, X.; Liu, L. Fabrication of Zein-Based Hydrophilic Nanoparticles for Efficient Gene Delivery by Layer-by-Layer Assembly. *Int. J. Biol. Macromol.* **2022**, *217*, 381–397.

(49) Leong, D. T.; Ng, K. W. Probing the Relevance of 3D Cancer Models in Nanomedicine Research. *Adv. Drug Deliv. Rev.* **2014**, *79–80*, 95–106.

(50) Kim, Y.; Jo, M.; Schmidt, J.; Luo, X.; Prakash, T. P.; Zhou, T.; Klein, S.; Xiao, X.; Post, N.; Yin, Z.; et al. Enhanced Potency of GalNAc-Conjugated Antisense Oligonucleotides in Hepatocellular Cancer Models. *Mol. Ther.* **2019**, *27* (9), 1547–1557.

(51) D'Souza, A. A.; Devarajan, P. V. Asialoglycoprotein Receptor Mediated Hepatocyte Targeting — Strategies and Applications. *J. Control. Release* **2015**, *203*, 126–139.

(52) Park, J.-H.; Cho, E.-W.; Shin, S. Y.; Lee, Y.-J.; Kim, K. L. Detection of the Asialoglycoprotein Receptor on Cell Lines of Extrahepatic Origin. *Biochem. Biophys. Res. Commun.* **1998**, *244* (1), 304–311.

(53) Palermo, E. F.; Lee, D.-K.; Ramamoorthy, A.; Kuroda, K. Role of Cationic Group Structure in Membrane Binding and Disruption by Amphiphilic Copolymers. *J. Phys. Chem. B* **2011**, *115* (2), 366–375.

(54) Ally, A.; Balasundaram, M.; Carlsen, R.; Chuah, E.; Clarke, A.; Dhalla, N.; Holt, R. A.; Jones, S. J. M.; Lee, D.; Ma, Y.; et al. Comprehensive and Integrative Genomic Characterization of Hepatocellular Carcinoma. *Cell* **2017**, *169* (7), 1327–1341.e23.

(55) Lozano, E.; Macias, R. I. R.; Monte, M. J.; Asensio, M.; del Carmen, S.; Sanchez-Vicente, L.; Alonso-Peña, M.; Al-Abdulla, R.; Munoz-Garrido, P.; Satriano, L.; et al. Causes of HOCT1-Dependent Cholangiocarcinoma Resistance to Sorafenib and Sensitization by Tumor-Selective Gene Therapy. *Hepatology* **2019**, *70* (4), 1246–1261.

(56) Younis, M. A.; Khalil, I. A.; Abd Elwakil, M. M.; Harashima, H. A Multifunctional Lipid-Based Nanodevice for the Highly Specific Codelivery of Sorafenib and Midkine SiRNA to Hepatic Cancer Cells. *Mol. Pharm.* **2019**, *16* (9), 4031–4044.

(57) Sun, W.; Wang, Y.; Cai, M.; Lin, L.; Chen, X.; Cao, Z.; Zhu, K.; Shuai, X.

Codelivery of Sorafenib and GPC3 SiRNA with PEI-Modified Liposomes for Hepatoma Therapy. *Biomater. Sci.* **2017**, *5* (12), 2468–2479.

(58) Zhao, Y.; Jian, W.; Gao, W.; Zheng, Y.-X.; Wang, Y.-K.; Zhou, Z.-Q.; Zhang, H.; Wang, C.-J. RNAi Silencing of C-Myc Inhibits Cell Migration, Invasion, and Proliferation in HepG2 Human Hepatocellular Carcinoma Cell Line: C-Myc Silencing in Hepatocellular Carcinoma Cell. *Cancer Cell Int.* **2013**, *13* (1), 23

CHAPTER 3

GLYCOPOLYMERS MEDIATE SUICIDE GENE THERAPY IN ASGPR-EXPRESSING HEPATOCELLULAR CARCINOMA CELLS IN TANDEM WITH DOCETAXEL

The contents of this chapter were adapted from:
Santo, D.; Cordeiro, R. A.; Mendonça, P. V; Serra, A. C.; Coelho, J. F. J.; Faneca, H. Glycopolymers Mediate Suicide Gene Therapy in ASGPR-Expressing Hepatocellular Carcinoma Cells in Tandem with Docetaxel. *Biomacromolecules* **2023** *https://doi.org/10.1021/acs.biomac.2c01329*

4.

4.1. Introduction

Hepatocellular carcinoma (HCC) represents approximately 75–85% of primary liver cancers and is third most common cause of cancer death worldwide.[1] In recent years, multiple kinase and immune checkpoint inhibitors have been approved as therapy approaches for patients with late-stage HCC.[2,3] However, due to their restricted indications, low response rate, drug toxicity/resistance and subsequent tumor relapse, the development of new antitumor strategies that can provide improved efficacy and reduce unexpected side effects is imperative.[4]

In this regard, gene therapy has become a promising therapeutic tool for cancer treatment.[5] Particularly, suicide gene therapy represents approximately 6.1% (194 out of 3180) of all gene therapy clinical trials performed worldwide in 2021.[6] The Herpes Simplex Virus thymidine kinase gene (*HSV-TK*) is the most commonly used suicide gene and involves the concomitant treatment with the antiviral prodrug ganciclovir (GCV).[7,8] This nontoxic prodrug is converted into activated toxic metabolites by the action of HSV-TK followed by endogenous kinases, causing cell death either by inducing chain termination during DNA synthesis or by affecting cell cycle progression.[9] Unfortunately, the clinical translation of suicide gene therapy is still limited by the poor therapeutic outcome and the low cancer cells specificity.[10] Therefore, the development of a high-performance suicide gene therapy strategy for the treatment of HCC requires the development of highly efficient and targeted gene delivery nanocarriers.

In this regard, sugar-based nanocarriers have been considered an appealing approach for the delivery of genetic material due to their inherent biocompatibility, colloidal stability and tissue-specific targeting.[11,12,] The development of reversibly deactivated radical polymerization (RDRP) techniques, namely atom transfer radical polymerization (ATRP) and reversible addition–fragmentation chain transfer polymerization (RAFT), allowed the synthesis of well-defined glycopolymers with precise molecular weight, diverse end-group functionalities, different compositions and a variety of architectures, could be readily prepared.[13,14] Lactobionic acid-functionalized nanocarriers, which are recognized by their biocompatibility and selective binding affinity, stand out as platforms for liver-specific gene delivery.[15] These multifunctional galactosylated molecules display high binding affinity with the asialoglycoprotein receptor (ASGPR), an endocytic cell surface receptor overexpressed on liver cancer cells compared to

hepatocytes,[16,17] which make lactobionic-based nanocarriers a powerful tool to deliver therapeutic genes into tumour cells to combat HCC. Reineke and Narain's groups have conducted a remarkable development on the research study of cationic glycopolymers and evaluation of their transfection ability as a function of various synthetic parameters, such as molecular weight,[18] cationic content,[19,20] carbohydrate content,[21] and glycopolymer composition (random/block copolymers).[22,11,13,14] Methacrylamide-based copolymers, synthetized by copolymerization between primary amine monomers, such as 3-aminopropyl methacrylamide[23] or 2-amino ethyl methacrylamide,[24,25] and carbohydrate-derived monomers, namely 3-gluconamidopropyl methacrylamide[26] and 2-lactobionamidoethyl methacrylamide,[27,28] are the most commonly used glycopolymers. Recently, Bockman et al. reported the synthesis of a N-acetyl-D-galactosamine (GalNAc)-derived monomer through a novel improved two-step route with high yield to prepare different diblock copolymers with 2-amino ethyl methacrylamide via RAFT polymerization. The transfection efficiency of the nanocarriers prepared with these glycopolymers was evaluated in HepG2 cells and depends on the GalNAc block length, which increases with the degree of polymerization of carbohydrate moiety [29]. In an another study, to understand the role of charge type of glycopolymers on transfection efficiency, Haibo Li and co-workers synthetized various poly(2-deoxy-2-methacrylamido glucopyranose)-*b*-poly(methacrylate amine) block copolymers, bearing primary, secondary, tertiary, or quaternary amine functionality.[30] Their results indicated that secondary-amine polymethacrylate-based copolymers exhibited higher gene delivery efficiency and lower cytotoxicity than glycopolymers containing more highly substituted amines. However, the potential of primary-amine polymethacrylate-containing glycopolymers as gene delivery nanosystems was not evaluated, as this polymer was not hydrosoluble, a crucial characteristic of polymers for biomedical applications.[31]

In this work, we proposed the development of a novel HCC-targeted glycopolymer-based nanocarrier to mediate suicide gene therapy, with powerful antitumor effect against HCC cells (Scheme 4). First, a mini-library of well-defined primary-amine polymethacrylate-based glycopolymers, with fixed degree of polymerization (DP) of 2-lactobionamidoethyl methacrylate (LAMA) and different DP values of 2-aminoethyl methacrylate (AMA), were synthesized by ARGET ATRP. The effect of primary amine content on the physicochemical properties, biological activity, biocompatibility and

ASGPR specificity of the nanocarriers were investigated. To boost the transfection efficiency and, thus the therapeutic potential of our best PAMA-*co*-PLAMA-based nanocarriers, HCC cells were pre-treated with a low concentration of docetaxel (DTX), a chemotherapeutic drug belonging to the category of microtubule depolymerization inhibitors.[32] This drug binds to the β-subunit of the tubulin protein of the microtubules and promotes the hyperstabilization of microtubule assemblies, which impairs the mitotic progression and, consequently, leads to cell cycle arrest. Furthermore, as microtubules play a critical role in intracellular dynamics transport, including the trafficking of nanocarriers to lysosomes after their uptake by endocytosis this drug may also be used to improve the transfection ability of nanocarriers by decreasing the entrapment inside the endosomal/lysosomal compartments.[33] Therefore, our hypothesis was that DTX at low concentration could enhance the antitumor effect of HSV-TK/GCV suicide gene therapy, by increasing the transfection efficiency of glycoplexes and inhibiting mitosis. To the best of our knowledge, this was the first research study that combines DTX with suicide gene therapy-mediated by methacrylate-based glycoplexes to combat HCC.

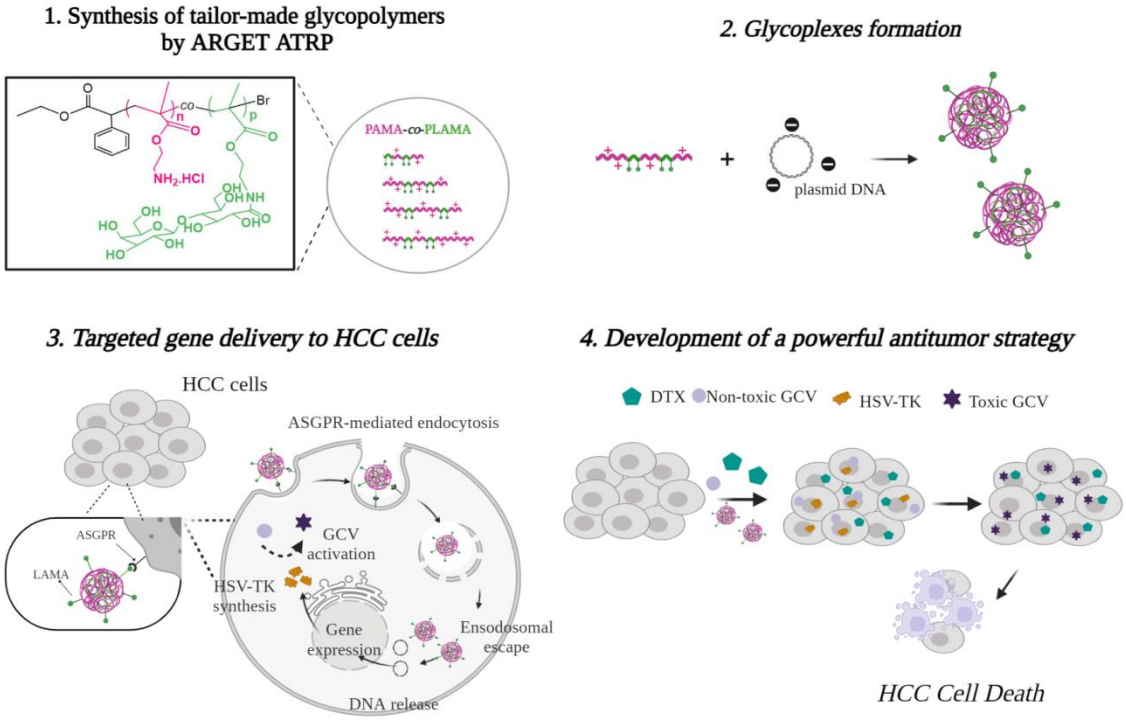

Scheme 4- Schematic illustration of the proposed anti-HCC therapeutic strategy based on the combinatorial effects of DTX with suicide gene therapy-mediated by PAMA-*co*-PLAMA-based glycoplexes.

4.2.Materials and Methods

Materials

Information regarding materials and methods is described in the Appendix B.

Synthesis and characterization of glycopolymers

Details about techniques and equipment are described in the Appendix B.

Typical procedure for the synthesis of PAMA-co-PLAMA by ARGET ATRP

AMA (1.51 g, 9.6 mmol), LAMA (0.6 g, 1.3 mmol), copper(II) bromide ($CuBr_2$) (7.13 mg, 32 μmol), tris(pyridine-2-ylmethyl)amine (TPMA) (37.1 mg, 127 μmol), and ethyl α- bromophenyl acetate (EBPA) (15.5 mg, 64 μmol) were dissolved in water/dimethylformamide (DMF) mixture (50/50, V/V) (3.5mL). The mixture was purged with nitrogen for 30 min in Schlenk flask. Then, the flask was placed under magnetic stirring at 60 °C and a previously deoxygenated ascorbic acid (AscA) solution (43 mM) was continuously added to the mixture via syringe pump at 1 μL/min during 4 h. The final reaction mixture was analyzed by ^1H nuclear magnetic resonance (NMR) spectroscopy and by aqueous size exclusion chromatography (SEC). After that, it was dialyzed (dialysis membrane MWCO = 3500) against deionized water and the glycopolymer was collected after freeze-drying process.

Formulation of polyplexes

Polymers were dissolved in ultra-pure water at pH 3 and blended with 1 μg of DNA plasmids encoding luciferase (pLuc), green fluorescent protein (pGFP) or HSV-TK (pTK) at the desired polymer/DNA N/P (+/−) charge ratio. The mixture solution was incubated for 15 min and was immediately used.

Transfection activity and interaction with target cells

The biological activity, transfection efficiency, cell viability and intracellular trafficking of the developed nanocarriers were evaluated according to Santo et al. and the procedures were described in the Supporting Information[39].

Antitumor activity

The *in vitro* antitumor effect induced by non-viral HSV-TK/GCV gene therapy, DTX or their combination was assessed in HepG2 cell line. Following 4 h incubation of HepG2 cells with $PAMA_{144}$-*co*-$PLAMA_{19}$-based polyplexes, in the presence or absence of different concentrations of DTX (0.006; 0.003; 0.0125; 0.0250;0.5; 0.1 μM) the cell culture medium was renewed with DMEM-HG containing 10% (V/V) FBS. 24 hours after, the cell culture medium was renewed with DMEM-HG with or without 100 μM of GCV and cells were further incubated for 5 days in 5% CO_2 at 37 °C. The cell viability was evaluated at 24 h, 72 h and 120 h by the Alamar Blue assay. After each measurement, the cell culture medium (with or without GCV) was renewed. In addition, the cell viability was also assessed at 120 h through sulforhodamine B (SRB) assay.[34]

The cell death mechanisms were assessed by flow cytometry using FITC-Annexin V and propidium iodide (PI) probes in 24-well culture plates. After 72 h of incubation with $PAMA_{144}$-*co*-$PLAMA_{19}$/pTK; $PAMA_{144}$-*co*-$PLAMA_{19}$/pTK + GCV; DTX: $PAMA_{144}$-*co*-$PLAMA_{19}$/pTK + DTX; and $PAMA_{144}$-*co*-$PLAMA_{19}$/pTK + GCV + DTX cells were harvested, washed and resuspended in 100 μL of binding buffer (10 mM HEPES (pH 7.4), 2.5 mM $CaCl_2$, 140 mM NaCl) containing 2 μL of FITC-annexin V and 1 μL of PI (0.05 mg/mL). Cells were incubated at RT and protected from light for 5 min and then analyzed (10,000 events) in a FACSCalibur flow cytometer (Becton Dickinson, USA). The data were analyzed using FlowJo software. Fluorescence images were obtained using fluorescein diacetate (5 mg/mL in acetone) and PI (2 mg/mL in PBS) for live/dead staining of HepG2 cells. After incubating for 15 minutes, the cells were washed and fixed with 4% paraformaldehyde solution (15 min, RT). The images were acquired with x20 magnification on an Axio Imager Z2 microscope (Zeiss, Munich, Germany) coupled to AxioCam HRc camera (Zeiss, Germany).

To evaluate the antitumor effect of the developed therapeutic strategy in a 3D cell culture model, $3x10^3$ $HepG^2$ cells/well were placed in 96-well cell culture round-bottom ultralow attachment microplates. After the initial 3 days of formation, spheroids were incubated, in the presence or absence of DTX (0.006 μM), with $PAMA_{144}$-*co*-$PLAMA_{19}$-based polyplexes, prepared at 50/1 N/P ratio with 0.5 μg of pTK per well. After 24 h of incubation, the cell culture medium was renewed by culture medium with or without GCV (100 μM) every 48 h. Microscopy images were obtained at 72 h, 120 h and 168 h. The images were acquired with x20 magnification (planapochromat objectives) in an Axio Observer Z1 widefield microscope coupled to digital CMOS

camera (ORCA Flash 4.0) (Zeiss®,Germany) and analyzed with Zen Blue software (Zeiss®, Germany). Analysis of spheroid areas was performed using the Zen Blue software. Fluorescence images were obtained using fluorescein diacetate (5 mg/mL in acetone) and PI (5 mg/mL in PBS) for live/dead staining of spheroids. After 45 min of incubation, the spheroids were washed and observed immediately. The PI mean fluorescence intensity (MFI) per spheroid area was calculated using ImageJ software. Six spheroids per treatment condition were analyzed and the results are representative of three independent experiments.

Statistical Analysis

All the results correspond to mean ± standard deviation (SD), achieved from triplicates and are representative of at least three independent experiments. Data were analyzed by GraphPad Prism (version 6.01 GraphPad Software Inc., San Diego, CA, USA) using one-way analysis of variance (ANOVA) followed by Dunnett test or using two-way ANOVA followed by Dunnett or Sidak tests. For all tests, statistical significance was considered for p-values < 0.05.

4.3. Results and Discussion

3.3.1. Synthesis and characterization of PAMA-co-PLAMA glycopolymers

To prepare new methacrylate-based glycopolymers with well-defined, functionalized and controlled structures and further developed a highly efficient and hepatocyte-specific gene delivery nanocarrier, a series of random PAMA-*co*-PLAMA glycopolymers were synthetized by ARGET ATRP. Lactobionic acid displays high binding affinity with the ASGPR and is capable of forming an amide bond between its carboxyl group and the amine groups of monomers or functional polymers, making lactobionic acid an ideal molecule for selectively target HCC cells.[17,35] In this regard, LAMA, an inexpensive lactobionic-acid derivative monomer, was synthetized by reacting AMA with lactobionolactone, without protecting group chemistry.[36]The chemical structure of the LAMA monomer was confirmed by ^{1}H and ^{13}C NMR spectroscopy (Figure B1, Appendix B) and it is in agreement with data reported in the literature.[36] Then, LAMA and AMA, a primary amine-containing monomer that will ensure the polyplex formation via electrostatic interaction with genetic material, were further polymerized through ARGET ATRP. Armes' group reported the polymerization

of LAMA and AMA, by ATRP in 3:2 methanol/water mixtures or in isopropanol/water mixtures using the CuBr/bipyridine complex as catalyst, to obtain different AMA- and LAMA-block copolymers.[36,37] However, for biomedical applications, the synthesis of glycopolymers by ARGET ATRP is advantageous, as it allows control over the molecular weight of the polymers using a much lower concentration of the metal catalyst.[38] Here, the synthesis of well-defined random copolymers was performed using a slow feeding of AscA as reducing agent in 1:1 DMF/water mixture at 60 ºC, without protecting group chemistry, avoiding the typically troublesome multistep protection/deprotection reactions of glycopolymers synthesis (Scheme 5).

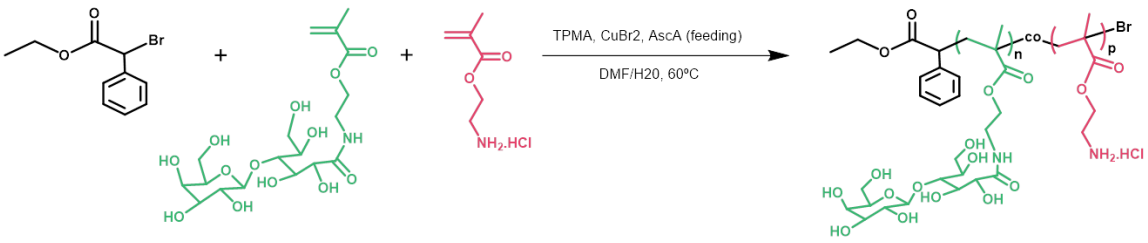

Scheme 5– Synthesis of for the random PAMA-*co*-PLAMA glycopolymers by ARGET ATRP.

The chain length of LAMA was fixed (DP = 20) and different DP values of AMA (DP = 55, 73, 88 and 144) were targeted to evaluate the effect of cationic content on the physicochemical properties, transfection capacity, cytotoxicity and targeting ability of the methacrylate-containing glycopolymers-based gene delivery nanocarriers (Table 7).

Table 7– Composition and molecular weight parameters of glycopolymers prepared by ARGET ATRP.

Polymer sample	DP		M_n^{th} x 10^{3a}	M_n^{SEC} x 10^{3b}	$Đ$
	AMA	LAMA			
$PLAMA_{38}$	-	38	18.4	25.4	1.05
$PAMA_{161}$[c]	161	N/A	25.7	26.9	1.10
PEG_{45}-*b*-$PAMA_{168}$[c]	168	N/A	29.9	28.8	1.10
$PAMA_{55}$-*co*- $PLAMA_{21}$	55	21	19.4	18.9	1.37
$PAMA_{73}$-*co*- $PLAMA_{21}$	73	21	22.0	23.4	1.36
$PAMA_{88}$-*co*- $PLAMA_{20}$	88	20	24.0	27.6	1.32
$PAMA_{144}$-*co*- $PLAMA_{19}$	144	19	33.0	38.7	1.31

Mn, number-average molecular weight; Đ, dispersity (Mw/Mn). [a]Determined from monomer conversion. Mn^{th}=[(AMA conversion/100)×DP_{AMA} × MW_{AMA}] + [(LAMA conversion/100) × DP_{LAMA} × MW_{LAMA}] + Mw_{EBPA}; [b] Determined by SEC using conventional calibration with PEG standards. [c] The synthesis and characterization of $PAMA_{161}$ and PEG_{45}-*b*-$PAMA_{168}$ was previously reported.[39]

A $PAMA_{161}$ homopolymer and a PEG_{45}-*b*-$PAMA_{168}$ block copolymer were also synthesized through the same technique, to be used as control samples, as we previously confirmed the potential of these polymers as gene delivery nanocarriers.[39] All polymers were purified by dialysis against water and collected by freeze–drying process, yielding solids with high water solubility, which enabled their application in gene delivery. Then, their chemical structure was analyzed by ^{1}H NMR spectroscopy and SEC (Figure B2 and Figure B4, Appendix B).

The results showed that the developed ARGET ATRP method yielded homopolymers and random glycopolymers with good control over molecular weight (Đ<1.4), as illustrated by representative monomodal SEC chromatograms (Figure B3, Appendix B) (Table 7).

The synthesis of these copolymers with controlled structure is very important to clarify the relationship between chemical structure and biological properties.

3.3.2. Physicochemical Characterization of Nanosystems

The physicochemical characteristics of polymeric-based nanocarriers play an important role in their capacity to mediate gene delivery into target cells. These include the ability to condense and protect DNA, the size, and the surface charge of the developed polyplexes. Thus, the physicochemical properties of PAMA-*co*-PLAMA-based nanocarriers were determined to evaluate their influence on transfection activity (Figure 20).

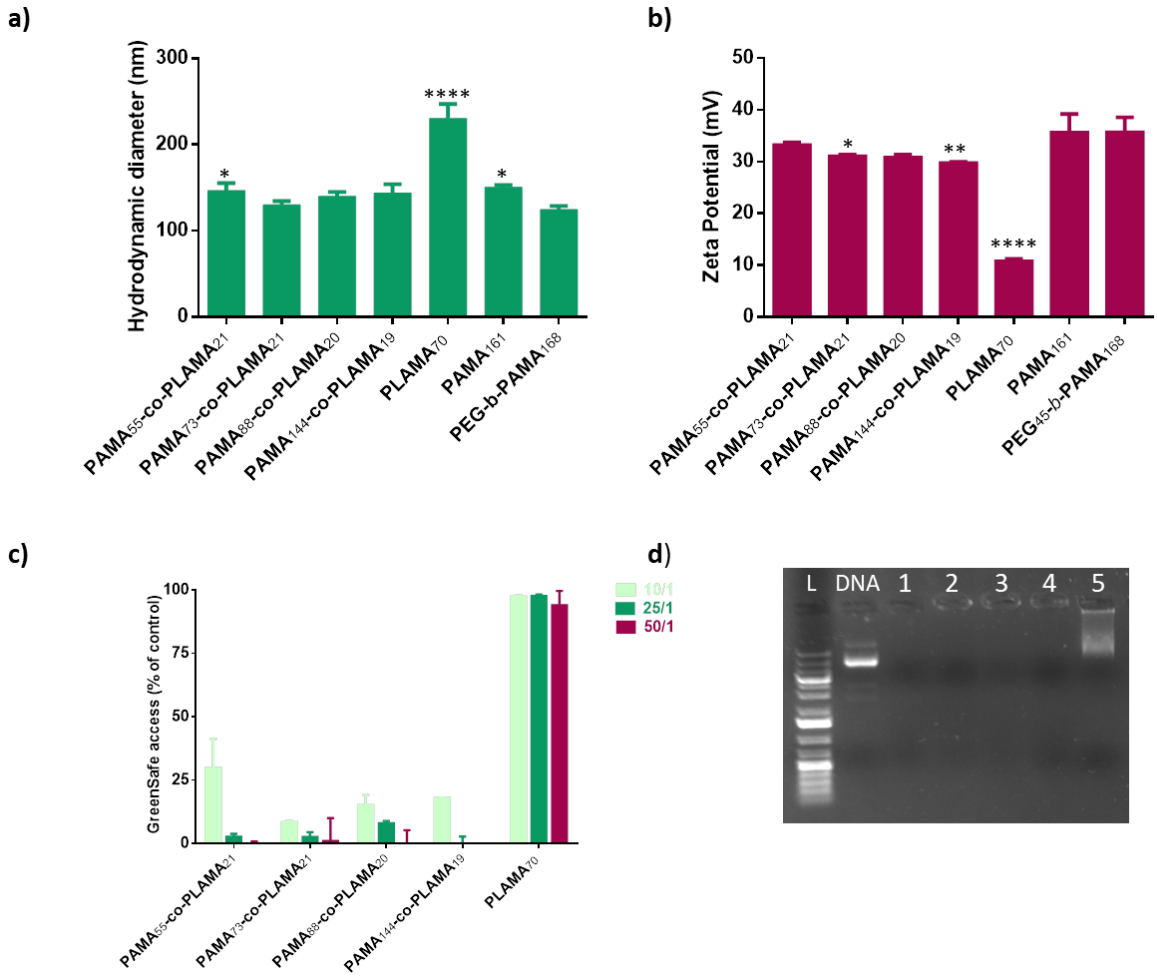

Figure 20– Physicochemical characterization of PAMA-co-PLAMA-based polyplexes. (a) Hydrodynamic diameter and (b) zeta potential of $PAMA_{55}$-*co*-$PLAMA_{21}$-, $PAMA_{73}$-*co*-$PLAMA_{21}$-, $PAMA_{88}$-*co*-$PLAMA_{20}$-, $PLAMA_{70}$-, $PAMA_{161}$- and PEG_{45}-*b*-$PAMA_{168}$-based polyplexes prepared at 50:1 N/P ratio, and $PAMA_{144}$-*co*-$PLAMA_{19}$- based polyplexes formulated at 25:1 N/P ratio. Asterisks (****$p < 0.0001$, **$p < 0.01$, and *$p < 0.05$) indicate values with statistical significance when compared to those obtained with PEG_{45}-*b*-$PAMA_{168}$-based polyplexes. (c) DNA complexation efficiency. (d) Gel electrophoresis of polyplexes prepared with different glycopolymers: L- DNA ladder (1 kb plus), DNA - Plasmid only, 1 - $PAMA_{55}$-*co*-$PLAMA_{21}$, 2 - $PAMA_{73}$-*co*-$PLAMA_{21}$, 3 - $PAMA_{88}$-*co*-$PLAMA_{20}$, 4 - $PAMA_{144}$-*co*-$PLAMA_{19}$, 5 - $PLAMA_{70}$.

The DLS measurements, presented in Figure 20a, revealed that all PAMA-*co*-PLAMA glycopolymers were able to efficiently condense pDNA into nanosized (130–150 nm) polyplexes. In addition, the results showed that the nanocarriers prepared with glycopolymers with different cationic contents presented similar hydrodynamic diameter, which may be justified by the fact that at the tested N/P ratios, a maximum

condensation of genetic material was reached and, consequently, no significant changes in size were observed. Moreover, $PLAMA_{70}$ homopolymer generated larger nanoparticles than cationic-containing glycopolymers, suggesting that they have a limited ability to condense genetic material.

Regarding the zeta potential of the developed nanocarriers, the results illustrated in Figure 20b, showed that their surface charge is positive, ranging between +10 and +35 mV. In addition, the results revealed that all the developed PAMA-*co*-PLAMA-based nanocarriers exhibited similar surface charge, which was slightly lower than that obtained for $PAMA_{161}$- and PEG_{45}-*b*-$PAMA_{168}$-based polyplexes. Moreover, nanocarriers prepared with the carbohydrate homopolymer exhibited lower zeta potential than polyplexes prepared with cationic-containing copolymers. These results indicate that carbohydrate-based nanosystems, when compared to PEGylated nanovehicles, provide a superior hydrophilic hindrance, which improves their capability to mask the excess of positive charge of nanocarriers.

To evaluate if the developed nanocarriers were able to condense the plasmid DNA, the Green Safe intercalation assay was performed. The results showed a decrease of Green Safe fluorescence with the increase of the N/P ratio of glycoplexes for all the developed formulations, except for $PLAMA_{70}$-based nanocarriers (Figure 20c). The glycoplexes generated with PLAMA homopolymer had the highest levels of intercalating agent access. This fact can be explained by the nature of the interactions of this glycopolymer with DNA, which probably occurs mostly via hydrogen bonding. On the other hand, for all developed PAMA-*co*-PLAMA-based polyplexes prepared at 25/1 and 50/1 N/P ratios, the results showed that these nanocarriers provided almost complete DNA condensation and protection.

The data obtained in the Green safe accessibility assays are consistent with those obtained in the agarose gel electrophoresis assays (Figure 20d).

3.3.3. Transfection activity and cytotoxicity of PAMA-co-PLAMA-based polyplexes

To the best of our knowledge, the effect of primary amine content on the transfection activity and cytotoxicity of methacrylate-based glycoplexes in gene delivery has never been studied. Therefore, to evaluate the potential of PAMA-*co*-PLAMA glycopolymers

as gene delivery nanosystems, a preliminary study was performed in HepG2 cells using luciferase as a reporter gene (Figure 21).

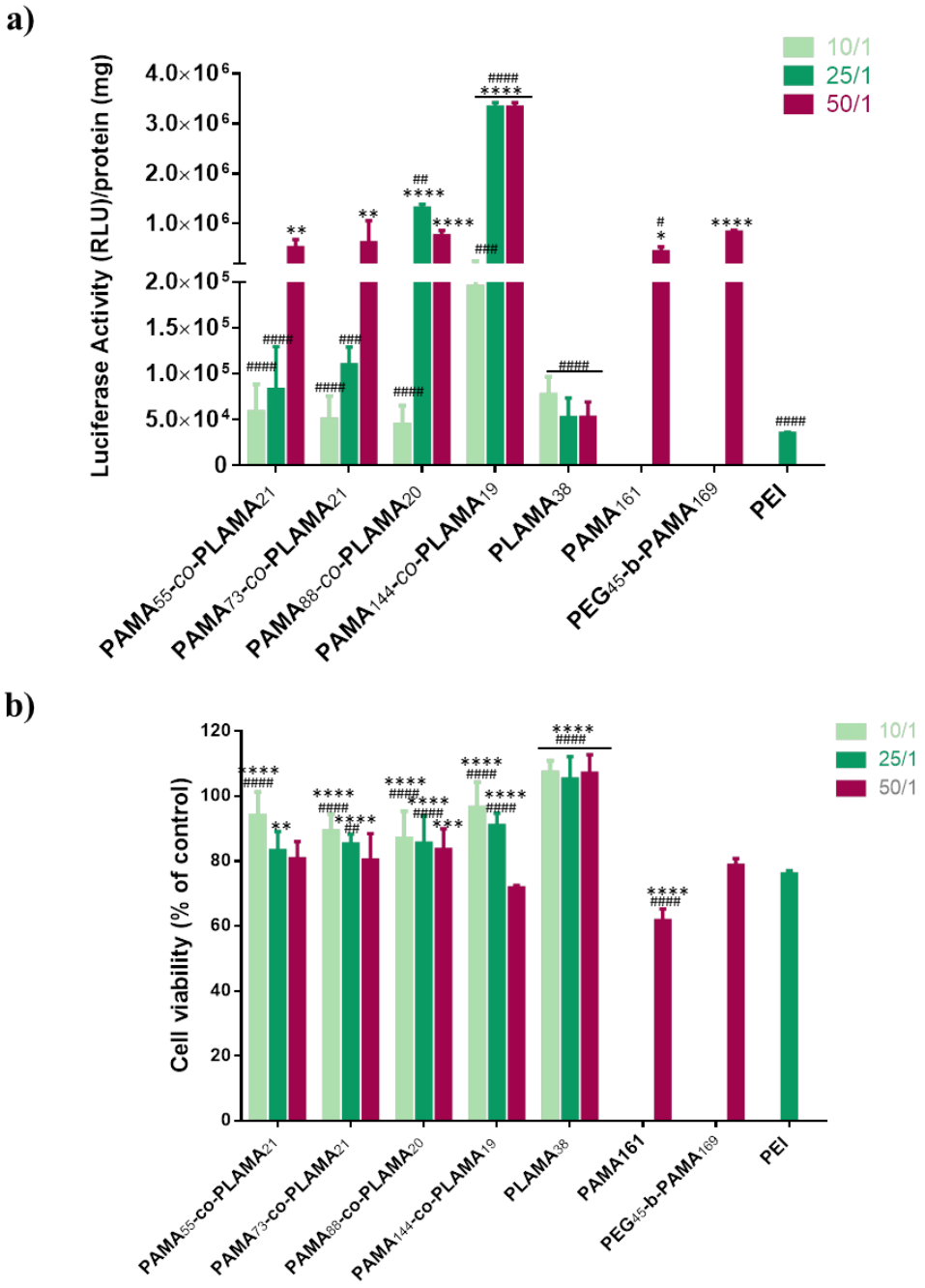

Figure 21– Transfection activity (a) and cytotoxicity (b) of PAMA-*co*-PLAMA-based nanocarriers in HepG2 cells. Polyplexes were prepared by complexing glycopolymers, $PAMA_{161}$ and PEG_{45}-*b*-$PAMA_{168}$ with DNA plasmid encoding luciferase, at different N/P ratios. Asterisks (****p < 0.0001, ***p < 0.001, **p < 0.01, and *p < 0.05) and cardinals (####p < 0.0001, ###p < 0.001, and #p < 0.05) indicate values with statistical significance when

compared to those obtained with the standard formulations, PEI-and PEG_{45}-*b*-$PAMA_{168}$-based polyplexes, respectively.

As shown in Figure 21a, the ability of the different nanocarriers to effectively deliver plasmid DNA into HepG2 cells depends on their N/P ratio and composition. The transfection activity of the developed PAMA-*co*-PLAMA-based polyplexes was generally improved by the increase of the tested N/P ratios. Nanocarriers prepared with $PAMA_{55}$-*co*-$PLAMA_{21}$ and $PAMA_{73}$-*co*-$PLAMA_{21}$ copolymers presented the highest gene reporter expression for 50/1 N/P ratio, while nanovehicles prepared with $PAMA_{88}$-*co*-$PLAMA_{20}$- and $PAMA_{144}$-*co*-$PLAMA_{19}$ glycopolymers, which have higher content of AMA, exhibited high levels of biological activity even for 25/1 N/P ratio. This fact could be related to higher amounts of cationic polymer, which establish multiple electrostatic interactions with endosomal membranes, facilitating the escape of genetic material from the endolysosomal pathway to the cytoplasm.[40] In addition, the results showed that the carbohydrate homopolymer $PLAMA_{38}$-based nanosystems promoted low transgene expression. This poor performance as gene delivery nanocarriers can be explained by their low ability to condense the genetic material, consequently allowing the premature release of DNA and/or enabling its degradation before reaching the nucleus (Figure 20d). Moreover, the results demonstrate that $PAMA_{144}$-*co*-$PLAMA_{19}$-based nanosystems presented the highest biological activity, exhibiting higher transgene expression than that $PAMA_{161}$- and PEG-*b*-$PAMA_{168}$-based polyplexes. This is a remarkable result because it has been reported that the glycopolymer-based nanosystems usually present lower transfection efficiency than the corresponding cationic homopolymers-based nanocarriers.[23,22]

Additionally, all the developed formulations exhibited higher transfection activity than that obtained with the gold-standard polymer for gene delivery application – the polyethylenimine (PEI). Cytotoxicity is one of the most common shortcoming of polymeric-based gene delivery nanosystems.[31] To overcome this drawback, without affecting the gene delivery efficacy, some modification of cationic polymers with different biocompatible molecules, such as PEG, have been explored.[39] In this regard, functionalization of cationic polymers with carbohydrates, ubiquitous components of biological systems, has been considered an attractive strategy to improve the biocompatibility of polymeric-based nanosystems.[41]

As illustrated in Figure 21b, the viability of HepG2 cells depends on the N/P ratio of polyplexes and their composition. In general, PAMA-*co*-PLAMA-based nanocarriers induced low cytotoxicity, with cell viability exceeding 80% for all formulations, except for $PAMA_{144}$-*co*-$PLAMA_{19}$-based complexes, which were prepared at N/P/ratio of 50/1 and exhibited a cytotoxicity of 30%. This reduction in cell viability can be explained by the multiple and strong interactions of the nanosystems with the cytomembranes, causing their destabilization and, consequently, influencing the metabolic activity of the cells.[42] Nevertheless, the data obtained showed that polyplexes based on $PAMA_{144}$-*co*-$PLAMA_{19}$ prepared at 25/1 N/P ratio presented an excellent biocompatible profile and induced much lower cytotoxicity than $PAMA_{161}$-, PEG_{45}-*b*-$PAMA_{168}$ and PEI-based nanocarriers.

To assess the influence of AMA content on transfection efficiency of PAMA-*co*-PLAMA-based nanocarriers, fluorescence microscopy was performed after transfection of HepG2 cells with glycoplexes prepared with plasmid DNA encoding green fluorescent protein (pgfp) (Figure 22).

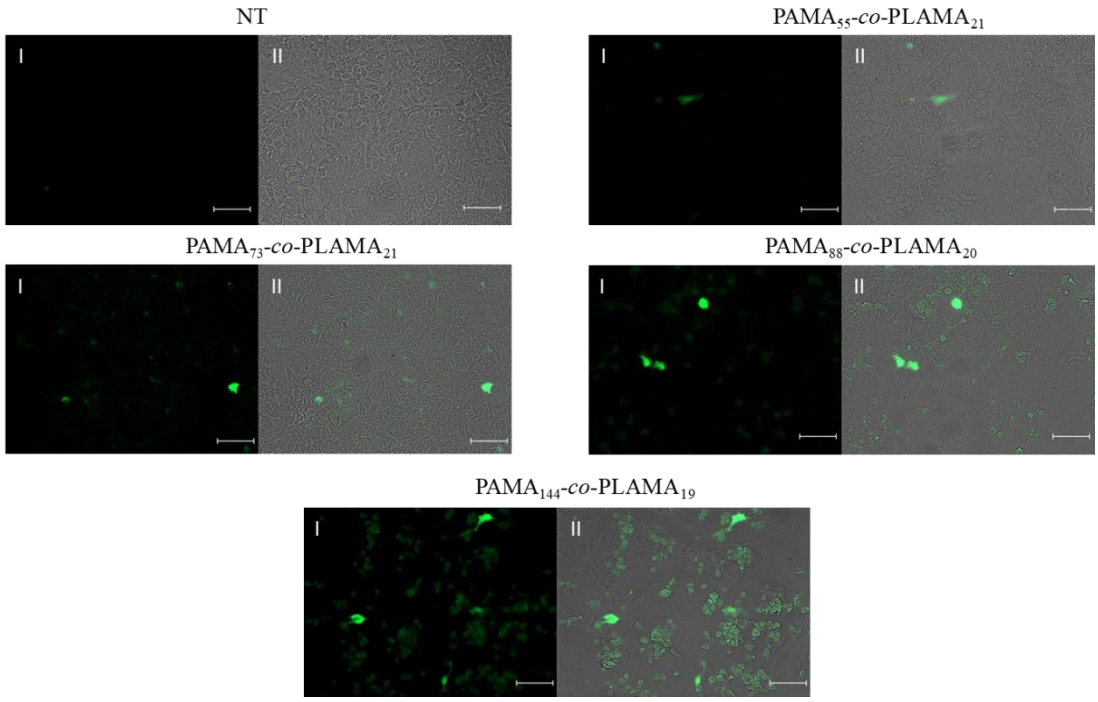

Figure 22– Transfection efficiency assessed by fluorescence microscopy in HepG2 cells. Typical fluorescence images (I) and overlapping (II) of fluorescence microscopy and phase contrast images of cells after transfection with different glycopolymers-based nanocarriers (scale bar = 50 μm).

The obtained results revealed that the transfection efficiency was improved by the increase of the polymerization of AMA, with the highest number of GFP-expressing cells being observed after transfection with $PAMA_{144}$-*co*-$PLAMA_{19}$-based polyplexes (Figure 22). In addition, these nanosystems promoted a large number of transfected cells than that obtained with PEG_{45}-*b*-$PAMA_{168}$- or PEI-based polyplexes (Figure B6, Appendix B).

3.3.4. ASGPR mediated targeted gene delivery to HCC cells

To improve the biocompatibility of cationic-based nanosystems, glycopolymers have been widely used as multivalent ligands to target lectin receptors overexpressed on the surface of cancer cells. The ASGPR binds specifically galactose moieties of desialylated glycoproteins and the binding affinity augments with the valence of the carbohydrate residues, a phenomenon termed as cluster glycoside effect.[43] To determine whether the developed PAMA-*co*-PLAMA-based polyplexes are specifically recognized by the ASGPR of HCC cells, a competition assay of transfection in the presence of asialofetuin, a natural ligand of ASGPR, or an antibody against the ASGPR was performed.

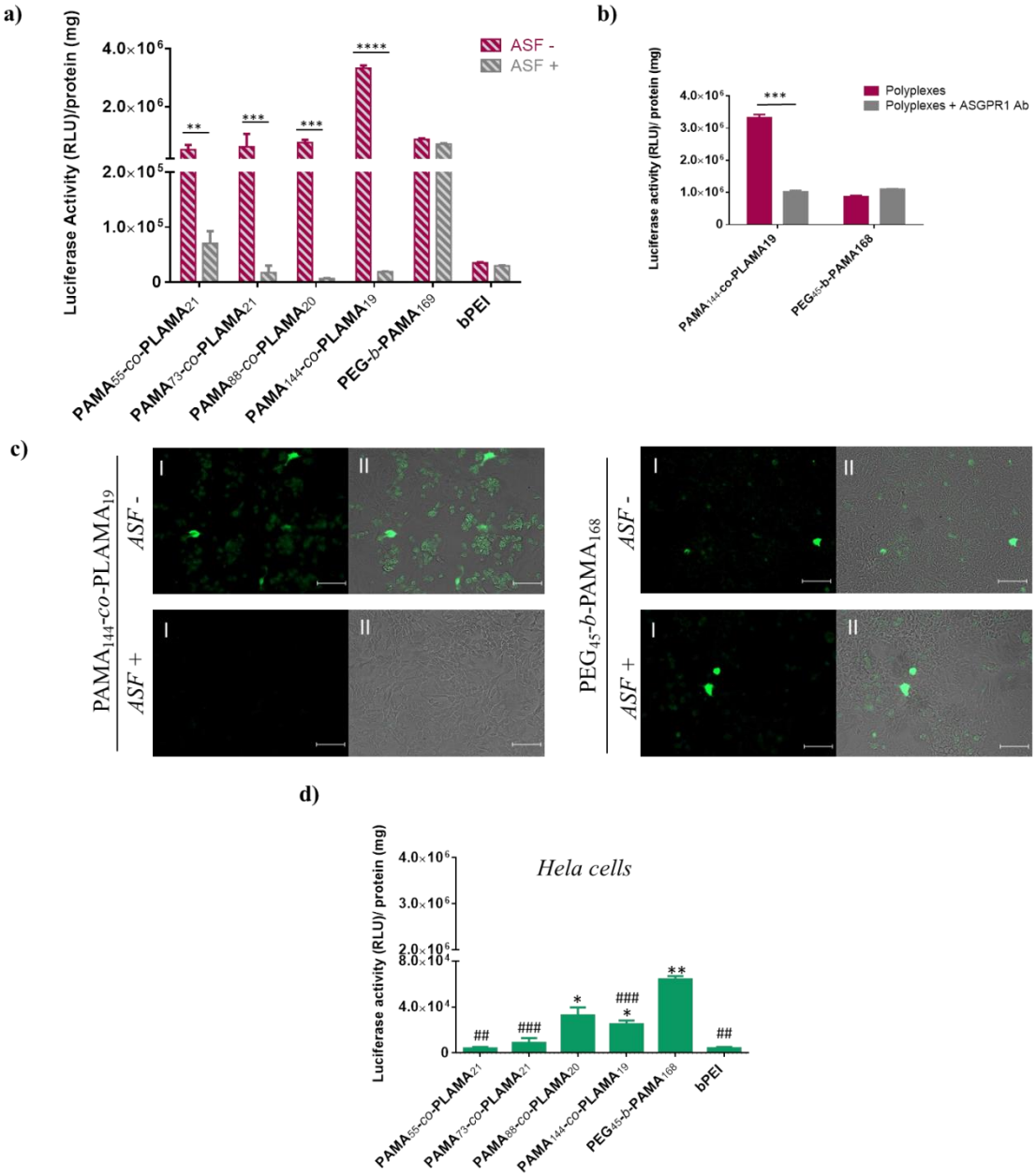

Figure 23– Effect of the presence of asialofetuin and an antibody against the ASGPR on biological activity of PAMA-*co*-PLAMA-based polyplexes in HepG2 cells. Biological activity of polyplexes in Hela cells. (a, b) Asterisks (****p < 0.0001, ***p < 0.001, **p < 0.01, and *p < 0.05) correspond to values that differ significantly from those obtained with e same formulations in the absence of asialofetuin or Ab against ASGPR. (c) Typical fluorescence images (I) and overlapping of fluorescence microscopy and phase contrast images (II) of cells transfected with different nanocarriers in the presence and absence of asialofetuin (scale bar = 100 μm). d) Asterisks (**p < 0.01 and *p < 0.05) and cardinals (###p < 0.001 and ##p < 0.01 indicate values with statistical significant differences when compared to those obtained with

PEI-based nanosystem at 25/1 N/P ratio, or with PEG_{45}-*b*-$PAMA_{168}$-based polyplexes, respectively.

The data presented in Figure 23a showed that the pretreatment of HepG2 cells with asialofetuin drastically reduced the transfection activity of PAMA-*co*-PLAMA-based polyplexes, while it did not significantly change the biological activity of PEI-, and PEG_{45}-*b*-$PAMA_{168}$-based nanocarriers. In addition, the effect of the preincubation of HepG2 cells with an antibody against the ASGPR on the biological activity of $PAMA_{144}$-*co*-$PLAMA_{19}$-based nanocarriers revealed that this pretreatment induced a strong reduction in their transfection activity. However, it did not affect the biological activity of PEG_{45}-*b*-$PAMA_{168}$-based nanocarriers (Figure 23b). To further confirm that our most promising formulation, $PAMA_{144}$-*co*-$PLAMA_{19}$-based nanocarriers prepared at 25/1 N/P ratio, was specifically recognized by the ASGPR of HepG2 cells, the effect of asialofetuin on transfection efficiency was also evaluated by fluorescence microscopy (Figure 23c). The results confirmed that asialofetuin bound to the ASGPR blocks the internalization of the developed formulation, consequently resulting in a significantly lower number of GFP-expressing cells than that observed in the absence of asialofetuin. On the other hand, the data showed that PEG-*b*-$PAMA_{168}$- or PEI-based nanocarriers promoted similar transfection efficiencies, regardless the presence or absence of asialofetuin, which highlights the fact that the developed glycoplexes are specifically recognized by the ASGPR expressed on the surface of HepG2 cells (Figure 23c and Figure B6). These assays were also performed in Hep3B cells and a similar decrease in the transfection activity of the developed glycoplexes was observed in the presence of ASGPR-competition agent, being this effect more pronounced with $PAMA_{144}$-*co*-$PLAMA_{19}$-based nanocarriers (Figure B7, Appendix B). In addition, the biological activity of PAMA-*co*-PLAMA-based polyplexes was also investigated in cells not expressing ASGPR (Hela cells) (Figure 23d)[22]. The results showed that the higher transfection activity of PLAMA-containing nanocarriers obtained in HepG2 and Hep3B cells, compared with PEI-based nanosystems, was not observed in Hela cells. In fact, in these cells the highest transfection efficiency was obtained with the non-targeted nanocarriers PEG-*b*-$PAMA_{168}$-based polyplexes. Overall, these results demonstrated that the developed nanocarriers with galactose residues have the ability to specifically bind ASGPR, enhancing both their cell internalization and transfection activity.

3.3.5. *The intracellular pathway of PAMA-co-PAMA-based nanocarriers*

The transfection efficiency of non-viral vectors is conditioned by multiple intracellular barriers, as cellular uptake and endolysosomal escape to nuclear internalization.[44,45] The interaction of nanocarriers with cells, and consequently their internalization, is affected by several parameters, in particular by their physicochemical properties and glycopolymer composition.[21]The cellular internalization of the developed nanocarriers, containing 1% fluorescein-labeled PAMA-*co*-PLAMA glycopolymer, was evaluated by confocal microscopy and flow cytometry, in the presence or absence of asialofetuin (Figure 24).

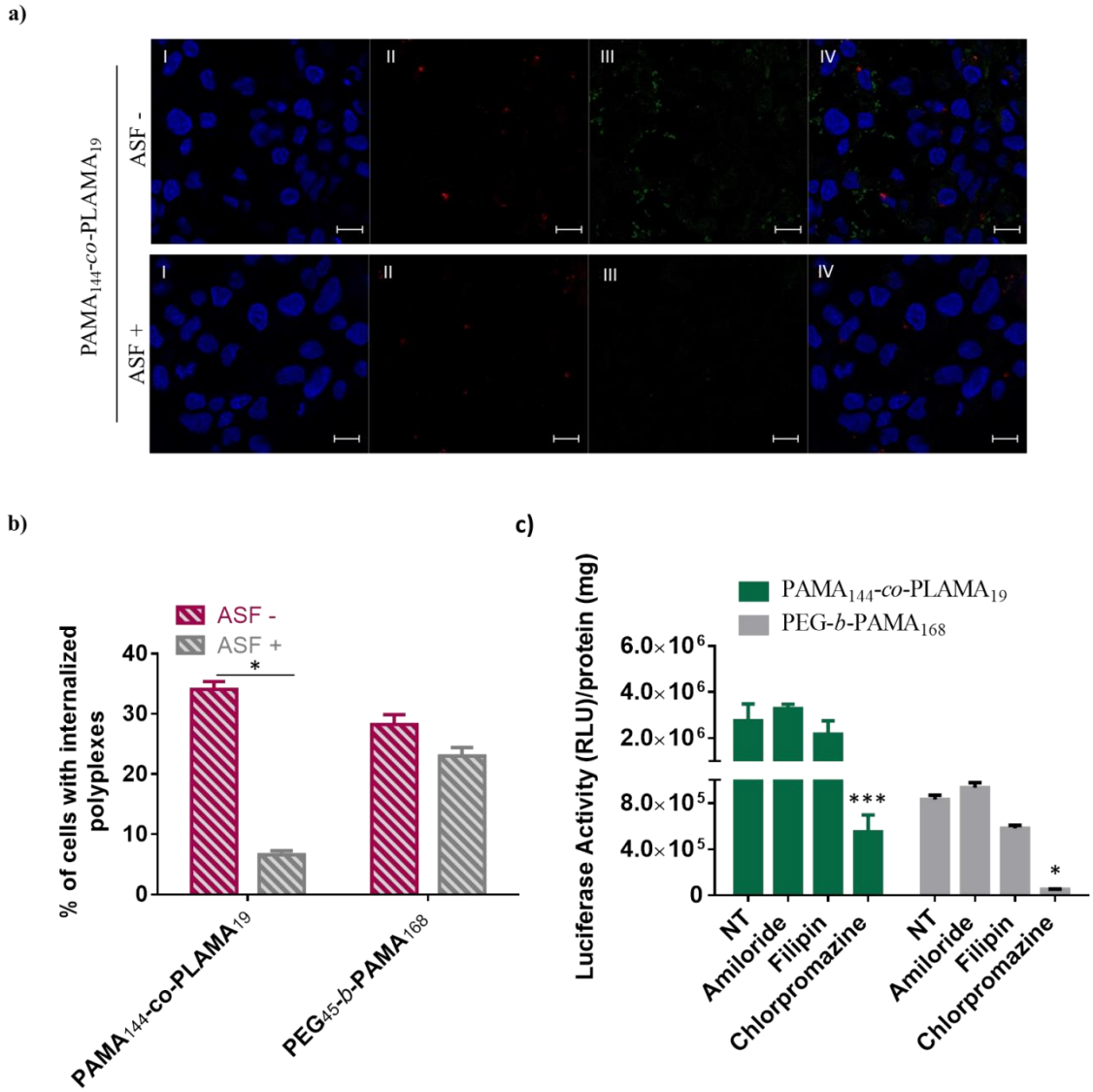

Figure 24- Effect of the presence of asialofetuin on cellular uptake of $PAMA_{144}$-*co*-$PLAMA_{19}$- and PEG_{45}-*b*-$PAMA_{168}$-based polyplexes, evaluated by confocal microscopy (a) and flow cytometry (b) and the influence of endocytosis inhibitors on their transfection ability (c). (a)

Representative confocal microscopic images of HepG 2 cells treated with $PAMA_{144}$-*co*-$PLAMA_{19}$-based nanocarriers (scale bar = 10 μm): (I) cell nucleus stained by DAPI (blue); (II) acidic cellular compartments stained with Lysotracker Red DND-99 (red); (III) polyplexes prepared with 1% fluorescein-labeled glycopolymer (green); and (IV) overlay of images I−III. (b) Asterisks (*$p < 0.05$) correspond to values which differed significantly from those obtained with the same formulations in the absence of asialofetuin. (c) HepG2 cells were treated or not treated (Nt) with endocytosis inhibitors: chlorpromazine (50 mM), filipin (1 μg/mL) and amiloride (0.25 mM). Asterisks (***$p < 0.001$ and *$p < 0.05$) indicate values with statistical significance compared to those measured in untreated cells (control).

The results shown in Figure 24a indicated that cellular internalization of $PAMA_{144}$-*co*-$PLAMA_{19}$-polyplexes was significantly inhibited by pretreatment with asialofetuin. In addition, it was not observed colocalization between the developed glycoplexes and lysosomal compartments (red fluorescence), which suggests that they have the ability to efficiently escape from the endolysosomal pathway to the cytoplasm, avoiding the subsequent DNA degradation in acidic cellular compartments. This observation can probably be explained by the high content of PAMA, a polymer containing primary amines that may interact and disrupt the endocytic membranes promoting the release of nanocarriers into the cell cytoplasm.[46] Furthermore, ASGPR-mediated cellular internalization of the developed nanocarriers was confirmed by flow cytometry (Figure 24b). As expected, the cellular internalization of $PAMA_{144}$-*co*-$PLAMA_{19}$-based nanocarriers decreased significantly in the presence of asialofetuin, whereas the uptake of PEG_{45}-*b*-$PAMA_{168}$-based polyplexes was not affected by the pretreatment with this glycoprotein. This result can be explained by the binding of asialofetuin to the ASGPR, which blocks the internalization of the LAMA-containing nanosystems, but not the internalization of PEG_{45}-*b*-$PAMA_{168}$-based nanocarriers, since the latter do not interact with the ASGPR. The extension of the interaction between glycopolymers and specific lectins depends on their molecular weight, composition, arrangement in the nanoparticle structure, and length of spacer groups between polymer backbone and the pendant carbohydrate groups.[23,47] For a fixed amount of carbohydrates, the increase of DP value of AMA resulted in a substantial decrease of the cellular internalization of PAMA-*co*-PLAMA-based nanocarriers (Figure B8, Appendix B). Despite the higher cellular internalization of $PAMA_{55}$-*co*-$PLAMA_{21}$-based polyplexes when compared to $PAMA_{144}$-*co*-$PLAMA_{19}$-based ones, their transfection activity was much lower, suggesting that the higher ability of our best formulation to effectively overcome the

multiple intracellular barriers. The pKa values of PAMA-*co*-PLAMA glycopolymers likely help to explain these differences between nanocarriers with different DP of AMA (Figure B5, Appendix B). The $PAMA_{144}$-*co*-$PLAMA_{19}$ glycopolymer has the lower pKa value and, consequently, the lower degree of protonation at physiological pH, resulting in a higher buffering capacity. The endocytic pathway has a critical role in the intracellular trafficking of nanocarriers and, consequently, in the transfection efficiency.[48] To evaluate the endocytic pathway involved in the cellular uptake of $PAMA_{144}$-*co*-$PLAMA_{19}$-based nanocarriers, their transfection activity was measured in the presence of various endocytic inhibitors (Figure 24c). Clathrin-mediated endocytosis was inhibited using chlorpromazine, caveolae-mediated endocytosis was blocked through the treatment with filipin, and amiloride was used to hinder macropinocytosis. Different concentrations of each endocytic inhibitor were used to define the lower drug concentration at which the inhibitor was efficient, without provoking significant toxicity (Figure B9 and Figure B10, Appendix B). In addition, the endocytic pathways engaged in the cellular uptake of non-targeted nanocarriers – PEG-*b*-$PAMA_{168}$-based nanosystems, was also evaluated. As shown in Figure 24c, pretreatment of HepG2 cells with chlorpromazine resulted in a significant reduction on transgene expression, suggesting that the clathrin-coated pit endocytic pathway is involved in the uptake of the developed $PAMA_{144}$-*co*-$PLAMA_{19}$-based nanocarriers. The physicochemical properties of these glycoplexes, namely their size of approximately 144 nm, were compatible with their internalization by clathrin-mediated endocytic pathway (Figure 20a). Moreover, this result confirmed the ASGPR-mediated cellular internalization, due to the specific binding of the galactose residues to this receptor. Regarding the PEG_{45}-*b*-$PAMA_{168}$-based polyplexes, the obtained data showed that the transgene expression was also negatively affected by the preincubation with chlorpromazine, indicating the involvement of clathrin-mediated endocytosis. This transfection activity reduction was not due to the toxicity of the endocytic inhibitors, as no significant changes in cell viability were observed for the selected concentrations (Figure B9 and Figure B10, Appendix B).

3.3.6. DTX as enhancer of antitumor activity mediated by suicide gene therapy

DTX is a standard first-line chemotherapeutic drug for the treatment of various cancers. However, clinical trials indicate that DTX does not seem to be safe and effective enough for patients suffering from advanced HCC.[49] This anticancer agent has multiple target processes, including apoptotic, angiogenic, and gene expression ones.[32] In addition, as an inhibitor of microtubule depolymerization, this second-generation taxane may also decrease the intracellular traffic of polyplexes to lysosomes, enhancing the transfection efficiency of non-viral vectors.[50,51] The *HSV-TK*/GCV gene therapy strategy focus on the delivery into tumor cells of a gene encoding the enzyme HSV-TK that metabolizes GCV to ganciclovir monophosphate, which in turn is phosphorylated to the triphosphate form by cellular kinases.[52] Since the latter compound is an analog of deoxyguanosine triphosphate, it will occur the inhibition of DNA polymerase and/or incorporation into DNA, resulting in chain termination and tumor cell death.[53] Moreover, suicide gene therapy yields better therapeutic outcomes due to the bystander effect involving the neighboring cancer cells, thus suppressing the necessity to deliver therapeutic genetic material to all tumor cells.[7]

Considering that one of the goals of this work was to develop an effective anti-HCC strategy, we investigated whether DTX as a transfection enhancer, together with its anticancer activity, would improve the therapeutic potential of the suicide gene therapy strategy mediated by the developed glycoplexes. To this end, we analyzed the effect of different DTX concentrations on luciferase gene expression in HepG2 cells transfected with $PAMA_{144}$-*co*-$PLAMA_{19}$/DNA nanosystems prepared at 25/1 N/P ratio (Figure 25).

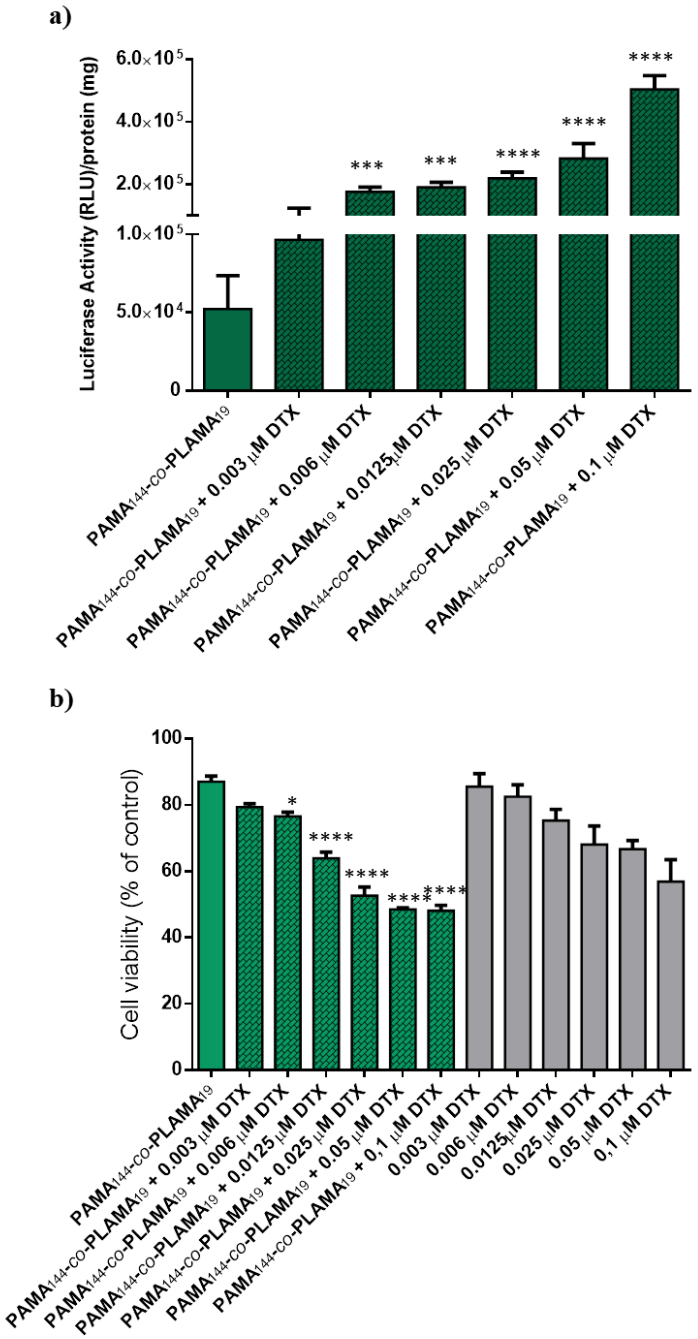

Figure 25– Effect of DTX concentration on the biological activity (a) and cytotoxicity (b) of $PAMA_{144}$-*co*-$PLAMA_{19}$-based glycoplexes, prepared at 25/1 N/P ratio, in HepG2 cells. Asterisks (****p < 0.0001, ***p < 0.001, **p < 0.01 and *p < 0.05) indicate values that significantly differ from those measured for $PAMA_{144}$-*co*-$PLAMA_{19}$-based nanocarriers in the absence of DTX.

The data presented in Figure 25a showed that pretreatment of HCC cells with DTX resulted in an increase of the biological activity of the nanocarriers. This booster effect was concentration-dependent and reached the highest effect at 0.1 μM DTX, under the

conditions tested and limited by the drug cytotoxicity. The cytoskeleton plays a pivotal role in different cellular processes, namely the maintenance of cell shape, mitosis, cell motility and intracellular trafficking of nanoparticles. Filopodia, actin projections that extend from the cell surface, actively detect glycoplexes in the extracellular milieu and internalize these nanoparticles into clathrin-coated vesicles, which are then transported along microtubules to the main cell body to deliver nucleic acids to the nucleus.[54] As DTX binds to the β-subunit of the tubulin protein of the microtubules and promotes the hyperstabilization of microtubule assemblies, it probably prevents the transport of glycoplexes to lysosomes. Thus, as previously reported by several authors, the increase in transgene expression induced by microtubule-targeting agents is probably due to the enhancement of intracellular trafficking from the endocytic pathway to the nucleus rather than an increase in cellular binding and internalization of nanosystems.[55,56] Increasing the concentration of DTX resulted in high levels of cytotoxicity, and as DTX treatment was performed in free form, it was critical to select a concentration that enhanced transfection activity without affecting the cell viability (Figure 25b). Therefore, the concentration of 0.006 μM, which tripled the transgene expression of the developed nanocarriers, was selected for further studies, namely those involving the delivery of the therapeutic gene.

In this regard, to evaluate the therapeutic potential resulting from the combination of suicide gene therapy strategy with a low concentration of DTX, HepG2 cells were treated with free drug or with $PAMA_{144}$-*co*-$PLAMA_{19}$-based nanosystems carrying the pTK plasmid, in the presence (combined therapy) or absence of DTX, followed by incubation for five days with 100 μM of ganciclovir (Figure 26**)**.

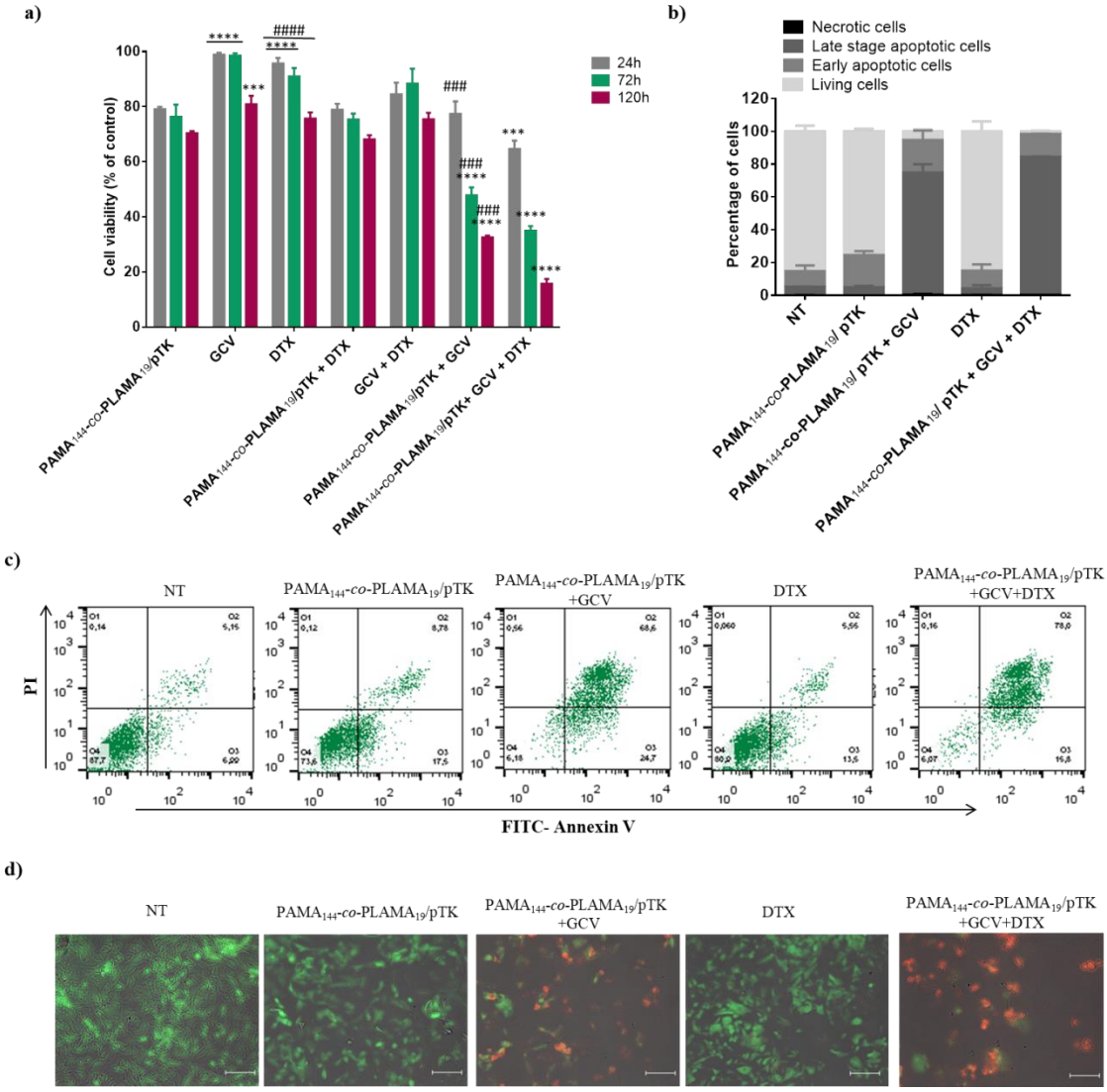

Figure 26- Therapeutic potential of the suicide gene therapy strategy mediated by the glycopolymer-based nanocarrier combined with DTX. Effect on viability (a) and apoptosis levels of HepG2 cells (b, c and d). HepG2 cells were treated with different antitumor strategies: suicide gene therapy ($PAMA_{144}$-*co*-$PLAMA_{19}$/pTK + GCV), chemotherapy (free DTX) and suicide gene therapy combined with chemotherapy ($PAMA_{144}$-*co*-$PLAMA_{19}$/pTK + GCV + DTX). a) The data are expressed as the percentage of cell viability with respect to untreated cells (control). Asterisks (****p <0.0001, ***p<0.001) indicate values that significantly differ from those measured for cells transfected with $PAMA_{144}$-*co*-$PLAMA_{19}$-based nanocarriers, containing 1 μg of pTK plasmid. Cardinals (####p < 0.0001 and ###p < 0.001) correspond to data from cells treated with each individual strategy ($PAMA_{144}$-*co*-$PLAMA_{19}$/pTK + GCV or DTX) which significantly differ from those obtained with cells treated with the combined therapy ($PAMA_{144}$-*co*-$PLAMA_{19}$/pTK + GCV + DTX). b) Percentage of viable, early apoptotic, late apoptotic/necrotic and necrotic cells obtained from flow cytometry analysis, measured after 72 h of treatment. c) Representative scatter plots of FITC-annexin V vs PI. Q1, necrotic cells;

Q2, late apoptotic/necrotic cells; Q3, early apoptotic cells, Q4, viable cells. d) Representative images of overlapping fluorescence microscopy and phase contrast of cells using fluorescein diacetate (green) and propidium iodide (red) staining for imaging live and dead cells, respectively (scale bar = 50 μm).

As shown in Figure 26a, the cytotoxic effect promoted by the HSV-TK/GCV gene therapy strategy or the combined approach is time-dependent, being the highest cytotoxic effect observed at the fifth day of treatment. After transfection with $PAMA_{144}$-*co*-$PLAMA_{19}$/pTK-based nanocarriers, followed by five days of treatment with 100 μM GGV, 68% of cell death was achieved. On the other hand, the treatment of non-transfected cells with DTX resulted only in a slight decrease of cell viability. However, the preincubation of cells with 0.006 μM DTX, followed by five days of treatment with 100 μM GGV resulted in 85% of cytotoxicity, showing an additive effect promoted by the combination of these two therapeutic approaches. As shown in Figure 26a, GCV was not toxic to non-transfected cells, either per se or in the presence of DTX, and no significant toxicity was measured upon transfection of cells in the absence of GCV treatment. To confirm these data, cytotoxicity was also measured through the SRB assay, which allows determination of cell viability in terms of cell proliferation, based on protein content relatively to untreated control cells, instead of metabolic activity. The results showed that the combined therapeutic strategy indeed produced a higher level of toxicity than that obtained with the individual approaches (Figure B11b, Appendix B). This additive effect was probably a consequence of the multiple effects associated with the combined strategy. Most notably, the small amount of DTX, which by itself does not cause a significant toxicity, could enhance the effect of the gene therapy strategy, by binding to beta-tubulin, inhibiting microtubule depolymerization, and consequently enhancing gene expression HSV-TK. Moreover, DTX many not only improve gene therapy strategy, but also directly contribute to antitumor effect by arresting the cell cycle at the mitosis level and reducing the expression of anti-apoptotic genes.[32]The molecular mechanism of cell death involved in the antitumor activity of the combined and individual strategies was evaluated by cell staining with annexin V and PI. As shown in Figure 26b and c, cells treated with our proposed combined therapeutic strategy ($PAMA_{144}$-*co*-$PLAMA_{19}$/pTK + GCV + DTX) had a higher percentage of non-viable apoptotic and/or necrotic cells after 72 h of incubation than cells treated with the individual strategies ($PAMA_{144}$-*co*-$PLAMA_{19}$/pTK + GCV or DTX). Furthermore, the negligible toxic effect of 0.006 μM DTX, confirmed the hypothesis that this chemotherapeutic drug, at this concentration, merely enhances the transfection ability of the developed glycoplexes, thereby increasing the success of the suicide gene therapy strategy. Moreover, a large number of necrotic (red) than viable cells (green) were observed with the developed combined strategy, compared with the individual therapeutic strategies (Figure 26d and Figure B11, Appendix B)

3D tumor spheroids have been used to overcome 2D culture constraints, by providing more realistic spatial/structural architecture and biophysiological relevant information, bridging the experimental gap between *in vivo* and *in vitro* results.[57,58] In order to evaluate the robustness of these therapeutic approaches, the antitumor effect of the combined strategy (PAMA$_{144}$-*co*-PLAMA$_{19}$/pTK + GCV + DTX) and of the individual approaches, suicide gene therapy (PAMA$_{144}$-*co*-PLAMA$_{19}$/pTK + GCV) and chemotherapy (DTX), was examined in HepG2 tumor spheroids.

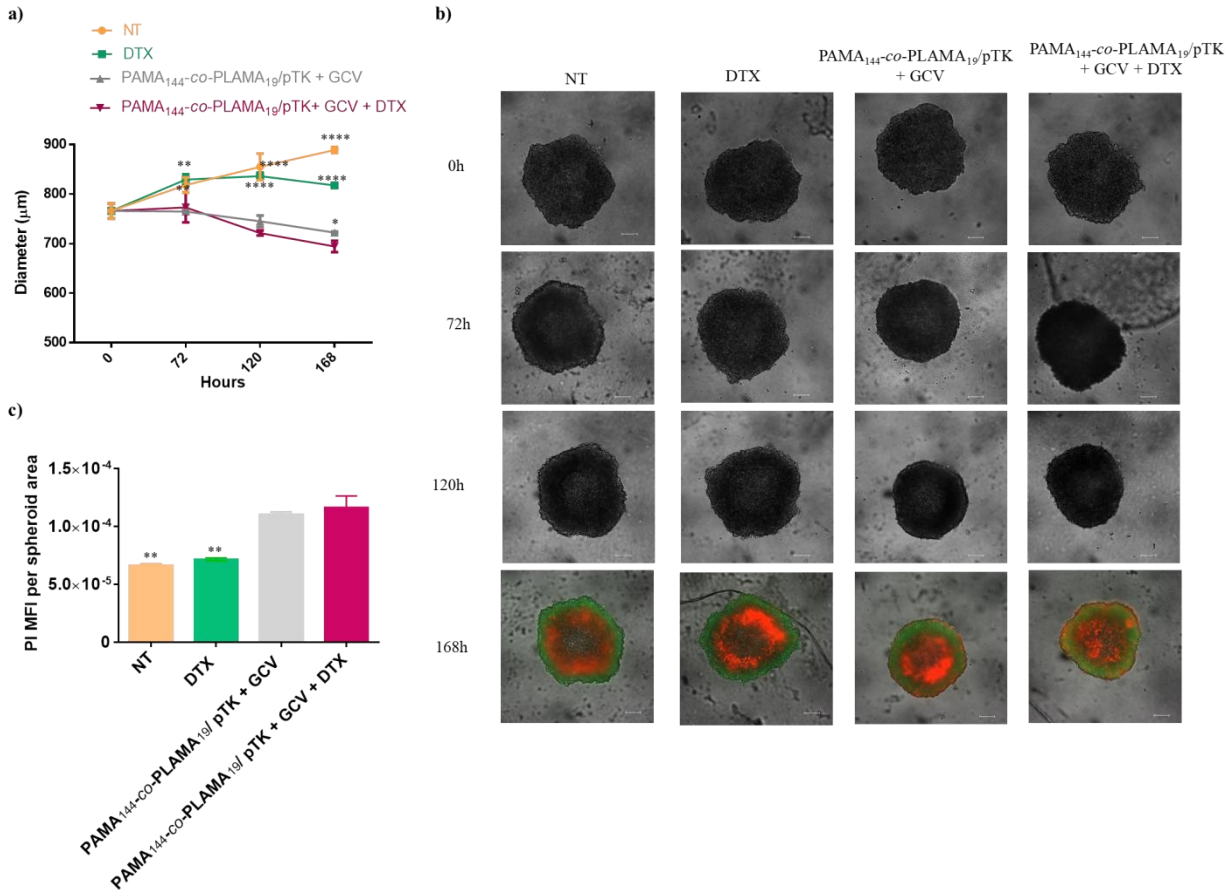

Figure 27– Effect of the suicide gene therapy strategy mediated by the glycopolymer-based nanocarriers combined with DTX on the tumor spheroid growth. HepG2-spheroids were treated with different antitumor strategies: suicide gene therapy (PAMA$_{144}$-*co*-PLAMA$_{19}$/pTK + GCV), DTX and suicide gene therapy combined with DTX (PAMA$_{144}$-*co*-PLAMA$_{19}$/pTK + GCV + DTX). a) Asterisks (****p <0.0001, ***p<0.001) correspond to data achieved with spheroids treated with each individual strategy and non-treated control, which significantly differ from those obtained with spheroids treated with the combined therapy (PAMA$_{144}$-*co*-PLAMA$_{19}$/pTK + GCV + DTX) . b) The microscopic images (scale bar = 200 µm) from 0 h to 120 h are phase contrast images, and the microscopic images for 168 h are fluorescence images using

fluorescein diacetate (green) and propidium iodide (red) staining for imaging live and dead cells, respectively. c) PI Mean Fluorescence Intensity (MFI) per spheroid area.

The results presented in Figure 27a and 27b show that after 168 h of transfection with $PAMA_{144}$-*co*-$PLAMA_{19}$/pTK- based nanocarriers, followed by treatment with 100 μM of GGV, the size of tumor spheroids decreased by 30%, whereas no significant change in their diameter was observed in non-transfected cells treated with 0.006 μM DTX. However, tumor spheroids treated with our proposed combined therapeutic strategy ($PAMA_{144}$-*co*-$PLAMA_{19}$/pTK + GCV + DTX) showed a reduction of 38% in the size. In addition, the PI mean fluorescence intensity (MIF) measurements showed that spheroids treated with PAMA144-co-PLAMA19/pTK + GCV or with PAMA144-co-PLAMA19/pTK + GCV + DTX exhibited a higher PI MIF per spheroid area than those treated with DTX or non-treated ones (Figure 27c), demonstrating the high therapeutic potential of suicide gene therapy combined with docetaxel.

4.4. Conclusion

In summary, we developed a novel glycopolymer-based nanocarrier and evaluated the antitumor effect resulting from the combination of HSV-TK suicide gene therapy, mediated by these HCC-targeted nanosystems, with low concentrations of DTX. To this end, a series of water-soluble PAMA-*co*-PLAMA random glycopolymers were synthesized by ARGET ATRP (without protection/deprotection chemistry). These polymethacrylate-based glycopolymers have shown to be capable of forming nanosystems for gene delivery with suitable physicochemical properties, high transfection efficiency, biocompatibility and ASGPR-specificity. In addition, our best formulation, $PAMA_{144}$-*co*-$PLAMA_{19}$-based polyplexes, showed excellent performance as suicide gene therapy mediators, with substantial antitumor effects enhanced by combination with DTX, even in hard-to-transfect multicellular tumor spheroids. Overall, the obtained results show the great potential of the $PAMA_{144}$-*co*-$PLAMA_{19}$ glycopolymer as an effective nanoplatform for gene delivery and that their combination with docetaxel represents a promising strategy for the treatment of HCC.

Acknowledgment

This work was financed by the European Regional Development Fund (ERDF) through the COMPETE 2020 program (Operational Program for Competitiveness and

Internationalization) and Portuguese national funds via FCT – Fundação para a Ciência e a Tecnologia, under projects: IF/01007/2015, POCI-01-0145-FEDER-30916, UIDB/04539/2020 and UIDP/04539/2020. Daniela Santo acknowledges FCT for the Grant: SFRH/BD/132601/2017. RC acknowledges financial support from FCT by Scientific Employment Stimulus - 2020.00186.CEECIND. The ^{1}H-NMR data was collected at the UC-NMR facility which is supported in part by FEDER –European Regional Development Fund through the COMPETE Programme (Operational Programme for Competitiveness) and by National Funds through FCT – Fundação para a Ciência e a Tecnologia (Portuguese Foundation for Science and Technology) through grants REEQ/481/QUI/2006, RECI/QEQ-QFI/0168/2012, CENTRO-07-CT62-FEDER-002012, and Rede Nacional de Ressonância Magnética Nuclear (RNRMN).

4.5. References

(1) Sung, H.; Ferlay, J.; Siegel, R. L.; Laversanne, M.; Soerjomataram, I.; Jemal, A.; Bray, F. Global Cancer Statistics 2020: GLOBOCAN Estimates of Incidence and Mortality Worldwide for 36 Cancers in 185 Countries. *CA. Cancer J. Clin.* **2021**, *71* (3), 209–249.

(2) Yang, J. D.; Hainaut, P.; Gores, G. J.; Amadou, A.; Plymoth, A.; Roberts, L. R. A Global View of Hepatocellular Carcinoma: Trends, Risk, Prevention and Management. *Nat. Rev. Gastroenterol. Hepatol.* **2019**, *16* (10), 589–604.

(3) Su, T.-H.; Hsu, S.-J.; Kao, J.-H. Paradigm Shift in the Treatment Options of Hepatocellular Carcinoma. *Liver Int.* **2022**, *42* (9), 2067–2079.

(4) Llovet, J. M.; Kelley, R. K.; Villanueva, A.; Singal, A. G.; Pikarsky, E.; Roayaie, S.; Lencioni, R.; Koike, K.; Zucman-Rossi, J.; Finn, R. S. Hepatocellular Carcinoma. *Nat. Rev. Dis. Prim.* **2021**, *7* (1), 6.

(5) Singh, V.; Khan, N.; Jayandharan, G. R. Vector Engineering, Strategies and Targets in Cancer Gene Therapy. *Cancer Gene Ther.* **2022**, *29* (5), 402–417.

(6) Gene Therapy Clinical Trials Worldwide. The Journal of Gene Medicine. *https://a873679.fmphost.com/fmi/webd/GTCT*.

(7) Sukumar, U. K.; Rajendran, J. C. B.; Gambhir, S. S.; Massoud, T. F.; Paulmurugan, R. SP94-Targeted Triblock Copolymer Nanoparticle Delivers Thymidine Kinase-P53-Nitroreductase Triple Therapeutic Gene and Restores Anticancer Function against Hepatocellular Carcinoma in Vivo. *ACS Appl.*

Mater. Interfaces **2020**, *12* (10), 11307–11319.

(8) Cordeiro, R. A.; Mendonça, P. V.; Coelho, J.; Faneca, H. Engineering Silica-Polymer Hybrid Nanosystems for Dual Drug and Gene Delivery. *Biomater. Adv.* **2022**, *135*, 212742.

(9) Malekshah, O. M.; Chen, X.; Nomani, A.; Sarkar, S.; Hatefi, A. Enzyme/Prodrug Systems for Cancer Gene Therapy. *Curr. Pharmacol. Reports* **2016**, *2* (6), 299–308.

(10) Vago, R.; Collico, V.; Zuppone, S.; Prosperi, D.; Colombo, M. Nanoparticle-Mediated Delivery of Suicide Genes in Cancer Therapy. *Pharmacol. Res.* **2016**, *111*, 619–641.

(11) Van Bruggen, C.; Hexum, J. K.; Tan, Z.; Dalal, R. J.; Reineke, T. M. Nonviral Gene Delivery with Cationic Glycopolymers. *Acc. Chem. Res.* **2019**, *52* (5), 1347–1358.

(12) Ma, Z.; Zhu, X. X. Copolymers Containing Carbohydrates and Other Biomolecules: Design, Synthesis and Applications. *J. Mater. Chem. B* **2019**, *7* (9), 1361–1378.

(13) Pramudya, I.; Chung, H. Recent Progress of Glycopolymer Synthesis for Biomedical Applications. *Biomater. Sci.* **2019**, *7* (12), 4848–4872.

(14) Galbis, J. A.; García-Martín, M. D. G.; De Paz, M. V.; Galbis, E. Synthetic Polymers from Sugar-Based Monomers. *Chem. Rev.* **2016**, *116* (3), 1600–1636.

(15) Thapa, B.; Kumar, P.; Zeng, H.; Narain, R. Asialoglycoprotein Receptor-Mediated Gene Delivery to Hepatocytes Using Galactosylated Polymers. *Biomacromolecules* **2015**, *16* (9), 3008–3020.

(16) Perrone, F.; Craparo, E. F.; Cemazar, M.; Kamensek, U.; Drago, S. E.; Dapas, B.; Scaggiante, B.; Zanconati, F.; Bonazza, D.; Grassi, M.; et al. Targeted Delivery of SiRNAs against Hepatocellular Carcinoma-Related Genes by a Galactosylated Polyaspartamide Copolymer. *J. Control. Release* **2021**, *330*, 1132–1151.

(17) Lu, J.; Wang, J.; Ling, D. Surface Engineering of Nanoparticles for Targeted Delivery to Hepatocellular Carcinoma. *Small* **2018**, *14* (5), 1702037.

(18) Ahmed, M.; Narain, R. The Effect of Molecular Weight, Compositions and Lectin Type on the Properties of Hyperbranched Glycopolymers as Non-Viral Gene Delivery Systems. *Biomaterials* **2012**, *33* (15), 3990–4001.

(19) Dhande, Y. K.; Wagh, B. S.; Hall, B. C.; Sprouse, D.; Hackett, P. B.; Reineke, T.

M. N-Acetylgalactosamine Block-Co-Polycations Form Stable Polyplexes with Plasmids and Promote Liver-Targeted Delivery. *Biomacromolecules* **2016**, *17* (3), 830–840.

(20) Smith, A. E.; Sizovs, A.; Grandinetti, G.; Xue, L.; Reineke, T. M. Diblock Glycopolymers Promote Colloidal Stability of Polyplexes and Effective PDNA and SiRNA Delivery under Physiological Salt and Serum Conditions. *Biomacromolecules* **2011**, *12* (8), 3015–3022.

(21) Chen, Y.; Diaz-Dussan, D.; Peng, Y.-Y.; Narain, R. Hydroxyl-Rich PGMA-Based Cationic Glycopolymers for Intracellular SiRNA Delivery: Biocompatibility and Effect of Sugar Decoration Degree. *Biomacromolecules* **2019**, *20* (5), 2068–2074.

(22) Thapa, B.; Kumar, P.; Zeng, H.; Narain, R. Asialoglycoprotein Receptor-Mediated Gene Delivery to Hepatocytes Using Galactosylated Polymers. *Biomacromolecules* **2015**, *16* (9), 3008–3020.

(23) Ahmed, M.; Narain, R. The Effect of Polymer Architecture, Composition, and Molecular Weight on the Properties of Glycopolymer-Based Non-Viral Gene Delivery Systems. *Biomaterials* **2011**, *32* (22), 5279–5290.

(24) Peng, Y. Y.; Diaz-Dussan, D.; Kumar, P.; Narain, R. Tumor Microenvironment-Regulated Redox Responsive Cationic Galactose-Based Hyperbranched Polymers for SiRNA Delivery. *Bioconjug. Chem.* **2019**, *30* (2), 405–412.

(25) Quan, S.; Kumar, P.; Narain, R. Cationic Galactose-Conjugated Copolymers for Epidermal Growth Factor (EGFR) Knockdown in Cervical Adenocarcinoma. *ACS Biomater. Sci. Eng.* **2016**, *2* (5), 853–859.

(26) Ahmed, M.; Deng, Z.; Liu, S.; Lafrenie, R.; Kumar, A.; Narain, R. Cationic Glyconanoparticles: Their Complexation with DNA, Cellular Uptake, and Transfection Efficiencies. *Bioconjug. Chem.* **2009**, *20* (11), 2169–2176.

(27) Singhsa, P.; Diaz-Dussan, D.; Manuspiya, H.; Narain, R. Well-Defined Cationic N-[3-(Dimethylamino)Propyl]Methacrylamide Hydrochloride-Based (Co)Polymers for SiRNA Delivery. *Biomacromolecules* **2018**, *19* (1), 209–221.

(28) Peng, Y. Y.; Diaz-Dussan, D.; Kumar, P.; Narain, R. Acid Degradable Cationic Galactose-Based Hyperbranched Polymers as Nanotherapeutic Vehicles for Epidermal Growth Factor Receptor (EGFR) Knockdown in Cervical Carcinoma. *Biomacromolecules* **2018**, *19* (10), 4052–4058.

(29) Bockman, M. R.; Dalal, R. J.; Kumar, R.; Reineke, T. M. Facile Synthesis of GalNAc Monomers and Block Polycations for Hepatocyte Gene Delivery. *Polym. Chem.* **2021**, *12* (28), 4063–4071.

(30) Li, H.; Cortez, M. A.; Phillips, H. R.; Wu, Y.; Reineke, T. M. Poly(2-Deoxy-2-Methacrylamido Glucopyranose)-b -Poly(Methacrylate Amine)s: Optimization of Diblock Glycopolycations for Nucleic Acid Delivery. *ACS Macro Lett.* **2013**, *2* (3), 230–235.

(31) Chen, J.; Wang, K.; Wu, J.; Tian, H.; Chen, X. Polycations for Gene Delivery: Dilemmas and Solutions. *Bioconjug. Chem.* **2019**, *30* (2), 338–349.

(32) Herbst, R. S.; Khuri, F. R. Mode of Action of Docetaxel – a Basis for Combination with Novel Anticancer Agents. *Cancer Treat. Rev.* **2003**, *29* (5), 407–415.

(33) Wang, L.; MacDonald, R. C. Effects of Microtubule-Depolymerizing Agents on the Transfection of Cultured Vascular Smooth Muscle Cells: Enhanced Expression with Free Drug and Especially with Drug–Gene Lipoplexes. *Mol. Ther.* **2004**, *9* (5), 729–737.

(34) Vichai, V.; Kirtikara, K. Sulforhodamine B Colorimetric Assay for Cytotoxicity Screening. *Nat. Protoc.* **2006**, *1* (3), 1112–1116.

(35) Alonso, S. Exploiting the Bioengineering Versatility of Lactobionic Acid in Targeted Nanosystems and Biomaterials. *J. Control. Release* **2018**, *287* (August), 216–234.

(36) Narain, R.; Armes, S. P. Synthesis and Aqueous Solution Properties of Novel Sugar Methacrylate-Based Homopolymers and Block Copolymers. *Biomacromolecules* **2003**, *4* (6), 1746–1758.

(37) Read, E. S.; Thompson, K. L.; Armes, S. P. Synthesis of Well-Defined Primary Amine-Based Homopolymers and Block Copolymers and Their Michael Addition Reactions with Acrylates and Acrylamides. *Polym. Chem.* **2010**, *1* (2), 221–230.

(38) Baker, S. L.; Kaupbayeva, B.; Lathwal, S.; Das, S. R.; Russell, A. J.; Matyjaszewski, K. Atom Transfer Radical Polymerization for Biorelated Hybrid Materials. *Biomacromolecules* **2019**, *20* (12), 4272–4298.

(39) Santo, D.; Mendonça, P. V; Lima, M. S.; Cordeiro, R. A.; Cabanas, L.; Serra, A.; Coelho, J. F. J.; Faneca, H. Poly(Ethylene Glycol)-Block-Poly(2-Aminoethyl

Methacrylate Hydrochloride)-Based Polyplexes as Serum-Tolerant Nanosystems for Enhanced Gene Delivery. *Mol. Pharm.* **2019**, *16* (5), 2129–2141.

(40) Bus, T.; Traeger, A.; Schubert, U. S. The Great Escape: How Cationic Polyplexes Overcome the Endosomal Barrier. *J. Mater. Chem. B* **2018**, *6* (43), 6904–6918.

(41) Zhao, L.; Li, Y.; Pei, D.; Huang, Q.; Zhang, H.; Yang, Z.; Li, F.; Shi, T. Glycopolymers/PEI Complexes as Serum-Tolerant Vectors for Enhanced Gene Delivery to Hepatocytes. *Carbohydr. Polym.* **2019**, *205*, 167–175.

(42) Tan, Z.; Dhande, Y. K.; Reineke, T. M. Cell Penetrating Polymers Containing Guanidinium Trigger Apoptosis in Human Hepatocellular Carcinoma Cells Unless Conjugated to a Targeting N-Acetyl-Galactosamine Block. *Bioconjug. Chem.* **2017**, *28* (12), 2985–2997.

(43) Huang, X.; Leroux, J. C.; Castagner, B. Well-Defined Multivalent Ligands for Hepatocytes Targeting via Asialoglycoprotein Receptor. *Bioconjug. Chem.* **2017**, *28* (2), 283–295.

(44) Monnery, B. D. Polycation-Mediated Transfection: Mechanisms of Internalization and Intracellular Trafficking. *Biomacromolecules* **2021**, *22* (10), 4060–4083.

(45) Kumar, R.; Santa Chalarca, C. F.; Bockman, M. R.; Bruggen, C. Van; Grimme, C. J.; Dalal, R. J.; Hanson, M. G.; Hexum, J. K.; Reineke, T. M. Polymeric Delivery of Therapeutic Nucleic Acids. *Chem. Rev.* **2021**, *121* (18), 11527–11652.

(46) Palermo, E. F.; Lee, D.-K.; Ramamoorthy, A.; Kuroda, K. Role of Cationic Group Structure in Membrane Binding and Disruption by Amphiphilic Copolymers. *J. Phys. Chem. B* **2011**, *115* (2), 366–375.

(47) Becer, C. R. The Glycopolymer Code: Synthesis of Glycopolymers and Multivalent Carbohydrate–Lectin Interactions. *Macromol. Rapid Commun.* **2012**, *33* (9), 742–752.

(48) Ingle, N. P.; Hexum, J. K.; Reineke, T. M. Polyplexes Are Endocytosed by and Trafficked within Filopodia. *Biomacromolecules* **2020**, *21* (4), 1379–1392.

(49) Hebbar, M.; Ernst, O.; Cattan, S.; Dominguez, S.; Oprea, C.; Mathurin, P.; Triboulet, J. P.; Paris, J. C.; Pruvot, F. R. Phase II Trial of Docetaxel Therapy in Patients with Advanced Hepatocellular Carcinoma. *Oncology* **2006**, *70* (2), 154–

158.

(50) Gu, J.; Hao, J.; Fang, X.; Sha, X. Factors Influencing the Transfection Efficiency and Cellular Uptake Mechanisms of Pluronic P123-Modified Polypropyleneimine/PDNA Polyplexes in Multidrug Resistant Breast Cancer Cells. *Colloids Surfaces B Biointerfaces* **2016**, *140*, 83–93.

(51) Vaughan, E. E.; Geiger, R. C.; Miller, A. M.; Loh-Marley, P. L.; Suzuki, T.; Miyata, N.; Dean, D. A. Microtubule Acetylation Through HDAC6 Inhibition Results in Increased Transfection Efficiency. *Mol. Ther.* **2008**, *16* (11), 1841–1847.

(52) Sheikh, S.; Ernst, D.; Keating, A. Prodrugs and Prodrug-Activated Systems in Gene Therapy. *Mol. Ther.* **2021**, *29* (5), 1716–1728.

(53) Vaughan, H. J.; Zamboni, C. G.; Hassan, L. F.; Radant, N. P.; Jacob, D.; Mease, R. C.; Minn, I.; Tzeng, S. Y.; Gabrielson, K. L.; Bhardwaj, P.; et al. Polymeric Nanoparticles for Dual-Targeted Theranostic Gene Delivery to Hepatocellular Carcinoma. *Sci. Adv.* **2022**, *8* (29), eabo6406.

(54) Ingle, N. P.; Hexum, J. K.; Reineke, T. M. Polyplexes Are Endocytosed by and Trafficked within Filopodia. *Biomacromolecules* **2020**.

(55) Faneca, H.; Faustino, A.; Pedroso de Lima, M. C. Synergistic Antitumoral Effect of Vinblastine and HSV-Tk/GCV Gene Therapy Mediated by Albumin-Associated Cationic Liposomes. *J. Control. Release* **2008**, *126* (2), 175–184.

(56) Barua, S.; Rege, K. The Influence of Mediators of Intracellular Trafficking on Transgene Expression Efficacy of Polymer–plasmid DNA Complexes. *Biomaterials* **2010**, *31* (22), 5894–5902.

(57) Rodrigues, T.; Kundu, B.; Silva-Correia, J.; Kundu, S. C.; Oliveira, J. M.; Reis, R. L.; Correlo, V. M. Emerging Tumor Spheroids Technologies for 3D in Vitro Cancer Modeling. *Pharmacol. Ther.* **2018**, *184*, 201–211.

(58) Sant, S.; Johnston, P. A. The Production of 3D Tumor Spheroids for Cancer Drug Discovery. *Drug Discov. Today Technol.* **2017**, *23*, 27–36.

(59) Britovsek, G. J. P.; England, J.; White, A. J. P. Non-Heme Iron(II) Complexes Containing Tripodal Tetradentate Nitrogen Ligands and Their Application in Alkane Oxidation Catalysis. *Inorg. Chem.* **2005**, *44* (22), 8125–8134.

CHAPTER 4

CONCLUDING REMARKS AND FUTURE PERSPECTIVES

4.1. Concluding remarks

Hepatocellular carcinoma is a challenging global health concern due to rising prevalence and high mortality worldwide. The future advances in the field of cancer gene therapy are largely dependent on the development of efficient and targeted gene delivery platforms that allow the achievement of the desired therapeutic effects and the reduction of the off-target effects. Cationic glycopolymers stand out as gene delivery nanosystems due to their biocompatibility and high binding affinity to the ASGPR, a target receptor overexpressed in HCC cells. The most commonly used glycopolymers are the methacrylamide-based ones that are prepared by copolymerization of primary amine monomers and carbohydrate-derived monomers. However, the lower susceptibility of these copolymers to hydrolysis, compared to their methacrylates counterparts, reduces their ability to promote the endolysosomal escape of genetic material and, thus, decreases their efficacy as gene delivery nanocarriers. Therefore, primary amine containing polymethacrylate-based glycopolymers exhibit higher potential as gene delivery nanosystems. Nevertheless, their synthesis procedure remains laborious and complex, with problems of solubilization and the need for protection/deprotection steps.

In this context, it was proposed the development of a highly efficient and HCC-specific polymethacrylate-based gene delivery nanosystem, and the evaluation of the antitumor effect resulting from the combination of gene therapy, mediated by these nanosystems, with low concentrations of different chemotherapeutic agents.

Thus, the first aim of this thesis was the synthesis of a library of tailor-made cationic glycopolymers, based on PAMA and PLAMA, with different compositions (block or random) and carbohydrate/cationic ratios. The synthesis of these well-defined glycopolymers was performed by ARGET ATRP, using a slow feeding of ascorbic acid for the regeneration of the activator, without protecting group chemistry, avoiding the typically troublesome multistep protection/deprotection reactions of glycopolymer synthesis. The results showed that the developed ARGET ATRP method yielded homopolymers, and random and diblock glycopolymers with good control over molecular weight. Among the different glycopolymers prepared, it was found that the nanocarriers generated with the random $PAMA_{114}$-*co*-$PLAMA_{20}$ copolymer presented higher transfection activity than that obtained with the $PAMA_{161}$-, PEG_{45}-*b*-$PAMA_{168}$- and PEI-based nanocarriers used as reference. These nanosystems exhibited higher

biological activity and biocompatibility than the glycoplexes prepared with the corresponding block glycopolymer. In addition, the inhibition of the transfection activity of these nanosystems in the presence of asialofetuin or an antibody against the ASGPR, in HCC cells, and the negligible biological activity in ASGPR-deficient cells, clearly demonstrated that $PAMA_{114}$-*co*-$PLAMA_{20}$-based polyplexes specifically bind to the ASGPR, being internalized by clathrin-mediated endocytosis. The expression of *c-MYC* was significantly inhibited upon transfections of HCC cells with $PAMA_{114}$-*co*-$PLAMA_{20}$/MYC shRNA nanosystems, which markedly increased the sensitivity of tumor cells to sorafenib (SF) treatment. Furthermore, the obtained results showed that *c-MYC* downregulation promoted a significantly decrease on tumor cell proliferation that was further reduced by combination with SF, which had only a slight effect by itself. Moreover, the data demonstrated that SF-induced apoptosis was synergistically enhanced by *c-MYC* downregulation in 2D and 3D HCC-tumor models.

The obtained results demonstrated the potential of $PAMA_{114}$-*co*-$PLAMA_{20}$-based nanocarriers as a HCC-targeted gene delivery nanosystem, and showed that the sensitization of tumor cells to SF, through *c-MYC* silencing, is a promising strategy for the treatment of HCC.

In the second part of this work, a wide range of well-defined primary amine polymethacrylate-based glycopolymers, with fixed DP of LAMA and different DP values of AMA, was synthesized by ARGET ATRP, to determine the effect of primary amine content on the physicochemical properties, biological activity, biocompatibility, and ASGPR specificity of the developed nanocarriers. These glycopolymers demonstrated to be capable of forming nanosystems for gene delivery with suitable physicochemical properties, high transfection efficiency, biocompatibility and ASGPR-specificity. Among the different glycopolymers produced with $PLAMA_{20}$ and different degrees of polymerization of AMA, it was shown that nanocarriers generated with $PAMA_{144}$-*co*-$PLAMA_{19}$ presented the highest transfection activity, when compared to those prepared with glycopolymers with lower content of AMA. In addition, these nanocarriers exhibited excellent performance as suicide gene therapy mediators, promoting a substantial antitumor effect that was further enhanced by combination with docetaxel (DTX), even in hard-to-transfect multicellular tumor spheroids. DTX, which by itself does not cause a significant toxicity at the used concentration, enhanced the effect of the gene therapy strategy, by binding to beta-tubulin, inhibiting microtubule

depolymerization and, consequently, enhancing *HSV-TK* gene expression. The obtained results demonstrated the great potential of the $PAMA_{144}$-*co*-$PLAMA_{19}$ glycopolymer as an effective nanoplatform for gene delivery, and that combination of *HSV-TK*/GCV suicide gene therapy, mediated by these nanosystems, with low amounts of docetaxel represents a promising strategy for the treatment of HCC.

To sum up, this PhD work allowed the development of new HCC-targeted gene delivery nanosystems and their application in the generation of different therapeutic strategies with high potential to treat HCC.

4.2. Future perspectives

The results presented in this project constitute an important basis to explore new avenues in the area of glycopolymer-based gene delivery nanocarriers and in their potential to mediate combined antitumor strategies for HCC treatment. Among several possibilities to continue this work, the following ideas are considered to be of particular relevance:

- To evaluate the polyplex stability (such as, against heparin replacement or DNase I agarose gel) as well as polyplex colloidal stability (i.e., in serum-rich cell culture medium);
- To evaluate the *in vivo* transfection capacity of $PAMA_{114}$-*co*-$PLAMA_{20}$- and $PAMA_{144}$-*co*-$PLAMA_{19}$-based polyplexes in an orthotopic animal model of HCC;
- To explore the *c-MYC* sensitization effect, namely by analyzing the levels of multiple target proteins associated with sorafenib resistance after the transfection with $PAMA_{114}$-*co*-$PLAMA_{20}$/MYC shRNA;
- To assess the antitumor effect of $PAMA_{114}$-*co*-$PLAMA_{20}$/MYC shRNA combined with low concentrations of sorafenib, including the involved antitumor mechanisms, in an orthotopic animal model of HCC;
- To further explore the antitumor effect of the developed suicide gene therapy strategy and its enhancement by combination with docetaxel;

- To evaluate the antitumor effect of the suicide gene therapy approach, mediated by the $PAMA_{144}$-*co*-$PLAMA_{19}$ glycopolymer, combined with docetaxel in an orthotopic animal model of HCC;

APPENDICES

APPENDIX A

SUPPORTING INFORMATION

THE SUPPLEMENTARY INFORMATION OF CHAPTER 2 IS PRESENTED IN THIS APPENDIX.

Synthesis and characterization of PAMA-b-PLAMA and PAMA-co-PLAMA glycopolymers

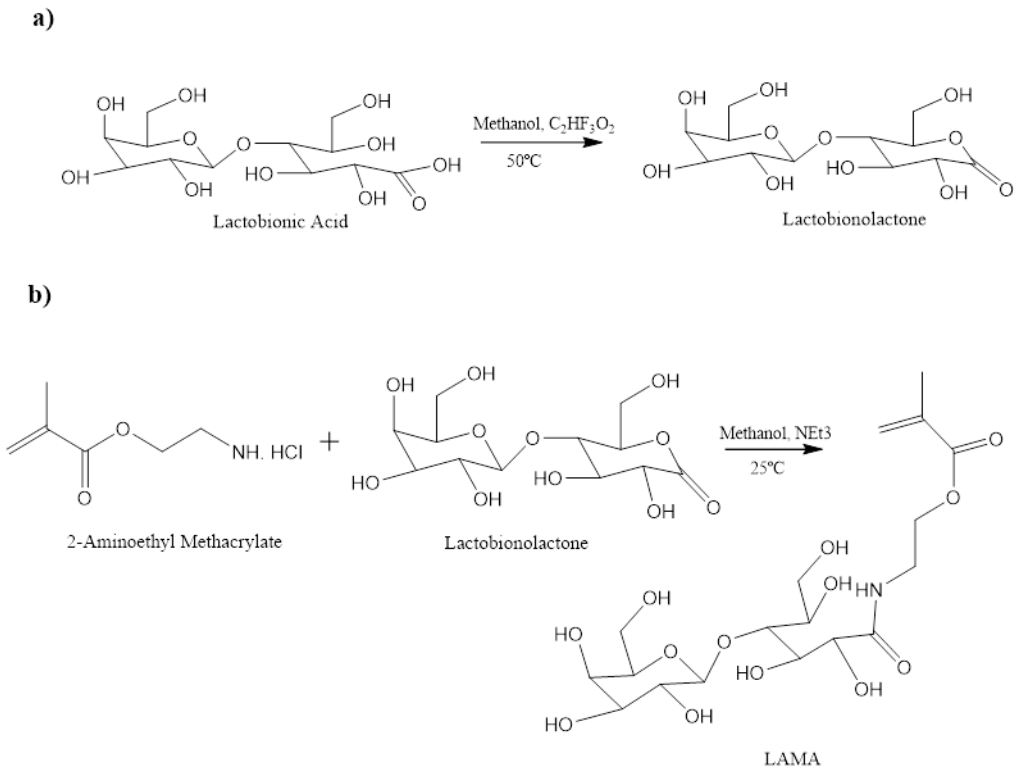

Scheme A1– Synthesis of 2-lactobionamidoethyl methacrylate (LAMA).a) Lactobionic acid was dissolved in anhydrous methanol at 50 ºC, in the presence of trifluoroacetic acid ($C_2HF_3O_2$), to obtain lactobionolactone. b) Lactobionolactone was dissolved in methanol, followed by the addition of 2-aminoethyl methacrylate hydrochloride, triethylamine (Net3) and hydroquinone at room temperature.

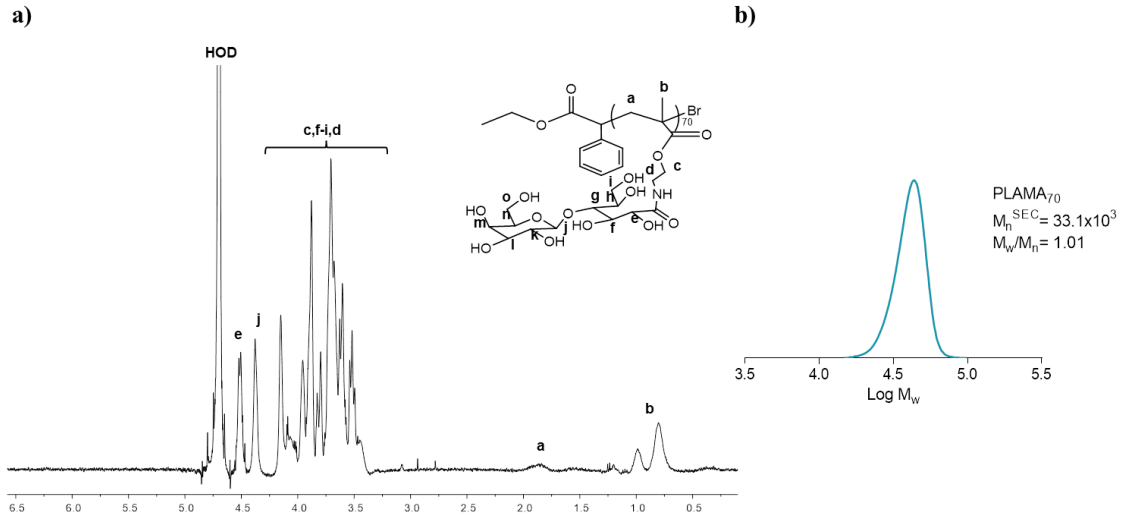

Figure A1- 400 MHz ^{1}H NMR spectrum in D_2O (a) and SEC trace (b) of the $PLAMA_{70}$ homopolymer prepared by ARGET ATRP.

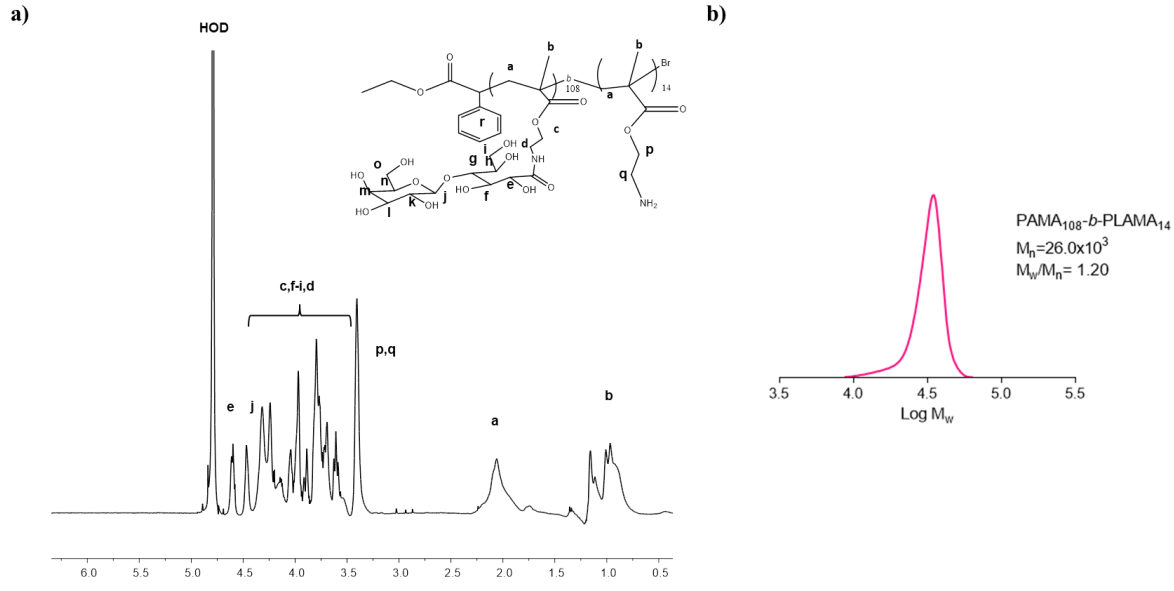

Figure A2– 400 MHz ^{1}H NMR spectrum in D_2O (a) and SEC trace (b) of the $PAMA_{108}$-*b*-$PLAMA_{14}$ block copolymer prepared by ARGET ATRP.

Physicochemical characterization of the nanosystems

Table A1– Statistical analysis of data presented in Figure 11a.

Experimental conditions	**p[a]**
$PAMA_{38}$-*co*-$PLAMA_{47}$ *vs*. all the other formulations	*

$PAMA_{50}$-*b*-$PLAMA_{49}$ *vs.* $PAMA_{114}$-*co*-$PLAMA_{20}$	*
$PAMA_{50}$-*b*-$PLAMA_{49}$ *vs.* $PAMA_{108}$-*b*-$PLAMA_{14}$	***
$PAMA_{50}$-*b*-$PLAMA_{49}$ *vs.* $PAMA_{94}$-*co*- $PLAMA_{9}$	***
$PAMA_{50}$-*b*-$PLAMA_{49}$ *vs.* $PAMA_{118}$-*b*-$PLAMA_{6}$	****
$PAMA_{50}$-*b*-$PLAMA_{49}$ *vs.* $PAMA_{87}$-*co*-$PLAMA_{42}$	**
$PAMA_{50}$-*b*-$PLAMA_{49}$ *vs.* $PAMA_{97}$-*b*-$PLAMA_{44}$	**
$PAMA_{50}$-*b*-$PLAMA_{49}$ *vs.* $PAMA_{92}$-*co*-$PLAMA_{95}$	*
$PAMA_{50}$-*b*-$PLAMA_{49}$ *vs.* $PAMA_{99}$-*b*-$PLAMA_{113}$	*
$PAMA_{50}$-*b*-$PLAMA_{49}$ *vs.* $PAMA_{161}$	*
$PAMA_{50}$-*b*-$PLAMA_{49}$ *vs.* PEG_{45}-*b*-$PAMA_{168}$	**
$PAMA_{114}$-*co*-$PLAMA_{20}$ *vs.* $PAMA_{108}$-*b*-$PLAMA_{14}$	*
$PAMA_{114}$-*co*-$PLAMA_{20}$ *vs.* $PAMA_{118}$-*b*-$PLAMA_{6}$	*
$PAMA_{114}$-*co*-$PLAMA_{20}$ *vs.* $PAMA_{92}$-*co*-$PLAMA_{95}$	*
$PAMA_{114}$-*co*-$PLAMA_{20}$ *vs.* $PAMA_{161}$	*
$PAMA_{108}$-*b*-$PLAMA_{14}$ *vs.* $PAMA_{94}$-*co*- $PLAMA_{9}$	**
$PAMA_{108}$-*b*-$PLAMA_{14}$ *vs.* $PAMA_{87}$-*co*-$PLAMA_{42}$	*
$PAMA_{108}$-*b*-$PLAMA_{14}$ *vs.* $PAMA_{92}$-*co*-$PLAMA_{95}$	**
$PAMA_{108}$-*b*-$PLAMA_{14}$ *vs.* $PAMA_{99}$-*b*-$PLAMA_{113}$	**
$PAMA_{108}$-*b*-$PLAMA_{14}$ *vs.* $PLAMA_{70}$	*
$PAMA_{108}$-*b*-$PLAMA_{14}$ *vs.* $PAMA_{161}$	**
$PAMA_{108}$-*b*-$PLAMA_{14}$ *vs.* PEG_{45}-*b*-$PAMA_{168}$	*
$PAMA_{94}$-*co*- $PLAMA_{9}$ *vs.* $PAMA_{118}$-*b*-$PLAMA_{6}$	**
$PAMA_{94}$-*co*- $PLAMA_{9}$ *vs.* $PAMA_{92}$-*co*-$PLAMA_{95}$	**
$PAMA_{94}$-*co*- $PLAMA_{9}$ *vs.* $PLAMA_{70}$	*
$PAMA_{94}$-*co*- $PLAMA_{9}$ *vs.* $PAMA_{161}$	**
$PAMA_{118}$-*b*-$PLAMA_{6}$ *vs.* $PAMA_{87}$-*co*-$PLAMA_{42}$	*
$PAMA_{118}$-*b*-$PLAMA_{6}$ *vs.* $PAMA_{92}$-*co*-$PLAMA_{95}$	****
$PAMA_{118}$-*b*-$PLAMA_{6}$ *vs.* $PAMA_{99}$-*b*-$PLAMA_{113}$	*
$PAMA_{118}$-*b*-$PLAMA_{6}$ *vs.* $PLAMA_{70}$	*
$PAMA_{118}$-*b*-$PLAMA_{6}$ *vs.* $PAMA_{161}$	***
$PAMA_{118}$-*b*-$PLAMA_{6}$ *vs.* PEG_{45}-*b*-$PAMA_{168}$	*
$PAMA_{87}$-*co*-$PLAMA_{42}$ *vs.* $PAMA_{92}$-*co*-$PLAMA_{95}$	***
$PAMA_{87}$-*co*-$PLAMA_{42}$ *vs.* $PLAMA_{70}$	*
$PAMA_{87}$-*co*-$PLAMA_{42}$ *vs.* $PAMA_{161}$	**
$PAMA_{97}$-*b*-$PLAMA_{44}$ *vs.* $PLAMA_{70}$	*
$PAMA_{92}$-*co*-$PLAMA_{95}$ *vs.* $PAMA_{99}$-*b*-$PLAMA_{113}$	*
$PAMA_{92}$-*co*-$PLAMA_{95}$ *vs.* PEG_{45}-*b*-$PAMA_{168}$	*
$PAMA_{99}$-*b*-$PLAMA_{113}$ *vs.* $PAMA_{161}$	*

[a]The statistical significance of differences between data was evaluated by one-way ANOVA using Turkey multiple comparisons test. Asterisks (****$p < 0.0001$, ***$p < 0.001$, **$p < 0.01$, and *$p < 0.05$) indicate values that differ significantly.

Table A2– Statistical analysis of data presented in Figure 11b.

Experimental conditions	**p[a]**
$PAMA_{38}$-*co*-$PLAMA_{47}$ *vs.* $PAMA_{114}$-*co*-$PLAMA_{20}$	**
$PAMA_{38}$-*co*-$PLAMA_{47}$ *vs.* $PAMA_{99}$-*b*-$PLAMA_{14}$	***
$PAMA_{38}$-*co*-$PLAMA_{47}$ *vs.* $PAMA_{99}$-*b*-$PLAMA_{113}$	****
$PAMA_{38}$-*co*-$PLAMA_{47}$ *vs.* $PLAMA_{70}$	****
$PAMA_{50}$-*b*-$PLAMA_{49}$ *vs.* $PAMA_{114}$-*co*-$PLAMA_{20}$	****
$PAMA_{50}$-*b*-$PLAMA_{49}$ *vs.* $PAMA_{94}$-*co*- $PLAMA_{9}$	**

$PAMA_{50}$-*b*-$PLAMA_{49}$ *vs.* $PAMA_{87}$-*co*-$PLAMA_{42}$	****
$PAMA_{50}$-*b*-$PLAMA_{49}$ *vs.* $PAMA_{99}$-*b*-$PLAMA_{113}$	**
$PAMA_{50}$-b-$PLAMA_{49}$ *vs.* $PLAMA_{70}$	****
$PAMA_{50}$-*b*-$PLAMA_{49}$ *vs.* $PAMA_{161}$	****
$PAMA_{50}$-*b*-$PLAMA_{49}$ *vs.* PEG_{45}-*b*-$PAMA_{168}$	****
$PAMA_{114}$-*co*-$PLAMA_{20}$ *vs.* $PAMA_{108}$-*b*-$PLAMA_{14}$	****
$PAMA_{114}$-*co*-$PLAMA_{20}$ *vs.* $PAMA_{118}$-*b*-$PLAMA_{6}$	****
$PAMA_{114}$-*co*-$PLAMA_{20}$ *vs.* $PAMA_{97}$-*b*-$PLAMA_{44}$	***
$PAMA_{114}$-*co*-$PLAMA_{20}$ *vs.* $PAMA_{92}$-*co*-$PLAMA_{95}$	****
$PAMA_{114}$-*co*-$PLAMA_{20}$ vs. $PAMA_{99}$-*b*-$PLAMA_{113}$	****
$PAMA_{114}$-*co*-$PLAMA_{20}$ *vs.* $PLAMA_{70}$	****
$PAMA_{108}$-*b*-$PLAMA_{14}$ *vs.* $PAMA_{94}$-*co*- PLAMA9	****
$PAMA_{108}$-*b*-$PLAMA_{14}$ *vs.* $PAMA_{87}$-*co*-$PLAMA_{42}$	****
$PAMA_{108}$-*b*-$PLAMA_{14}$ *vs.* $PAMA_{97}$-*b*-$PLAMA_{44}$	**
$PAMA_{108}$-*b*-$PLAMA_{14}$ *vs.* $PAMA_{92}$-*co*-$PLAMA_{95}$	*
$PAMA_{108}$-*b*-$PLAMA_{14}$ *vs.* $PLAMA_{70}$	****
$PAMA_{108}$-*b*-$PLAMA_{14}$ *vs.* $PAMA_{161}$	****
$PAMA_{108}$-*b*-$PLAMA_{14}$ *vs.* PEG_{45}-*b*-$PAMA_{168}$	****
$PAMA_{94}$-*co*- $PLAMA_{9}$ *vs.* $PAMA_{118}$-*b*-$PLAMA_{6}$	**
$PAMA_{94}$-*co*- $PLAMA_{9}$ *vs.* $PAMA_{99}$-*b*-$PLAMA_{113}$	****
$PAMA_{94}$-*co*- $PLAMA_{9}$ *vs.* $PLAMA_{70}$	****
$PAMA_{118}$-*b*-$PLAMA_{6}$ *vs.* $PAMA_{87}$-*co*-$PLAMA_{42}$	****
$PAMA_{118}$-*b*-$PLAMA_{6}$ *vs.* $PAMA_{99}$-*b*-$PLAMA_{113}$	**
$PAMA_{118}$-*b*-$PLAMA_{6}$ *vs.* $PLAMA_{70}$	****
$PAMA_{118}$-*b*-$PLAMA_{6}$ *vs.* $PAMA_{161}$	****
$PAMA_{118}$-*b*-$PLAMA_{6}$ *vs.* PEG_{45}-*b*-$PAMA_{168}$	****
$PAMA_{87}$-*co*-$PLAMA_{42}$ *vs.* $PAMA_{97}$-*b*-$PLAMA_{44}$	**
$PAMA_{87}$-*co*-$PLAMA_{42}$ *vs.* $PAMA_{92}$-*co*-$PLAMA_{95}$	**
$PAMA_{87}$-*co*-$PLAMA_{42}$ *vs.* $PAMA_{99}$-*b*-$PLAMA_{113}$	****
$PAMA_{87}$-*co*-$PLAMA_{42}$ *vs.* $PLAMA_{70}$	****
$PAMA_{97}$-*b*-$PLAMA_{44}$ *vs.* $PAMA_{99}$-*b*-$PLAMA_{113}$	****
$PAMA_{97}$-*b*-$PLAMA_{44}$ *vs.* $PLAMA_{70}$	****
$PAMA_{97}$-*b*-$PLAMA_{44}$ *vs.* $PAMA_{161}$	**
$PAMA_{97}$-*b*-$PLAMA_{44}$ *vs.* PEG_{45}-*b*-$PAMA_{168}$	**
$PAMA_{92}$-*co*-$PLAMA_{95}$ *vs.* $PAMA_{99}$-*b*-$PLAMA_{113}$	****
$PAMA_{92}$-*co*-$PLAMA_{95}$ *vs.* $PLAMA_{70}$	****
$PAMA_{92}$-*co*-$PLAMA_{95}$ *vs.* $PAMA_{161}$	**
$PAMA_{92}$-*co*-$PLAMA_{95}$ *vs.* PEG_{45}-*b*-$PAMA_{168}$	**
$PAMA_{99}$-*b*-$PLAMA_{113}$ *vs.* $PLAMA_{70}$	****
$PAMA_{99}$-b-$PLAMA_{113}$ vs. $PAMA_{161}$	****
$PAMA_{99}$-*b*-$PLAMA_{113}$ *vs.* PEG_{45}-*b*-$PAMA_{168}$	****
$PLAMA_{70}$ *vs.* $PAMA_{161}$	****
$PLAMA_{70}$ *vs.* PEG_{45}-*b*-$PAMA_{168}$	****

[a]The statistical significance of differences between data was evaluated by one-way ANOVA using Turkey multiple comparisons test. Asterisks (****$p < 0.0001$, ***$p < 0.001$, **$p < 0.01$, and *$p < 0.05$) indicate values that differ significantly.

Transfection activity and cytotoxicity of glycopolymers-based polyplexes

Table A3– Statistical analysis of data presented inFigure 12a and 10b..

N/P ratio	Experimental conditions	p[a]
Rndom glycopolymers		
50/1	$PAMA_{38}$-*co*-$PLAMA_{47}$ *vs.* $PAMA_{114}$-*co*-$PLAMA_{20}$	***
	$PAMA_{87}$-*co*-$PLAMA_{42}$ *vs.* $PAMA_{114}$-*co*-$PLAMA_{20}$	**
	$PAMA_{94}$-*co*-$PLAMA_{9}$ *vs.* $PAMA_{114}$-*co*-$PLAMA_{20}$	**
	$PAMA_{114}$-*co*-$PLAMA_{20}$ *vs.* $PAMA_{92}$-*co*-$PLAMA_{95}$	***
75/1	$PAMA_{38}$-*co*-$PLAMA_{47}$ *vs.* $PAMA_{87}$-*co*-$PLAMA_{42}$	*
	$PAMA_{38}$-*co*-$PLAMA_{47}$ *vs.* $PAMA_{114}$-*co*-$PLAMA_{20}$	****
	$PAMA_{87}$-*co*-$PLAMA_{42}$ *vs.* $PAMA_{114}$-*co*-$PLAMA_{20}$	****
	$PAMA_{94}$-*co*-$PLAMA_{9}$ *vs.* $PAMA_{114}$-*co*-$PLAMA_{20}$	****
	$PAMA_{114}$-*co*-$PLAMA_{20}$ *vs.* $PAMA_{92}$-*co*-$PLAMA_{95}$	****
100/1	$PAMA_{38}$-*co*-$PLAMA_{47}$ *vs.* $PAMA_{114}$-*co*-$PLAMA_{20}$	****
	$PAMA_{87}$-*co*-$PLAMA_{42}$ *vs.* $PAMA_{114}$-*co*-$PLAMA_{20}$	****
	$PAMA_{94}$-*co*-$PLAMA_{9}$ *vs.* $PAMA_{114}$-*co*-$PLAMA_{20}$	****
	$PAMA_{114}$-*co*-$PLAMA_{20}$ *vs.* $PAMA_{92}$-*co*-$PLAMA_{95}$	****
Block glycopolymers		
50/1	$PAMA_{50}$-*b*-$PLAMA_{49}$ *vs.* $PAMA_{108}$-*b*-$PLAMA_{14}$	***
	$PAMA_{108}$-*b*-$PLAMA_{14}$ *vs.* $PAMA_{99}$-*b*-$PLAMA_{113}$	***
75/1	$PAMA_{50}$-*b*-$PLAMA_{49}$ *vs.* $PAMA_{108}$-*b*-$PLAMA_{14}$	***
	$PAMA_{50}$-*b*-$PLAMA_{49}$ *vs.* $PAMA_{99}$-*b*-$PLAMA_{113}$	**
	$PAMA_{97}$-*b*-$PLAMA_{44}$ *vs.* $PAMA_{108}$-*b*-$PLAMA_{14}$	*
	$PAMA_{118}$-*b*-$PLAMA_{6}$ *vs.* $PAMA_{108}$-*b*-$PLAMA_{14}$	***
	$PAMA_{118}$-*b*-$PLAMA_{6}$ *vs.* $PAMA_{99}$-*b*-$PLAMA_{113}$	**
100/1	$PAMA_{50}$-*b*-$PLAMA_{49}$ *vs.* $PAMA_{108}$-*b*-$PLAMA_{14}$	*
	$PAMA_{97}$-*b*-$PLAMA_{44}$ *vs.* $PAMA_{108}$-*b*-$PLAMA_{14}$	*
	$PAMA_{108}$-*b*-$PLAMA_{14}$ *vs.* $PAMA_{99}$-*b*-$PLAMA_{113}$	*

[a]The statistical significance of differences between data was evaluated by two-way ANOVA using Turkey multiple comparisons test. Asterisks (****$p < 0.0001$, ***$p < 0.001$, **$p < 0.01$, and *$p < 0.05$) indicate values that differ significantly.

Table A4– Statistical analysis of data presented in **Figure 13**.

N/P ratio	Experimental conditions	p[a]
Random glycopolymers		
10/1	$PAMA_{38}$-*co*-$PLAMA_{47}$ *vs.* $PAMA_{87}$-*co*-$PLAMA_{42}$	**
	$PAMA_{87}$-*co*-$PLAMA_{42}$ *vs.* $PAMA_{94}$-*co*-$PLAMA_{9}$	*
	$PAMA_{87}$-*co*-$PLAMA_{42}$ *vs.* $PAMA_{114}$-*co*-$PLAMA_{20}$	**
50/1	$PAMA_{38}$-*co*-$PLAMA_{47}$ *vs.* $PAMA_{94}$-*co*-$PLAMA_{9}$	*
	$PAMA_{38}$-*co*-$PLAMA_{47}$ *vs.* $PAMA_{114}$-*co*-$PLAMA_{20}$	*
	$PAMA_{87}$-*co*-$PLAMA_{42}$ *vs.* $PAMA_{114}$-*co*-$PLAMA_{20}$	*
	$PAMA_{87}$-*co*-$PLAMA_{42}$ *vs.* $PAMA_{92}$-*co*-$PLAMA_{95}$	*
	$PAMA_{94}$-*co*-$PLAMA_{9}$ *vs.* $PAMA_{92}$-*co*-$PLAMA_{95}$	****
	$PAMA_{114}$-*co*-$PLAMA_{20}$ *vs.* $PAMA_{92}$-*co*-$PLAMA_{95}$	****
75/1	$PAMA_{38}$-*co*-$PLAMA_{47}$ *vs.* $PAMA_{87}$-*co*-$PLAMA_{42}$	****
	$PAMA_{38}$-*co*-$PLAMA_{47}$ *vs.* $PAMA_{94}$-*co*-$PLAMA_{9}$	**
	$PAMA_{38}$-*co*-$PLAMA_{47}$ *vs.* $PAMA_{114}$-*co*-$PLAMA_{20}$	****
	$PAMA_{87}$-*co*-$PLAMA_{42}$ *vs.* $PAMA_{94}$-*co*-$PLAMA_{9}$	**
	$PAMA_{87}$-*co*-$PLAMA_{42}$ *vs.* $PAMA_{92}$-*co*-$PLAMA_{95}$	****
	$PAMA_{94}$-*co*-$PLAMA_{9}$ *vs.* $PAMA_{92}$-*co*-$PLAMA_{95}$	****
	$PAMA_{114}$-*co*-$PLAMA_{20}$ *vs.* $PAMA_{92}$-*co*-$PLAMA_{95}$	****

100/1	$PAMA_{38}$-*co*-$PLAMA_{47}$ *vs.* $PAMA_{87}$-*co*-$PLAMA_{42}$	****
	$PAMA_{38}$-*co*-$PLAMA_{47}$ *vs.* $PAMA_{94}$-*co*-$PLAMA_{9}$	****
	$PAMA_{38}$-*co*-$PLAMA_{47}$ *vs.* $PAMA_{114}$-*co*-$PLAMA_{20}$	****
	$PAMA_{87}$-*co*-$PLAMA_{42}$ *vs.* $PAMA_{92}$-*co*-$PLAMA_{95}$	****
	$PAMA_{94}$-*co*-$PLAMA_{9}$ *vs.* $PAMA_{92}$-*co*-$PLAMA_{95}$	****
	$PAMA_{114}$-*co*-$PLAMA_{20}$ *vs.* $PAMA_{92}$-*co*-$PLAMA_{95}$	****
Block glycopolymers		
10/1	$PAMA_{50}$-*b*-$PLAMA_{49}$ *vs.* $PAMA_{97}$-*b*-$PLAMA_{44}$	****
	$PAMA_{97}$-*b*-$PLAMA_{44}$ *vs.* $PAMA_{118}$-*b*-$PLAMA_{6}$	***
	$PAMA_{97}$-*b*-$PLAMA_{44}$ *vs.* $PAMA_{108}$-*b*-$PLAMA_{14}$	*
	$PAMA_{97}$-*b*-$PLAMA_{44}$ *vs.* $PAMA_{99}$-*b*-$PLAMA_{113}$	*
25/1	$PAMA_{97}$-*b*-$PLAMA_{44}$ *vs.* $PAMA_{108}$-*b*-$PLAMA_{14}$	*
50/1	$PAMA_{118}$-*b*-$PLAMA_{6}$ *vs.* $PAMA_{99}$-*b*-$PLAMA_{113}$	***
	$PAMA_{108}$-*b*-$PLAMA_{14}$ *vs.* $PAMA_{99}$-*b*-$PLAMA_{113}$	*
100/1	$PAMA_{50}$-*b*-$PLAMA_{49}$ *vs.* $PAMA_{118}$-*b*-$PLAMA_{6}$	***
	$PAMA_{97}$-*b*-PLAMA44 *vs.* $PAMA_{99}$-*b*-$PLAMA_{113}$	***
	$PAMA_{118}$-*b*-$PLAMA_{6}$ *vs.* $PAMA_{108}$-*b*-$PLAMA_{14}$	***
	$PAMA_{118}$-*b*-$PLAMA_{6}$ vs. $PAMA_{99}$-*b*-$PLAMA_{113}$	****

[a]The statistical significance of differences between data was evaluated by two-way ANOVA using Turkey multiple comparisons test. Asterisks (****$p < 0.0001$, ***$p < 0.001$, **$p < 0.01$, and *$p < 0.05$) indicate values that differ significantly.

a)

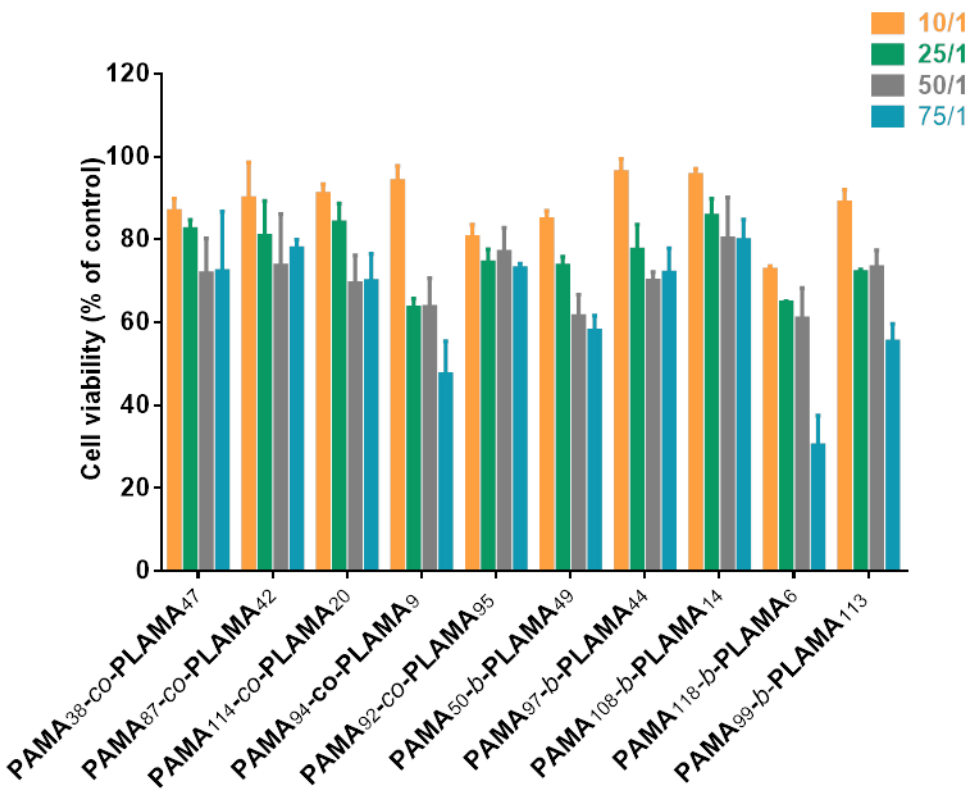
10/1
25/1
50/1
75/1
Cell viability (% of control)
120
100
80
60
40
20
0
PAMA38-co-PLAMA47
PAMA87-co-PLAMA42
PAMA114-co-PLAMA20
PAMA94-co-PLAMA9
PAMA92-co-PLAMA95
PAMA50-b-PLAMA49
PAMA97-b-PLAMA44
PAMA108-b-PLAMA14
PAMA118-b-PLAMA6
PAMA99-b-PLAMA113

b)

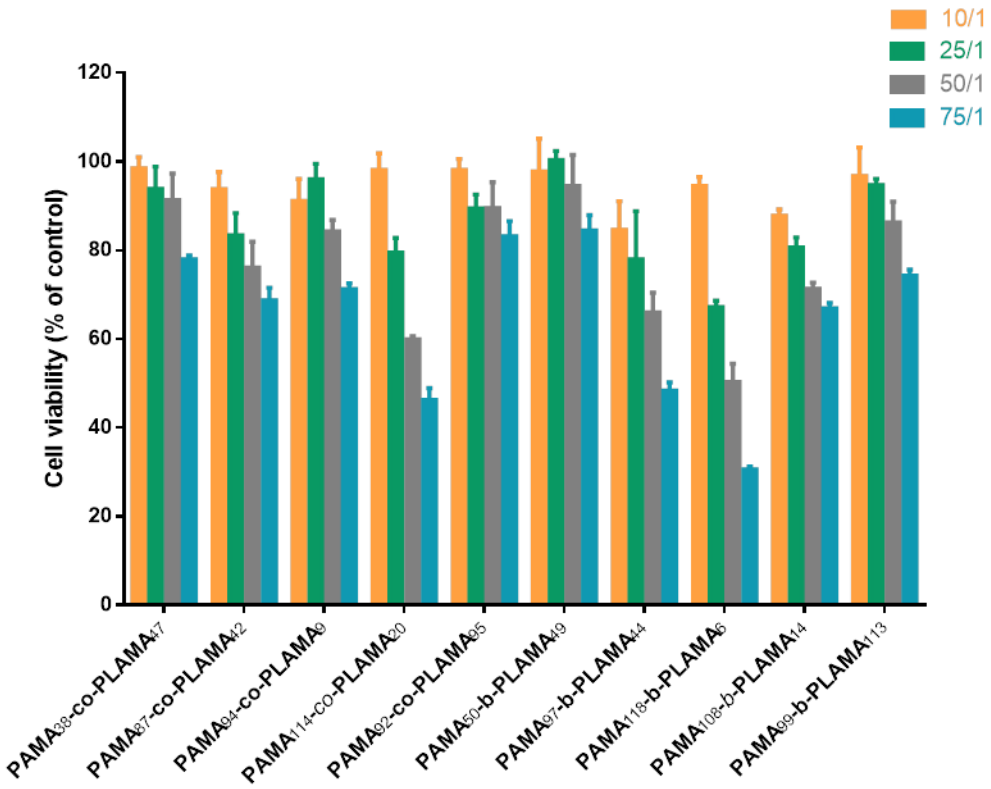
10/1
25/1
50/1
75/1
Cell viability (% of control)
120
100
80
60
40
20
0
PAMA38-co-PLAMA47
PAMA87-co-PLAMA42
PAMA94-co-PLAMA9
PAMA114-co-PLAMA20
PAMA92-co-PLAMA95
PAMA50-b-PLAMA49
PAMA97-b-PLAMA44
PAMA118-b-PLAMA6
PAMA108-b-PLAMA14
PAMA99-b-PLAMA113

Figure A3– Cytotoxicity of random- and diblock-based glycoplexes in Hep3B (a) and Huh-7 (b) cells. Polyplexes were prepared by complexing the glycopolymers with 1 μg of plasmid DNA encoding luciferase (pCMV.Luc), at different N/P ratios. The results correspond to mean ± SD, achieved from triplicates, and are representative of at least three independent experiments.

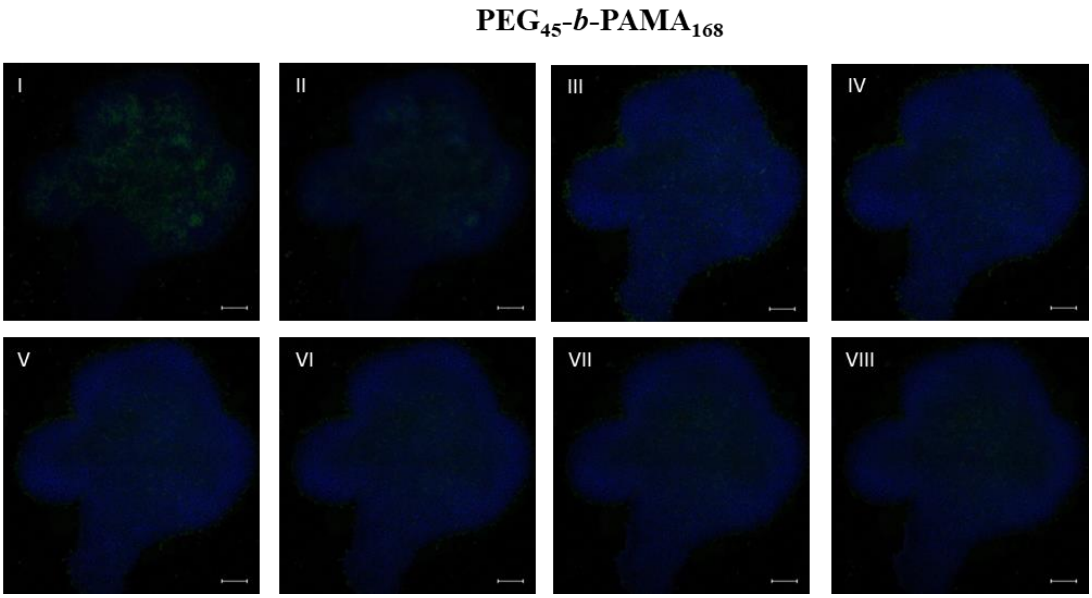

Figure A4– Representative Z-stack confocal microscopic images of tumor spheroids treated with PEG_{45}-*b*-$PAMA_{168}$-based nanosystems formulated at 50/1 N/P ratio. Polyplexes were prepared by complexing the copolymer with 0.5 μg of pCMV.gfp, at 50/1 N/P ratios. The cell nucleus was stained with DAPI (blue). Scale bar = 100 μm.

Asialoglycoprotein receptor-targeted glycoplexes

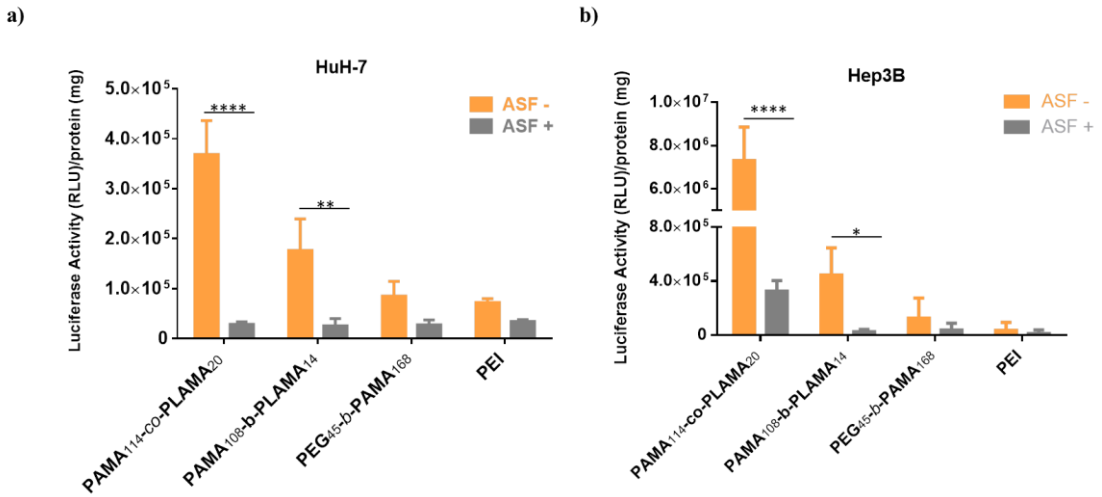

Figure A5– Effect of the presence of asialofetuin on the biological activity Huh-7 (a) and Hep3B cells transfected with different polyplexes. Asialofetuin was added to cells 1 h before the addition of polyplexes. Polyplexes were prepared by complexing the polymers with 1 μg of pCMV.Luc, at their optimal N/P ratio. The results correspond to mean ± SD, achieved from

triplicates, and are representative of at least three independent experiments. Asterisks (****p < 0.0001, ***p < 0.001, **p < 0.01 and *p < 0.05) correspond to values that differ significantly from those obtained with the same formulations in the absence of asialofetuin.

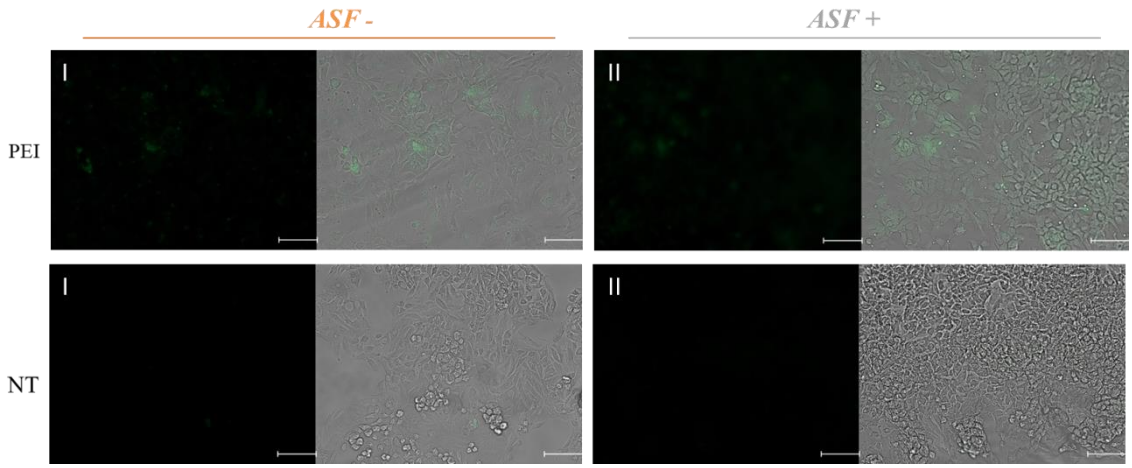

Figure A6– Effect of the presence of asialofetuin on the transfection efficiency of HepG2 cells transfected with PEI-based polyplexes and untreated control. Asialofetuin was added to cells 1 h before the addition of polyplexes. Polyplexes were prepared by complexing the polymers with 1 µg of pCMV.GFP, at their optimal N/P ratio. Fluorescence microscopy (I) and overlapping of fluorescence microscopy and phase contrast images (II) of cells transfected with different formulations at 50:1 N/P ratio (scale bar = 50 µm).

The endocytosis and intracellular fate of glycoplexes

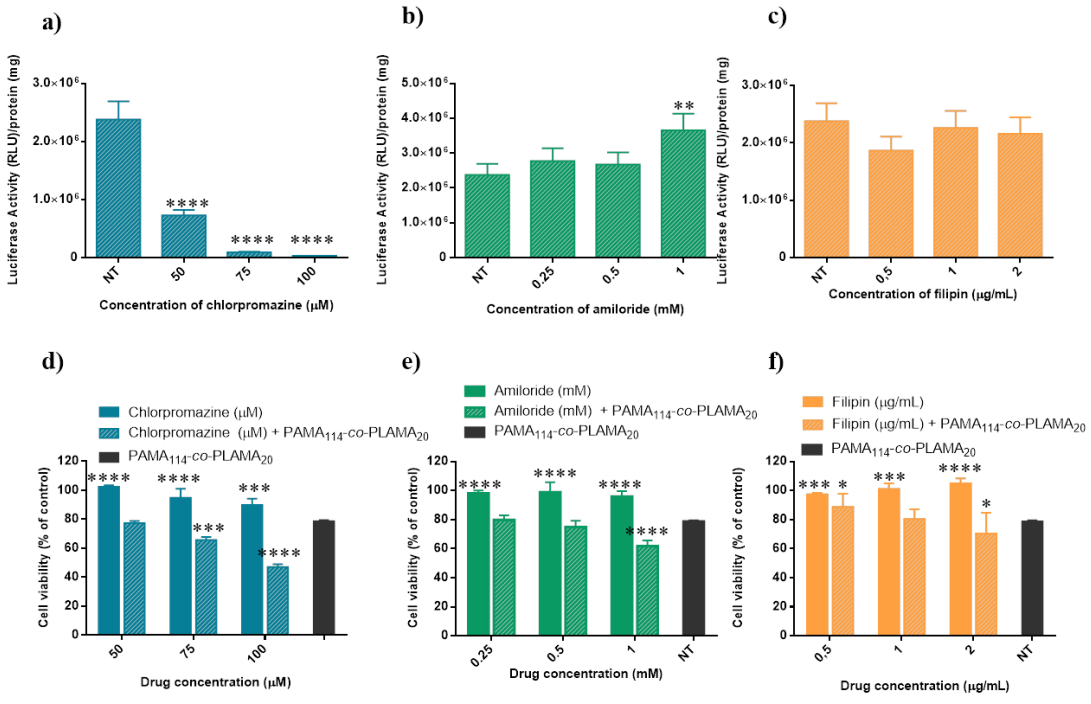

Figure A7– Effect of endocytosis inhibitors on the transfection activity (a), (b), (c) and toxicity (d), (e), (f) of $PAMA_{114}$-*co*-$PLAMA_{20}$-based polyplexes. HepG2 cells were pretreated with chlorpromazine (50; 75; 100 µM), amiloride (0.25; 0.5; 1 mM) or filipin (0.5; 1; 2 µg.mL^{-1}) and transfected with $PAMA_{114}$-*co*-$PLAMA_{21}$-based polyplexes prepared with 1 µg of pCMV.Luc at 50/1 N/P ratio. The results correspond to mean ± SD, achieved from triplicates, and are representative of at least three independent experiments. Asterisks (****p <0.0001, ***p < 0.001, **p < 0.01 and *p < 0.05) indicate values that differ significantly from those measured in the control (cells not-treated with endocytosis inhibitors).

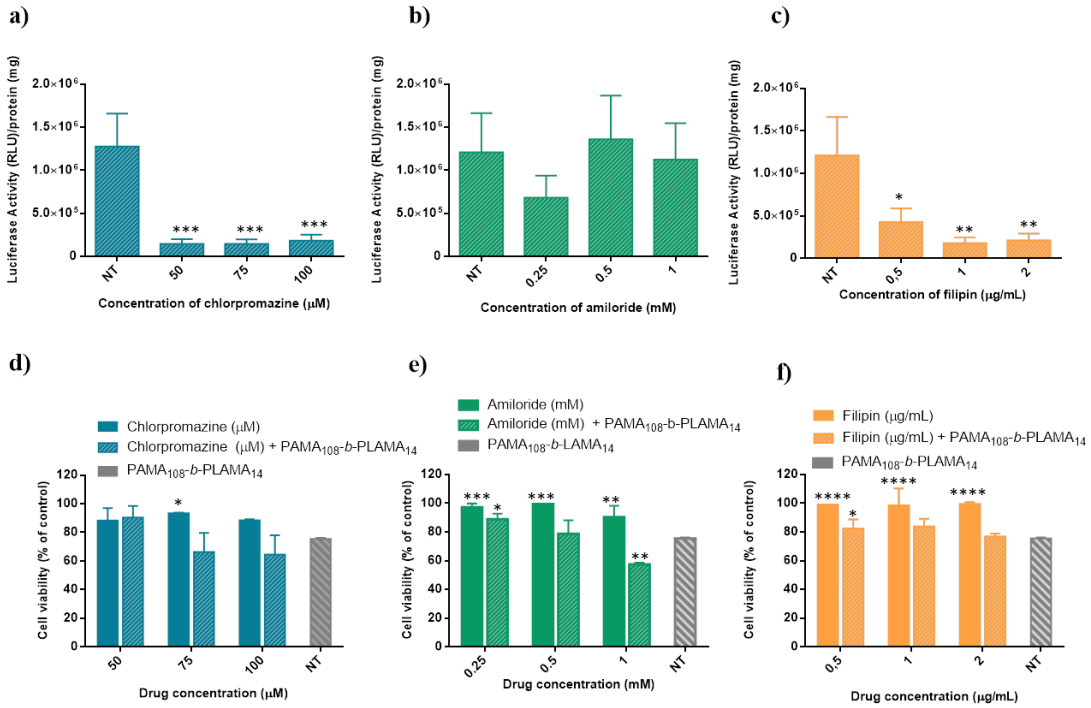

Figure A8– Effect of endocytosis inhibitors on the transfection activity (a), (b), (c) and toxicity (d), (e), (f) of $PAMA_{108}$-*b*-$PLAMA_{14}$-based polyplexes. HepG2 cells were pretreated with chlorpromazine (50; 75; 100 µM), amiloride (0.25; 0.5; 1 mM) or filipin (0.5; 1; 2 µg.mL^{-1}) and transfected with $PAMA_{108}$-*b*-$PLAMA_{14}$-based polyplexes prepared with 1 µg of pCMV.Luc at 50/1 N/P ratio. The results correspond to mean ± SD, achieved from triplicates, and are representative of at least three independent experiments. Asterisks (****p <0.0001, ***p < 0.001, **p < 0.01 and *p < 0.05) indicate values that differ significantly from those measured in the control (cells not-treated with endocytosis inhibitors).

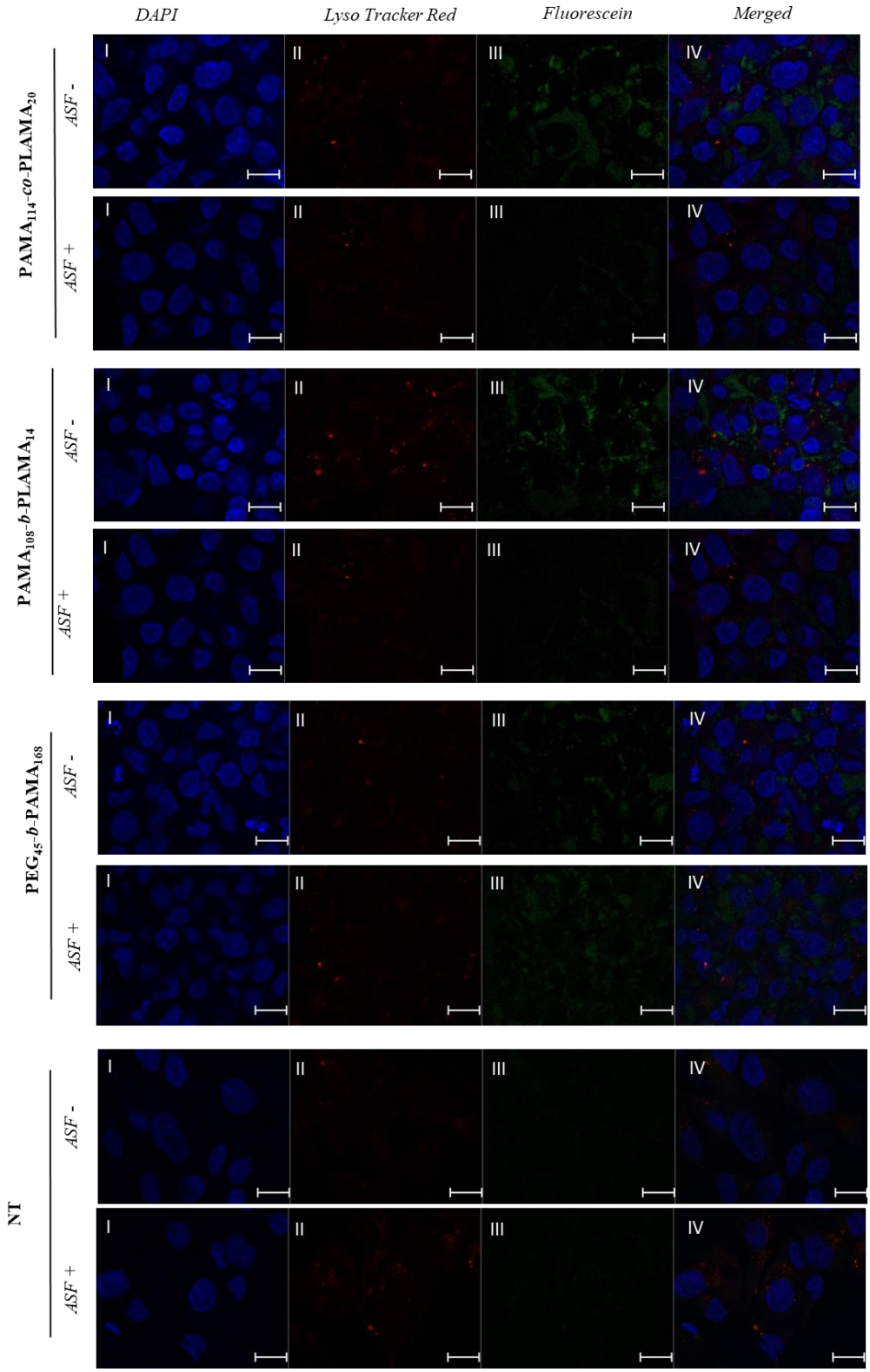

Figure A9– Effect of asialofetuin on cellular uptake of polyplexes in HepG2 cells evaluated by confocal microscopy. Asialofetuin was added to the cells 1 h before the addition of the polyplexes. Polyplexes were prepared by complexing the polymers, containing 1% of fluorescein-labeled glycopolymer, with 1 μg of pCMV.Luc, at their optimal N/P ratio. Scale bar = 10 μm. (I) cell nucleus stained by DAPI (blue); (II) acidic cell compartments labeled with

Lysotracker Red DND-99 (red); (III) polyplexes were prepared with 1% fluorescein-labeled glycopolymer (green); (IV) overlay of images I−III.

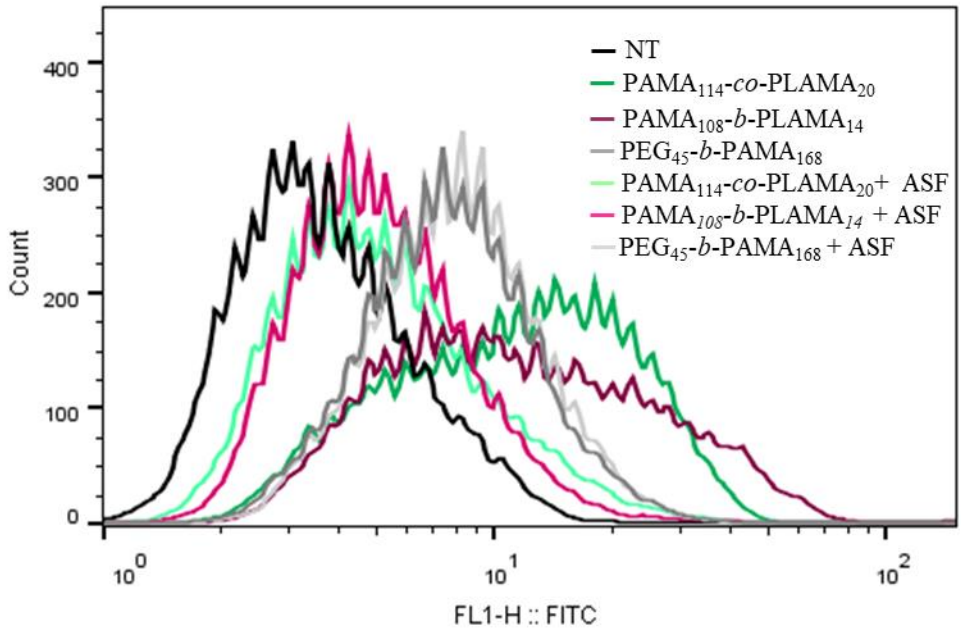

Figure A10– Effect of asialofetuin on cellular internalization of polyplexes on HepG2 cells. Asialofetuin was added to cells 1 h before the addition of polyplexes. Polyplexes were prepared by complexing the polymers, containing 1% of fluorescein-labeled glycopolymer, with 1 μg of pCMV.Luc, at their optimal N/P ratio. The uptake was evaluated by flow cytometry, in terms of percentage of positive cell population, compared to untreated control cells.

c-MYC downregulation to enhance sorafenib antitumor effect

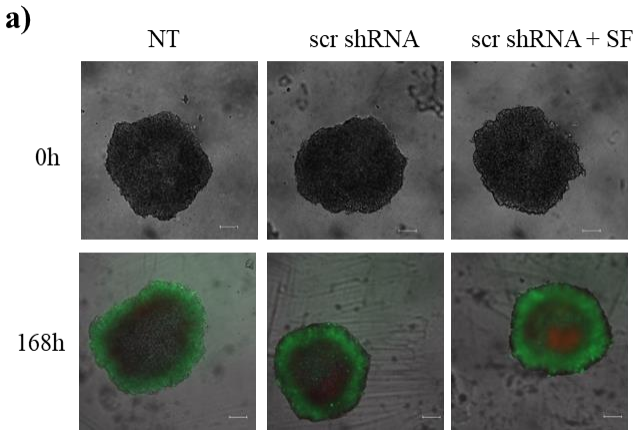

Figure A10– Effect of the non-targeting shRNA combined or not with SF (Scr shRNA and Scr shRNA + SF) on tumor spheroids growth. The microscopic images (scale bar = 200 μm) for 0 h are phase contrast images, and the microscopic images for 168 h are fluorescence images using fluorescein diacetate (green) and propidium iodide (red) staining for imaging live and dead cells, respectively.

APPENDIX B

SUPPORTING INFORMATION

THE SUPPLEMENTARY INFORMATION OF CHAPTER 3 IS PRESENTED IN THIS APPENDIX.

Materials

2-Aminoethyl methacrylate hydrochloride (AMA; ≥95%, Polysciences), ascorbic acid (AscA; Sigma-Aldrich), ASGPR monoclonal antibody (Thermo Fisher), asialofetuin (Sigma-Aldrich), amiloride hydrochloride (Sigma-Aldrich), bovine serum albumin (BSA; Sigma-Aldrich), chlorpromazine (Sigma-Aldrich), copper(II) bromide (CuBr2; 99.999%, Sigma-Aldrich), deuterium oxide (D2O; Euroiso-top, +99.9% D), DC protein assay (Bio-Rad), 4,6-diamidino-2-phenylindole (DAPI, 1 μg mL−1) (Thermo Fisher Scientific), dimethylformamide (DMF, Fisher Scientific), docetaxel solution (DTX, HIKMA), Dulbecco's modified Eagle's medium-high glucose (DMEM-HG; Sigma-Aldrich), D-luciferin sodium salt (Synchem, 99%), ethyl α- bromophenyl acetate (EBPA; Alfa Aesar), filipin (Sigma-Aldrich), fluorescein o-methacrylate monomer (FMO, Sigma-Aldrich), fluorescein diacetate (Sigma-Aldrich) FluoroshieldTM (Sigma-Aldrich), Green Safe (Nzytech), lactobionic acid (Thermo Fisher Scientific), Lysotrack Red DND-99 (Thermo Fisher Scientific), PEI (branched, Mw 25 000) (Sigma-Aldrich), DNA plasmids encoding luciferase (pLuc), green fluorescent protein (GFP, pgfp) and HSV-TK (pTK) (Vical), resazurin sodium salt (Sigma-Aldrich), 2-propanol (Fisher Scientific), propidium iodide (Sigma-Aldrich). Methanol was dried over CaH2 and distilled before use. Triethylamine (≥99.5%, Sigma-Aldrich) was distilled before use. Tris(pyridine-2-ylmethyl)amine (TPMA) was synthesized as reported in the literature.[1]

Methods

Synthesis and characterization of glycopolymers

Techniques

A syringe pump (KDS Scientific, Legato 101) was used for the continuous feeding of the reducing agent at the rate of 1 μL/min. The molecular weight parameters of the polymers were determined by using a size exclusion chromatography (SEC) system equipped with an online degasser, a refractive index (RI) detector and a set of columns: Shodex OHpak SB-G guard column, OHpak SB-804HQ and OHpak SB-802.5HQ columns. The polymers were eluted at a flow rate of 0.5 mL/min with 0.1 M Na_2SO_4 (aq)/1 wt% acetic acid/0.02% NaN_3 at 40 °C. Before the injection, the samples were filtered through a polytetrafluoroethylene (PTFE) membrane with 0.45 μm pore. The

system was calibrated with five narrow PEG standards and the polymers number-average molecular weights (M_n^{SEC}) and dispersity ($Đ = M_w/M_n$) were determined by conventional calibration using the Clarity software version 2.8.2.648.400. MHz ^{1}H NMR spectra were recorded on a Bruker Avance III 400 MHz spectrometer, with a 5-mm TIX triple resonance detection probe, in D_2O. Conversion of monomers was determined by integration of monomers NMR signals using the MestRenova software version: 10.0.1-14719.

Synthesis of 2-lactobionamidoethyl methacrylate (LAMA)

LAMA was synthesized according to a previously reported procedure.[2] Firstly, lactobionic acid was converted to the corresponding lactobionolactone. For that, lactobionic acid (4.0 g, 11.2 mmol) was dissolved in anhydrous methanol (25 mL) at 50 ºC, in the presence of trifluoroacetic acid as a catalyst (0.1 g, 1.1 mmol), followed by vacuum distillation to recover lactobionolactone. After that, lactobionolactone (1.5 g, 4.5 mmol) was dissolved in methanol at 50 ºC, followed by the addition of 2-aminoethyl methacrylate hydrochloride (1.5 g, 9.0 mmol), triethylamine (1.27 mL) and hydroquinone (0.05 g) at room temperature. The mixture was stirred for 6 h, concentrated by rotary evaporation and precipitated in 2-propanol. The white solid (LAMA) formed was filtered, washed with 2-propanol and dried under vacuum (yield = 81%).

Then, their chemical structure was characterized by 1H NMR spectroscopy (Figure 1a and Figure S2a, Supporting Information) and SEC (Figure 1b and Figure S2b, Supporting Information).

Synthesis of fluorescein-labeled glycopolymer

AMA (0.54g, 3.7 mmol), LAMA (0.25 g, 532 μmol), fluorescein o-methacrylate (FMO) (53.3 mg, 133 μmol), $CuBr_2$ (2.97 mg, 13.3 μmol), TPMA (15.5 mg, 53 μmol), and EBPA (6.5 mg, 26 μmol) were dissolved in water/DMF mixture (50/50, V/V) (3.5mL). The mixture was added to a 10 mL round-bottom Schlenk flask, equipped with a magnetic stir bar, and purged with nitrogen for 30 min. The flask was placed in an oil bath at 60 °C and a deoxygenated AscA solution (43 mM) was continuously injected into the reaction medium using a syringe pump at the rate of 1 μL/min. The reaction was stopped after 3 h, and a sample was collected for ^{1}H NMR spectroscopy to

determine the monomers (FMO, AMA and LAMA) conversion. The final reaction mixture was dialyzed (dialysis membrane MWCO = 3500) against deionized water and the glycopolymer was recovered by freeze-drying.

Physicochemical characterization of polyplexes

Green Safe Intercalation Assay

The accessibility to DNA of the polyplexes was analyzed using Green Safe intercalation assay. The polyplexes were prepared as described above and after 15 min, 50 μL of each sample was transferred into a black 96-well plate (Costar, Cambridge, CA, USA). Then, 50 μL of Green Safe solution (0.00002 % (V/V)) was added to polyplexes. Following 10 min incubation, fluorescence was measured in a SpectraMax Gemini EM fluorometer (Molecular Devices, Sunnyvale, CA, USA) at the excitation wavelength of 490 nm and emission wavelength of 530 nm. The fluorescence scale was calibrated such that the initial fluorescence of Green Safe (50 μL of Green Safe solution was added to 50 μL of Milli-Q water) was set as residual fluorescence. The value of fluorescence obtained with 1 μg of naked DNA (control) was set as 100%. The amount of DNA available to interact with the probe was calculated by subtracting the values of residual fluorescence from those obtained for the samples and expressed as the percentage of the control.

Agarose Gel Electrophoresis Assay

To evaluate the complexation of the DNA with the copolymers an electrophoresis in agarose gel was performed. Polyplexes were prepared and, after 15 min, 20 μL of each sample was added to 5 μL of loading buffer. 20 μL of each blend were transferred to a 1% agarose gel prepared in TBE solution and containing 1.5 μL of Green Safe. The electrophoresis was set to 30 min at 80 mV. Sample visualization takes place in a GelDoc® (BioRad®, USA) system using the QuantityOne® program.

Dynamic Light Scattering and Zeta Potential Analysis

Dynamic light scattering (DLS) measurements were performed on a Zetasizer Nano-ZS (Malvern Instruments Ltd. UK). The particle size distribution (in intensity) and average hydrodynamic diameter (z-average) were determined with Zetasizer 7.13 software. Measurements were made at 25 °C and at a backward scattering angle of 173°. ζ-

Potential measurements were performed using a Zetasizer Nano-ZS (Malvern Instruments Ltd., UK) coupled to laser Doppler electrophoresis and determined using a Smoluchovski model.

Cell Culture

Human hepatocellular carcinoma cells (HepG2 and Hep3B cell lines) and human epithelial cervical carcinoma cells (HeLa cell line) were maintained at 37 °C, under 5% CO_2, in Dulbecco's modified Eagle's medium-high glucose (DMEM-HG, Sigma-Aldrich), supplemented with 10% (V/V) heat inactivated fetal bovine serum (FBS, Sigma-Aldrich), penicillin (100 U/mL), and streptomycin (100 μg/mL). All cells were grown in monolayers and were detached by treatment with a 0.25% trypsin solution (Sigma-Aldrich).

Transfection Activity

The biological activity of the different polyplexes was determined by luminescence, using luciferase as a reporter gene (pLuc plasmid), in HepG2 and Hep3B cells. Briefly, the HepG2 (8×10^4 cells/well), Hep3B (3.5×10^4 cells/well) and HeLa (5×10^4 cells/well) cells were seeded onto 48-well culture plates 24 h prior to incubation with polyplexes. The cells were used at 70% confluence, and polyplexes containing 1 μg of p.Luc were added to the cells previously covered with DMEM-HG containing 10% (v/v) FBS. After 4 h of incubation, the transfection medium was replaced with fresh DMEM-HG, and the cells were further incubated for 48 h. At this time, the cells were washed twice with PBS, and 100 μL of lysis buffer was added to each well. The quantification of luciferase expression in cell lysates was evaluated by measuring the light production by luciferase in a FLUOstar Omega Microplate Reader (BMG Labtech, USA). The protein content of the lysates was measured by the DC protein assay reagent (Biorad, CA, USA) using BSA as a standard. The data were expressed as relative light units of luciferase per milligram of total cell protein. For the competitive studies, the culture medium containing 1 mg/mL of asialofetuin (ASF) or 40 μg/ml of antibody against the ASGP-R (ASGPR1 Ab) was added to cells 1 h before the addition of nanosystems and maintained during the 4 h of transfection. In the endocytic pathway studies, the culture medium containing different inhibitors (75 μM chlorpromazine, 0.25 mM amiloride or 2 μg/mL filipin) was added to cells 1 h before the polyplex addition and maintained

during the 4 h of transfection. To evaluate the effect of docetaxel (DTX) as enhancer of transfection activity, the culture medium containing different concentrations of DTX (0.003; 0.006; 0.0125; 0.025; 0,05 or 0.1 μM) was added to cells 1 h before the addition of nanosystems and maintained during the 4 h of transfection.

Transfection Efficiency

To evaluate the transfection efficiency of our formulations, green fluorescent protein (GFP) expression was evaluated in HCC cells by fluorescence microscopy. Briefly, the HepG2 (1.1×10^5 cells/well) and Hep3B (7.5×10^4 cells/well) cells were seeded on 24-well plates (the wells were previously covered with a coverslip), and after 24 h, polyplexes containing 2 μg of pgfp were added to the cells previously covered with 0.5 mL of DMEM-HG with serum. After 4 h of incubation (5% CO_2 at 37 °C), the transfection medium was replaced with DMEM-HG containing 10% (V/V) FBS and antibiotics, and the cells were further incubated for 48 h. After that, the cells were washed twice with PBS, fixed with 4% paraformaldehyde for 15 min at room temperature, and then mounted in Fluoroshield medium. The images (original magnification ×20) were obtained on an Axio Imager Z2 microscope (Zeiss, Munich, Germany) using an AxioCam HRc camera (Zeiss, Germany).

Cell Viability Assay

Cell viability under different experimental conditions was assessed by an Alamar Blue assay. After 48 h of transfection, the cells were incubated with DMEM containing 10% (V/V) Alamar Blue dye, prepared from a 0.1 $mg.mL^{-1}$ stock solution of Alamar Blue. After 1 h incubation period at 37 °C, the absorbance of the medium was measured at 570 (A_{570}) and 600 (A_{600}) nm in SPECTRAmax PLUS 384 spectrophotometer (Molecular Devices, USA). Cell viability was calculated, as percentage of the nontreated control cells, according to the formula: [($A_{570} - A_{600}$) of treated cells × 100]/[($A_{570} - A_{600}$) of control cells].

Cell uptake

Polyplexes were prepared with 1% of fluorescein-labeled FMO_2-*co*-$PAMA_{103}$-*co*-$PLAMA_{19}$ at their optimal N/P ratio. HepG2 cells were seeded on 24-well plates at a density of 1.6×10^5 cells/well and, after 24 h, polyplexes containing the glycopolymer

labeled with fluorescein were added to cells previously covered with 0.5 mL of DMEM-HG with serum. After 4 h incubation (5% CO_2 at 37 °C), cells were washed twice with PBS, detached with trypsin, and then washed and resuspended in PBS. To quench external fluorescence, trypan blue was added to each sample 1 min before FACSCalibur flow cytometer (Becton Dickinson, NJ, USA) analysis, at a final concentration of 0.05% (V/V). In the competitive studies, the culture medium containing 2 mg/mL of asialofetuin was added to cells 30 min before the addition of nanosystems and maintained during the 4 h of transfection. Live cells were gated by forward/side scattering from a total of 20000 events, and data was analyzed using FlowJo software.

Intracellular distribution of polyplexes

Confocal laser scanning microscopy was used to visualize the intracellular distribution of polyplexes prepared with 1% of fluorescein-labeled glycopolymer at their optimal N/P ratio. The HepG2 cells were seeded in 24-well culture plates (previously covered with a coverslip) at an initial density of 1.5×10^5 cells/well and, after 24 h, polyplexes were added to the cells previously covered with 0.5 mL of DMEM-HG with serum. In the competitive studies, the culture medium containing 2 mg/mL of asialofetuin was added to cells 30 min before the addition of nanosystems and maintained during the 4 h of transfection. After this period of incubation (5% CO_2 at 37 °C), the transfection medium was removed, and the cells were washed with PBS and incubated for 30 min with 200 nM Lysotrack Red DND-99, which labels the acidic compartments of living cells. Thereafter, the cells were washed three times with PBS and fixed with 4% paraformaldehyde solution for 15 min at room temperature. Nuclei labeling was accomplished through 5 min of incubation at room temperature with the fluorescent DNA binding dye DAPI (1 μg/mL). The cells were then mounted in Fluoroshield medium, and images were taken in a Zeiss LSM 710 Axio Observer microscope (Zeiss, Gottingen, Germany) with a Plan-Apochromat 63×/1.40 oil differential interference contrast (DIC) M27 objective at the excitation wavelengths of 405 nm for DAPI (blue), 488 nm for fluorescein (green), and 561 nm for Lysotracker (red).

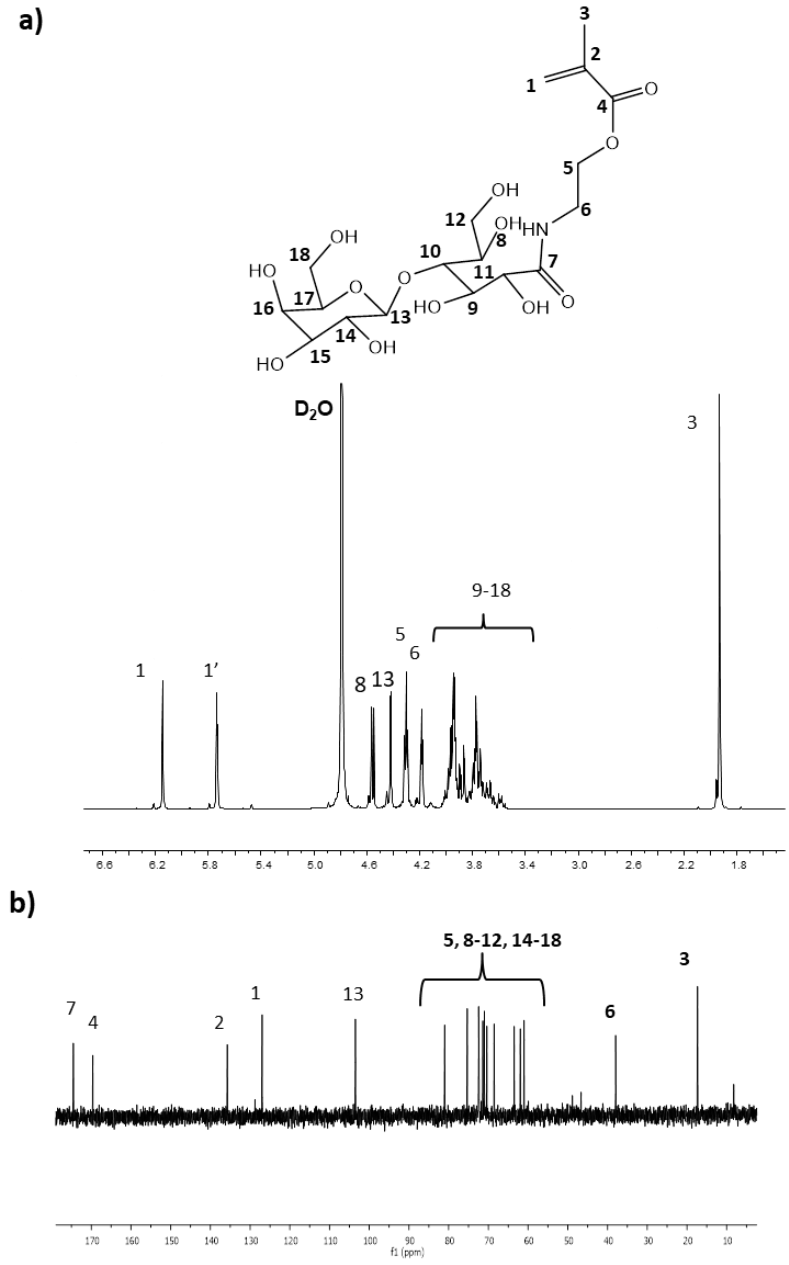

Figure B1– ^{1}H (a) and ^{13}C (b) NMR spectra (D_2O, 400 MHz) for the LAMA monomer.

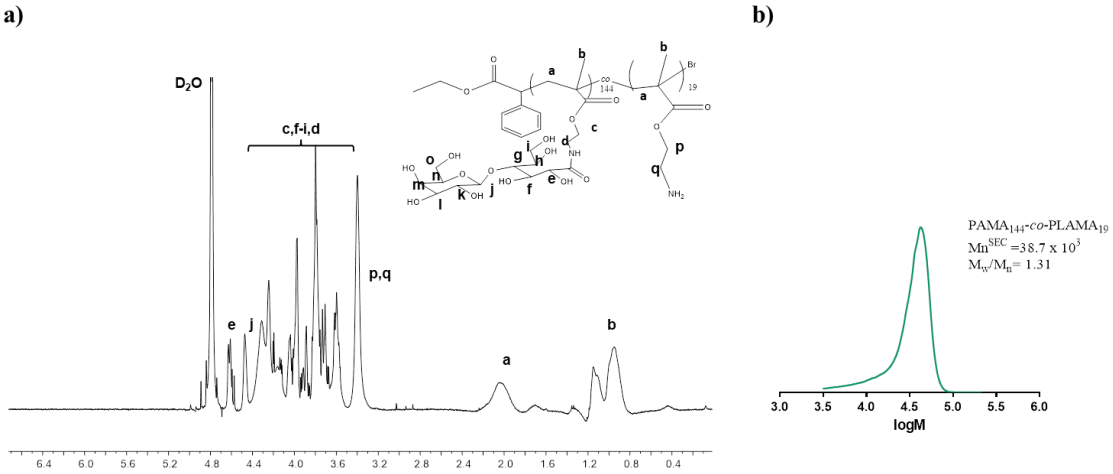

Figure B2– ^{1}H NMR spectrum (D_2O, 400 MHz) (a) and SEC trace (b) of the $PAMA_{144}$-*co*-$PLAMA_{19}$ random copolymer prepared by ARGET ATRP.

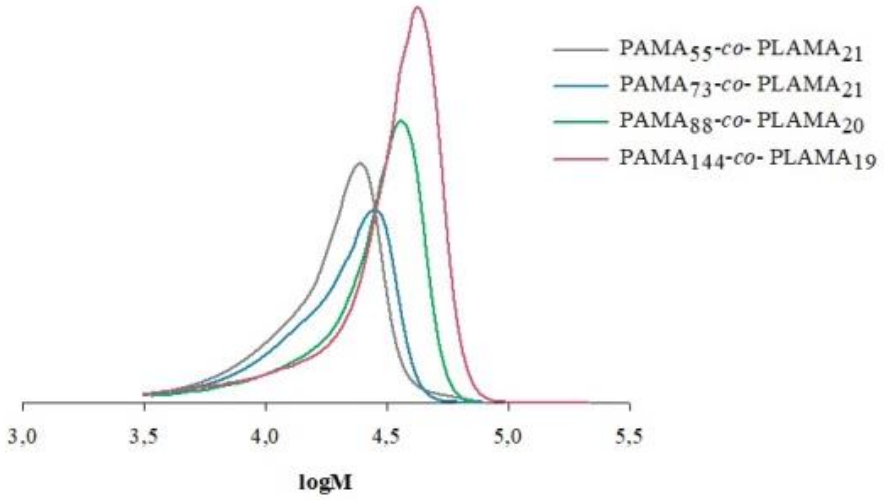

Figure B3– SEC traces of the PAMA-*co*-PLAMA random copolymers prepared by ARGET ATRP.

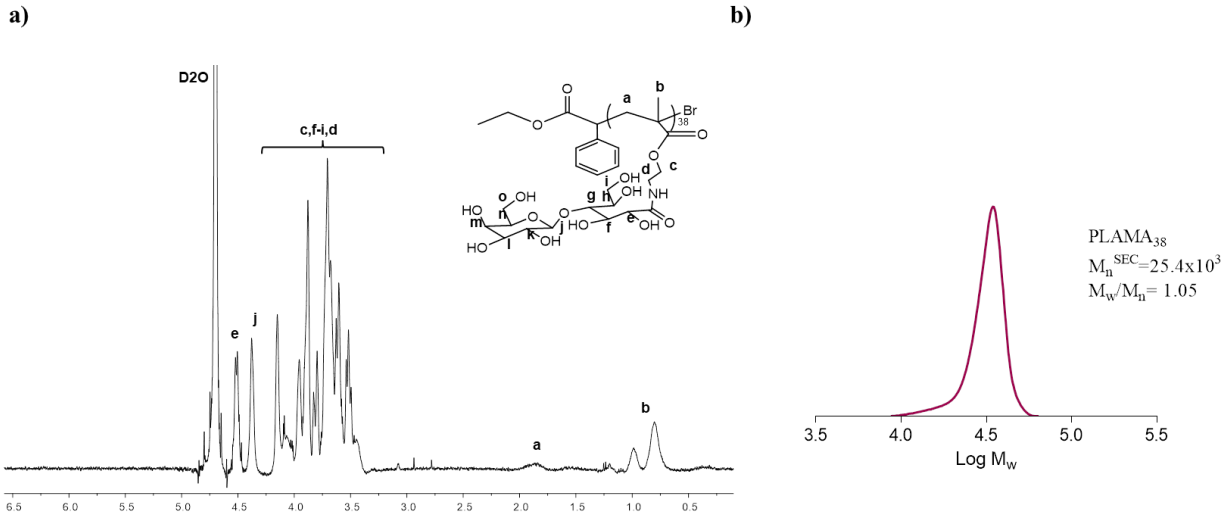

Figure B4– ^{1}H NMR spectrum (D_2O, 400 MHz) (a) and SEC trace (b) of the $PLAMA_{38}$-Br homopolymer prepared by ARGET ATRP.

Acid-base Titration for pKa Determination

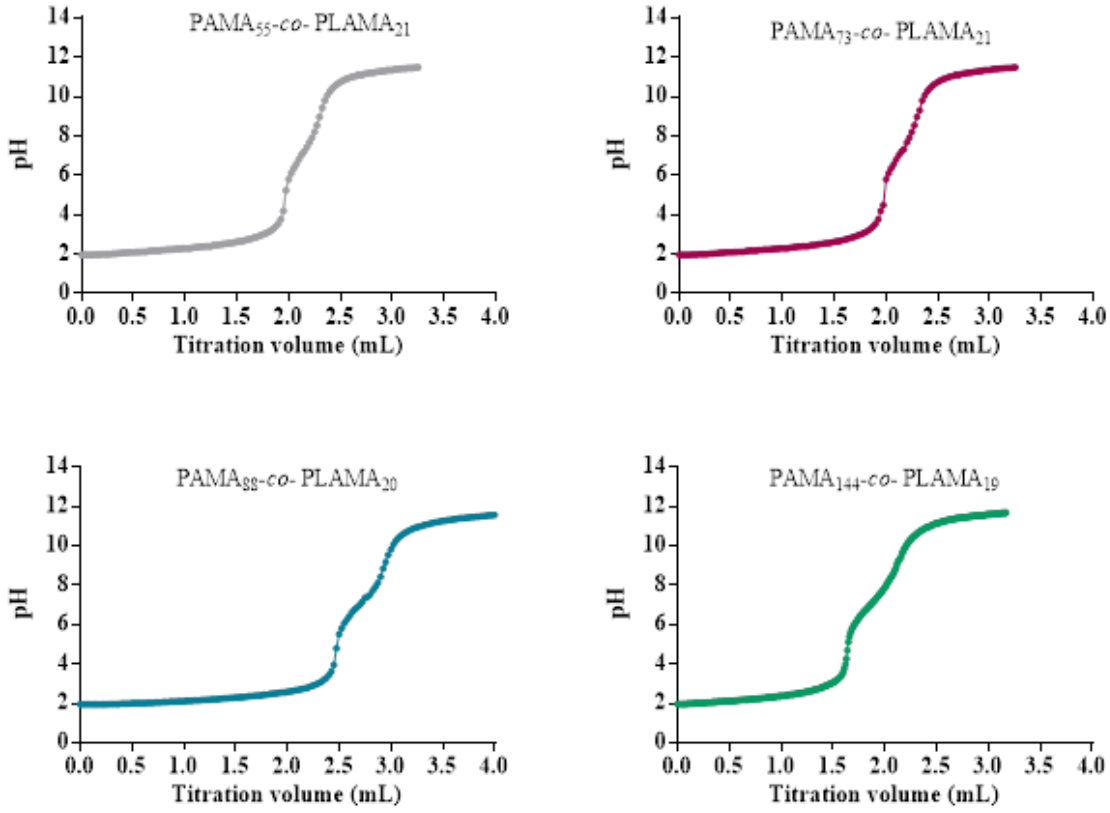

Glycopolymer	*pKa*

$PAMA_{55}$-*co*- $PLAMA_{21}$	7.2
$PAMA_{73}$-*co*- $PLAMA_{21}$	7.2
$PAMA_{88}$-*co*- $PLAMA_{20}$	7.1
$PAMA_{144}$-*co*- $PLAMA_{19}$	7.0

Figure B5– Potentiometric titration curves of PAMA-co-PLAMA glycopolymers. Glycopolymers were dissolved in acidic water (pH=3) and the polymeric solutions were acidified to pH 2 with 1% (V/V) HCl and titrated with 0.1M NaOH.

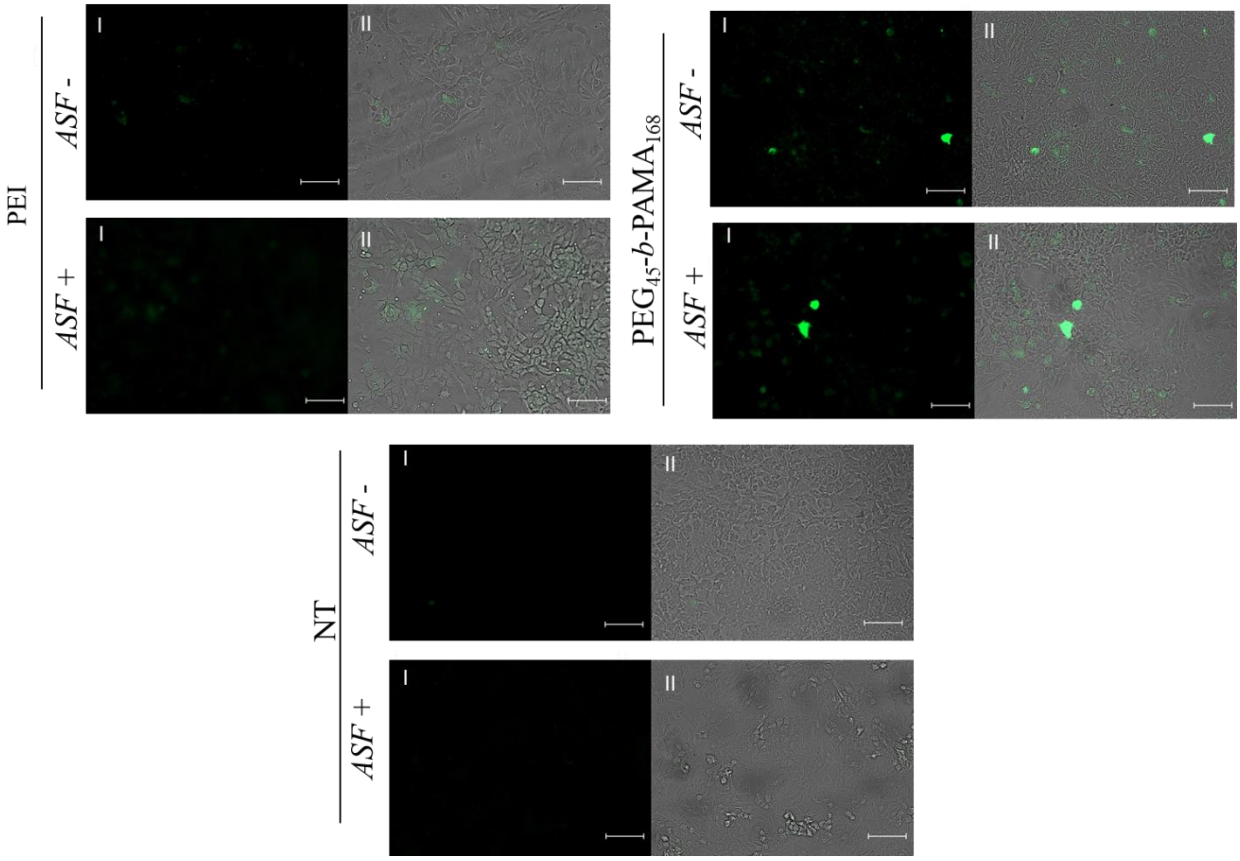

Figure B6– Effect of the presence of asialofetuin on the transfection efficiency of PEI- and PEG_{45}-*b*-$PAMA_{168}$ based polyplexes in HepG2 cells. Typical fluorescence images (I) and overlapping of fluorescence microscopy and phase contrast images (II) of cells (scale bar = 10 μm).

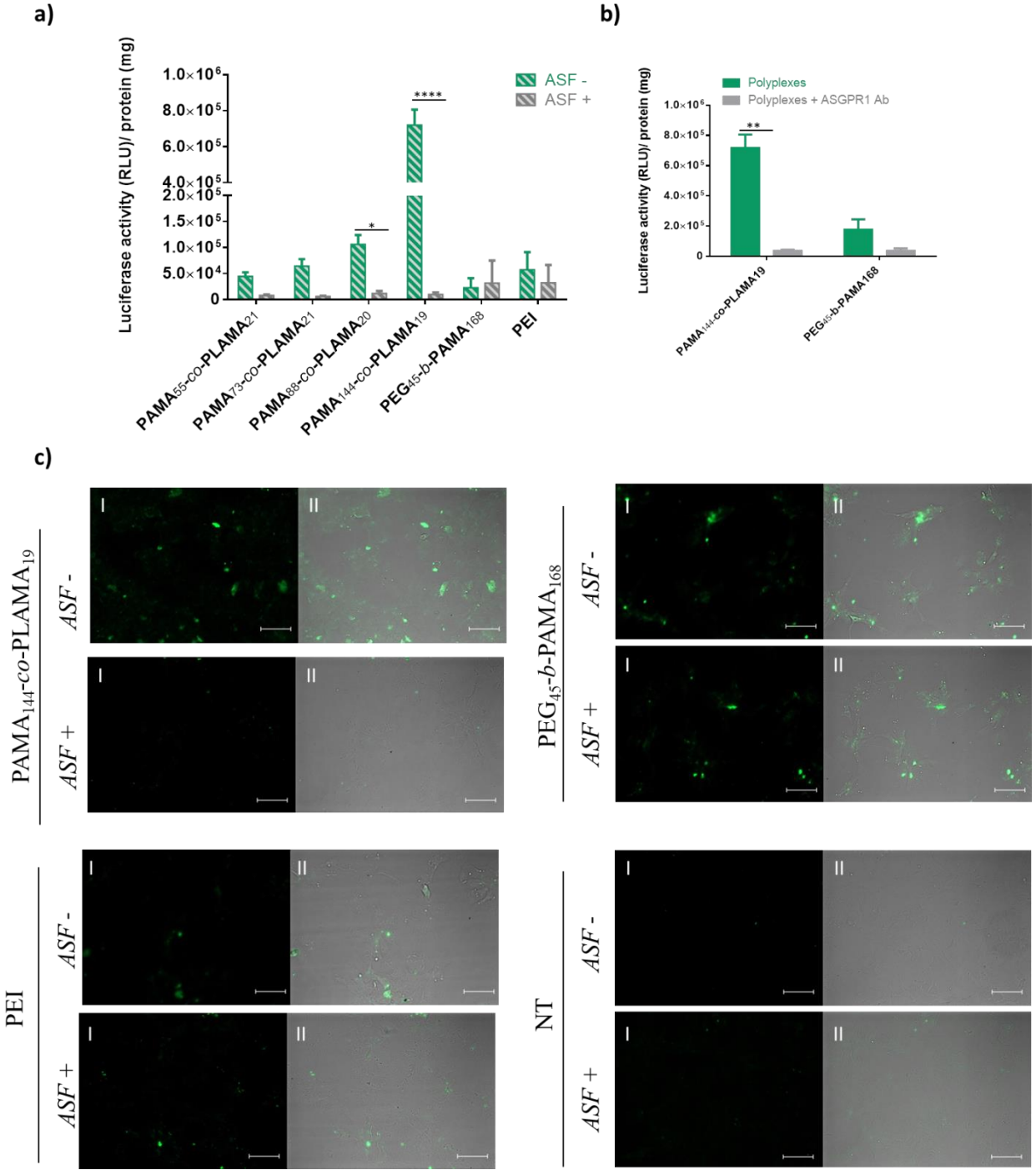

Figure B7– Effect of the presence of asialofetuin and an antibody against the ASGPR on biological activity of PAMA-*co*-PLAMA-based polyplexes in Hep3B cells. (a, b) Asterisks (****p < 0.0001, **p < 0.01 and *p < 0.05) correspond to values that differ significantly from those obtained with the same nanocarrier in the absence of ASGPR-competition agent. (c) Typical fluorescence images (I) and overlapping of fluorescence microscopy and phase contrast images (II) of cells transfected with different nanocarriers and non-treated cells in the presence and absence of asialofetuin (scale bar = 50 μm). Typical fluorescence images (I) and

overlapping (II) of fluorescence microscopy and phase contrast images of cells transfected with different glycopolymers-based nanocarriers (scale bar = 50 μm).

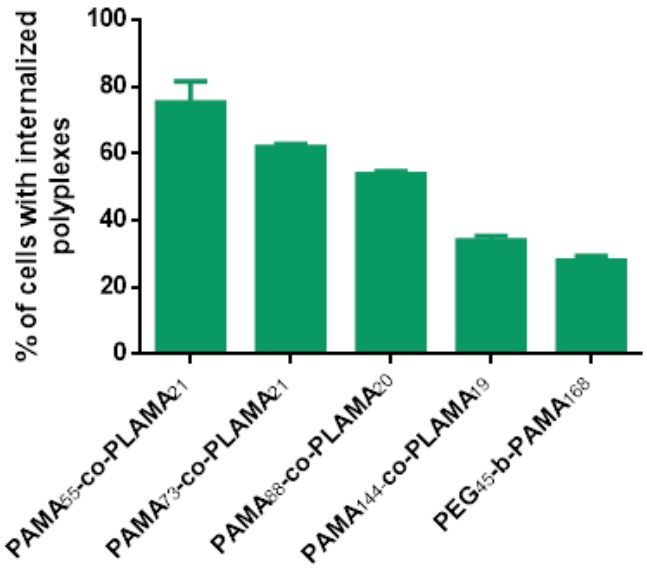

Figure B8– Cellular internalization of PAMA-*co*-PLAMA-based polyplexes evaluated by flow cytometry. Polyplexes were prepared by complexing the copolymers, containing 1% fluorescein-labeled glycopolymer, with 2 μg of DNA plasmid encoding luciferase at their optimal N/P ratios.

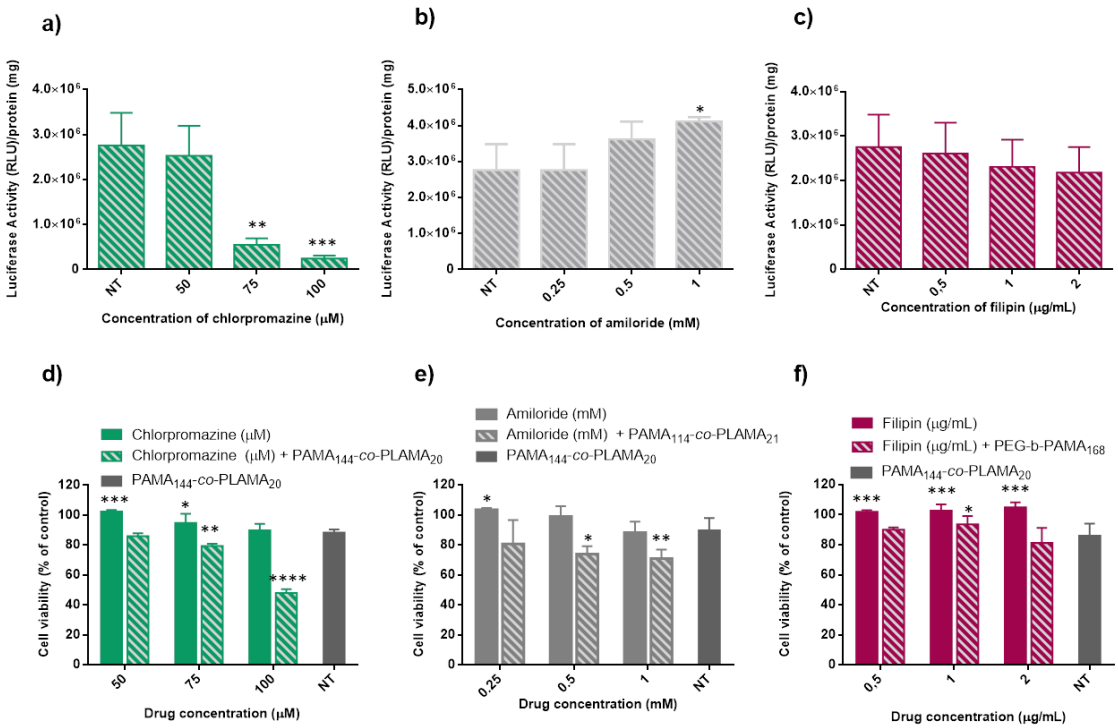

Figure B9– Effect of endocytosis inhibitors on the transfection activity (a), (b), (c) and toxicity (d), (e), (f) of $PAMA_{114}$-*co*-$PLAMA_{21}$-based polyplexes. HepG2 cells were pretreated with chlorpromazine (50; 75; 100 µM) or amiloride (0.25; 0.5; 1 mM) or filipin (0.5; 1; 2 µg.mL^{-1}) and transfected with $PAMA_{114}$-*co*-$PLAMA_{21}$-based polyplexes prepared with 1 µg of pCMV.Luc at 25/1 N/P ratio. Asterisks (****p <0.0001, ***p < 0.001, **p < 0.01 and *p < 0.05) indicate values that differ significantly from those measured in the control (cells not-treated with endocytosis inhibitors).

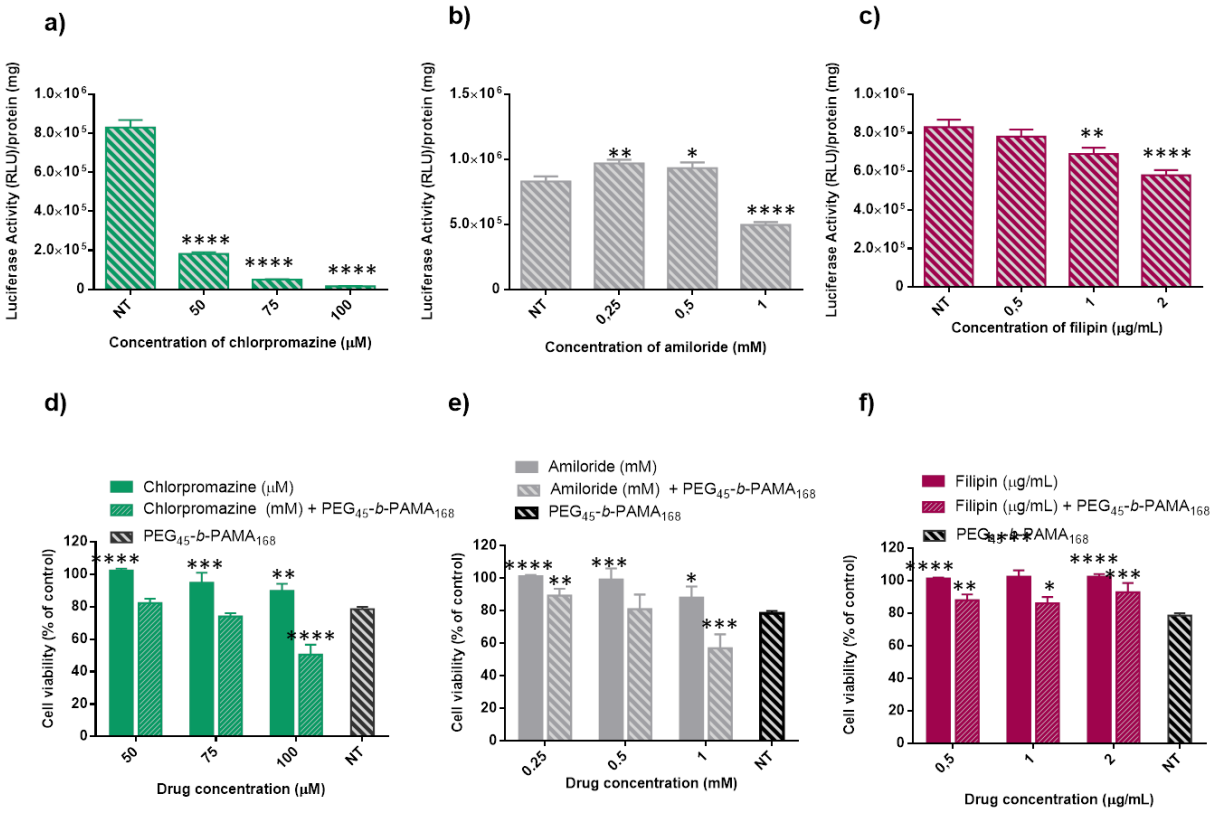

Figure B10– Effect of endocytosis inhibitors on the transfection activity (a), (b), (c) and toxicity (d), (e), (f) of PEG45-b-PAMA168-based polyplexes. HepG2 cells were pretreated with chlorpromazine (50; 75; 100 µM) or amiloride (0.25; 0.5; 1 mM) or filipin (0.5; 1; 2 µg.mL-1) and transfected with PEG45-b-PAMA168-based polyplexes prepared with 1 µg of pCMV.Luc at 50/1 N/P ratio. Asterisks (****p <0.0001, ***p < 0.001, **p < 0.01 and *p < 0.05) indicate values that differ significantly from those measured in the control (cells not-treated with endocytosis inhibitors).

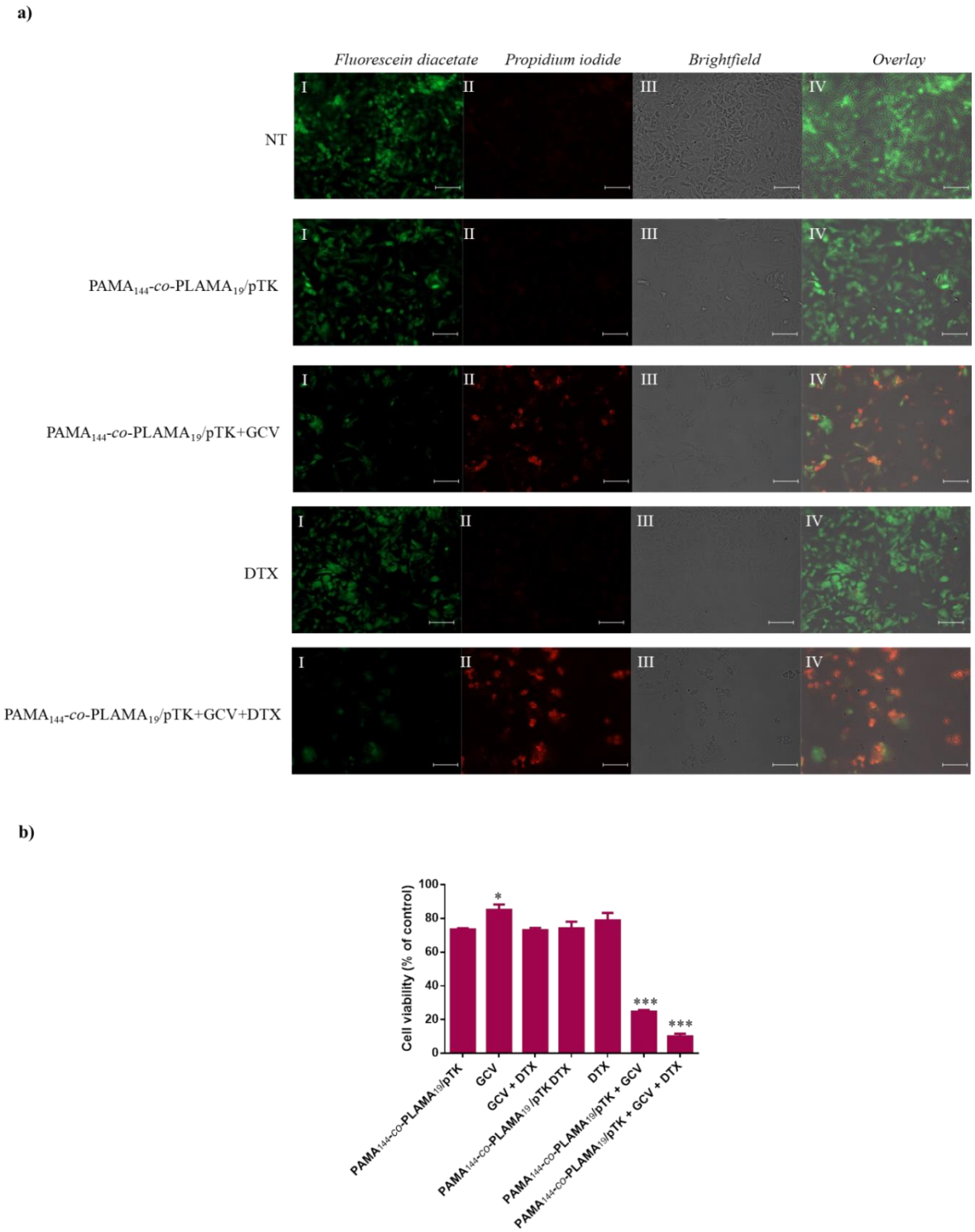

Figure B11–Therapeutic potential of the suicide gene therapy strategy mediated by the glycopolymer-based nanocarrier combined with docetaxel in HepG2 cells. a) Representative images of fluorescence microscopy and phase contrast of cells using fluorescein diacetate (green) and propidium iodide (red) staining for imaging live and dead cells, respectively (scale bar = 50 μm). b) Cell viability evaluated by the SRB assay. Asterisks (****p <0.0001,

∗∗∗p<0.001) indicate values that significantly differ from those measured for cells transfected with PAMA144-co-PLAMA19-based nanocarriers, containing 1 μg of pTK plasmid.

References

(1) Britovsek, G. J. P.; England, J.; White, A. J. P. Non-Heme Iron(II) Complexes Containing Tripodal Tetradentate Nitrogen Ligands and Their Application in Alkane Oxidation Catalysis. *Inorg. Chem.* **2005**, *44* (22), 8125–8134.

(2) Narain, R.; Armes, S. P. Synthesis and Aqueous Solution Properties of Novel Sugar Methacrylate-Based Homopolymers and Block Copolymers. *Biomacromolecules* **2003**, *4* (6), 1746–1758.